ChemRxiv™

doi.org/10.26434/chemrxiv.7771493.v1

Electrochemically Driven, Ni-Catalyzed Aryl Amination: Scope, Mechanism, and Applications

Yu Kawamata, Julien Vantourout, David P. Hickey, Peng Bai, Longrui Chen, Qinglong Hou, Wenhua Qiao, Koushik Barman, Martin A. Edwards, Alberto F. Garrido-Castro, Justine N. deGruyter, Hugh Nakamura, Kyle W. Knouse, Chuanguang Qin, Khalyd J. Clay, Denghui Bao, Chao Li, Jeremy T. Starr, Carmen N. Garcia-Irizarry, Neal Sach, Henry S. White, Matthew Neurock, Shelley D. Minteer, Phil Baran

Submitted date: 26/02/2019 • Posted date: 28/02/2019

Licence: CC BY-NC-ND 4.0

Citation information: Kawamata, Yu; Vantourout, Julien; Hickey, David P.; Bai, Peng; Chen, Longrui; Hou, Qinglong; et al. (2019): Electrochemically Driven, Ni-Catalyzed Aryl Amination: Scope, Mechanism, and Applications. ChemRxiv. Preprint.

C–N cross-coupling is one of the most valuable and widespread transformations in organic synthesis. Largely dominated by Pd- and Cu-based catalytic systems, it has proven to be a staple transformation for those in both academia and industry. The current study presents the development and mechanistic understanding of an electrochemically driven, Ni-catalyzed method for achieving this reaction of high strategic importance. Through a series of electrochemical, computational, kinetic, and empirical experiments the key mechanistic features of this reaction have been unraveled, leading to a second generation set of conditions that is applicable to a broad range of aryl halides and amine nucleophiles, including complex examples on oligopeptides, medicinally-relevant heterocycles, natural products, and sugars. Full disclosure of the current limitations as well as procedures for both batch and flow scale-ups (100 gram) are also described.

File list (2)

e-Amination 2.0 - Manuscript.pdf (9.67 MiB) view on ChemRxiv • download file

e-Amination 2.0 - Supporting information.pdf (49.03 MiB) view on ChemRxiv • download file

Electrochemically Driven, Ni-Catalyzed Aryl Amination: Scope, Mechanism, and Applications

Yu Kawamata,[1,7] Julien C. Vantourout,[1] David P. Hickey,[2,7] Peng Bai,[3,7] Longrui Chen,[4] Qinglong Hou,[4] Wenhua Qiao,[4] Koushik Barman,[2,7] Martin A. Edwards,[2,7] Alberto F. Garrido-Castro,[1] Justine N. deGruyter,[1] Hugh Nakamura,[1] Kyle Knouse,[1] Chuanguang Qin,[1] Khalyd J. Clay,[1] Denghui Bao,[4] Chao Li,[1] Jeremy T. Starr,[5] Carmen Garcia-Irizarry,[5] Neal Sach,[6] Henry S. White,[2,7] Matthew Neurock,*[3,7] Shelley D. Minteer,*[2,7] Phil S. Baran*[1,7]

[1]Department of Chemistry, The Scripps Research Institute, 10550 North Torrey Pines Road, La Jolla, California 92037, United States.

[2]Department of Chemistry, University of Utah, 315 South 1400 East, Salt Lake City, Utah 84112, United States.

[3]Department of Chemical Engineering and Materials Science, University of Minnesota, Minneapolis, MN 55455, United States.

[4]Asymchem Life Science (Tianjin), Tianjin Economic-Technological Development Zone, Tianjin 300457, China.

[5]Discovery Sciences, Medicine Design, Pfizer Global Research and Development, 445 Eastern Point Road, Groton, Connecticut 06340, United States.

[6]Department of Chemistry, La Jolla Laboratories, Pfizer, 10770 Science Center Drive, San Diego, CA 92121, United States.

[7]NSF Center for Synthetic Organic Electrochemistry

ABSTRACT: C–N cross-coupling is one of the most valuable and widespread transformations in organic synthesis. Largely dominated by Pd- and Cu-based catalytic systems, it has proven to be a staple transformation for those in both academia and industry. The current study presents the development and mechanistic understanding of an electrochemically driven, Ni-catalyzed method for achieving this reaction of high strategic importance. Through a series of electrochemical, computational, kinetic, and empirical experiments the key mechanistic features of this reaction have been unraveled, leading to a second generation set of conditions that is applicable to a broad range of aryl halides and amine nucleophiles, including complex examples on oligopeptides, medicinally-relevant heterocycles, natural products, and sugars. Full disclosure of the current limitations as well as procedures for both batch and flow scale-ups (100 gram) are also described.

Introduction

Given the ubiquitous nature of the aniline motif in drugs and natural products, there is a constant need for the development of methods for mild and selective C(sp^2)–N bond formation.[1] Currently, the stalwart methods to achieve cross-coupling of aryl halides and amines employ Pd- (Buchwald-Hartwig) and Cu-based (Ullmann) catalysts, which rank among one of the most employed transformations in modern pharmaceutical development.[2] Indeed, there exists a myriad of reports investigating the classic limitations of these reactions such as the use of strong base and elevated temperature.[1] Despite these reports, there is still documented and anecdotal evidence that several classes of amines or aryl halides remain particularly challenging substrates for C–N cross-coupling. As an example, the coupling of secondary alkyl amines and oligopeptides proceeds in low yields even under the most modern sets of conditions.[3]

Synthetic organic electrochemistry enables precise redox control to achieve either known transformations with less waste or to accomplish otherwise-intractable transformations.[4] Examples from our own lab range from the anodic generation of alkyl radicals from sulfinate salts[5] to the C–H oxidation of allylic[6] and unactivated sites.[7] Interactions with industrial collaborators in both process and medicinal chemistry inspired us to evaluate an electrochemical approach to C–N cross coupling. In 2017, we reported a Ni-catalyzed aryl amination—coined as e-amination—that exhibited a wide substrate scope for the coupling of aryl halides and triflates with amines, alcohols, and amides.[8] The reaction uses commercial reticulated vitreous carbon (RVC) and Ni-foam electrodes in concert with an inexpensive and abundant Ni catalyst at room temperature. We speculated the success of this transformation relies on the curious co-existence of multiple different Ni-oxidation states in the same reaction vessel, a task perfectly suited to electrochemistry. Critical assessment of the original conditions revealed that aryl halide coupling partners were largely limited to electron-poor derivatives and attempts with historically challenging heteroaryl halides were deemed unsatisfactory. Additionally, the choice of amine was restricted to primary and secondary alkyl substrates;

functionalized amines, including amino acids and oligopeptides, did not perform well.

The limitations in scope were attributed to a lack of understanding in the catalytic system. For instance, it was not clear what oxidation state of Ni was engaging in oxidative addition, the identity of the rate-determining step, or even the effect of simple experimental parameters such as ligand, electrolyte, or solvent. Thus, a comprehensive understanding of the reaction mechanism was needed in order to improve the previous set of conditions, with particular interest in identifying the rate-determining step, along with the ligation and oxidation states of catalytically active species. In this Article, a detailed reaction profile for e-amination is delineated, enabled by the strategic union of nuanced electrochemical analysis, DFT calculations, and empirical optimization. This collaborative endeavor facilitated the development of a robust, well-defined, catalytic system resulting in a greatly expanded substrate scope.

Background and Historical Context

Figure 1 graphically outlines the history of Ni-catalyzed C–N cross coupling.[9] In 1950, Hughes and co-workers reported the first example of Ni mediated C–N cross-coupling between chlorobenzene and methylamine using $NiCl_2$ at 200 °C (Figure 1A).[10] Several decades later, Cramer[11] and Cristau[12] conducted comprehensive studies on the C–N bond formation between chlorobenzene and different amine coupling partners in the presence of a Ni^0 catalyst at elevated temperatures (100 °C to 230 °C). The limited substrate scope did not favor the uptake of this potentially valuable transformation. It was not until 1997, when Buchwald and co-workers explored Ni^0-catalyzed amination in a synthetic context, that significant interest in Ni-catalyzed C–N cross coupling emerged.[13] As recognized, Ni-based amination reactions might be more practical than related Pd-systems on large scale due to cost considerations. Moreover, owing to its high reactivity towards less reactive electrophiles such as aryl chlorides, Ni-catalysis provides an alternative approach to palladium and copper catalysis. However, the requirements of air-sensitive Ni^0 catalysts, high temperatures, and strong alkoxide bases remained important unsolved drawbacks that significantly curtailed the adoption of such systems.

Through the years, several groups tackled the challenges and limitations associated with the Ni-catalyzed C–N bond formation (Figure 1B). Nolan,[14] Buchwald,[15] Doyle,[16] and Stewart [17] independently addressed the air sensitivity issue of Ni^0 catalysts by developing innovative air stable Ni precatalysts. In 2010, Nicasio *et al.* reported the first room temperature amination reaction of heteroaromatic chlorides using a bulky allylnickel chloride/*N*-heterocyclic carbene complex as a well-defined precatalyst **1**.[18] Despite all these advances, the scope of the Ni-catalyzed amination of aryl halides has been limited to the coupling of secondary alkylamines and arylamines, while primary alkylamines, one of the most significant classes of amines for such cross coupling, have been shown to couple only with activated aryl chlorides. As a breakthrough for this problem, Hartwig and Stradiotto *et al.* independently reported the Ni-catalyzed amination for a broad range of unactivated aryl/heteroaryl chlorides and bromides with primary aliphatic amines.[19] However, secondary aliphatic amines have proven to be poor coupling partners under their developed conditions and the use of sophisticated ligands and air-sensitive catalysts such as **2** and **3** lowered the practicality of the reaction. These pioneering developments highlight the difficulty in finding an efficient, general and practical set of conditions for the Ni-catalyzed amination of aryl halides.

As a totally different approach to improve Ni-catalyzed amination, Hillhouse and co-workers demonstrated dramatic acceleration of C–N reductive elimination by using an oxidant in the context of aliphatic systems (Figure 1C).[20] In 2012, Nakamura and co-workers suggested that facile C–N bond formation could be achieved under similar oxidative conditions for aryl systems as well.[21] Therefore, the reductive elimination event can be promoted by the intermediacy of a high-valent Ni species accessible via oxidation. These results point to a critical challenge to achieve Ni-catalyzed amination of aryl halides; namely, the coexistence of a low-valent Ni catalyst to favor oxidative addition with a high-valent Ni catalyst to facilitate reductive elimination. In 2016, Buchwald, MacMillan and co-workers elegantly employed photoinduced electron transfer to allow mild generation of active Ni^0 species and oxidatively-induced reductive elimination in the same pot using an Ir photosensitizer (Figure 1D).[22] Subsequently, our group reported an electrochemical approach to Ni-catalyzed amination (e-amination) that proceeds smoothly at room temperature or below without the aid of a strong inorganic base or co-catalyst, together with a promising substrate scope (Figure 1E).[8]

Mechanistic Studies of e-Amination

As alluded to above, e-amination likely involves accessing disparate Ni-oxidation states; the initial low-valent Ni (Ni^0 or Ni^I) for oxidative addition and the intermediate high-valent state (Ni^{III}) required for efficient reductive elimination must harmoniously coexist in the same vessel. Realization of such contradictory redox events in a simultaneous manner is challenging under conventional chemical conditions but ideally suited to an electrochemical setup. In this section a careful study to demystify the underlying steps of the catalytic cycle is presented.

Extensive mechanistic studies involving detailed electrochemical analysis and DFT calculation have led to elucidation of the mechanistic underpinnings of the e-amination, which is now presented in Figure 2A. First, the ligation state of the Ni^{II} precatalyst was determined by UV-Vis spectroscopy (Figure 2B [A]). Concentration profiles for each NiL_nBr_2 ligation state (L = Mebpy) were constructed using reported λ_{max} values and molar absorption coefficients.[23] Interestingly, the data suggested a mixed and dynamic Ni^{II} ligation states, and predominant species varies depending on the ligand/Ni^{II} ratio. Importantly, the ligation profile suggests a substantial portion of Ni^{II} remains unligated when the ligand is present in only one equivalent relative to Ni^{II}. The presence of unligated Ni^{II} species is postulated to be undesirable because overreduction of such species could lead to excessive Ni^0 aggregation which would manifest as Ni-black deposition on the cathode. Consequently, the UV-Vis study suggested the possibility of more efficient catalysis with higher ligand loading.

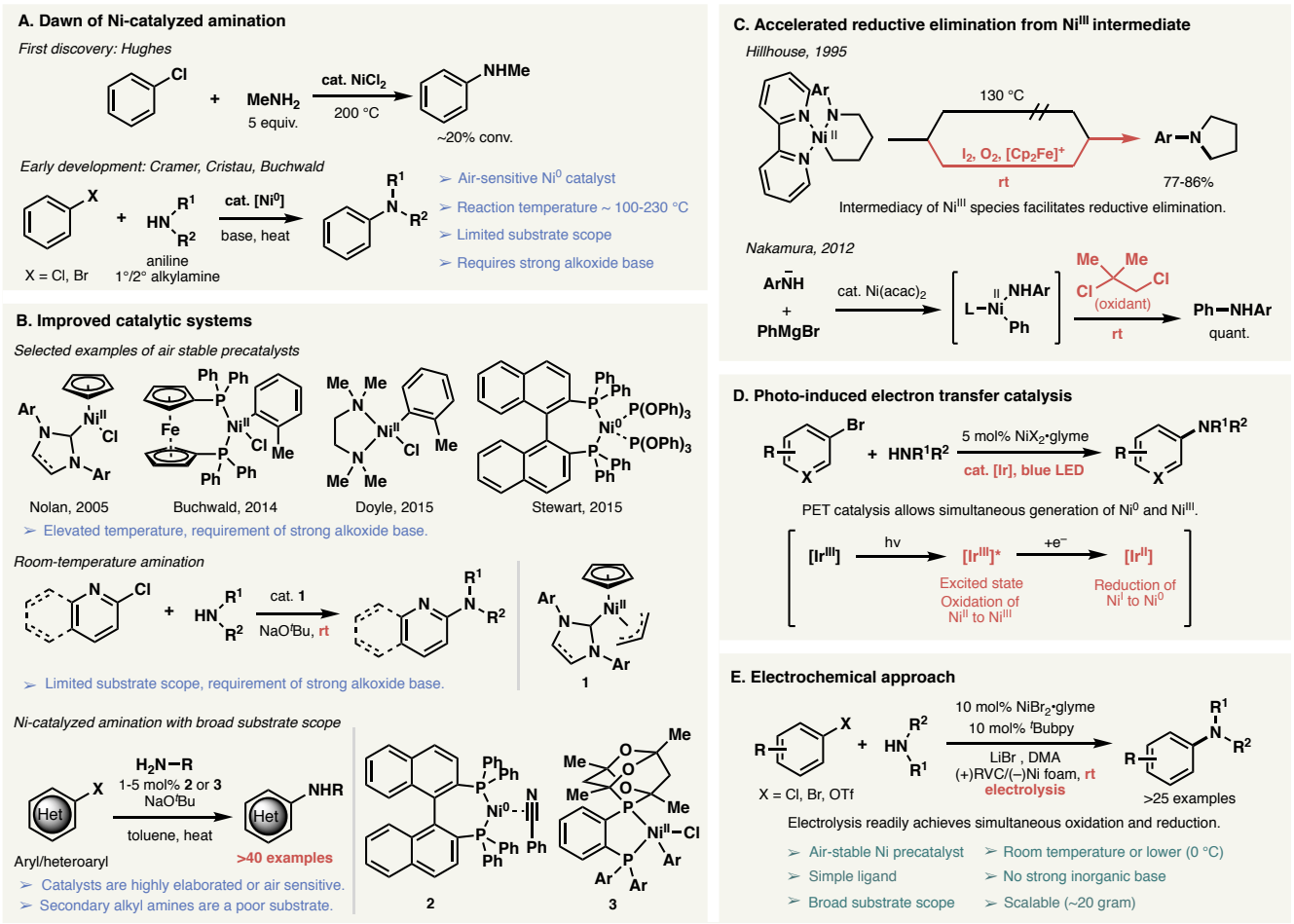

Figure 1. (A) Discovery of Ni-catalyzed amination; (B) Improvement of catalytic systems; (C) Accelerated reductive elimination via Ni^{III} intermediate; (D) Ni-catalyzed amination with photo-induced electron transfer catalysis; (E) Electrochemical, Ni-catalyzed amination (e-amination).

In parallel to these experiments, we performed density-functional theory (DFT) calculations were performed using the M06-L exchange-correlation functional, 6-31+G** basis set, and Stuttgart/Dresden effective core potentials, which took into account solvation effects with the SMD model using DMF as the implicit solvent to gain more insight about this equilibrium. The binding of the first Mebpy ligand ($Ni^{II}Br_2 \rightarrow Ni^{II}LBr_2$) is substantially exothermic with the calculated energy difference between unligated and mono-ligated species ΔE = -323 kJ/mol (See SI for details). Although much smaller energy gains are observed for the binding of the second and third ligands due to steric constraints, the energy differences indicate facile ligand association/dissociation is thermodynamically feasible. In reality the situation is likely competitive binding between the ligand, DMF, and amine nucleophile. Hence, the population of various Ni^{II} complexes is dependent on the molar fractions of all solution phase compounds, which creates a dynamic and complex ligation situation.

To shed light on the electrochemical reduction of $Ni^{II}(Mebpy)_nBr_2$, DMF solution of $NiBr_2{\bullet}3H_2O$ with various concentrations of Mebpy was analyzed by square wave voltammetry (SWV, Figure 2B [B]). There are two distinct sets of redox features grouped in the range of -0.8 to -1.2 V and -1.5 to -1.8 V (all potentials are reported vs $Ag/AgNO_3$). Computational analysis of various $Ni^{II}(Mebpy)_nBr_2$ oxidation states (See SI for details) suggests that these experimentally observed redox potentials are similar to the calculated values for the Ni(II/I) and Ni(I/0) redox transitions. The large difference between the two redox couples suggest that the Ni^{I} species is likely formed predominantly under constant current conditions to initiate oxidative addition. Electrochemical analysis of $Ni^{II}(Mebpy)_nBr_2$ reduction using a microelectrode suggests that the nature of this step is complicated and the involvement of Ni^0 cannot be completely ruled out (See SI for details). However, the combination of computational evidence, SWV analysis, and the variety of known comproportionation pathways resulting in the rapid formation of Ni^{I} lead us to the conclusion that Ni^{I} is most likely the active species toward oxidative addition.[24]

Cyclic voltammograms (CVs) of $Ni^{II}(Mebpy)Br_2$ in the absence and presence of 4-bromoanisole as an electrophile indicated the ability of Ni^{I} to undergo oxidative addition under the reaction conditions (Figure 2B [C][D]). A loss of electrochemical reversibility of the Ni(II/I) redox couple upon addition of 4-bromoanisole suggests oxidative addition is occurring rapidly relative to the time scale of the CV (100 mV/s), indicating this step is unlikely to be the rate-determining step. Reaction energy profiles determined by DFT (Figure 2B [C][D], bottom) further corroborate this conclusion; after endothermic ligand dissociation at ΔE = 99 kJ/mol, oxidative addition occurs with relatively low activation energy $\Delta E^{\ddagger}$ = 73 kJ/mol. As indicated, this oxidative addition is quite exothermic (ΔE = -162 kJ/mol). This means that all $Ni^{II}(Mebpy)_nBr_2$ (n = 1-3) could undergo rapid

oxidative addition upon reduction due to the relatively small activation barrier and large energy gain, even considering the unfavorable ligand dissociation to create open coordination sites. DFT results also suggest that the generated Ni^{III}(Mebpy)(Ar)Br_2 **5a** (Ar = 4-$CF_3C_6H_4$) can be readily reduced to Ni^{II}(Mebpy)(Ar)Br **7a** (E_{red} ~ -0.5 V vs $Ag/AgNO_3$), which is experimentally supported by the observed increase in reductive current of the Ni(II/I) redox couple in the presence of aryl halide substrate.

The evidence for rapid oxidative addition suggests that either amine coordination/deprotonation or reductive elimination is rate-determining in the overall catalytic cycle. Experimentally, the reaction with a sterically demanding *t*-butyl amine became sluggish, indicating that slow coordination/deprotonation of the amine nucleophile is potentially rate-determining (Figure 2B [E][F], top). To further determine the energetic requirements of amine coordination versus deprotonation, we examined the coupling of morpholine with 4-trifluoromethylbromobenzene. The DFT results showed that in the absence of steric constraints, the dative amine coordination should be relatively facile, with energy release around ΔE = -46 kJ/mol for this step, while the subsequent deprotonation from the basic amine causes a large energy increase (ΔE = 193 kJ/mol) and similarly large values for the ensuing reductive elimination (ΔE ~ 204 kJ/mol, black line). However, when excess free amine molecules exist in solution, their action as a base in the deprotonation of the coordinated amine compensates for the large positive ΔE for this step (similarly accomplished by the addition of an exogenous base such as DBU). In addition, ΔE for reductive elimination drastically decreases if the Ni^{II} complex is oxidized to Ni^{III} one. Overall, combination of additional base and oxidation of Ni^{II} to Ni^{III} afford an energetically feasible reaction pathway.

To experimentally verify the oxidation of Ni^{II} to Ni^{III}, intermediate Ni^{II}(^{t}Bubpy)(4-$MeOC_6H_4$)Br **12** was synthesized independently and cyclic voltammetry of **12** was studied in the presence or absence of hexyl amine. Neither **12** nor hexyl amine showed electrochemical oxidation within the electrochemical solvent/electrolyte window (Figure 2B [E][F] middle). However, the addition of a large excess of hexyl amine into the DMF solution of **12** (100 equivalents with respect to Ni) results in the formation of a complex that is oxidized irreversibly at ~0.8 V, which again indicates slow amine coordination/deprotonation on the Ni^{II}L(Ar)Br intermediate **7**.

Taken together, our results are consistent with the mechanism illustrated in Figure 2A involving [A] the dynamic ligation state of Ni^{II} precatalyst, [B] the electrochemical reduction of Ni^{II} to a Ni^{I} species **4** at the cathode, [C] the rapid oxidative addition of Ni^{I} to an aryl halide generating a transient Ni^{III} species **5**, [D] a second electrochemical reduction at the cathode resulting in a stable Ni^{II} aryl intermediate **7**, [E] the coordination of the amine and rate-limiting deprotonation to the intermediate **8**, [F] the electrochemical oxidation at the anode to generate a high-energy Ni^{III} complex **6**, followed by rapid reductive elimination to produce the arylamine product while regenerating **4** as the active catalyst. Basic kinetic analysis is in good agreement with this mechanistic picture (See SI for detail).

It should be noted the current mechanistic evidence does permit the possibility of a self-sustaining Ni^{I}/Ni^{III} cycle (Figure 2A, step [G]) in which Ni^{III}L(Ar)Br_2 **5** is not immediately reduced at the cathode, but undergoes amine coordination/deprotonation to generate the intermediate **6**. A similar Ni^{I}/Ni^{III} cycle is also proposed by Miyake and co-workers in their photochemical amination work recently investigated.[25] The feasibility of this Ni^{I}/Ni^{III} pathway was tested by performing the reaction with a catalytic amount of electricity (Figure 2B [G]). While 5% yield of **10** was obtained after 15 minutes electrolysis/3 hours stirring, the current efficiency was merely 27%, which clearly suggests that continuous electrolysis is necessary in order to achieve appreciable yields. This apparent inefficiency of Ni^{I}/Ni^{III} cycle could be explained by the comproportionation of **4** and **5** to generate stable Ni^{II} intermediate **7**, considering redox potential of Ni(II/I) obtained by SWV (~ -1 V) and calculated reduction potential of **5a** (-0.5 V). Therefore, the role of electricity is constant regeneration of the key catalytic species such as **4** and **6** throughout the duration of the reaction.

Collectively, the mechanistic results suggest the ligand/Ni^{II} ratio should be optimized to afford enhanced reactivity by avoiding deleterious Ni^{0} deposit. Furthermore, the addition of appropriate amount of external base would appear to facilitate the rate-limiting deprotonation. With these mechanistic nuances in mind, we began our forays on expanding the scope of e-amination.

Optimization

Minimal arylation of glutamic acid di-*tert*-butyl ester (**14)** was observed under our previously reported e-amination conditions (Table 1A, conditions A), and therefore it was selected as a model reaction to validate the insights obtained from the above mechanistic study. A slight improvement was observed by changing the electrolyte from LiBr to tetra-*n*-butylammonium bromide (conditions B). As suggested by the UV-Vis spectroscopic study, increasing the ligand/Ni^{II} ratio from 1/1 to 2/1 was found to be far superior with a greater than four-fold increase in yield obtained (conditions C). Although increasing the ligand loading further (ligand/Ni^{II} = 3/1, conditions D) seemed to have no effect on the yield, deposition of nickel black on the cathode was observed in some cases when 20 mol% ligand was employed; this phenomenon was almost completely suppressed at 30 mol%. Therefore, conditions D were chosen as the standard conditions for additional optimization with the impact of several reaction parameters

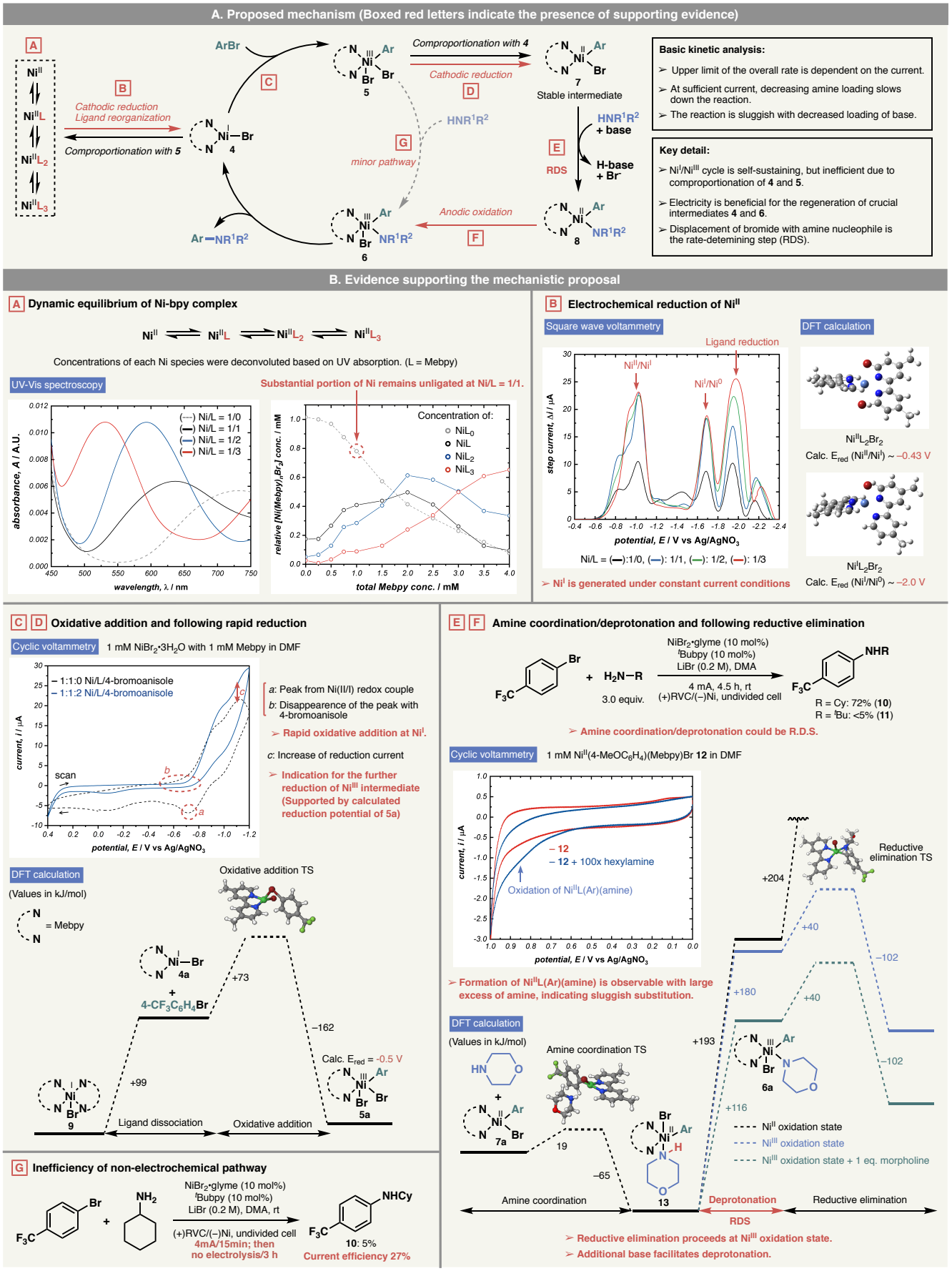

Figure 2. (A) Proposed mechanism; (B) Experimental and computational evidence to support the proposed mechanism; subpanels [A]-[G] represent evidence for each elementary step.

summarized in Table 1B. As generally observed in transition-metal catalyzed coupling reactions, the choice of ligand was found to be crucial for the success of this reaction. After extensive screening of different ligand architectures (see SI for the complete list), the best result was obtained with simple, unsubstituted bipyridine (bpy, entry 1). This is fortuitous considering that the ligand is the most expensive component of this amination system. Similar results were also obtained with Mebpy (entry 2), whereas more sterically demanding 6,6'-Mebpy completely shut down the reaction (entry 3), indicating that this reaction is rather sensitive to the steric environment around the Ni catalyst. Pyridine-oxazoline ligands were found to be similarly effective for the of **14** (entry 4), but later were found not to be generally applicable. Reduced quantities of DBU were found to be deleterious to the reaction (entry 5), in good agreement with DFT calculations that the rate-determining step—displacement of the bromide on the intermediate **7** with the amine nucleophile—is facilitated by an external base (*vide supra*). Highly polar and aprotic solvents were found to be suitable for this reaction (entries 6-7), as these solvents have ideal characteristics for electrochemical synthesis: good solubility of the electrolyte and the Ni-catalyst, high dielectric constant required for efficient conductivity, and an appropriate electrochemical window.[26] With regard to the counterion of the electrolyte, perchlorate and chloride were slightly less efficient than bromide (entries 8 and 9). Concentration of the electrolyte did not have a major impact on the reaction despite the apparent voltage difference (entry 10, terminal potential 3-4 V for 0.2 M vs 4-6 V for 0.05 M). Finally, it was found that $Ni(bpy)_3Br_2$ (**17**),[27] a bench-stable and free-flowing solid with no apparent hygroscopicity, was an ideal precatalyst, which improves operational simplicity of this reaction by removing the need for the preparing stock solutions of hygroscopic $NiBr_2 \cdot 3H_2O$ (entry 11). The preparation of this known precatalyst is exceedingly simple as illustrated in Table 1C and is currently being commercialized (Sigma-Aldrich ALD00608).

A. Initial re-optimization

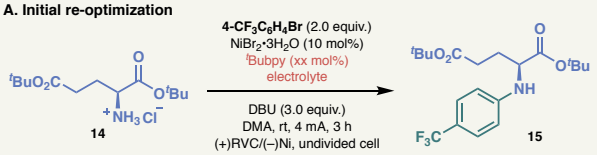

Conditions	Electrolyte	ligand loading	Yield
A	LiBr (0.2 M)	10 mol%	<5%
B	^{n}Bu$_4$N•Br (0.05 M)	10 mol%	9%
C	^{n}Bu$_4$N•Br (0.05 M)	20 mol%	38%
D	^{n}Bu$_4$N•Br (0.05 M)	30 mol%	38%

B. Impact of various reaction parameters

Entry	Change from conditions D	Yield
1	Ligand = bpy	52%
2	Ligand = Mebpy	40%
3	Ligand = 6,6'-Mebpy	<5%
4	Ligand = **16**	40%
5	1.0 equiv. DBU	5%
6	Solvent = NMP	42%
7	Solvent = DMF	27%
8	$Et_4N \cdot ClO_4$ (0.05 M)	45%
9	$Et_4N \cdot Cl$ (0.05 M)	42%
10	^{n}Bu$_4$N•Br (0.20 M)	54%
11	10 mol% $Ni(bpy)_3Br_2$, ^{n}Bu$_4$N•Br (0.20 M), 4 h	63%[a]

[a] 66% ee was determined by chiral HPLC analysis.

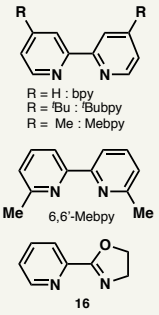

C. Synthesis of Ni precatalyst

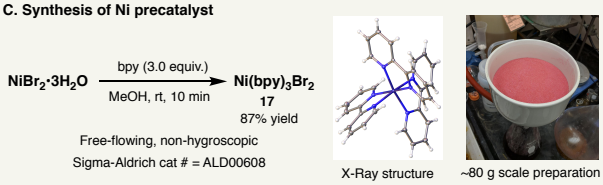

Table 1. (A) Initial re-optimization of amino acid arylation; (B) Effect of various reaction parameters; (C) Simple preparation of the precatalyst $Ni(bpy)_3Br_2$ **17**.

Scope and Applications of e-Amination

Encouraged by the successful arylation of glutamic acid ester **14**, the generality of the revised electrochemical C–N bond formation on various amino acid esters was explored (Table 2A). Using readily-available amino acid hydrochloride salts as starting materials, various amino acid esters (including non-canonical amino acids) were arylated efficiently with 4-trifluoromethylbromobenzene. Reactions were conveniently carried out in an undivided cell with a readily-available RVC anode and a nickel foam cathode. Yields under the previous conditions are shown in parentheses, which highlight the drastic improvement afforded under the revised conditions. Although there have been multiple precedents for the arylation of amino acid esters employing palladium[28,] and copper catalysis,[29] this is the first example of successful C–N bond formation on amino acid esters by Ni-catalysis. Racemization was minimized by short reaction times at ambient temperature.[3] Of note, the sulfide in **24** and the indole ring in **26**—both of which are commonly considered to be labile under oxidative conditions—were found to be compatible.

As an extension of this scope, *N*-acetyl-4-bromoindole **29** was chosen (Table 2B) as an emblematic substrate for challenging C–N coupling.[30] Similar systems were reported to require large amount of copper salt for traditional Ullmann coupling conditions,[31] and applications of Buchwald-Hartwig coupling was found to be challenging.[32] Not surprisingly, our first-generation conditions for e-amination failed to deliver the desired coupling product **31** (entry 1). The optimized conditions documented herein did in fact afforded **31** in 16% yield (entry 2), and ultimately a small screening of electrolyte, amount of base, ligands, nickel source (entries 3-7) was required to arrive at a workable solution (entry 7, 32%). Based on the conditions in entry 7, scale-up of the reaction was attempted with a slight change of substrate and electrolyte concentration. Fortunately, e-amination performed on a larger scale delivered superior yield, presumably due to the higher concentration of the substrate and more appropriate current density (entry 8, 51%). This small study demonstrates that like other C–N cross couplings, re-adjustment of reaction parameters such as precatalyst, ligand, and concentration of the substrate may be necessary for the success of certain substrate classes. In our initial report, a limited substrate scope of heteroaryl amination was documented.[8] Considering that heteroaryl amines are

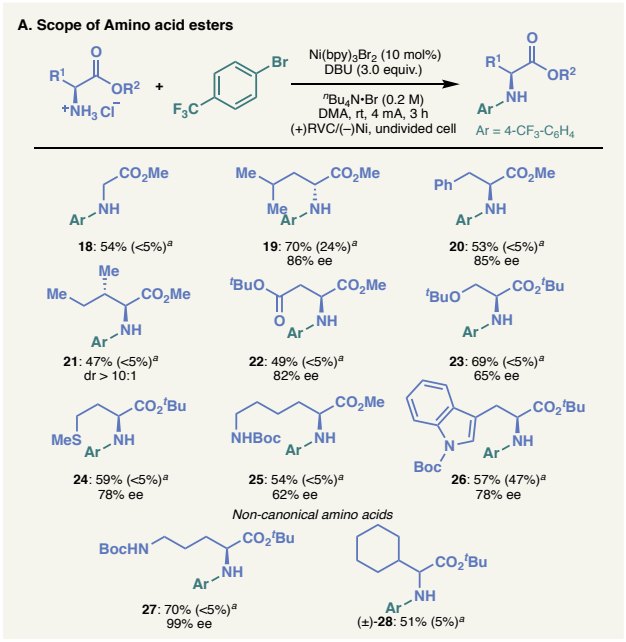

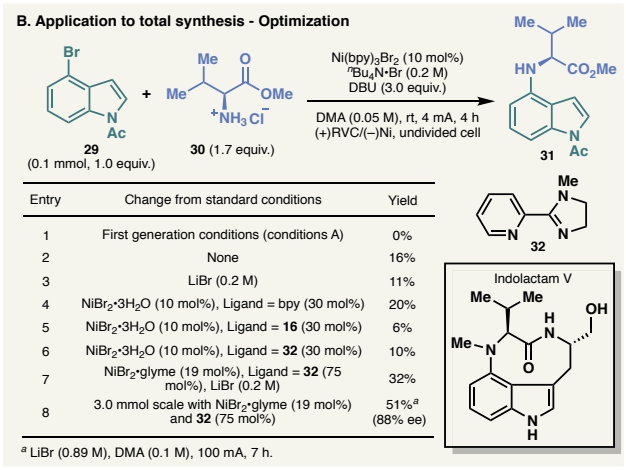

Entry	Change from standard conditions	Yield
1	First generation conditions (conditions A)	0%
2	None	16%
3	LiBr (0.2 M)	11%
4	$NiBr_2{\cdot}3H_2O$ (10 mol%), Ligand = bpy (30 mol%)	20%
5	$NiBr_2{\cdot}3H_2O$ (10 mol%), Ligand = **16** (30 mol%)	6%
6	$NiBr_2{\cdot}3H_2O$ (10 mol%), Ligand = **32** (30 mol%)	10%
7	$NiBr_2$•glyme (19 mol%), Ligand = **32** (75 mol%), LiBr (0.2 M)	32%
8	3.0 mmol scale with $NiBr_2$•glyme (19 mol%) and **32** (75 mol%)	51%[a] (88% ee)

[a] LiBr (0.89 M), DMA (0.1 M), 100 mA, 7 h.

Table 2. (A) Arylation of amino acid esters. [a] () indicates yield under previous conditions (conditions A). (B) Optimization for the coupling of *N*-acetyl-4-bromoindole **29** with valine methyl ester **30**.

essential in medicinal chemistry, a more complete survey of this class of molecules was undertaken. *N*-Boc-piperazine was chosen as the amine coupling partner, since: (1) this motif frequently appears in pharmaceuticals, and (2) secondary amines are sometimes troublesome coupling partners even with state-of-the-art palladium catalysis at room temperature.[3] As shown in Table 3, a wide range of heteroaryl halides deriving from quinoline (**33**, **34**), indole (**31**, **35**), benzofuran (**36**), pyridines (**37**-**39**), thiophene (**40**, **41**), thiazole (**42**), pyrimidine (**43**) and azaindazole (**44**) were successfully coupled with *N*-Boc-piperazine under essentially identical conditions optimized for amino acid esters. Both aryl bromides and chlorides were found to be competent in this reaction. Most of the heterocycles included in this table are privileged scaffolds in pharmaceuticals.[33] The high functional group tolerance of this reaction deserves further comment. For instance, the free anilinic amine in **39** remained untouched. Sulfur-containing heterocycles afforded the desired coupling products **40**-**43**, despite the fact that sulfur is

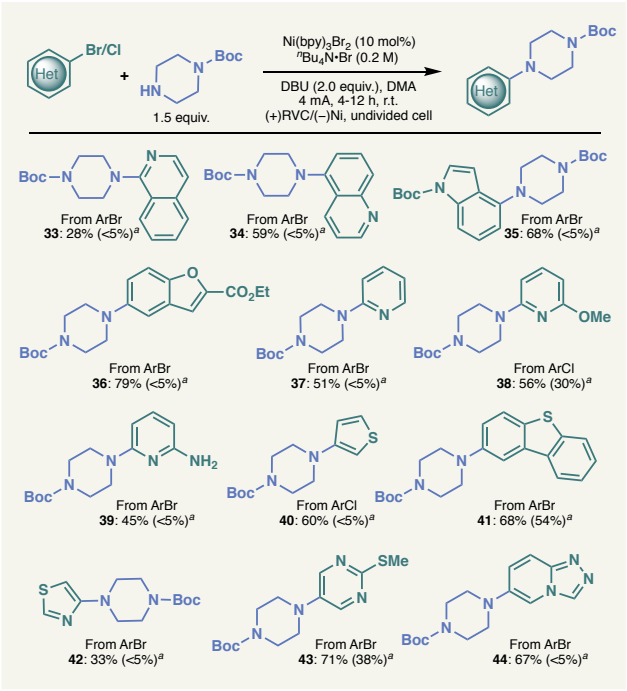

Table 3. Amination of heteroaryl halides with *N*-Boc-piperazine. [a] () indicates yield under previous conditions (conditions A)

commonly considered to be poisonous to transition-metal catalysts with the C–S bond being particularly labile in Ni-catalysis.[34]

To further explore the capability of electrochemical C–N bond formation, the reaction was applied to more challenging substrates. Table 4A illustrates C–N bond formation on nucleoside analogs. TBS-protected 1-(4-bromophenyl)ribose was successfully coupled with both primary and secondary amines. This method enables rapid access to various substituted 1-arylribose, which is potentially useful for the study of artificial base-pairs to expand the genetic alphabet.[35] Likewise, arylation of 3-amino thymidine was also successful without protection on thymine. More interestingly, the powerful electrochemical C–N bond formation furnished a unique dinucleoside analog **5oa** linked by an aniline moiety, which is a highly intriguing linker due to its non-hydrolyzable nature.

Another interesting application of this method was found in oligopeptide modification (Table 4B). Slight modification to the established conditions were made to achieve synthetically useful efficiency. Thus, the use of a LiBr electrolyte was found to give higher yield than tetra-*n*-butylammonium bromide, and DBU was omitted by using an excess amine coupling partner to avoid undesired racemization. With these modifications, e-amination on pendant 4-bromophenylalanine residues proceeded surprisingly well with only a catalytic amount of Ni precatalyst in several cases. Various functional groups in canonical amino acids were tolerated in protected form, as demonstrated in the products **51**-**55**. More strikingly, the unprotected nona-peptide afforded the desired amination product **56** in appreciable yield. To the best of our knowledge, this is the first example of Ni-catalyzed C–N bond formation on oligopeptides, which holds promise for further application of such chemistry to biomolecule modifications. This work is a complementary addition to the growing area of transition-metal mediated oligopeptide functionalization.[36]

As we previously demonstrated in a batch decagram scale reaction (Table 4C, top), the e-amination is easily scalable. Compound **58** is an important intermediate for the synthesis of vilazodone, a drug recently approved by FDA for the treatment of major depressive disorder.[37] Previously, **58** was prepared by four steps from salicylaldehyde in 26% overall yield,[38] though a more straightforward synthesis is possible by using Pd-catalyzed amination to form the C–N bond between benzofuran fragment and piperidine.[39] As an alternative approach, e-amination of **59** with *N*-Boc-piperidine was evaluated to prepare a closely-related compound **36**. After a brief investigation, it was found that tetra-*n*-butylammonium bromide could be replaced with inexpensive sodium bromide to further reduce the cost of the production. Moreover, the RVC electrode was found to be replaceable with an even simpler carbon felt electrode. A 100 g scale reaction was successfully carried out by employing a flow system with only a small drop in yield (64% in 100 g vs 79%

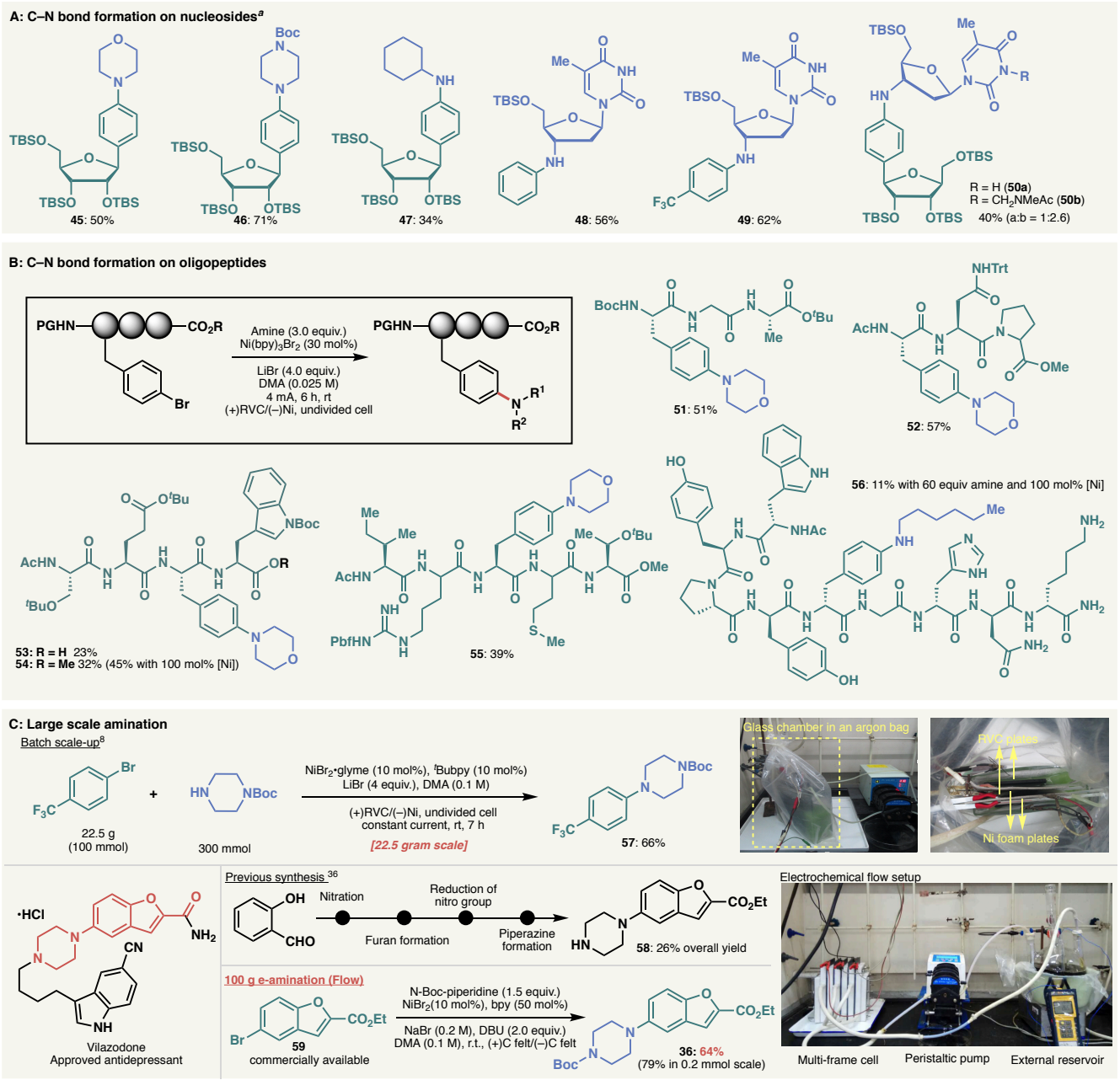

Table 4. (A) C–N bond formation on nucleosides. [a] Reaction conditions: 10 mol% $Ni(bpy)_3Br_2$, $^nBu_4N$•Br (0.2 M), DBU (2.0 equiv.), DMA (0.025-0.05 M), (+)RVC/(−)Ni, 4 mA, r.t. in undivided cell. (B) C–N bond formation on oligopeptides. (C) Synthesis of arylomycin analogs. (D) Scale-up synthesis of compound **36**.

in 0.2 mmol). Notably, the multi-frame cell set up used in this scale-up study accommodates various reaction scales simply by changing the number of frames (See SI for details). This scale-up example clearly illustrates the simplicity and low-cost of scaling up e-amination.

Applicability of other nucleophiles and limitations of the e-amination

Finally, the efficiency of the modified conditions (higher ligand loading together with the use of DBU as an external base) over the first-generation conditions (Conditions A) as well as limitations of e-amination are illustrated in Table 5. In the case

of substrates previously described,[8] the desired products **64**-**72** were obtained in similar or slightly higher yields under the modified conditions. With regard to the applicability of other types of nitrogen nucleophiles, a lactam and ammonia were both found to be competent (**74**, **75**). However, e-amination with aniline and sulfonamide were not successful due to low nucleophilicity of these coupling partners (**73**, **76**). Coupling with oxygen-based nucleophile was also found to be feasible as exemplified in the formation of **77**-**79**. Phenol was not a suitable nucleophile likely due to its susceptibility toward oxidation (**80**). In contrast to relatively predictable reactivity of nucleophiles, the reactivity of the aryl bromides seems to be rather difficult to interpret. Some heteroaryl bromides gave complex mixtures, whereas others were unreactive. It implies that multiple mechanistic scenarios could exist in e-amination, depending on the sub strate used. Oxidative addition, rather than amine

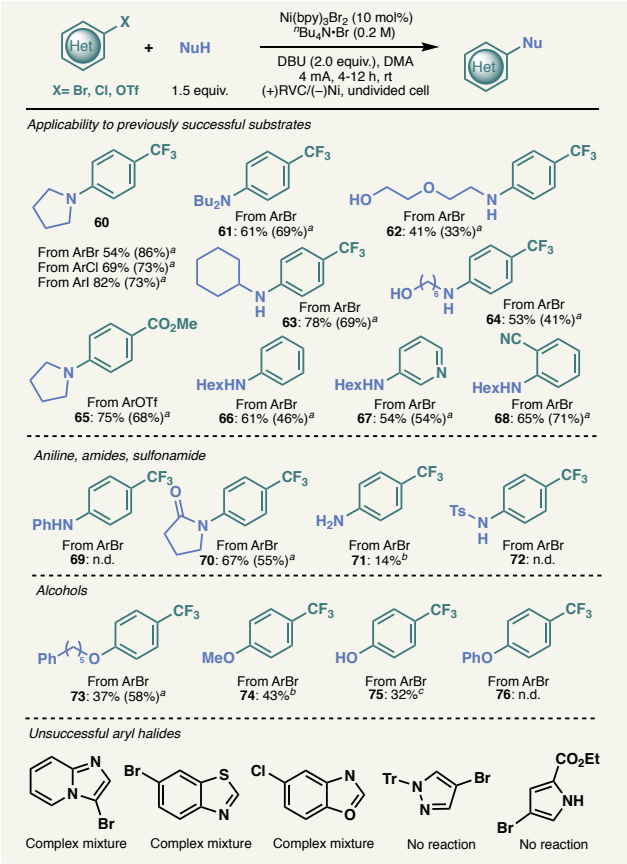

Table 5. Comparison to previously-successful substrates and limitations of e-amination. [a] Data obtained from ref 8. [b] 10 equiv. of nucleophile used. [c] 20 equiv. of water used.

coordination/deprotonation might be the possible rate-determining step in some of these cases.

Conclusion

The present study commenced with a deep interrogation of the mechanism of e-amination in order to demystify the nature of the catalytic cycle and aid in the elucidation of more general and robust conditions. By applying a range of techniques, from empirical optimizations to DFT calculations and kinetic studies, a second-generation set of conditions was invented using a simple Ni-precatalyst. The scope of e-amination was significantly expanded and supplemented with multiple applications. The use of e-amination is not limited to small scale applications and simple setups for both batch and flow scale up are delineated. Finally, this unique method for C–N bond formation has been field tested in multiple programs within the labs of our industrial collaborators. The mainstream adoption of electrochemistry in areas like medicinal chemistry has been stymied by a lack of standardized equipment and reaction classes that are relevant to drug discovery. It is anticipated that the current work will be an important step in accelerating the adoption of this useful means of controlling redox states in organic synthesis.

ASSOCIATED CONTENT

Supporting Information

The Supporting Information is available free of charge on the ACS Publications website.

Experimental procedures, additional electrochemical analysis data, the detail of DFT calculation and compound characterization data. (PDF)

X-ray crystallographic data for compound **17** (CIF)

AUTHOR INFORMATION

Corresponding Author

*mneurock@umn.edu
*minteer@chem.utah.edu
*pbaran@scripps.edu

Present Addresses

†Peng Bai: Department of Chemical Engineering, University of Massachusetts, Amherst, MA, 01003, United States.
†Alberto F. Garrido-Castro: Department of Organic Chemistry, Universidad Autónoma de Madrid, Madrid, 28049, Spain.
† Chuanguang Qin: Department of Applied Chemistry, School of Natural and Applied Sciences, Northwestern Polytechnical University, 127 Youyixilu, Xi'an, 710072, Shaanxi, P. R. China.
† Chao Li: National Institute of Biological Sciences, Beijing, 7 Science Park Road ZGC Life Science Park, Beijing, China.

Author Contributions

The manuscript was written through contributions of all authors. All authors have given approval to the final version of the manuscript.

Funding Sources

Financial support for this work was provided by NIH (GM-118176), CCI NSF Synthetic Organic Electrosynthesis Center (#1740656), George E. Hewitt foundation for postdoctoral fellowship (Y.K.), Universidad Autónoma de Madrid (A.F.G.-C.), NSF GRFP for graduate support (D.S.P. and J.N.D.) and JSPS for postdoctoral fellowship (H. N.).

ACKNOWLEDGMENT

We thank Prof. Donna Blackmond for assistance in interpreting the kinetics data. We also thank Dr. D.-H. Huang and Dr. L. Pasternack for NMR spectroscopic assistance, Prof. A. L. Rheingold, Dr. C. E. Moore and Dr. Milan Gembicky for X- ray crystallographic analysis, Dr. Jason Chen and Brittany Sanchez (Scripps Automated Synthesis Facility) for assistance with HPLC, HRMS and LCMS. We gratefully acknowledge Dr. Jinshan Chen for helpful discussions during the early stage of this work. We also greatly appreciate insightful discussion with Dr. Martin D. Eastgate, Dr. Amy C. Hart and Dr. Jennifer X. Qiao.

REFERENCES

(1) For selected reviews, see: (a) Ruiz-Castillo, P.; Buchwald, S. L. Applications of Palladium-Catalyzed C–N Cross-Coupling Reactions. *Chem. Rev*. **2016**, *116*, 12564–12649. (b) Beletskaya, I. P.; Cheprakov, A. V. The Complementary Competitors: Palladium and Copper in C–N Cross-Coupling Reactions. *Organometallics* **2012**, *31*, 7753–7808. (c) Fischer, C.; Koenig, B. Palladium- and Copper-Mediated *N*-Aryl Bond Formation Reactions for the Synthesis of Biological Active Compounds. *Beilstein J. Org. Chem*. **2011**, *7*, 59–74.
(2) Brown, D. G.; Boström, J. Analysis of Past and Present Synthetic Methodologies on Medicinal Chemistry: Where Have All the New Reactions Gone? *J. Med. Chem.* **2016**, *59*, 4443–4458.
(3) (a) Dennis, J. M.; White, N. A.; Liu, R. Y.; Buchwald, S. L. Breaking the Base Barrier: an Electron-Deficient Palladium Catalyst Enables the Use of a Common Soluble Base in C–N Coupling. *J. Am. Chem. Soc*. **2018**, *140*, 4721–4725. (b) Lee, H. G.; Lautrette, G.; Pentelute, B. L.; Buchwald, S. L. Palladium-Mediated Arylation of Lysine in Unprotected Peptides. *Angew. Chem. Int. Ed*. **2017**, *56*, 3177–3181. (c) Balraju, V.; Iqbal, J. Synthesis of Cyclic Peptides Constrained with Biarylamine Linkers Using Buchwald−Hartwig C−N Coupling#. *J. Org. Chem*. **2006**, *71*, 8954–8956.
(4) For selected reviews, see: (a) Yan, M.; Kawamata, Y.; Baran, P. S. Synthetic Organic Electrochemical Methods Since 2000: on the Verge of a Renaissance. *Chem. Rev*. **2017**, *117*, 13230–13319. (b) Horn, E. J.; Rosen, B. R.; Baran, P. S. Synthetic Organic Electrochemistry: an Enabling and Innately Sustainable Method. *ACS Cent. Sci*. **2016**, *2*, 302–308. (c) Francke, R.; Little, R. D. Redox Catalysis in Organic Electrosynthesis: Basic Principles and Recent Developments. *Chem. Soc. Rev*. **2014**, *43*, 2492–2521. (d) Yoshida, J.-I.; Kataoka, K.; Horcajada, R.; Nagaki, A. Modern Strategies in Electroorganic Synthesis. *Chem. Rev*. **2008**, *108*, 2265–2299. (e) Moeller, K. D. Synthetic Applications of Anodic Electrochemistry. *Tetrahedron* **2000**, *56*, 9527.
(5) O'Brien, A. G.; Maruyama, A.; Inokuma, Y.; Fujita, M.; Baran, P. S.; Blackmond, D. G. Radical C–H Functionalization of Heteroarenes Under Electrochemical Control. *Angew. Chem. Int. Ed*. **2014**, *53*, 11868–11871.
(6) Horn, E. J.; Rosen, B. R.; Chen, Y.; Tang, J.; Chen, K.; Eastgate, M. D.; Baran, P. S. Scalable and Sustainable Electrochemical Allylic C–H Oxidation. *Nature* **2016**, *533*, 77–81.
(7) Kawamata, Y.; Yan, M.; Liu, Z.; Bao, D.-H.; Chen, J.; Starr, J. T.; Baran, P. S. Scalable, Electrochemical Oxidation of Unactivated C–H Bonds. *J. Am. Chem. Soc*. **2017**, *139*, 7448–7451.
(8) Li, C.; Kawamata, Y.; Nakamura, H.; Vantourout, J. C.; Liu, Z.; Hou, Q.; Bao, D.; Starr, J. T.; Chen, J.; Yan, M.; et al. Electrochemically Enabled, Nickel-Catalyzed Amination. *Angew. Chem. Int. Ed*. **2017**, *56*, 13088–13093.
(9) Marín, M.; Rama, R. J.; Nicasio, M. C. Ni-Catalyzed Amination Reactions: an Overview. *Chem. Rec*. **2016**, *16*, 1819–1832.
(10) Hughes, E. C.; Veatch, F.; Elersich, V. *N*-Methylaniline From Chlorobenzene and Methylamine. *Ind. Eng. Chem*. **1950**, *42*, 787–790.
(11) Cramer, R.; Coulson, D. R. Nickel-Catalyzed Displacement Reactions of Aryl Halides. *J. Org. Chem*. **1975**, *40*, 2267–2273. (12) Cristau, H.-J.; Desmurs, J.-R. Arylation of Hard Heteroatomic Nucleophiles Using Bromoarenes Substrates and Cu, Ni, Pd-Catalysts; Industrial Chemistry Library; Elsevier, 1995; Vol. 7, pp 240–263.
(13) Wolfe, J. P.; Buchwald, S. L. Nickel-Catalyzed Amination of Aryl Chlorides. *J. Am. Chem. Soc*. **1997**, *119*, 6054–6058.
(14) Kelly, R. A.; Scott, N. M.; Díez-González, S.; Stevens, E. D.; Nolan, S. P. Simple Synthesis of CpNi(NHC)Cl Complexes (Cp = Cyclopentadienyl; NHC = *N*-Heterocyclic Carbene). *Organometallics* **2005**, *24*, 3442–3447.
(15) Park, N. H.; Teverovskiy, G.; Buchwald, S. L. Development of an Air-Stable Nickel Precatalyst for the Amination of Aryl Chlorides, Sulfamates, Mesylates, and Triflates. *Org. Lett*. **2013**, *16*, 220–223.
(16) Shields, J. D.; Gray, E. E.; Doyle, A. G. A Modular, Air-Stable Nickel Precatalyst. *Org. Lett*. **2015**, *17*, 2166–2169.
(17) Kampmann, S. S.; Skelton, B. W.; Wild, D. A.; Koutsantonis, G. A.; Stewart, S. G. An Air-Stable Nickel(0) Phosphite Precatalyst for Primary Alkylamine C-N Cross-Coupling Reactions. *Eur. J. Org. Chem*. **2015**, *2015*, 5995–6004.
(18) Iglesias, M. J.; Prieto, A.; Nicasio, M. C. Well-Defined Allylnickel Chloride/*N*-Heterocyclic Carbene [(NHC)Ni(Allyl)Cl] Complexes as Highly Active Precatalysts for C–N and C–S Cross-Coupling Reactions. *Adv. Synth. Catal*. **2010**, *352*, 1949–1954.
(19) (a) Ge, S.; Green, R. A.; Hartwig, J. F. Controlling First-Row Catalysts: Amination of Aryl and Heteroaryl Chlorides and Bromides with Primary Aliphatic Amines Catalyzed by a BINAP-Ligated Single-Component Ni(0) Complex. *J. Am. Chem. Soc.* **2014**, *136*, 1617–1627. (b) Lavoie, C. M.; MacQueen, P. M.; Rotta-Loria, N. L.; Sawatzky, R. S.; Borzenko, A.; Chisholm, A. J.; Hargreaves, B. K. V.; McDonald, R.; Ferguson, M. J.; Stradiotto, M. Challenging Nickel-Catalysed Amine Arylations Enabled by Tailored Ancillary Ligand Design. *Nature Commun*. **2016**, *7*, 1–11.
(20) (a) Koo, K.; Hillhouse, G. L. Carbon-Nitrogen Bond Formation by Reductive Elimination From Nickel(II) Amido Alkyl Complexes. *Organometallics* **1995**, *14,* 4421–4423. (b) Koo, K.; Hillhouse, G. L. Indoline Synthesis via Coupling of Phenethyl Grignard Reagents with Organoazides Mediated by (Alkylphosphine)Nickel(II) Complexes. *Organometallics* **1996**, *15,* 2669–2671. (c) Mindiola, D. J.; Hillhouse, G. L. Terminal Amido and Imido Complexes of Three-Coordinate Nickel. *J. Am. Chem. Soc*. **2001**, *123*, 4623–4624. (d) Lin, B. L.; Clough, C. R.; Hillhouse, G. L. Interactions of Aziridines with Nickel Complexes: Oxidative-Addition and Reductive-Elimination Reactions That Break and Make C−N Bonds. *J. Am. Chem. Soc.* **2002**, *124*, 2890–2891.
(21) Ilies, L.; Matsubara, T.; Nakamura, E. Nickel-Catalyzed Synthesis of Diarylamines via Oxidatively Induced C–N Bond Formation at Room Temperature. *Org. Lett*. **2012**, *14*, 5570–5573.
(22) Corcoran, E. B.; Pirnot, M. T.; Lin, S.; Dreher, S. D.; DiRocco, D. A.; Davies, I. W.; Buchwald, S. L.; MacMillan, D. W. C. Aryl Amination Using Ligand-Free Ni(II) Salts and Photoredox Catalysis. *Science* **2016**, *353*, 279–283.
(23) Vander Griend, D. A.; Bediako, D. K.; DeVries, M. J.; DeJong, N. A.; Heeringa, L. P. Detailed Spectroscopic, Thermodynamic, and Kinetic Characterization of Nickel(II) Complexes with 2,2'-Bipyridine and 1,10-Phenanthroline Attained via Equilibrium-Restricted Factor Analysis. *Inorg. Chem*. **2008**, *47*, 656–662.
(24) Lappin, A. G.; McAuley, A. The Redox Chemistry of Nickel; Advances in Inorganic Chemistry; Elsevier, 1988; Vol. 32, pp 241–295.
(25) Lim, C.-H.; Kudisch, M.; Bin Liu; Miyake, G. M. C–N Cross-Coupling via Photoexcitation of Nickel–Amine Complexes. *J. Am. Chem. Soc*. **2018**, *140*, 7667–7673.
(26) DMA seems to be oxidized under the reaction conditions as evident from the formation of aminal product **52b**. However, this oxidation is likely to prevent undesirable consumption of amine nucleophile.
(27) Dhar, S. K.; Basolo, F. Thermal Decomposition of the Tris (2,2'-Bipyridine) Complexes of Some First Row Transition Group Elements in the Solid State. *J. Inorg. Nucl. Chem.* **1963**, *25*, 37–44.
(28) (a) Froese, R. D. J.; Lombardi, C.; Pompeo, M.; Rucker, R. P.; Organ, M. G. Designing Pd–*N*-Heterocyclic Carbene Complexes for High Reactivity and Selectivity for Cross-Coupling Applications. *Acc. Chem. Res*. **2017**, *50*, 2244–2253. (b) King, S. M.; Buchwald, S. L. Development of a Method for the *N*-Arylation of Amino Acid Esters with Aryl Triflates. *Org. Lett*. **2016**, *18*, 4128–4131. (c) Sharif, S.; Mitchell, D.; Rodriguez, M. J.; Farmer, J. L.; Organ, M. G. *N*-Heteroarylation of Optically Pure α-Amino Esters Using the *Pd-PEPPSI-IPent^{Cl}-o-picoline* Precatalyst. *Chem. Eur. J*. **2016**, *22*, 14860–14863. (d) Hammoud, H.; Schmitt, M.; Blaise, E.; Bihel, F.; Bourguignon, J.-J. *N*-Heteroarylation of Chiral α-Aminoesters by Means of Palladium-Catalyzed Buchwald–Hartwig Reaction. *J. Org. Chem*. **2013**, *78*, 7930–7937. (e) Surasani, R.; Kalita, D.; Rao, A. V. D.; Chandrasekhar, K. B. Palladium-Catalyzed C–N and C–O Bond Formation of *N*-Substituted 4-Bromo-7-Azaindoles with Amides, Amines, Amino Acid Esters and Phenols. *Beilstein J. Org. Chem.* **2012**, *8*, 2004–2018. (f) Becica, J.; Dobereiner, G. E. Acceleration of Pd-Catalyzed Amide *N*-Arylations Using Cocatalytic Metal Triflates: Substrate Scope and Mechanistic Study. *ACS Catal*. **2017**, *7*, 5862–5870.
(29) (a) Sharma, K. K.; Sharma, S.; Kudwal, A.; Jain, R. Room Temperature *N*-Arylation of Amino Acids and Peptides Using Copper(I) and α-Diketone. *Org. Biomol. Chem*. **2015**, *13*, 4637–4641. (b) Ma, D.; Xia, C. CuI-Catalyzed Coupling Reaction of *β*-Amino Acids or Esters with Aryl Halides at Temperature Lower Than That Employed in the Normal Ullmann Reaction. Facile Synthesis of SB-214857. *Org. Lett*. **2001**, *3*, 2583–2586.
(30) Nakamura, H.; Yasui, K.; Kanda, Y.; Baran, P. S. 11-Step Total Synthesis of Teleocidins B-1−B-4. *J. Am. Chem. Soc*. Articles ASAP.

(31) (a) Noji, T.; Okano, K.; Tokuyama, H. A Concise Total Synthesis of (-)-Indolactam V. *Tetrahedron* **2015**, *71*, 3833–3837. (b) Haynes-Smith, J.; Diaz, I.; Billingsley, K. L. Modular Total Synthesis of Protein Kinase C Activator (-)-Indolactam V. *Org. Lett*. **2016**, *18*, 2008–2011.
(32) Mari, M.; Bartoccini, F.; Piersanti, G. Synthesis of (-)-Epi-Indolactam V by an Intramolecular Buchwald-Hartwig C–N Coupling Cyclization Reaction. *J. Org. Chem*. **2013**, *78*, 7727–7734.
(33) Welsch, M. E.; Snyder, S. A.; Stockwell, B. R. Privileged Scaffolds for Library Design and Drug Discovery. *Curr. Opin. Chem. Biol*. **2010**, *14*, 347–361.
(34) For recent reviews on C–S bond functionalization by nickel catalysis, see: (a) Otsuka, S.; Nogi, K.; Yorimitsu, H. C–S Bond Activation. *Top. Curr. Chem*. **2018**, *376*, 1–39. (b) Rentner, J.; Kljajic, M.; Offner, L.; Breinbauer, R. Recent Advances and Applications of Reductive Desulfurization in Organic Synthesis. *Tetrahedron* **2014**, *70*, 8983–9027. (c) Wang, L.; He, W.; Yu, Z. Transition-Metal Mediated Carbon–Sulfur Bond Activation and Transformations. *Chem. Soc. Rev*. **2013**, *42*, 599–621. (d) Pan, F.; Shi, Z.-J. Recent Advances in Transition-Metal-Catalyzed C–S Activation: From Thioester to (Hetero)Aryl Thioether. *ACS Catal*. **2013**, *4*, 280–288.
(35) (a) Feldman, A. W.; Romesberg, F. E. Expansion of the Genetic Alphabet: a Chemist's Approach to Synthetic Biology. *Acc. Chem. Res*. **2018**, *51*, 394–403. (b) Joubert, N.; Urban, M.; Pohl, R.; Hocek, M. Modular Synthesis of 4-Aryl- and 4-Amino-Substituted Benzene *C*-2'-Deoxyribonucleosides. *Synthesis* **2008**, 1918–1932. (c) Wang, L.; Schultz, P. G. Expanding the Genetic Code. *Chem. Commun*. **2001**, 1–11.
(36) (a) Pentelute, B.; Zhang, C.; Vinogradova, E.; Spokoyny, A.; Buchwald, S. Arylation Chemistry for Bioconjugation. *Angew. Chem. Int. Ed*. **2018**, accepted article. (b) deGruyter, J. N.; Malins, L. R.; Baran, P. S. Residue-Specific Peptide Modification: a Chemist's Guide. *Biochemistry* **2017**, *56*, 3863–3873.
(37) Hu, B.; Song, Q.; Xu, Y. Scale-Up Synthesis of Antidepressant Drug Vilazodone. *Org. Process Res. Dev*. **2012**, *16*, 1552–1557.
(38) Renuka, J.; Reddy, K. I.; Srihari, K.; Jeankumar, V. U.; Shravan, M.; Sridevi, J. P.; Yogeeswari, P.; Babu, K. S.; Sriram, D. Design, Synthesis, Biological Evaluation of Substituted Benzofurans as DNA gyraseB Inhibitors of *Mycobacterium Tuberculosis*. *Bioorg. Med. Chem*. **2014**, *22*, 4924–4934.
(39) Shao, Q.-L.; Jiang, Z.-J.; Su, W.-K. Solvent-Free Mechanochemical Buchwald-Hartwig Amination of Aryl Chlorides Without Inert Gas Protection. *Tetrahedron Lett*. **2018**, *59*, 2277–2280.

Insert Table of Contents artwork here

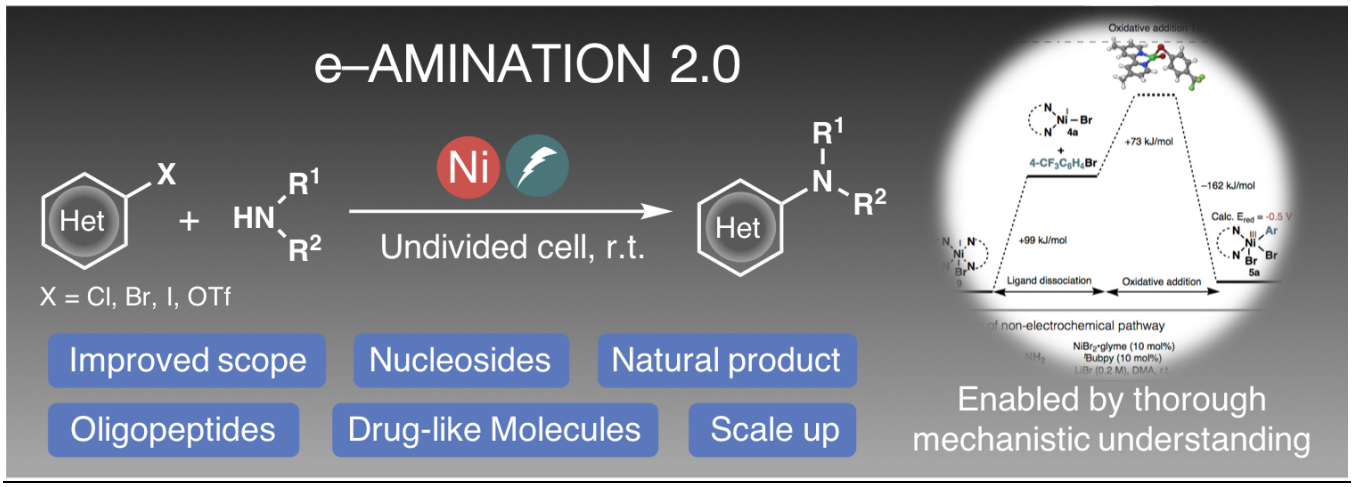

e-Amination 2.0 - Manuscript.pdf (9.67 MiB) view on ChemRxiv • download file

Supplementary Materials for

Electrochemically Driven, Ni-Catalyzed Aryl Amination: Scope, Mechanism, and Applications

Yu Kawamata,[1,7] Julien C. Vantourout,[1] David P. Hickey,[2,7] Peng Bai,[3,7] Longrui Chen,[4] Qinglong Hou,[4] Wenhua Qiao,[4] Koushik Barman,[2,7] Martin A. Edwards,[2,7] Alberto F. Garrido-Castro,[1] Justine N. deGruyter,[1] Hugh Nakamura,[1] Kyle Knouse,[1] Chuanguang Qin,[1] Khalyd J. Clay,[1] Denghui Bao,[4] Chao Li,[1] Jeremy T. Starr,[5] Carmen Garcia-Irizarry,[5] Neal Sach,[6] Henry S. White,[2,7] Matthew Neurock,*[3,7] Shelley D. Minteer,*[2,7] Phil S. Baran*[1,7]

[1] Department of Chemistry, The Scripps Research Institute, 10550 North Torrey Pines Road, La Jolla, California 92037, United State

[2]Department of Chemistry, University of Utah, 315 South 1400 East, Salt Lake City, Utah 84112, United States

[3]Department of Chemical Engineering and Materials Science, University of Minnesota, Minneapolis, MN 55455, United States

[4]Asymchem Life Science (Tianjin), Tianjin Economic-Technological Development Zone, Tianjin 300457, China

[5]Discovery Sciences, Medicine Design, Pfizer Global Research and Development, 445 Eastern Point Road, Groton, Connecticut 06340, United States

[6]Department of Chemistry, La Jolla Laboratories, Pfizer, 10770 Science Center Drive, San Diego, CA 92121, USA.

[7]NSF Center for Synthetic Organic Electrochemistry

Correspondence to:
Matthew Neurock: mneurock@umn.edu
Shelley D. Minteer: minteer@chem.utah.edu
Phil S. Baran: pbaran@scripps.edu

Table of Contents

General Methods

Instruments

Reagents were purchased at the highest commercial quality grade and used without further purification, unless otherwise stated. Yields refer to chromatographically and spectroscopically (^{1}H NMR) homogeneous material, unless otherwise stated. Reactions were monitored by thin layer chromatography (TLC) carried out on 0.25 mm E. Merck silica plates (60F-254), using shortwave UV light and $KMnO_4$ for visualization. Flash column chromatography was performed using E. Merck silica gel (60, particle size 0.043 – 0.063 mm). NMR spectra were recorded on Bruker AVIII-600 instruments and Bruker AV400 for ^{19}F were calibrated using residual undeuterated solvent as an internal reference ($CDCl_3$: 7.26 ppm ^{1}H NMR, 77.16 ppm ^{13}C NMR. The following abbreviations were used to explain NMR peak multiplicities: s = singlet, d = doublet, t = triplet, q = quartet, p = pentet, m = multiplet, br = broad. High–resolution mass spectra (HRMS) were recorded on an Agilent LCMS TOF mass spectrometer using electrospray ionization time-of-flight (ESI-TOF) reflectron experiments. The enantiomeric excesses were determined with Waters UPC^2 SFC equipped with a photodiode array detector or an Agilent Technologies 1220 Infinity II LC HPLC. Optical rotations were recorded on a Rudolph Research Analytical Autopol III Automatic Polarimeter.

Electrode materials and dimensions

The RVC electrodes were purchased from commercial RVC block (purchased from ULTRAMET, 80 ppi, 14.40” x 13.86” x 8”) and Ni foam electrodes were furnished from Nickel Foam (1.5 mm x 100 mm x 250 mm for Battery, Electric Capacity etc. purchased from eBay).

For experiments using 5 mL IKA ElectraSyn vial, the dimensions of the RVC anode were 47 mm x 8 mm x 2 mm; the dimensions of Ni foam cathode were 0.8 cm × 4.7 × 0.1 cm (the submerged exterior surface areas of the anode and cathode were approximately 0.8 cm × 1.5 cm on 0.1 mmol scale). For experiments on larger scales, dimensions of electrodes have been specified in the relevant experimental section.

$Ni(bpy)_3Br_2$ catalyst

Preparation

To a 1 L round bottom flask was added a saturated solution of 2,2'-bipyridine (450 mmol) in MeOH (100 mL) followed by the addition of a solution of $NiBr_2 \bullet 3H_2O$ (150 mmol) in MeOH (100 mL). The mixture immediately turned red and a pink precipitate was formed (*note: the reaction is exothermic*). After cooling to ambient temperature, acetone (150 mL) was added to induce more precipitation and the pink solid was filtered. This solid was used as catalyst without further purification (88 g, 87% yield). Aldrich catalog number ALD00608.

X-ray crystallographic data of compound 17

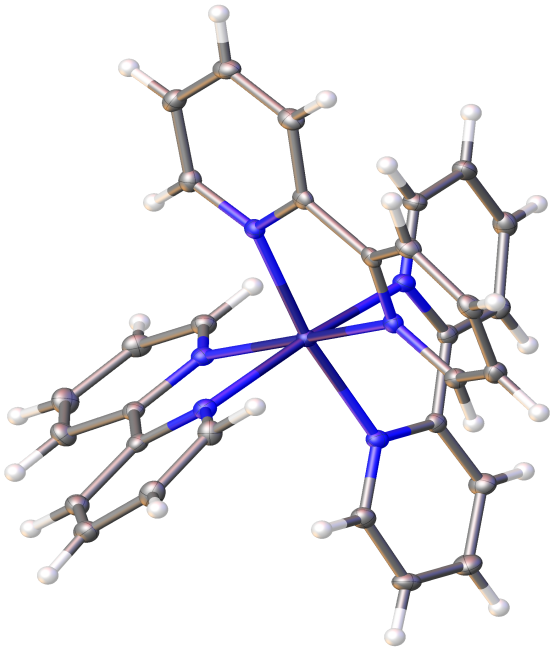

The structure of $[Ni(bpy)_3]Br_2$ and $[Ni(bpy)_3](ClO_4)_2$ were determined by single crystal X-ray diffraction. It was confirmed that nickel ion is ligated by three bpy ligands in both structures. However, due to the disorder of bromide counter aninon, structural refinement was not completely successful. Accordingly, the graphic and cif file of $[Ni(bpy)_3](ClO_4)_2$ were provided for the publication.

Empirical formula	C30 H24 Cl2 N6 Ni O8	
Molecular formula	C30 H24 N6 Ni, 2(Cl O4)	
Formula weight	726.16	
Temperature	100.0 K	
Wavelength	0.71073 Å	
Crystal system	Monoclinic	
Space group	C 1 2/c 1	
Unit cell dimensions	a = 17.0095(9) Å	α= 90°.
	b = 10.7266(6) Å	β= 91.4250(10)°.
	c = 15.9498(9) Å	γ = 90°.
Volume	2909.2(3) $Å^3$	
Z	4	
Density (calculated)	1.658 Mg/m^3	
Absorption coefficient	0.916 mm^{-1}	
F(000)	1488	
Crystal size	0.125 x 0.1 x 0.09 mm^3	
Crystal color, habit	pink block	
Theta range for data collection	2.245 to 27.102°.	
Index ranges	-16<=h<=21, -13<=k<=13, -20<=l<=20	
Reflections collected	10973	
Independent reflections	3212 [R(int) = 0.0371]	
Completeness to theta = 25.242°	100.0 %	
Absorption correction	Semi-empirical from equivalents	

Max. and min. transmission	0.6468 and 0.5945
Refinement method	Full-matrix least-squares on F^2
Data / restraints / parameters	3212 / 0 / 213
Goodness-of-fit on F^2	1.052
Final R indices [I>2sigma(I)]	R1 = 0.0283, wR2 = 0.0711
R indices (all data)	R1 = 0.0322, wR2 = 0.0737
Largest diff. peak and hole	0.381 and -0.437 e.$Å^{-3}$

Table 2. Atomic coordinates (x 10^4) and equivalent isotropic displacement parameters ($Å^2$x 10^3)

	x	y	z	U(eq)
Ni(1)	5000	5319(1)	2500	9(1)
N(1)	4396(1)	3905(1)	1859(1)	11(1)
N(2)	3993(1)	5138(1)	3216(1)	11(1)
N(3)	5438(1)	6800(1)	3192(1)	11(1)
C(1)	4617(1)	3347(2)	1148(1)	13(1)
C(2)	4223(1)	2336(2)	802(1)	15(1)
C(3)	3569(1)	1885(2)	1206(1)	17(1)
C(4)	3335(1)	2445(2)	1941(1)	15(1)
C(5)	3764(1)	3456(2)	2254(1)	11(1)
C(6)	3559(1)	4115(2)	3036(1)	11(1)
C(7)	2970(1)	3704(2)	3560(1)	14(1)
C(8)	2822(1)	4379(2)	4281(1)	15(1)
C(9)	3238(1)	5467(2)	4445(1)	16(1)
C(10)	3818(1)	5813(2)	3897(1)	14(1)
C(11)	5816(1)	6715(2)	3942(1)	13(1)
C(12)	5937(1)	7735(2)	4458(1)	14(1)
C(13)	5665(1)	8890(2)	4191(1)	15(1)
C(14)	5300(1)	8999(2)	3405(1)	14(1)
C(15)	5199(1)	7931(2)	2920(1)	11(1)
Cl(1)	6763(1)	9937(1)	1374(1)	14(1)

O(1)	6649(1)	9248(1)	2130(1)	26(1)
O(2)	6177(1)	10907(1)	1292(1)	27(1)
O(3)	7536(1)	10499(1)	1393(1)	24(1)
O(4)	6691(1)	9114(1)	660(1)	29(1)

Substrate Synthesis and Characterization

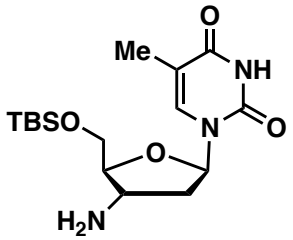

3-amino-thymidine derivative was prepared following a known procedure.[1]

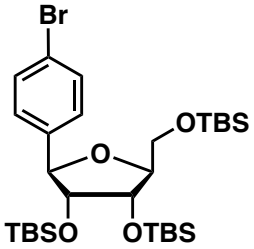

1-(4-bromophenyl)-ribose derivative was prepared following a known procedure.[2]

General and Graphical Procedure

General procedure for small scale (0.05-0.2 mmol) reactions

An ElectraSyn vial (5 mL) with a stir bar was charged with $Ni(bpy)_3Br_2$ (10 mol%), TBAB (0.4 mmol, 0.2 M), aryl halide, amine, DBU and DMA (2.0 mL). [Liquid compounds were added after the addition of DMA. The order of the addition does not affect the result. The amount of aryl halide, amine and DBU in individual case are indicated in the characterization section] The ElectraSyn vial cap equipped with anode (RVC) and cathode (Ni foam) were inserted into the mixture (See below for the graphical guide. If electrode area submerged into the solution is less than 1.0 cm, add more solvent.). The vial was then evacuated and backfilled with an argon balloon. This cycle was repeated twice. The reaction mixture was electrolyzed under a constant current of 4 mA until complete consumption of the starting material as judged by TLC. After the reaction, the ElectraSyn vial cap was removed and electrodes were rinsed with a mixture of organic solvents (EtOAc:hexanes = 1:1), which was combined with the crude mixture. Aqueous sat. NH_4Cl was then added to the combined solutions; the resulting solution was extracted with a mixture of organic solvents (EtOAc:hexanes = 1:1). The combined organic layers were dried over anhydrous Na_2SO_4 and concentrated *in vacuo*. The crude material was purified by column chromatography or preparative thin-layer chromatography (PTLC) to furnish the desired product.

Graphical guide

Photos were taken from the coupling between 4-bromobenzotrifluoride and glutamic acid di-tert-butyl ester.


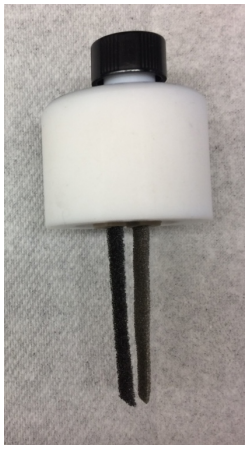

(Left) ElectraSyn 2.0. ***(Middle)*** ElectraSyn 2.0 vial (5 mL). ***(Right)*** ElectraSyn 2.0 cap equipped with RVC (left side) and Nickel electrodes (right side).

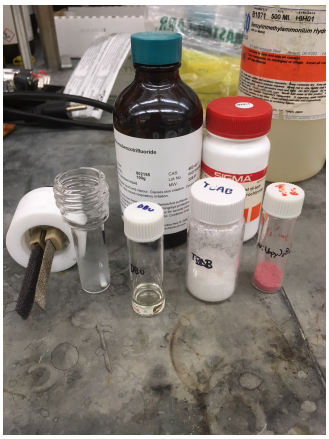

(Left) Materials used in the reaction. ***(Middle)*** Wrapping Teflon tape helps to keep a good sealing during a reaction. ***(Right)*** The appearance of the mixture after the addition of all solid components.

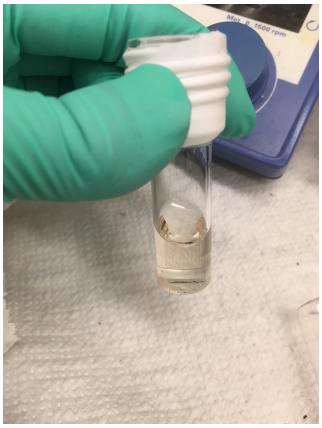
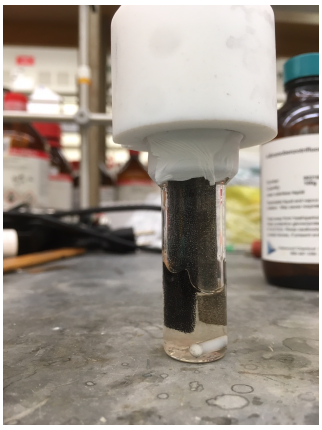
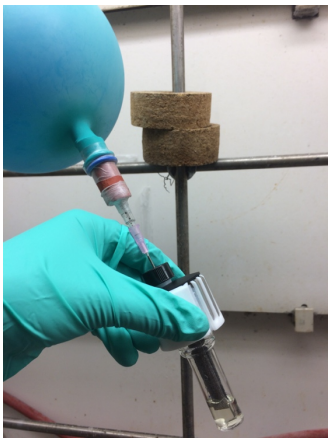

(Left) After the addition of DMA. ***(Middle)*** The cap was tightly screwed into the vial. Ensure > 1cm of the electrodes are submerged into the solution**.** If not, please add more solvent. ***(Right)*** The reaction vessel was connected to a vacuum line through a needle. The reaction vessel was backfilled with an argon balloon [***Right*** was repeated for three cycles].


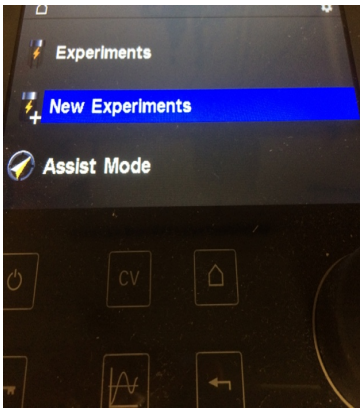

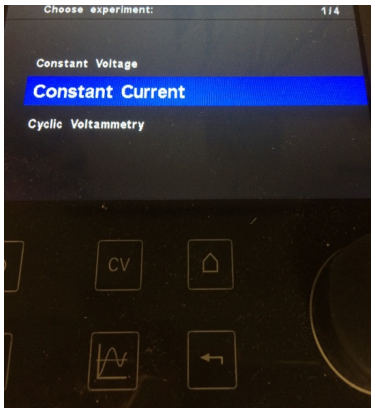

(Left) The electrochemical cell was plugged into ElectraSyn 2.0. ***(Middle)*** Select New experiments. ***(Right)*** Select Constant Current.

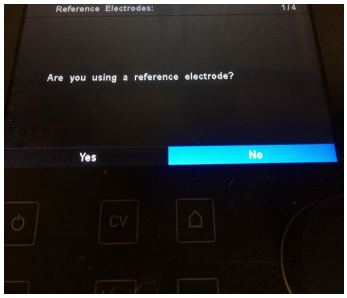

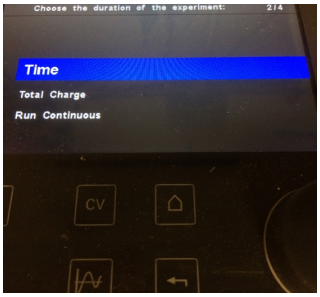

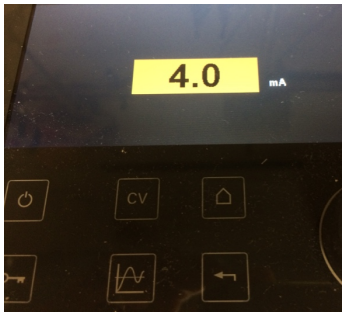

(Left) No use of reference electrode. ***(Middle)*** Select Time. ***(Right)*** Adjust the current value.

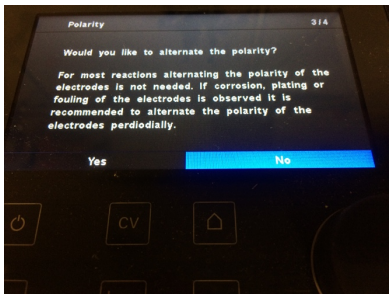

(Left) Define the “time”. ***(Middle)*** Indicate the “mmol” of the substrate. ***(Right)*** No alternate polarity.

Peptide Synthesis, general amination procedure and purification

Methods for peptide synthesis

HPLC analysis were conducted on a Waters Autopurification LC with a Waters XBridge C18 column (4.6x150 mm, 3.5 ⌈m). Fractionation was triggered by a Waters QDa single quadruple mass spec in ESI^+ single ion or ESI^- single ions recoding modes. UV detection was monitored at 261 nm.

Solvent A: 0.1 M aqueous triethylammonium acetate Solvent B: acetonitrile
1.5 mL/min, 25 °C.
Gradient: 5–90% B over 11 minutes

Preparative HPLC were conducted on the same instrument as above and were based on the HPLC analysis using the methods describe below:

RT: Method: %B:
0-2 min Narrow 5-20 %B
2-4 min Narrow 1 10-25 %B
4-5 min Narrow 2 15-35 %B
5-6 min Narrow 3 25-45 %B
6-7 min Narrow 4 35-55 %B
7-8 min Narrow 5 45-65 %B
8-9 min Narrow 6 55-75 %B
9-11 min Narrow 7 65-95 %B

Materials

Commercial materials were used as received unless otherwise noted. Amino acids and coupling reagents were obtained from Novabiochem or Combi-blocks. 2-CTC resin was purchased from Chem Impex (1.0 – 2.0 mmol/g). Solid-phase reaction vessels and pressure caps were purchased from Torviq.

Solid phase peptide synthesis

General procedure. 2-CTC resin

2-CTC resin (1.0 equiv., substitution = 1.0 – 2.0 mmol/g) was swollen in dry DCM for 30 min then washed with DCM (5 x 3 mL) and DMF (5 x 3 mL). A solution of the Fmoc-AA-OH (2.0 equiv.) and *N*,*N*-diisopropylethylamine (DIPEA, 4.0 equiv.) in DMF (final concentration 0.1 M) was added to the resin (1.0 equiv.) and agitated at room temperature. After 16 h, the resin was washed with DMF (5 x 3 mL), DCM (5 x 3 mL), and DMF (5 x 3 mL). A capping step was performed as described below and the resin-bound residue was submitted to iterative peptide assembly (Fmoc-SPPS).

The loading efficiency was evaluated through treatment of the resin with 20% piperidine/DMF (3 mL, 2 × 3 min) to deprotect the Fmoc group. The combined deprotection solutions were diluted to 10 mL with 20% piperidine/DMF. An aliquot of this mixture (50 μL) was diluted 200-fold with 20% piperidine/DMF and the UV absorbance of the piperidine-fulvene adduct was measured (λ = 301 nm, ε = 7800 M^{-1} cm^{-1}) to quantify the amount of amino acid loaded onto the resin. The theoretical maximum for the reported yields of all isolated peptides are based on the numerical value obtained from the resin loading.

General iterative peptide assembly (Fmoc-SPPS)

Peptides were elongated using iterative Fmoc-solid-phase peptide synthesis (Fmoc-SPPS), according to the following general protocols:

Deprotection: The resin was treated with 20% piperidine/DMF (3 mL, 2 x 3 min) and washed with DMF (5 x 3 mL), DCM (5 x 3 mL) and DMF (5 x 3 mL).

General amino acid coupling: A preactivated solution of protected amino acid (4 equiv.), PyBOP (4 equiv.), and *N*-methylmorpholine (NMM) (8 equiv.) in DMF (final concentration 0.1 M) was added to the resin. After 1 h, the resin was washed with DMF (5 x 3 mL), DCM (5 x 3 mL) and DMF (5 x 3 mL).

Capping: Acetic anhydride/pyridine (1:9 v/v) was added to the resin (3 mL). After 3 min the resin was washed with DMF (5 x 3 mL), DCM (5 x 3 mL) and DMF (5 x 3 mL).

Cleavage: A mixture of DCM and HFIP (95:5 v/v) was added to the resin. After 2 h, the resin was washed with DCM (3 x 2 mL).

Work-up: The combined cleavage solution and DCM washes were concentrated under a stream of nitrogen. The residue was treated with cold Et2O to precipitate the crude peptide, which was subsequently dissolved

in water/acetonitrile containing 0.1% TFA, filtered and used crude in the next esterification or amidation steps except otherwise stated.

Esterification: The crude peptide was dissolved in MeOH (0.25 M) and was titrated with TMS diazomethane solution until yellow color remains. Solvent was removed under *vacuo* and the residue was treated with cold Et_2O to precipitate the crude peptide, which was subsequently dissolved in water/acetonitrile, filtered and purified by reverse-phase HPLC.

General procedure for the coupling of side chain protected peptides – 0.05 mmol scale.

An ElectraSyn vial (5 mL) with a stir bar was charged with $Ni(bpy)_3Br_2$ (0.3 or 1 equiv.), LiBr (4 equiv.), side chain protected *N*-acetylated methyl ester/acid or amide peptide (1 equiv.), amine (3 equiv.), and DMA (2.0 mL). [Liquid compounds were added after the addition of DMA. The order of the addition does not affect the result]. The ElectraSyn vial cap equipped with anode (RVC) and cathode (Ni foam) was inserted into the mixture. The vial was then evacuated and backfilled with an argon balloon. This cycle was repeated twice. The reaction mixture was electrolyzed under a constant current of 4 mA for 6 hours. After the reaction, the ElectraSyn vial cap was removed and electrodes were rinsed with the mixture of organic solvents (EtOAc:hexane = 2:1), which was combined with the crude mixture. Aqueous sat. NH_4Cl was then added to the combined solution; the resulting solution was extracted with the mixture of organic solvents (EtOAc:hexane = 2:1). The combined organic layer was dried over anhydrous Na_2SO_4 and concentrated *in vacuo*. The crude material was purified by preparative HPLC to furnish the desired product.

Mechanistic investigation (Figure 2)

Kinetic experiments

Method

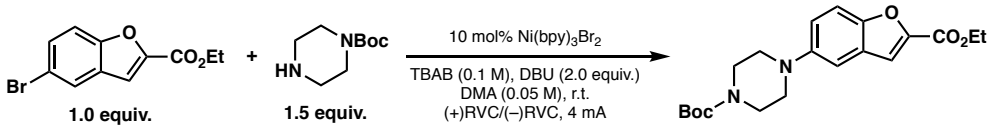

Kinetic experiments were carried out using LCMS analysis following the general e-amination procedure described above. Aliquots were taken at different times (please see graphics for more details) and the conversion was measured against an internal standard (4,4-di-*tert*-butylbiphenyl).

Results

The product formation was monitored by varying one of the parameters under the above conditions. The results showed that the rate of product formation was largely independent of the loading of amine, DBU and Ni catalyst, whereas current value (mA) had large effect on the rate of product formation. This indicates that, if all chemical steps are fast enough, the rate determining step is electron transfer between an electrode and an intermediate. However, the slower rate with 0.75 equiv. anime indicates that the rate determining step in this case is likely a chemical step, rather than electron transfer step. Under the conditions with 0.75 equiv. amine, the rate increase was observed with higher Ni loading.

Amine loading

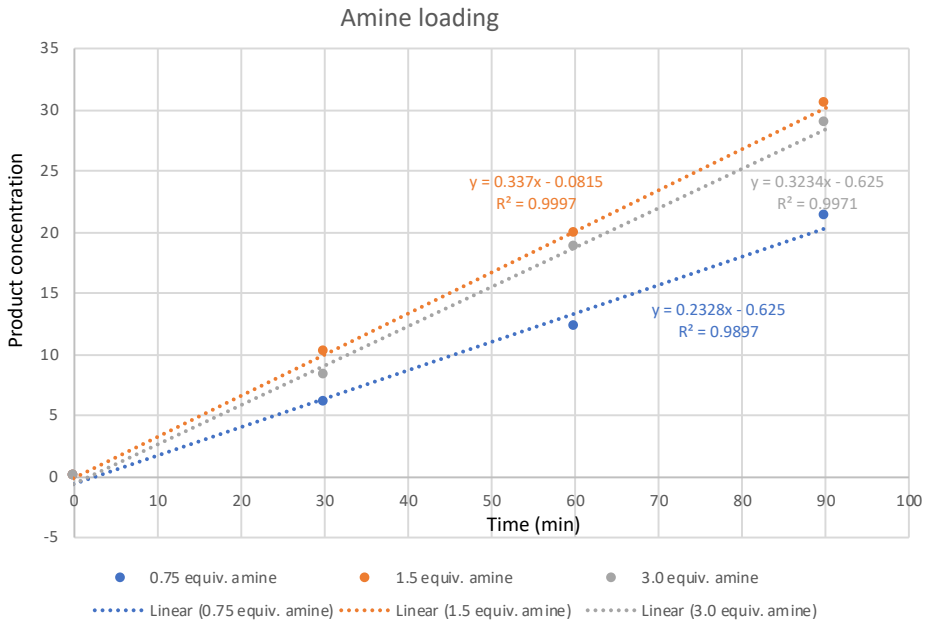

Base loading

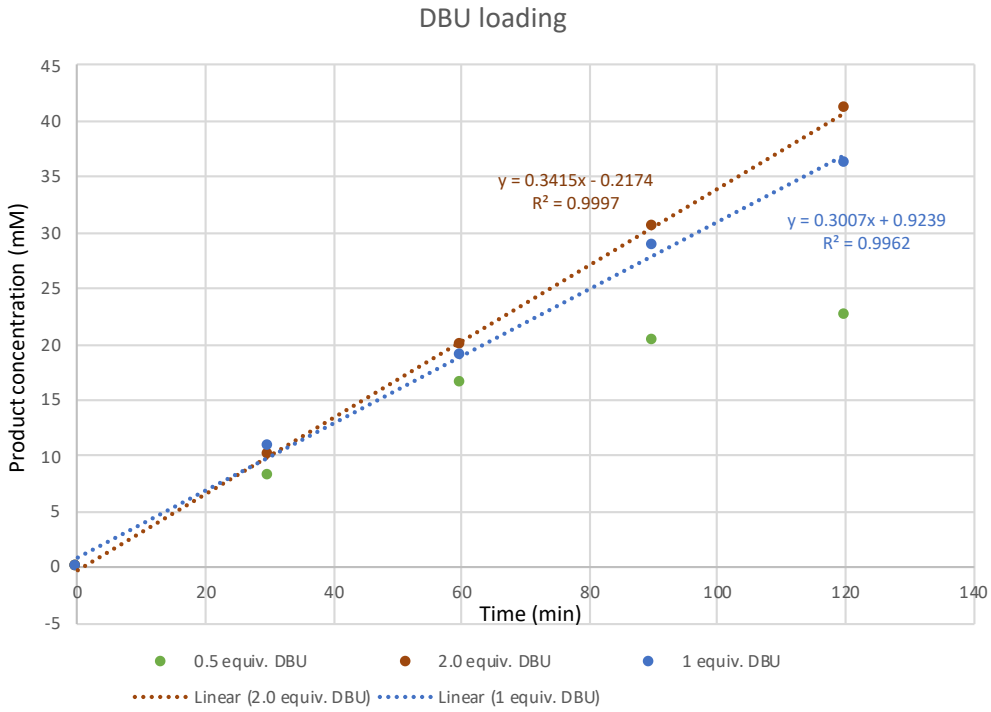

Nickel catalyst loading

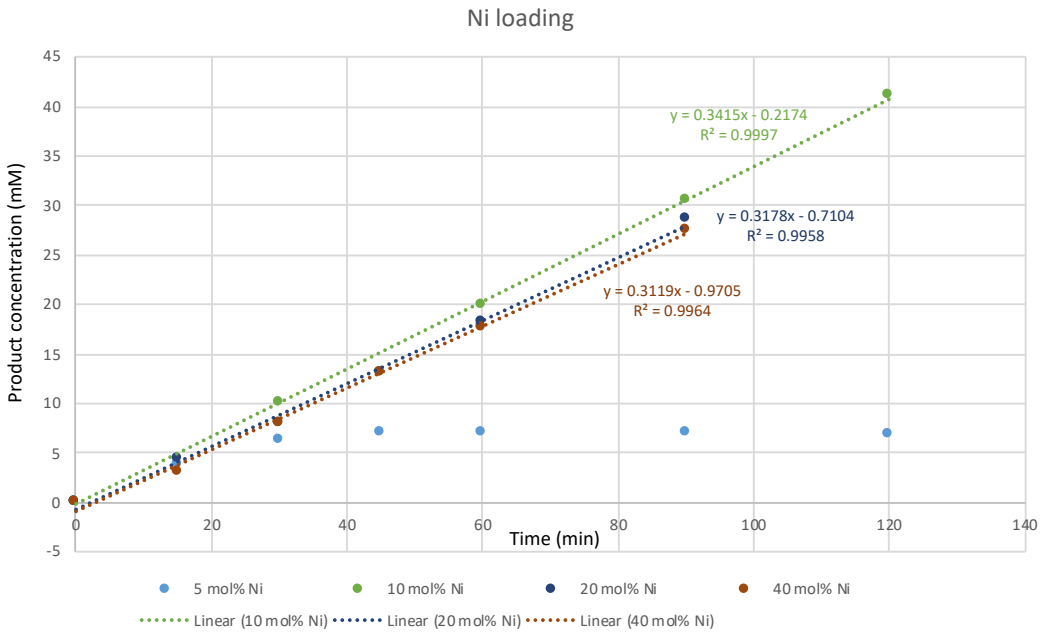

Effect of current

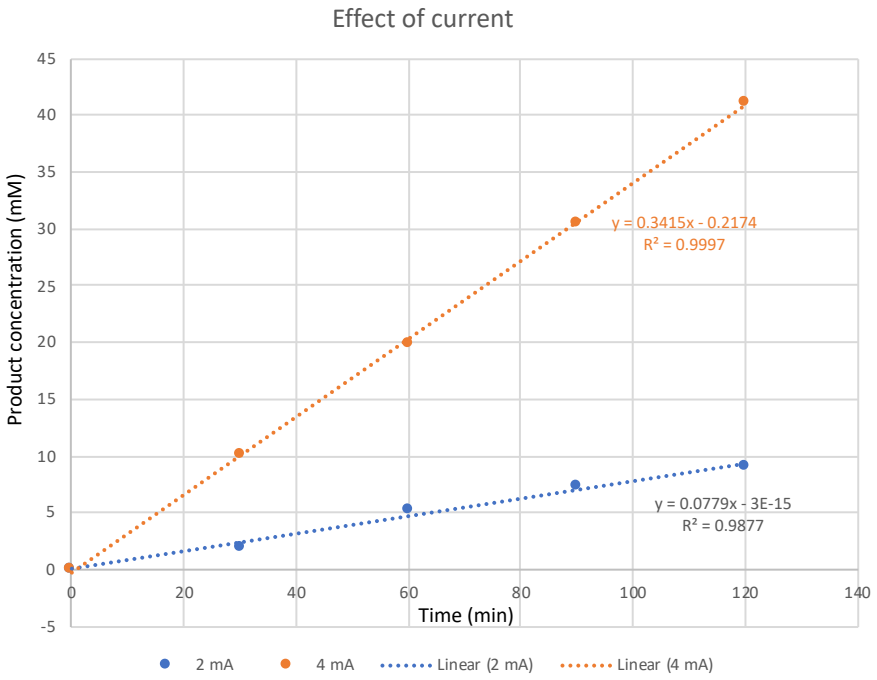

Effect of Nickel catalyst loading at low concentration of amine

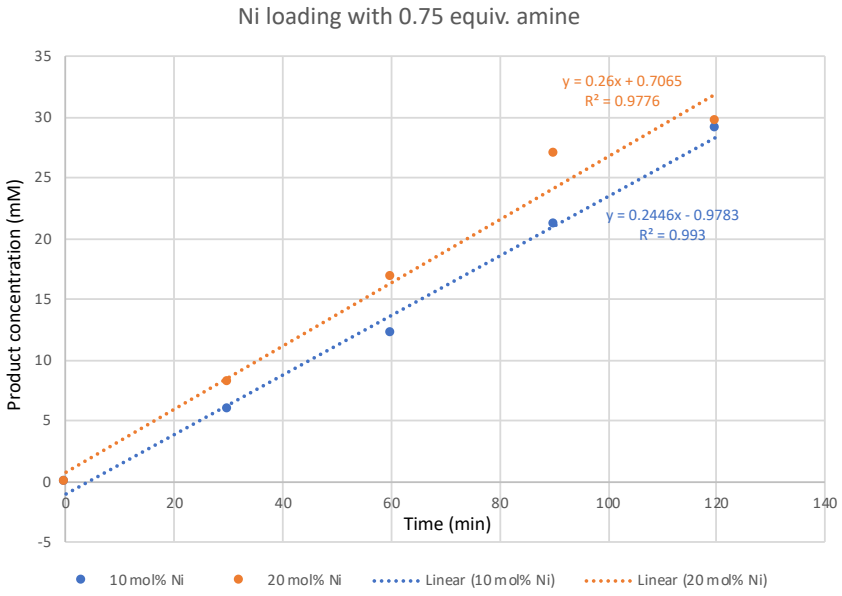

UV-Vis Analysis

Method

Spectrophotometric experiments were carried out using a Thermo Scientific Evolution 260Bio UV-Vis Spectrophotometer. Absorbance was monitored between 450 and 750 nm with a path length of 1 cm using a solution of 100 mM NBu_4Br in dry DMF as a background solution. Background-subtracted spectra were obtained for solutions of 1 mM $NiBr_2•3H_2O$ in the presence of 0, 0.25, 0.5, 0.75, 1, 1.5, 2, 2.5, 3, 3.5, and 4 mM 4,4'-dimethyl-2,2'-bipyridine.

Electrochemical Analysis

Method

Electrochemical experiments for mechanistic analysis were carried out using a Biologic SP-150 potentiostat using a 3-electrode cell with a 3 mm glassy carbon working electrode, a platinum mesh counter electrode, and a $Ag/AgNO_3$ (10 mM) reference electrode unless otherwise noted. Cyclic voltammetry and square wave voltammetry experiments were performed using1 mM $NiBr_2•3H_2O$ as a Ni(II) species and 4,4'-dimethyl-2,2'-bipyridine (Mebpy) as a ligand with 100 mM NBu_4Br in dry DMF as a supporting electrolyte/solvent system under an atmosphere of Ar with 3.2% H_2 and less than 3 ppm O_2. All glassware for electrochemical analysis were flame dried prior to use. Unless otherwise noted, SWVs were performed from positive to negative potential with an amplitude of 20 mV, frequency of 40 Hz, and a step potential of 5 mV. Throughout the manuscript, positive current corresponds to reduction while negative current corresponds to oxidation. Electrochemical oxidative addition experiments were performed using solutions containing 1 mM $NiBr_2•3H_2O$ with 1 mM Mebpy, where CVs were run at 100 mV s^{-1} in the absence of any electrophile, then again in the presence of 30 mM p-bromoanisole ($MeOC_6H_4Br$). Electrochemical experiments to determine the effect of amine on the oxidation window of Ni(II)($MeOC_6H_4$)(Mebpy)Br were carried out using 1 mM Ni complex in the absence and presence of 100 mM hexylamine at 100 mV s^{-1} and 20 mV s^{-1}. For experiments used to determine the diffusion coefficient and number of electrons transferred; prior to electrochemical measurements, the Pt microelectrode was cleaned by polishing in 50 nm alumina slurry and rinsed with acetone. Electrochemical data were recorded with a CH Instruments 760E bipotentiostat (1 kHz sampling frequency) in a two-electrode configuration, employing the 25 μm diameter Pt microdisk as the working electrode and a leakless Ag/AgCl electrode (eDAQ) as the reference/counter electrode. The entire electrochemical cell was inside a home-built Faraday cage.

Results

Voltammetric Analysis of $Ni(Mebpy)_nBr_2$ Complexes

Cyclic voltammetry (CV) and square wave voltammetry (SWV) were used to characterize the reversibility and ligation state of each Ni(II) complex. SWVs of $NiBr_2$ in the presence of various concentrations of Mebpy reveal a complex series of peaks that are generally clustered around -1 V, -1.7 V and -1.9 V. Comparing this with SWVs of $NiBr_2$ and Mebpy individually, suggests that the peaks around -1 V are

consistent with a Ni(II/I) redox couple, while the peak at -1.9 V matches closely the authentic peak for Mebpy reduction, leaving the peak at -1.7 V as likely to resulting from a second electrochemical reduction of the $Ni(Mebpy)_nBr_2$ complex. Upon application of -2.1 V to a solution of 1 mM $NiBr_2$, Ni(0) could be observed precipitating out of solution (coincides with increased reductive current at an onset potential of -1.95 V, below).

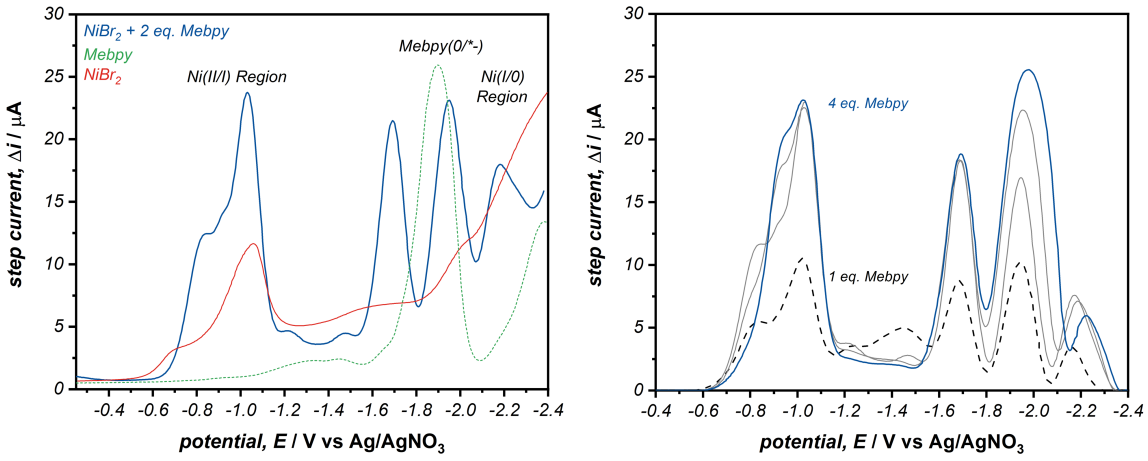

Representative SWVs of ***(left)*** 1mM $NiBr_2 \cdot 3H_2O$ (–), 1 mM Mebpy (---), and $NiBr_2$/Mebpy 1:2 (–); or ***(right)*** 1 mM $NiBr_2 \cdot 3H_2O$ in the presence of 1, 2, 3, or 4 equivalents of Mebpy.

The peak step current (i_p) for a SWV corresponds to the concentration of a species in solution (directly comparable assuming equivalent diffusion coefficients and number of electrons transferred). Therefore, i_p was measured as a function of Mebpy concentration to generate a profile of ligation states for $Ni(Mebpy)_nBr_2$. The resulting profiles were then correlated to spectrophotometric data (primary text) to assign the reduction potentials of $Ni(Mebpy)Br_2$, $Ni(Mebpy)_2Br_2$, and $Ni(Mebpy)_3Br_2$ as -0.82 ± 0.02 V, -0.94 ± 0.02 V, and -1.03 ± 0.01 V respectively.

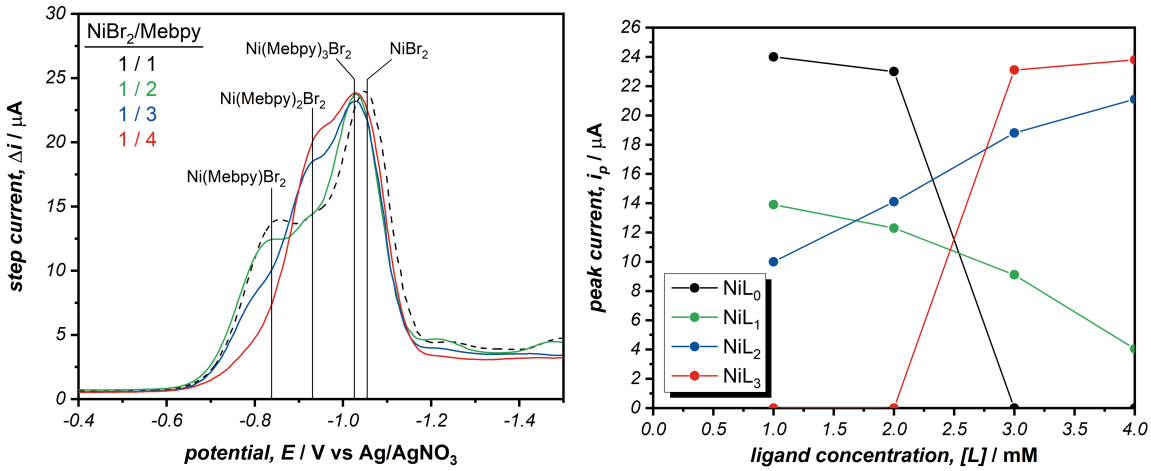

(*Left*) Representative SWVs 1 mM $NiBr_2 \bullet 3H_2O$ in the presence of 1 (---), 2 (–), 3 (–), or 4 (–) equivalents of Mebpy, and **(*right*)** profiles of the peak step current (i_p) for the four observed redox features corresponding to various ligation states of $Ni(Mebpy)_nBr_2$.

Cyclic voltammetry of $NiBr_2$ in the presence of either one, two or three equivalents of Mebpy (below) reveal the variably reversible nature of each ligation state. The loss of reversibility for Ni(II) species with one equivalent of Mebpy is largely attributed to the formation of insoluble Ni(0) species at the edge of the CV window. While isolation of peaks is complicated slightly by their overlapping nature, peak currents for all observed peaks are linear with square root of the corresponding scan rate. This suggests that adsorbed species are not playing a significant role in the catalytic cycle. Increased concentration of Mebpy alters the shape and number of reductive peaks without dramatically altering the profile of corresponding oxidative peaks. The primary oxidative features include a pair of peaks at -0.65 V and -0.85 V that most closely correspond to the reductive peaks of $Ni(Mebpy)Br_2$ and $Ni(Mebpy)_3Br_2$ (potentials determined by SWV and correlated by peak separation, where E_{ipc}-E_{ipa} approaches 81 mV for the peaks assigned to $Ni(Mebpy)Br_2$ and 64 mV for the peaks assigned to $Ni(Mebpy)_3Br_2$). The precise determination of ligation states is experimentally challenging; however, electrochemical analysis suggests that ligation state is dynamic and dependent on the oxidation state of Ni.

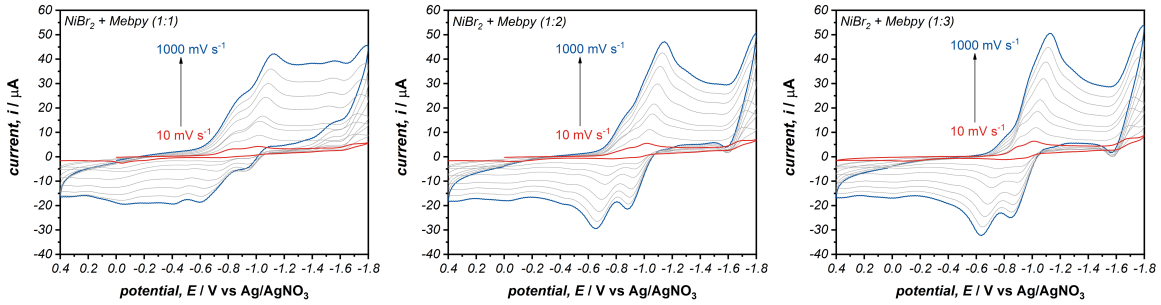

Representative CVs at variable scan rates of 1 mM $NiBr_2 \bullet 3H_2O$ in the presence of either 1 mM **(*left*)**, 2 mM **(*center*)** or 3 mM **(*right*)** Mebypy. CVs were performed at scan rates of 10, 50, 100, 200, 400, 600, 800, and 1000 mV s^{-1}.

Previous studies have employed microelectrode analysis to suggest that the initial electrochemical reduction of bpy-ligated Ni(II) species is a two-electron transfer resulting in Ni(0).[3] Similar analysis of $Ni(Mebpy)_nBr_2$ under synthetically relevant conditions using a two-step process. First, the diffusion coefficient was calculated from a temporal decay of the current at a microelectrode upon the application of a potential step. Next, the number of electrons transferred was calculated from the steady-state diffusion-limited current at the electrode, through rearrangement of the analytical expression for this current, which includes the diffusion coefficient, determined in the first step.

Determination of Diffusion coefficient (D)

The diffusion coefficient of the Ni(Mebpy)$_n$Br$_2$ complex in DMF (D) was calculated from the current response of a microelectrode to a potential step, as described previously.[4] Briefly, a 25 µm diameter Pt microdisk electrode (CH Instruments) was initially held at a potential of -0.4 V vs Ag/AgCl in a DMF solution containing the Ni(Mebpy)$_n$Br$_2$ complex with excess supporting electrolyte (0.1 M TBAB). At this potential, no oxidation or reduction of the complex occurs (Fig. 1, left). The potential was then stepped to -1.25 V vs Ag/AgCl, a potential sufficient to reduce the complex at a diffusion-limited rate, while the current response, i_d, was recorded (Fig 1, right).

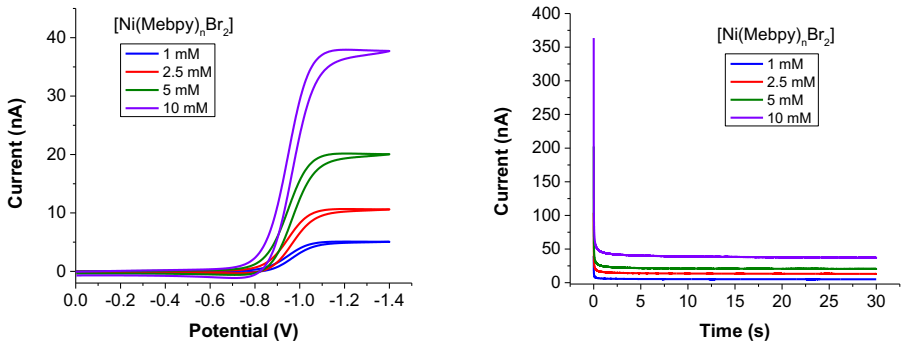

Figure 1. Cyclic voltammetry ***(left)*** and chronoamperometry ***(right)*** of the Ni(Mebpy)$_n$Br$_2$ complex (concentrations as given in legend) at a 25 µm diameter disk Pt microelectrode. The solution contained 0.1 M TBAB in DMF, and the concentration of 4,4′ -dimethyl-2,2′ -dipyridyl was selected to be at 2 equivalents w.r.t. Ni. In the chronoamperometric experiment, the potential was stepped from -0.4 V to -1.25 V vs Ag/AgCl at t = 0 s. For the voltammetry experiment, the scan rate is 20 mV s^{-1}.

A plot of i_d, normalized by dividing by the steady-state diffusion limited current, i_{ss}, vs $1/\sqrt{t}$ was then made (Figure 2), where i_{ss} was obtained from the limit of the current response at long times (30 s). A fit of a straight line gives a slope (S) that is related to the diffusion coefficient through:

$$D = \pi a^2/16S^2$$

where a is the electrode radius. Note, normalizing i_{ss} means this method can be used to determine D without knowledge of the number of electrons transferred during the electrochemical process (n) or the concentration of redox species (C), as noted by their absence in the above equation. From the slope measured from Figure 2, we calculate D = 0.5(±0.1) x 10^{-5} cm^2 s^{-1}.

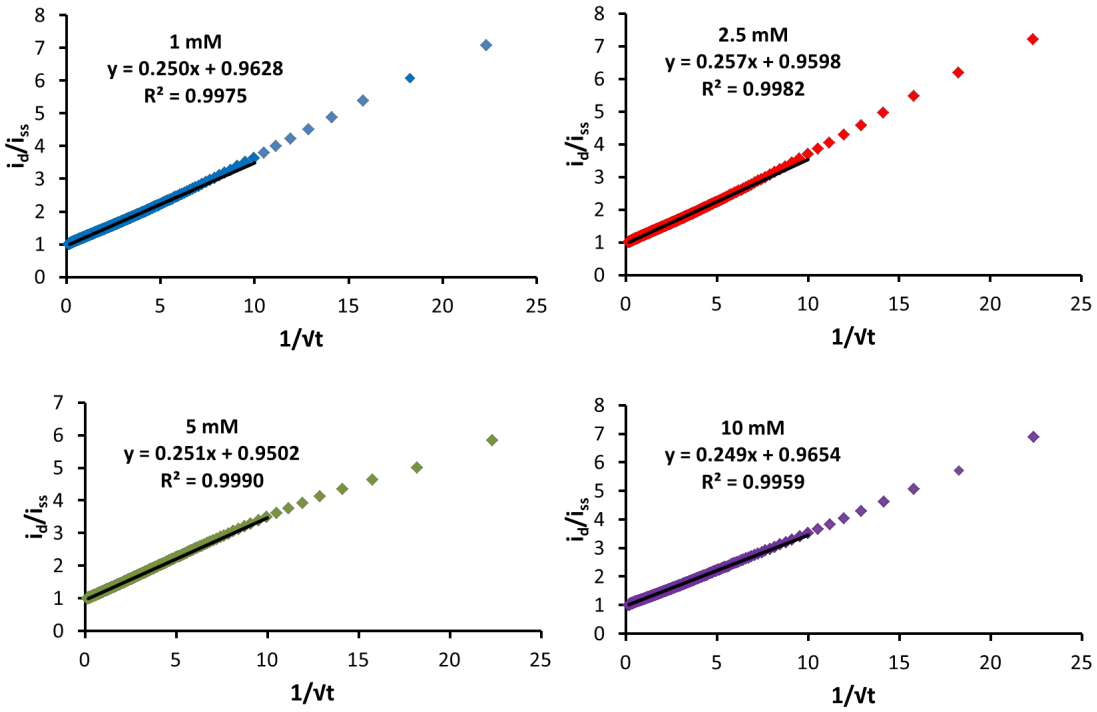

Figure 2. The plot of i_d /i_{ss} *vs* $1/\sqrt{t}$ from the chronoamperometric response for different concentration of the $Ni(Mebpy)_nBr_2$ complex. Solid lines show least-squares best fits to the data (''<10.0 $s^{-1/2}$'') to obtain D. Conditions as described in caption of **Figure 1**.

Measurement of the *D* in solutions containing 4 different concentrations of $Ni(Mebpy)_nBr_2$, all gave diffusion coefficients that agreed within error.

Number of Electrons Transferred (n)

The steady-state diffusion-limited current at an inlaid micro-disk electrode is described by:[5]

$i_{ss}=4nFCDa$

where F is Faraday's constant and the other variables are as described above. Rearrangement of this equation gives the number of electrons transferred during the reduction as a function of the measured steady-state current, $n = i_{ss}/naFCD$. From i_{ss}, obtained from cyclic voltammetry (Fig. 1, right), and the value of $D = 0.5(\pm0.1) \times 10^{-5}$ cm^2 s^{-1}, we obtain $n = 1.9 \pm 0.2$, i.e., the reduction of the Ni(Mebpy)$_n$Br$_2$ complex is a 2-electron process.

While the precise nature of the Ni oxidation state at the electrode interface remains unclear, several previous studies have demonstrated both that Ni(I) can be generated in appreciable quantities at the electrode surface (e.g. by comproportionation of Ni(0)/Ni(II)),[6] and that oxidative addition to Ni(I)(bpy)$_n$ species is thermodynamically preferential to oxidative addition to Ni(0)(bpy) complexes.[7]

DFT calculations

Computational method

All density-functional theory calculations were performed using the Gaussian 16 software package, revision A.03, with the M06-L exchange-correlation functional, and 6-31+G(d,p) basis set.[8,9] The Stuttgart/Dresden effective core potentials ECP10MDF[10] and ECP28MWB[11] were used on Ni and Br atoms, and solvation effects were taken into account using the SMD model[12] with DMF as the implicit solvent. SCF cycles were converged to 10^{-8} Ha while geometry optimizations were stopped after maximum force, root-mean-square force, maximum displacement, and root-mean-square displacement dropped below 4.5×10^{-4} Ha/a_0, 3.0×10^{-4} Ha/a_0, 1.8×10^{-3} a_0, and 1.2×10^{-3} a_0, respectively. The reported reaction energetics correspond to the spin states with the lowest energies, and the nudged elastic band method[13,14] was used to locate transition states. The experimental solvation free energies of H^+ and Br^- in DMF[15] were used for the calculation of standard reduction potentials (vs. SHE), and the resulting values were then converted to the Ag/AgNO$_3$ (10 mM) reference by subtracting 0.5 V.[16]

Ligand binding and reduction potential

Calculated ligand binding and reduction potentials in DMF (vs. 10 mM $Ag/AgNO_3$). L = 4,4'-Mebpy.

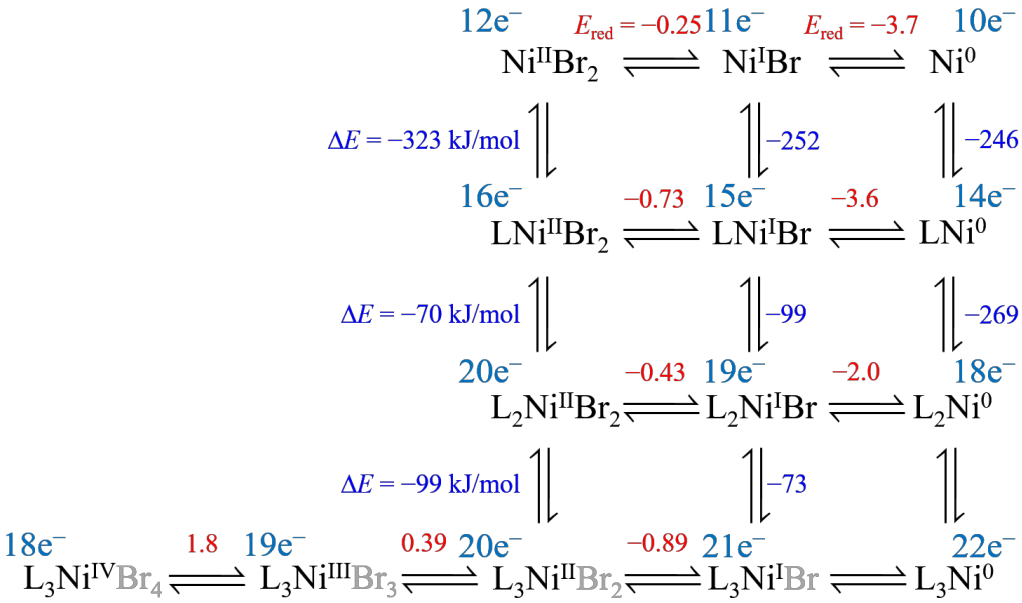

Ligand Screening (Table 1)

Initial ligand screening for the arylation of 4-bromothiazole

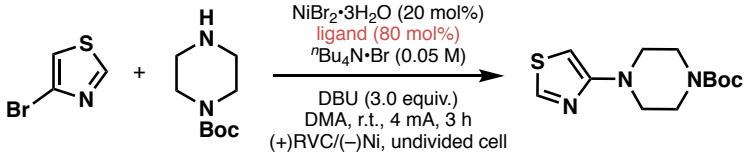

Effective ligands

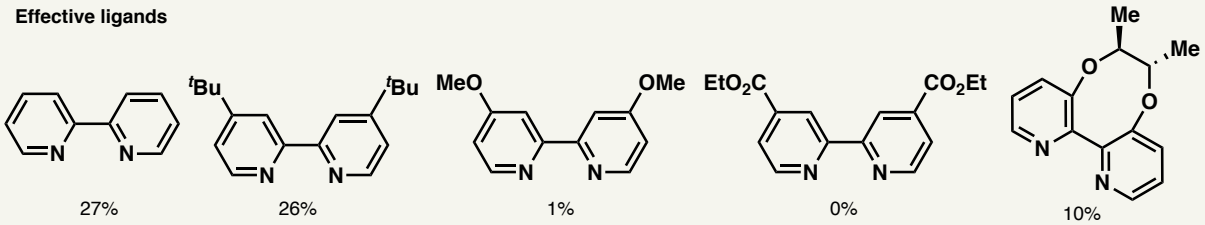

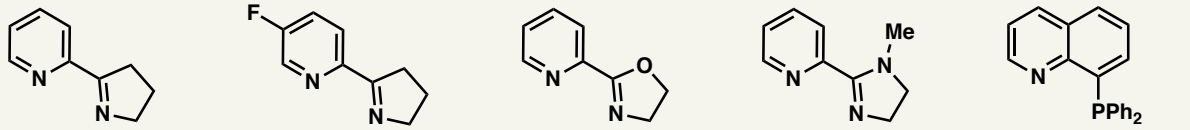

Ineffective ligands (0% yield)

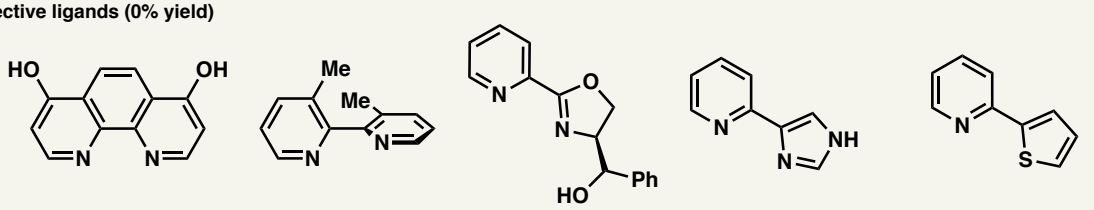

R = H, Me, NH_2 X = O, S

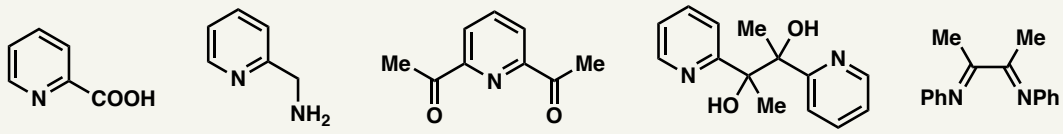

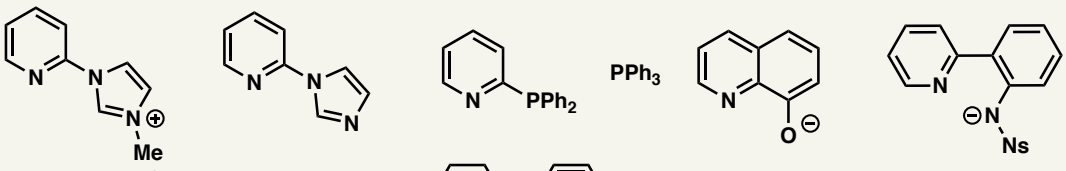

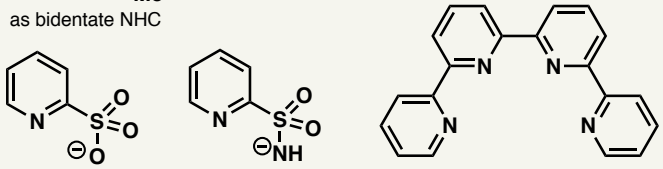

Second ligand screening focusing on electronic/steric tuning of effective types of ligands

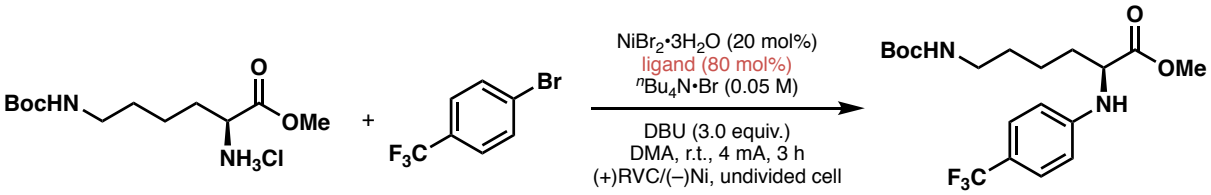

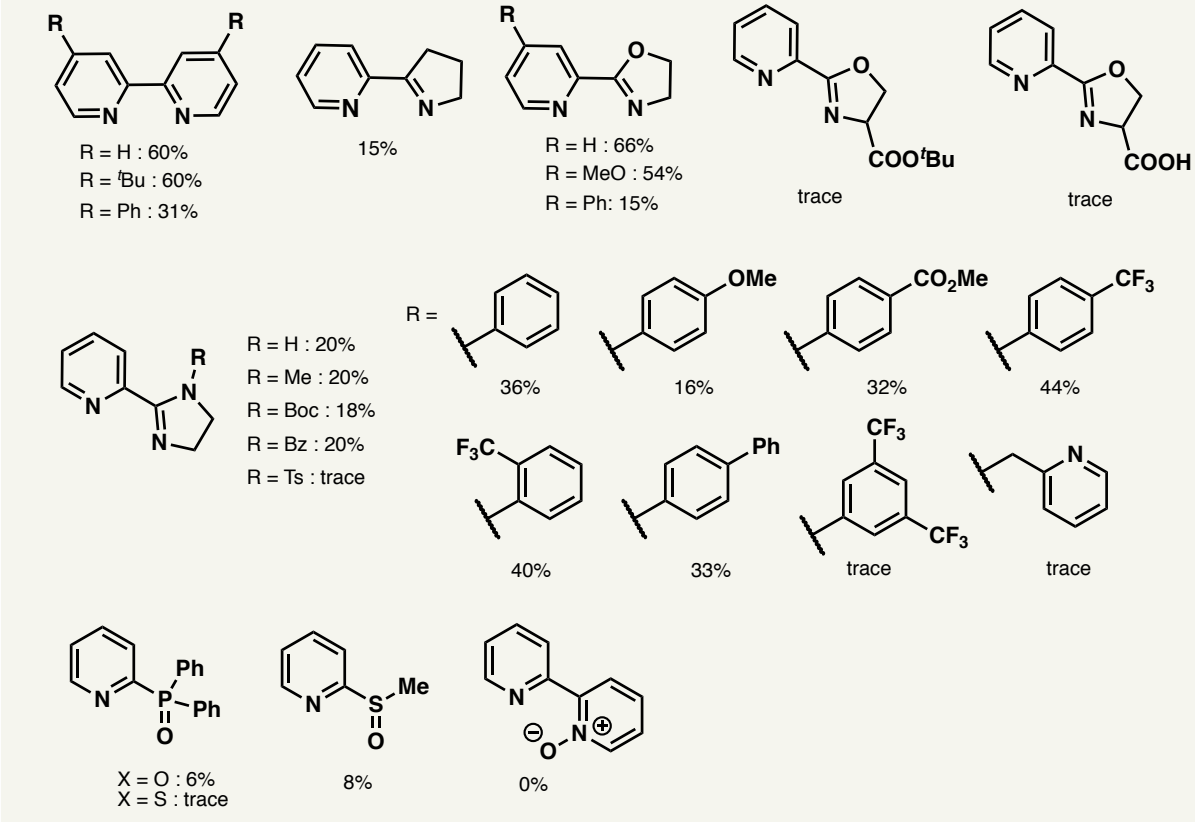

Trouble shooting & FAQ

Q. What can I do if the yield of the reaction is not reproducible?

A. Check the voltage of the reaction. From our experiences, if the cell voltage is too high (above 6 V at 4 mA on 0.2 mmol scale without a reference electrode), this reaction does not proceed well. Normal operational voltage range for this reaction is around 2.5V–5V.

When a high voltage is noted:
• Ensure there is sufficient contact between the electrode and the reaction solution. If not, please add more solvent containing 0.2 M TBAB to decrease the resistance in the circuit.
• Increasing the concentration of electrolyte helps to reduce the resistance of the cell.
• Reducing the current value also helps to decrease the reaction potential. Please note that longer reaction time is required in this case to ensure the passage of the same amount of electrical charge.

If the reaction voltage is unlikely to be the cause of irreproducibility, make sure that the reaction is degassed and the cap is screwed tightly. Though the reaction is not extremely sensitive to either oxygen or water, irreproducible results have been observed by insufficient sealing of the reaction cell. One easy way to improve sealing is to wrap Teflon tape around the rim of the vial, as described in Graphical guide.

Q. What are the suitable current values for reactions on different scales?

A. We typically use 4 mA on 0.2 mmol scales with exceptions noted in the procedure of each coupling reaction. The submerged exterior anode area is approximately 1.5 cm × 1 cm; the submerged exterior cathode area is approximately 1.5 cm × 1 cm.

Q. Where can I get the materials to construct the electrochemical cell?

A. Although in this work we used materials that we purchased previously, everything required for setting up this reaction can be obtained from IKA (https://www.ika.com/fr/Produits-Lab-Eq/Electrochemistry-Kit-csp-516/).

Q. Is this reaction sensitive to water?

A. A small amount of water (100–300 mol%) does not significantly affect the outcome.

Q. How air sensitive is the reaction?

A. The reaction is not particularly air sensitive as it proceeds without freeze-pump-thaw. However, evacuation-argon backfill cycle is still required as running the reaction under air results in much lower yield.

Q. How stable is $Ni(bpy)_3Br_2$?

A. This catalyst is indefinitely bench-stable, free-flowing pink powder. In addition, no sign of hygroscopic nature has been observed.

Q. Do other ligands work?

A. Please see the ligand screening section above

Q. Is stirring crucial for this reaction.

A. Stirring is critical—without stirring, the potential of the reaction could increase, leading to low yields. Our preferred stirring rate is from 500 to 1000 rpm.

Q. What is the byproduct of this reaction?

A. The major side reactions were homocoupling and proto-dehalogenation of the aryl halide. Occasionally, phenols (from the oxidation of aryl halides) could be detected, albeit in small quantities.

Q. What can I do if lots of starting materials remain after electrolysis?

A. One can increase the reaction time, use a higher current. If black deposit is observed at the Ni cathode, increasing ligand loading helps to slow down this undesired Ni deposition.

Q. How can I optimize the reaction if lots of homocoupling dimer or dehalogenation byproducts were detected at the end of the reaction?

A. One can change the ratio of amine and aryl halide. Alternatively, one can also increase the amount of DBU for the enhancement of amine nucleophilicity.

Q. Would it affect the yield if the electrolysis is conducted for longer, after the consumption of starting materials?

A. Longer reaction times can lead to the over-oxidation of amination products. Therefore, stopping the reaction after disappearance of starting materials by TLC/GC is recommended.

Characterization Data

Table 2-a – Scope of Amino acid esters

Compound 15

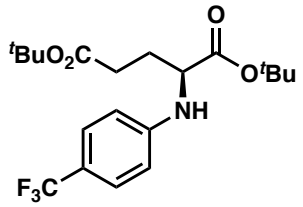

L-glutamic acid di-*tert*-butyl ester hydrochloride (0.1 mmol), 4-trifluormethylbromobenzene (0.2 mmol), DBU (0.3 mmol). Electrolysis was conducted for 4 h following the general procedure. The crude material was purified by PTLC (silica gel, hexanes:EtOAc = 10:1) to give the **15** as a white solid (63% yield).

R_f = 0.5 (hexanes:EtOAc = 5:1)

^{1}H NMR (600 MHz, $CDCl_3$) δ 7.39 (d, *J* = 8.4 Hz, 2H), 6.62 (d, *J* = 8.5 Hz, 2H), 4.59 (s, 1H), 4.03 (s, 1H), 2.31-2.43 (m, 2H), 2.01-2.14 (m, 2H), 1.45 (s, 9H), 1.44 (s, 9H) ppm.

^{13}C NMR (151 MHz, $CDCl_3$) δ 172.4, 172.3, 149.7, 126.8 (q, *J* = 3.8 Hz), 125.0 (q, *J* = 270.4 Hz), 119.8 (q, *J* = 32.6 Hz), 112.6, 82.5, 80.9, 56.2, 31.6, 28.2, 28.1, 27.8 ppm.

^{19}F NMR (376 MHz, $CDCl_3$) δ -61.39 ppm.

HRMS (ESI-TOF): calc'd for $C_{20}H_{29}F_3NO_4$ ($[M+H]^+$) 404.2049, found 404.2062.

Compound 18

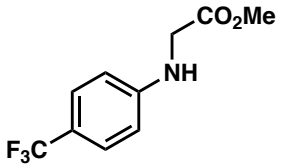

Glycine methyl ester hydrochloride (0.1 mmol), 4-trifluormethylbromobenzene (0.2 mmol), DBU (0.3 mmol). Electrolysis was conducted for 3 h following the general procedure. The crude material was purified by PTLC (silica gel, hexanes:EtOAc = 3:1) to give the **18** as a white solid (54% yield).

R_f = 0.5 (hexanes:EtOAc = 3:1)

^{1}H NMR (600 MHz, $CDCl_3$) δ 7.43 (d, *J* = 8.4 Hz, 2H), 6.61 (d, *J* = 8.5 Hz, 2H), 4.62 (s, 1H), 3.94 (d, *J* = 5.3 Hz, 2H), 3.81 (s, 3H) ppm.

^{13}C NMR (151 MHz, $CDCl_3$) δ 171.1, 149.5, 126.9 (q, *J* = 3.8 Hz), 125.0 (q, *J* = 270.4 Hz), 120.0 (q, *J* = 32.6 Hz), 112.3, 52.6, 45.2 ppm.

^{19}F NMR (376 MHz, $CDCl_3$) δ -61.41 ppm.

HRMS (ESI-TOF): calc'd for $C_{10}H_{11}F_3NO_2$ ($[M+H]^+$) 234.0742, found 234.0743.

Compound 19

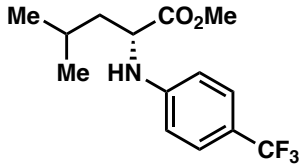

D-leucine methyl ester hydrochloride (0.1 mmol), 4-trifluormethylbromobenzene (0.2 mmol), DBU (0.3 mmol). Electrolysis was conducted for 3 h following the general procedure. The crude material was purified by PTLC (silica gel, hexanes:EtOAc = 5:1) to give the **19** as a colorless oil (70% yield).

***R**_f* = 0.6 (hexanes:EtOAc = 5:1)

^{1}H NMR (600 MHz, $CDCl_3$) δ 7.40 (d, *J* = 8.4 Hz, 2H), 6.62 (d, *J* = 8.5 Hz, 2H), 4.30 (d, *J* = 8.9 Hz, 1H), 4.12 (td, *J* = 8.5, 6.1 Hz, 1H), 3.73 (s, 3H), 1.78 (dp, *J* = 13.2, 6.6 Hz, 1H), 1.73 – 1.62 (m, 2H), 1.00 (d, *J* = 6.6 Hz, 3H), 0.95 (d, *J* = 6.5 Hz, 3H) ppm.

^{13}C NMR (151 MHz, $CDCl_3$) δ 174.6, 149.6, 126.9 (q, *J* = 3.8 Hz), 124.8 (q, *J* = 270.4 Hz), 120.0 (q, *J* = 32.7 Hz), 112.6, 54.8, 52.4, 42.2, 25.0, 22.8, 22.3 ppm.

^{19}F NMR (376 MHz, $CDCl_3$) δ -61.45 ppm.

HRMS (ESI-TOF): calc'd for $C_{14}H_{19}F_3NO_2$ ($[M+H]^+$) 290.1368, found 290.1369.

Chiral SFC: IG column (3 μm, 4.6x250 mm) under isocratic conditions [3% MeOH / CO_2 (4 mL/min), 1600 psi backpressure] at 30 °C. The enantiomers were detected by UV light (260 nm). t_R (major) = 1.179 min, t_R (minor) = 1.825 min, 86% *ee*.

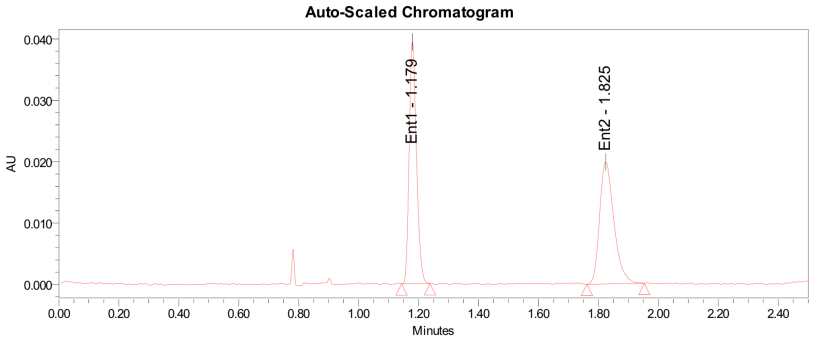

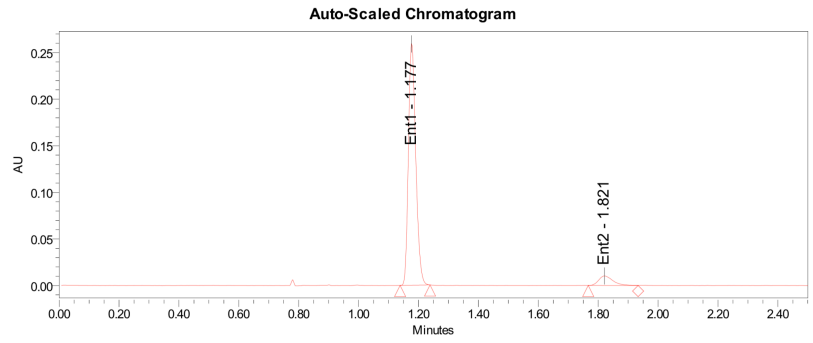

Compound 20

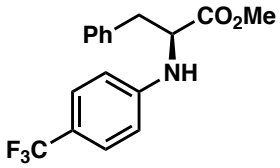

L-phenylalanine methyl ester hydrochloride (0.1 mmol), 4-trifluormethylbromobenzene (0.2 mmol), DBU (0.3 mmol). Electrolysis was conducted for 3 h following the general procedure. The crude material was purified by PTLC (silica gel, hexanes:EtOAc = 5:1) to give the **20** as a white solid (53% yield).

R_f = 0.5 (hexanes:EtOAc = 5:1)

^{1}H NMR (600 MHz, $CDCl_3$) δ 7.41 (d, *J* = 8.6 Hz, 2H), 7.31 (t, *J* = 7.3 Hz, 2H), 7.26 (t, *J* = 7.3 Hz, 1H), 7.15 (d, *J* = 7.2 Hz, 2H), 6.60 (d, *J* = 8.6 Hz, 2H), 4.49 (d, *J* = 7.9 Hz, 1H), 4.43 – 4.40 (m, 1H), 3.71 (s, 3H), 3.20 (dd, *J* = 13.7, 5.8 Hz, 1H), 3.12 (dd, *J* = 13.7, 6.2 Hz, 1H) ppm.

^{13}C NMR (151 MHz, $CDCl_3$) δ 173.0, 149.0, 135.94, 129.4, 128.8, 127.4, 126.9 (q, *J* = 3.7 Hz), 125.5 (q, *J* = 270.3 Hz) 120.1 (q, *J* = 32.6 Hz), 112.7, 57.20, 52.43, 38.5 ppm.

^{19}F NMR (376 MHz, $CDCl_3$) δ -61.43 ppm.

HRMS (ESI-TOF): calc'd for $C_{17}H_{17}F_3NO_2$ ($[M+H]^+$) 324.1211, found 324.1218.

Chiral SFC: IG column (3 μm, 4.6x250 mm) under isocratic conditions [3% MeOH / CO_2 (4 mL/min), 1600 psi backpressure] at 30 °C. The enantiomers were detected by UV light (260 nm). t_R (minor) = 1.329 min, t_R (major) = 1.739 min, 85% *ee*.

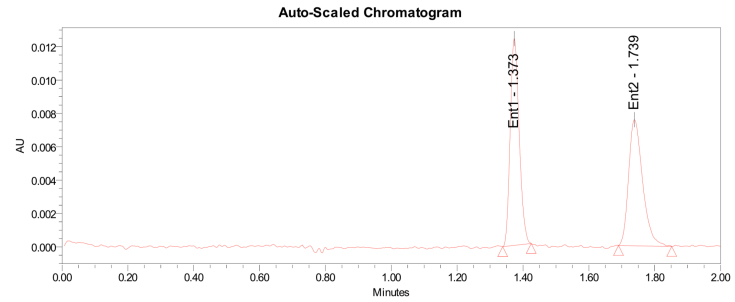

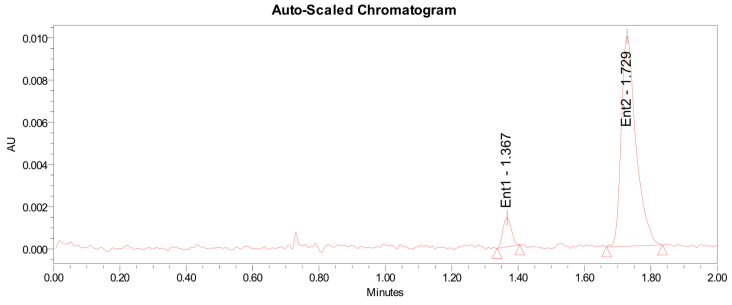

Compound 21

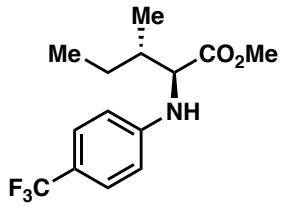

L-isoleucine methyl ester hydrochloride (0.1 mmol), 4-trifluormethylbromobenzene (0.2 mmol), DBU (0.3 mmol). Electrolysis was conducted for 3 h following the general procedure. The crude material was purified by PTLC (silica gel, hexanes:EtOAc = 10:1) to give the **21** as a colorless liquid (47% yield).

R_f = 0.6 (hexanes:EtOAc = 10:1)

^{1}H NMR (600 MHz, $CDCl_3$) δ 7.39 (d, *J* = 8.4 Hz, 2H), 6.62 (d, *J* = 8.5 Hz, 2H), 4.47 (br, 1H), 4.00 (d, *J* = 5.8 Hz, 1H), 3.73 (s, 3H), 1.85-1.92 (m, 1H), 1.58-1.65 (m, 1H), 1.27-1.34 (m, 1H), 0.96-0.98 (m, 6H) ppm.

^{13}C NMR (151 MHz, $CDCl_3$) δ 173.5, 149.7, 126.9 (q, *J* = 3.8 Hz), 125.0 (q, *J* = 270.3 Hz), 119.8 (q, *J* = 32.7 Hz), 112.6, 60.7, 52.2, 38.1, 25.8, 15.6, 11.6 ppm.

^{19}F NMR (376 MHz, $CDCl_3$) δ -61.42 ppm.

HRMS (ESI-TOF): calc'd for $C_{14}H_{19}F_3NO_2$ ($[M+H]^+$) 290.1368, found 290.1375.

Compound 22

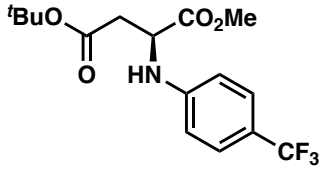

H-Asp(O^{t}Bu)-OMe•HCl (0.1 mmol), 4-trifluormethylbromobenzene (0.2 mmol), DBU (0.3 mmol). Electrolysis was conducted for 3 h following the general procedure. The crude material was purified by PTLC (silica gel, hexanes:EtOAc = 5:1) to give the **22** as a white solid (49% yield).

***R**$_f$* = 0.5 (hexanes:EtOAc = 10:1)

^{1}H NMR (600 MHz, CDCl$_3$) δ 7.42 (d, *J* = 8.4 Hz, 2H), 6.66 (d, *J* = 8.4 Hz, 2H), 4.83 (d, *J* = 8.4 Hz, 1H), 4.43 (dt, *J* = 8.5, 5.5 Hz, 1H), 2.82 (dd, *J* = 15.9, 5.6 Hz, 1H), 2.77 (dd, *J* = 15.9, 5.5 Hz, 1H), 1.44 (s, 9H) ppm.

^{13}C NMR (151 MHz, CDCl$_3$) δ 172.5, 169.6, 149.0, 126.9 (q, *J* = 3.8 Hz), 124.9 (q, *J* = 270.6 Hz), 120.3 (q, *J* = 32.7 Hz), 112.8, 82.0, 53.0, 52.8, 38.4, 28.14 ppm.

^{19}F NMR (376 MHz, CDCl$_3$) δ -61.49 ppm.

HRMS (ESI-TOF): calc'd for $C_{16}H_{21}F_3NO_4$ ([M+H]$^+$) 348.1423, found 348.1429.

Chiral SFC: IG column (3 μm, 4.6x250 mm) under isocratic conditions [3% MeOH / CO_2 (4 mL/min), 1600 psi backpressure] at 30 °C. The enantiomers were detected by UV light (260 nm). t_R (minor) = 1.270 min, t_R (major) = 1.670 min, 82% *ee*.

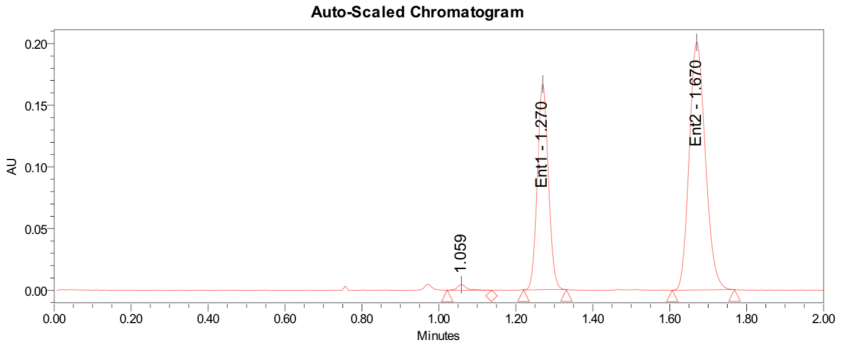

Compound 23

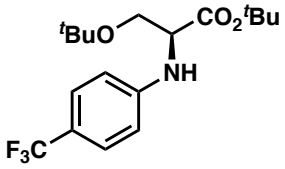

H-Ser(O^{t}Bu)-O^{t}Bu•HCl (0.1 mmol), 4-trifluormethylbromobenzene (0.2 mmol), DBU (0.3 mmol). Electrolysis was conducted for 3 h following the general procedure. The crude material was purified by PTLC (silica gel, hexanes:EtOAc = 20:1) to give the **23** as a white solid (69% yield).

R_f = 0.6 (hexanes:EtOAc = 10:1)

^{1}H NMR (600 MHz, $CDCl_3$) δ 7.39 (d, J = 8.4 Hz, 2H), 6.62 (d, J = 8.5 Hz, 2H), 4.82 (d, J = 8.8 Hz, 1H), 4.09 (dt, J = 8.8, 3.8 Hz, 1H), 3.78 (dd, J = 8.6, 3.7 Hz, 1H), 3.65 (dd, J = 8.6, 3.8 Hz, 1H), 1.45 (s, 9H), 1.17 (s, 9H) ppm.

^{13}C NMR (151 MHz, $CDCl_3$) δ 170.7, 149.9, 126.7 (q, J = 3.8 Hz), 125.1 (q, J = 270.3 Hz), 119.6 (q, J = 32.6 Hz), 112.7, 82.0, 73.5, 62.4, 57.0, 28.2, 27.5 ppm.

^{19}F NMR (376 MHz, $CDCl_3$) δ -61.32 ppm.

HRMS (ESI-TOF): calc'd for $C_{16}H_{27}F_3NO_3$ ($[M+H]^+$) 362.1943, found 362.1946.

Chiral SFC: IG column (3 μm, 4.6x250 mm) under isocratic conditions [3% MeOH / CO_2 (4 mL/min), 1600 psi backpressure] at 30 °C. The enantiomers were detected by UV light (260 nm). t_R (minor) = 1.105 min, t_R (major) = 1.249 min, 64% *ee*.

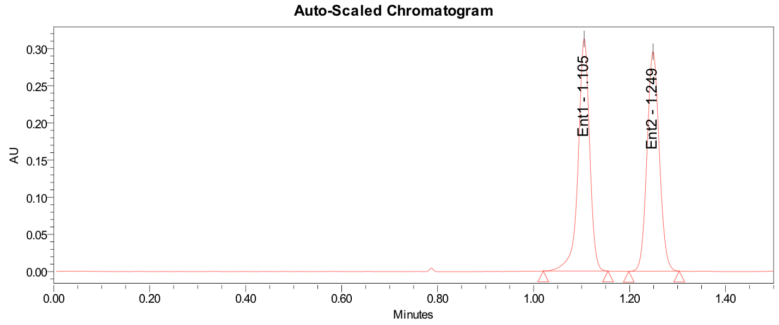

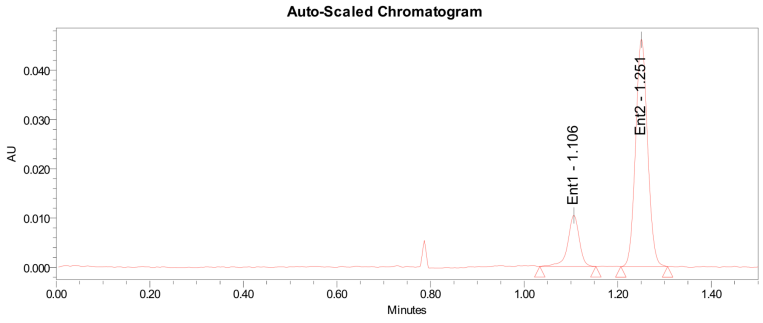

Compound 24

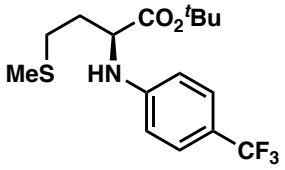

L-Methionine *tert*-butyl ester hydrochloride (0.1 mmol), 4-trifluormethylbromobenzene (0.2 mmol), DBU (0.3 mmol). Electrolysis was conducted for 3 h following the general procedure. The crude material was purified by PTLC (silica gel, hexanes:EtOAc = 4:1) to give the **24** as a white solid (59% yield).

R_f = 0.5 (hexanes:EtOAc = 3:1)

^{1}H NMR (600 MHz, $CDCl_3$) δ 7.40 (d, *J* = 8.5 Hz, 2H), 6.65 (d, *J* = 8.5 Hz, 2H), 4.54 (d, *J* = 8.4 Hz, 1H), 4.17 (q, *J* = 7.1 Hz, 1H), 2.60 (t, *J* = 7.4 Hz, 2H), 2.07-2.16 (m, 4H), 2.00 (dq, *J* = 14.1, 7.1 Hz, 1H), 1.45 (s, 9H) ppm.

^{13}C NMR (151 MHz, $CDCl_3$) δ 172.3, 149.6, 126.8 (q, *J* = 3.7 Hz), 125.0 (q, *J* = 270.3 Hz), 119.9 (q, *J* = 32.7 Hz), 11287, 82.6, 55.7, 32.2, 30.3, 28.2, 15.7 ppm.

^{19}F NMR (376 MHz, $CDCl_3$) δ -61.41 ppm.

HRMS (ESI-TOF): calc'd for $C_{16}H_{23}F_3NO_2S$ ($[M+H]^+$) 350.1402, found 350.1408.

Chiral SFC: IG column (3 μm, 4.6x250 mm) under isocratic conditions [3% MeOH / CO2 (4 mL/min), 1600 psi backpressure] at 30 °C. The enantiomers were detected by UV light (260 nm). t_R (minor) = 1.228 min, t_R (major) = 1.793 min, 78% *ee*.

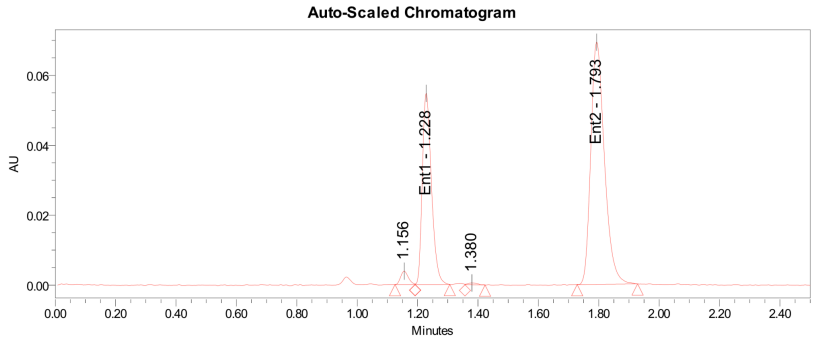

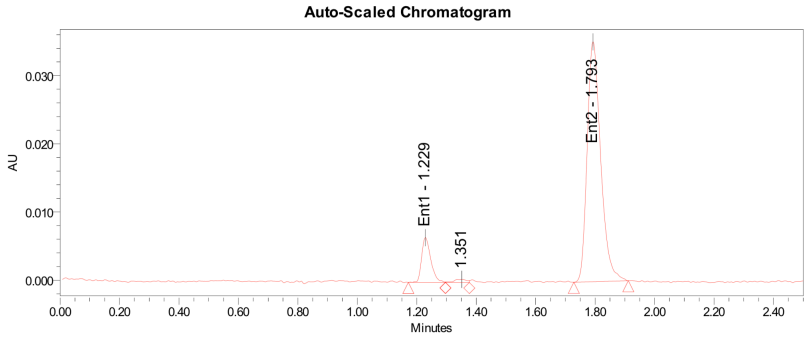

Compound 25

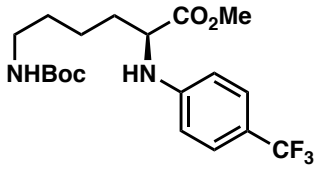

H-Lys(Boc)-OMe•HCl (0.1 mmol), 4-trifluormethylbromobenzene (0.2 mmol), DBU (0.3 mmol). Electrolysis was conducted for 3 h following the general procedure. The crude material was purified by PTLC (silica gel, hexanes:EtOAc = 2:1) to give the **25** as a white solid (54% yield).

R_f = 0.3 (hexanes:EtOAc = 3:1)

^{1}H NMR (600 MHz, $CDCl_3$) δ 7.39 (d, *J* = 8.5 Hz, 2H), 6.60 (d, *J* = 8.6 Hz, 2H), 4.54 (s, 2H), 4.09 (q, *J* = 7.1 Hz, 1H), 3.73 (s, 3H), 3.19 – 3.04 (m, 2H), 1.86-1.92 (m, 1H), 1.77-1.83 (m, 1H), 1.39-1.54 (m, 13H) ppm.

^{13}C NMR (151 MHz, $CDCl_3$) δ 185.7, 174.0, 156.2, 149.4, 126.9 (q, *J* = 3.8 Hz), 124.9 (q, *J* = 270.5 Hz), 119.9 (q, *J* = 33.4, 32.5 Hz), 112.5, 56.0, 52.5, 40.2, 32.4, 30.0, 28.5, 22.8 ppm.

^{19}F NMR (376 MHz, $CDCl_3$) δ -61.42 ppm.

HRMS (ESI-TOF): calc'd for $C_{19}H_{28}F_3N_2O_4$ ($[M+H]^+$) 405.2001, found 405.2004.

Chiral SFC: IG column (3 μm, 4.6x250 mm) under isocratic conditions [3% MeOH / CO2 (4 mL/min), 1600 psi backpressure] at 30 °C. The enantiomers were detected by UV light (260 nm). t_R (major) = 1.558 min, t_R (minor) = 1.885 min, 62% *ee*.

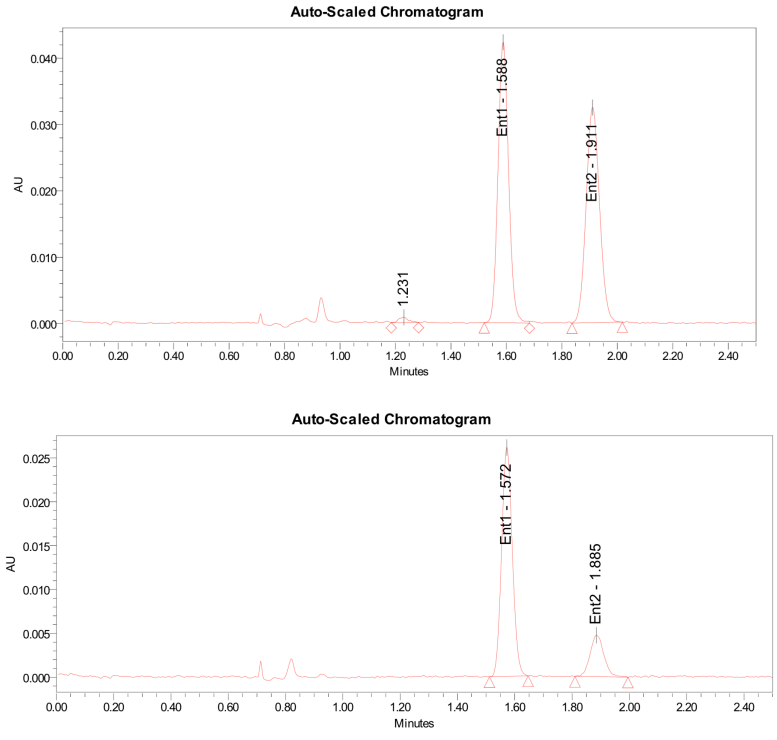

Compound 26

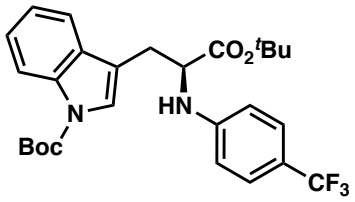

H-Trp(Boc)-O^{t}Bu•HCl (0.1 mmol), 4-trifluormethylbromobenzene (0.2 mmol), DBU (0.3 mmol). Electrolysis was conducted for 3 h following the general procedure. The crude material was purified by PTLC (silica gel, hexanes:EtOAc = 10:1) to give the **26** as a pale yellow liquid (57% yield).

R_f = 0.5 (hexanes:EtOAc = 10:1)

^{1}H NMR (600 MHz, $CDCl_3$) δ 8.14 (s, 1H), 7.44 (m, 4H), 7.33 (t, *J* = 7.4 Hz, 1H), 7.23 (t, *J* = 7.5 Hz, 1H), 6.61 (d, *J* = 8.6 Hz, 2H), 4.59 (d, *J* = 7.9 Hz, 1H), 4.37 (dd, *J* = 8.0, 4.0 Hz, 1H), 3.27 (dd, *J* = 14.6, 5.9 Hz, 1H), 3.20 (dd, *J* = 14.7, 5.9 Hz, 1H), 1.65 (s, 9H), 1.39 (s, 9H) ppm.

^{13}C NMR (151 MHz, $CDCl_3$) δ 171.7, 149.7, 149.2, 135.5, 130.7, 126.8 (q, *J* = 3.7 Hz), 125.0 (q, *J* = 270.3 Hz), 124.7, 124.4, 122.7, 119.8 (q, *J* = 32.7 Hz), 119.1, 115.4, 115.2, 112.7, 82.6, 56.7, 28.3, 28.1 ppm.

^{19}F NMR (376 MHz, $CDCl_3$) δ -61.36 ppm.

HRMS (ESI-TOF): calc'd for $C_{27}H_{32}F_3N_2O_4$ ($[M+H]^+$) 505.2314, found 505.2310.

Chiral SFC: IG column (3 μm, 4.6x250 mm) under isocratic conditions [3% MeOH / CO_2 (4 mL/min), 1600 psi backpressure] at 30 °C. The enantiomers were detected by UV light (260 nm). t_R (minor) = 1.385 min, t_R (major) = 1.633 min, 78% *ee*.

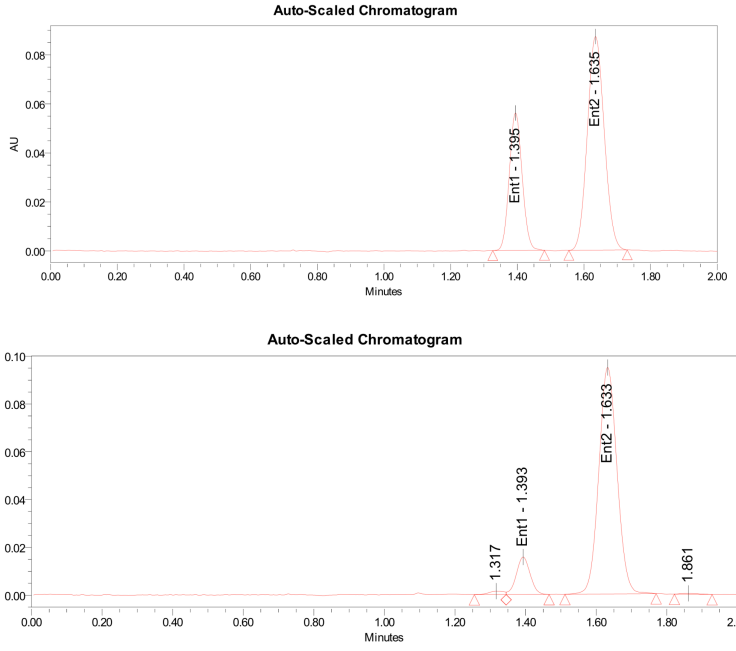

Compound 27

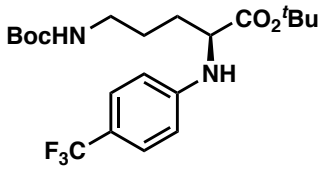

H-Orn(Boc)-O^{t}Bu•HCl (0.1 mmol), 4-trifluormethylbromobenzene (0.2 mmol), DBU (0.3 mmol). Electrolysis was conducted for 3 h following the general procedure. The crude material was purified by PTLC (silica gel, hexanes:EtOAc = 5:1) to give the **27** as a white solid (70% yield).

R_f = 0.3 (hexanes:EtOAc = 5:1)

^{1}H NMR (600 MHz, CDCl$_3$) δ 7.27-7.48 (m, 2H), 6.57-6.92 (m, 2H), 4.84-5.15 (m, 1H), 4.02-4.23 (m, 2H), 3.18-3.22 (m, 2H), 1.84-1.91 (m, 1H), 1.61-1.80 (m, 3H), 1.35-1.53 (m, 18H) ppm.

^{13}C NMR (151 MHz, CDCl$_3$) δ 171.8, 159.3, 155.7, 150.7, 126.7 (q, J = 3.7 Hz), 125.1 (q, J = 270.4 Hz), 118.8 (q, J = 33.5, 32.6 Hz), 115.6, 111.9, 82.4, 80.2, 53.70, 43.0, 30.8, 28.5, 28.1, 24.9 ppm.

^{19}F NMR (376 MHz, CDCl$_3$) δ -61.21, -61.65 ppm.

HRMS (ESI-TOF): calc'd for $C_{21}H_{32}F_3N_2O_4$ ([M+H]$^+$) 433.2314, found 433.2320.

Chiral SFC: IG column (3 μm, 4.6x250 mm) under isocratic conditions [3% MeOH / CO_2 (4 mL/min), 1600 psi backpressure] at 30 °C. The enantiomers were detected by UV light (260 nm). t_R (major) = 1.371 min, t_R (minor) = 1.485 min, 99% *ee*.

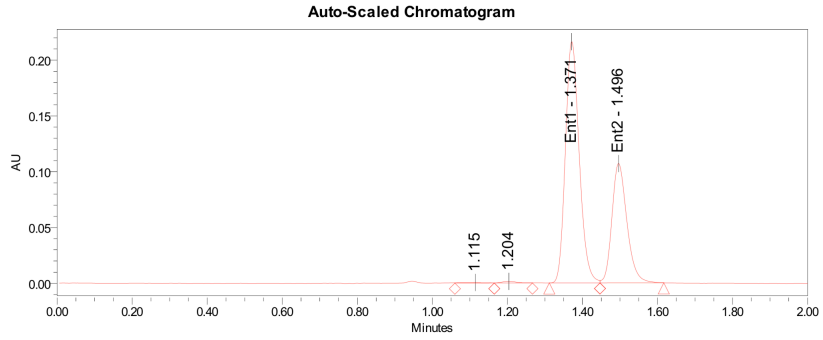

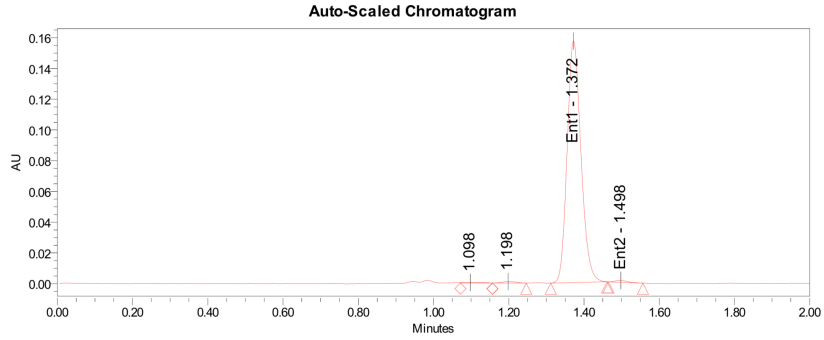

Compound 28

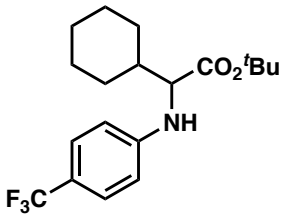

tert-Butyl 2-amino-2-cyclohexylacetate (0.1 mmol), 4-trifluormethylbromobenzene (0.2 mmol), DBU (0.3 mmol). Electrolysis was conducted for 3 h following the general procedure. The crude material was purified by PTLC (silica gel, hexanes:EtOAc = 20:1) to give the **28** as a white solid (51% yield).

R_f = 0.6 (hexanes:EtOAc = 10:1)

^{1}H NMR (600 MHz, $CDCl_3$) δ 7.38 (d, *J* = 8.8 Hz, 2H), 6.62 (d, *J* = 8.5 Hz, 2H), 4.47 (d, *J* = 8.4 Hz, 1H), 3.79 (dd, *J* = 8.2, 5.7 Hz, 1H), 1.66-1.81 (m, 6H), 1.44 (s, 9H), 1.11-1.30 (m, 5H) ppm.

^{13}C NMR (151 MHz, $CDCl_3$) δ 172.2, 150.2, 126.7 (q, *J* = 3.8 Hz), 125.0 (q, *J* = 270.3 Hz), 119.4 (q, *J* = 32.6 Hz), 112.6, 82.1, 61.9, 41.4, 29.6, 29.2, 26.3, 26.3, 26.2 ppm.

^{19}F NMR (376 MHz, $CDCl_3$) δ -61.33 ppm.

HRMS (ESI-TOF): calc'd for $C_{19}H_{27}F_3NO_2$ ($[M+H]^+$) 358.1994, found 358.1997.

Table 2-b – Application to total synthesis

Optimization table

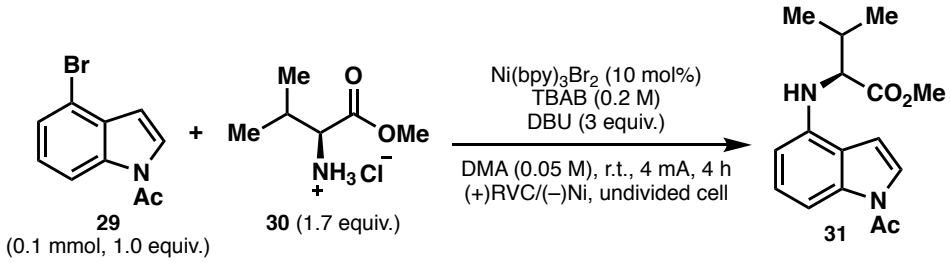

Optimization was conducted following the general procedure. The results are summarized below:

Entry	Change from standard conditions	Yield
1	First generation conditions (conditions A)	0%
2	None	16%
3	LiBr (0.2 M)	11%
4	$NiBr_2 \cdot 3H_2O$ (10 mol%), Ligand = bpy (30 mol%)	20%
5	$NiBr_2 \cdot 3H_2O$ (10 mol%), Ligand = **16** (30 mol%)	6%
6	$NiBr_2 \cdot 3H_2O$ (10 mol%), Ligand = **32** (30 mol%)	10%
7	$NiBr_2$•glyme (19 mol%), Ligand = **32** (75 mol%), LiBr (0.2 M)	32%
8	3.0 mmol scale with $NiBr_2$•glyme (19 mol%) and **32** (75 mol%)	51%[a]

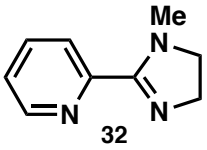

[a] LiBr (0.89 M), DMA (0.1 M), 100 mA, 7 h.

Large scale experiment (entry 8)

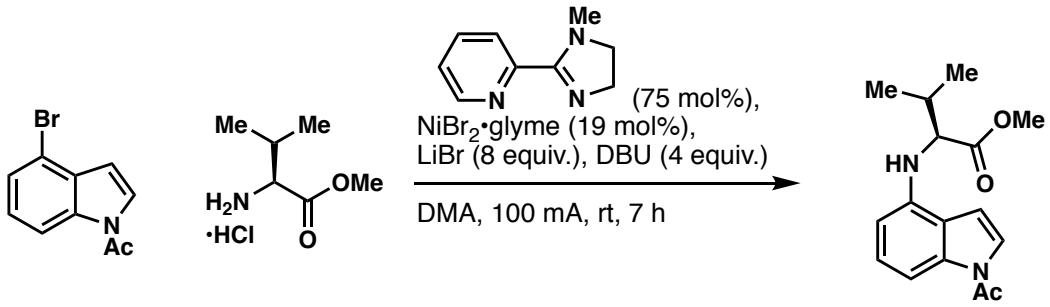

To a cell were added compound **29** (735 mg, 3.09 mmol), **30** (991 mg, 5.87 mmol, 1.9 equiv.), **32** (375 mg, 2.32 mmol, 75 mol%), LiBr solution (14 mL, 2.0 M in DMA, 8 equiv.), DBU (1.75 mL, 11.7 mmol, 4 equiv.) and DMA (13.9 mL). RVC anode and Ni form cathode were inserted into the mixture. A solution of $NiBr_2$•glyme (181 mg, 0.587 mmol, 19 mol%) in DMA (3.6 mL) was added then the reaction mixture was electrolyzed under a constant current of 100 mA for 7 h at room temperature. After the reaction, the reaction was quenched with water. The resulting mixture was extracted with Et_2O (x3). The combined organic layer was dried over anhydrous $MgSO_4$ and concentrated under reduced pressure. The crude material was purified by column chromatography (silica, 10:1 to 3:2 hexane:EtOAc) to afford 475 mg (51%) of compound **31**.

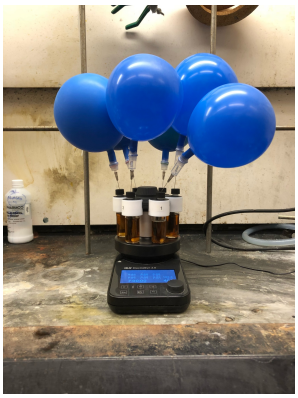

Physical State: yellow oil.

^{1}H NMR (600 MHz, $CDCl_3$): δ 7.83 (d, *J* = 8.3 Hz, 1H), 7.34 (d, *J* = 3.8 Hz, 1H), 7.19 (t, *J* = 8.1 Hz, 1H), 6.65 (d, *J* = 3.9 Hz, 1H), 6.44 (d, *J* = 7.9 Hz, 1H), 4.41 (s, 1H), 4.02 (d, *J* = 5.8 Hz, 1H), 3.72 (s, 3H), 2.62 (s, 3H), 2.19 (dq, *J* = 13.4, 6.5 Hz, 1H), 1.10 (d, *J* = 6.8 Hz, 3H), 1.05 (d, *J* = 6.7 Hz, 3H).

^{13}C NMR (151 MHz, $CDCl_3$): δ 174.33, 140.36, 136.50, 126.62, 123.39, 119.10, 105.28, 105.27, 62.57, 52.09, 31.82, 24.26, 18.94.

HRMS (ESI-TOF): calcd for $C_{16}H_{20}N_2O_3$ $[M+H]^+$: 289.1547, found: 289.1555.

TLC: R_f = 0.33 (3:2 hexanes:EtOAc, $Ce_2(SO_4)_3$ in phosphomolybdic acid).

$[\alpha]_D^{20}$ = −3.3 (c 0.392, $CHCl_3$).

Table 3 – Amination of heteroaryl halides with N-Boc-piperazine

Compound 33

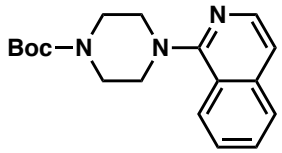

N-Boc-piperazine (0.3 mmol), 1-bromoisoquinoline (0.2 mmol), DBU (0.4 mmol). Electrolysis was conducted for 4 h following the general procedure. The crude material was purified by PTLC (silica gel, hexanes:EtOAc = 2:1) to give the **33** as a white solid (28% yield). The spectrum matched with the reported values.[17]

R_f = 0.4 (hexanes:EtOAc = 2:1)

Compound 34

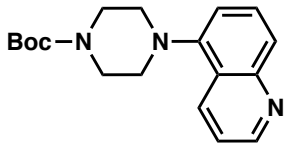

N-Boc-piperazine (0.3 mmol), 5-bromoquinoline (0.2 mmol), DBU (0.4 mmol). Electrolysis was conducted for 6 h following the general procedure. The crude material was purified by PTLC (silica gel, hexanes:EtOAc = 1:1) to give the **34** as off-white solid (59% yield).

R_f = 0.4 (hexanes:EtOAc = 2:1)

^{1}H NMR (600 MHz, $CDCl_3$) δ 8.89 (d, *J* = 4.1 Hz, 1H), 8.51 (d, *J* = 8.5 Hz, 1H), 7.83 (d, *J* = 8.5 Hz, 1H), 7.62 (t, *J* = 8.0 Hz, 1H), 7.39 (dd, *J* = 8.5, 4.2 Hz, 1H), 7.11 (d, *J* = 8.3 Hz, 1H), 3.69 (br, 4H), 3.03 (br, 4H), 1.50 (s, 9H) ppm.

^{13}C NMR (151 MHz, $CDCl_3$) δ 155.0, 150.4, 149.6, 149.6, 132.1, 129.5, 125.3, 124.2, 120.5, 115.5, 80.1, 53.3, 44.2 (br), 28.6 ppm.

HRMS (ESI-TOF): calc'd for $C_{18}H_{24}N_3O_2$ ($[M+H]^+$) 314.1869, found 314.1879.

Compound 35

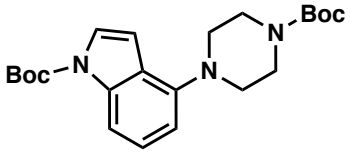

N-Boc-piperazine (0.3 mmol), *N*-Boc-4-bromoindole (0.2 mmol), DBU (0.4 mmol). Electrolysis was conducted for 7 h following the general procedure. The crude material was purified by PTLC (silica gel, hexanes:EtOAc = 5:1) to give the **35** as off-white solid (68% yield).

R_f = 0.5 (hexanes:EtOAc = 5:1)

^{1}H NMR (600 MHz, $CDCl_3$) δ 7.85 (d, *J* = 7.9 Hz, 1H), 7.56 (d, *J* = 3.6 Hz, 1H), 7.23 (t, *J* = 8.0 Hz, 1H), 6.74 (d, *J* = 7.7 Hz, 1H), 6.58 (d, *J* = 3.7 Hz, 1H), 3.66 (br, 4H), 3.11 (br, 4H), 1.67 (s, 9H), 1.50 (s, 9H) ppm.

^{13}C NMR (151 MHz, $CDCl_3$) δ 155.0, 149.9, 145.8, 136.4, 125.0, 124.8, 124.3, 110.6, 110.4, 105.4, 83.9, 79.9, 51.8, 44.1 (br), 28.6, 28.3 ppm.

HRMS (ESI-TOF): calc'd for $C_{22}H_{32}N_3O_4$ ($[M+H]^+$) 403.2393, found 403.2400.

Compound 36

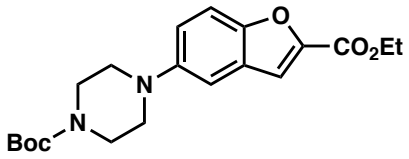

N-Boc-piperazine (0.3 mmol), ethyl 5-bromobenzofuran-2-carboxylate (0.2 mmol), DBU (0.4 mmol). Electrolysis was conducted for 6 h following the general procedure. The crude material was purified by PTLC (silica gel, hexanes:EtOAc = 3:1) to give the **36** as pale yellow solid (79% yield). The spectrum matched with the reported values.[18]

Compound 37

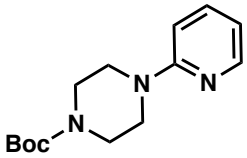

N-Boc-piperazine (0.3 mmol), 2-bromopyridine (0.2 mmol), DBU (0.4 mmol). Electrolysis was conducted for 4 h following the general procedure. The crude material was purified by PTLC (silica gel, hexanes:EtOAc = 3:1) to give the **37** as a white solid (51% yield). The spectrum matched with the reported values.[17]

Compound 38

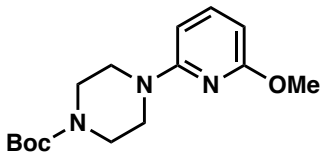

N-Boc-piperazine (0.3 mmol), 6-methoxy-2-chloropyridine (0.2 mmol), DBU (0.4 mmol). Electrolysis was conducted for 4 h following the general procedure. The crude material was purified by PTLC (silica gel, hexanes:EtOAc = 4:1) to give the **38** as off-white solid (56% yield).

R_f = 0.4 (hexanes:EtOAc = 4:1)

^{1}H NMR (600 MHz, $CDCl_3$) δ 7.40 (t, *J* = 7.9 Hz, 1H), 6.15 (d, *J* = 8.0 Hz, 1H), 6.09 (d, *J* = 7.9 Hz, 1H), 3.85 (s, 3H), 3.48-3.53 (m, 8H), 1.48 (s, 9H) ppm.

^{13}C NMR (151 MHz, $CDCl_3$) δ 163.2, 158.2, 154.9, 140.3, 98.7, 98.4, 80.0, 53.1, 45.2, 43.4 (br), 28.5 ppm.

HRMS (ESI-TOF): calc'd for $C_{15}H_{24}N_3O_3$ ($[M+H]^+$) 294.1818, found 294.1823.

Compound 39

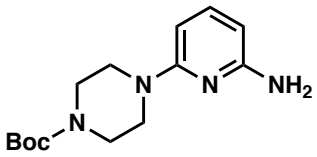

N-Boc-piperazine (0.3 mmol), 2-amino-6-bromopyridine (0.2 mmol), DBU (0.4 mmol). Electrolysis was conducted for 4 h following the general procedure. The crude material was purified by PTLC (silica gel, hexanes:EtOAc = 1:1) to give the **39** as off-white solid (45% yield).

R_f = 0.4 (hexanes:EtOAc = 1:1)

^{1}H NMR (600 MHz, $CDCl_3$) δ 7.27 (t, *J* = 7.9 Hz, 1H), 5.98 (d, *J* = 8.1 Hz, 1H), 5.88 (d, *J* = 7.7 Hz, 1H), 4.21 (br, 2H), 3.43-3.50 (m, 8H), 1.47 (s, 9H) ppm.

^{13}C NMR (151 MHz, $CDCl_3$) δ 158.9, 157.4, 155.0, 139.5, 97.8, 96.6, 79.9, 45.2, 43.5 (br), 28.6 ppm.

HRMS (ESI-TOF): calc'd for $C_{14}H_{23}N_4O_2$ ($[M+H]^+$) 279.1821, found 279.1827.

Compound 40

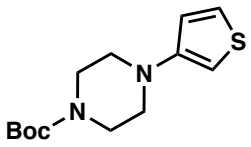

N-Boc-piperazine (0.3 mmol), 3-chlorothiophene (0.2 mmol), DBU (0.4 mmol). Electrolysis was conducted for 6 h following the general procedure. The crude material was purified by PTLC (silica gel, hexanes:EtOAc = 5:1) to give the **40** as a white solid (60% yield).

R_f = 0.6 (hexanes:EtOAc = 5:1)

^{1}H NMR (600 MHz, $CDCl_3$) δ 77.24 (dd, *J* = 5.2, 3.1 Hz, 1H), 6.86 (dd, *J* = 5.3, 1.5 Hz, 1H), 6.21 (dd, *J* = 3.0, 1.5 Hz, 1H), 3.55-3.57 (m, 4H), 3.03-3.05 (m, 4H), 1.47 (s, 9H) ppm.

^{13}C NMR (151 MHz, $CDCl_3$) δ 154.8, 152.3, 125.7, 120.3, 101.2, 80.0, 50.6, 43.5 (br), 28.5 ppm.

HRMS (ESI-TOF): calc'd for $C_{13}H_{21}N_2O_2S$ ($[M+H]^+$) 269.1324, found 269.1329.

Compound 41

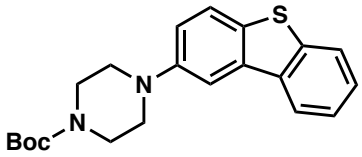

N-Boc-piperazine (0.3 mmol), 2-bromodibenzothiophene (0.2 mmol), DBU (0.4 mmol). Electrolysis was conducted for 7 h following the general procedure. The crude material was purified by PTLC (silica gel, hexanes:EtOAc = 5:1) to give the **41** as a white solid (68% yield).

R_f = 0.5 (hexanes:EtOAc = 5:1)

^{1}H NMR (600 MHz, $CDCl_3$) δ 8.10 (dd, *J* = 6.0, 3.2 Hz, 1H), 7.83 (dd, *J* = 5.8, 3.2 Hz, 1H), 7.72 (d, *J* = 8.7 Hz, 1H), 7.66 (s, 1H), 7.43 (dd, *J* = 6.0, 3.2 Hz, 2H), 7.16 (dd, *J* = 8.7, 2.3 Hz, 1H), 3.66 (br, 4H), 3.22 (br, 4H), 1.52 (s, 9H) ppm.

^{13}C NMR (151 MHz, $CDCl_3$) δ 154.9, 149.4, 140.5, 136.6, 135.6, 131.7, 126.7, 124.3, 123.3, 123.1, 121.5, 118.7, 109.2, 80.1, 50.7, 43.8 (br), 28.6 ppm.

HRMS (ESI-TOF): calc'd for $C_{21}H_{25}N_2O_2S$ ($[M+H]^+$) 369.1637, found 369.1641.

Compound 42

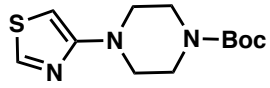

N-Boc-piperazine (0.3 mmol), 4-bromothiazole (0.2 mmol), DBU (0.4 mmol). Electrolysis was conducted for 4 h following the general procedure. The crude material was purified by PTLC (silica gel, hexanes:EtOAc = 3:1) to give the **42** as a white solid (33% yield).

R_f = 0.5 (hexanes:EtOAc = 3:1)

^{1}H NMR (600 MHz, $CDCl_3$) δ 8.60 (d, *J* = 2.1 Hz, 1H), 5.96 (d, *J* = 2.1 Hz, 1H), 3.57-3.58 (m, 4H), 3.25-3.27 (m, 4H), 1.47 (s, 9H) ppm.

^{13}C NMR (151 MHz, $CDCl_3$) δ 162.7, 154.9, 151.4, 90.6, 80.1, 48.82, 43.36 (br), 28.55 ppm.

HRMS (ESI-TOF): calc'd for $C_{12}H_{20}N_3O_2$ ($[M+H]^+$) 270.1276, found 270.1275.

Compound 43

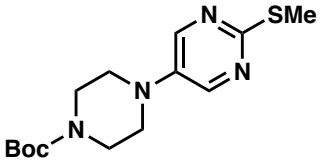

N-Boc-piperazine (0.3 mmol), 4-bromo-1-methylthiopyrimidine (0.2 mmol), DBU (0.4 mmol). Electrolysis was conducted for 4 h following the general procedure. The crude material was purified by PTLC (silica gel, hexanes:CH_2Cl_2:EtOAc = 1:1:0.5) to give the **43** as a white solid (71% yield).

R_f = 0.6 (hexanes:CH_2Cl_2:EtOAc = 1:1:0.5)

^{1}H NMR (600 MHz, $CDCl_3$) δ 8.23 (s, 2H), 3.57-3.59 (m, 4H), 3.09-3.08 (m, 4H), 2.53 (s, 3H), 1.46 (s, 9H) ppm.

^{13}C NMR (151 MHz, $CDCl_3$) δ 162.9, 154.6, 146.3, 141.3, 80.3, 48.8, 43.3 (br), 28.5, 14.4 ppm.

HRMS (ESI-TOF): calc'd for $C_{14}H_{23}N_4O_2S$ ($[M+H]^+$) 311.1542, found 311.1545.

Compound 44

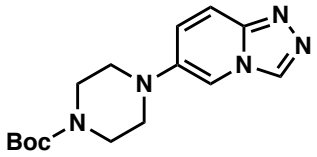

N-Boc-piperazine (0.3 mmol), 6-bromo-[1,2,4]triazolo[4,3-a]pyridine (0.2 mmol), DBU (0.4 mmol). Electrolysis was conducted for 4 h following the general procedure. The crude material was purified by PTLC (silica gel, CH_2Cl_2:MeOH = 20:1) to give the **44** as pale-blue liquid (67% yield).

$\boldsymbol{R_f}$ = 0.2 (CH_2Cl_2:MeOH = 10:1)

^{1}H NMR (600 MHz, $CDCl_3$) δ 8.71 (s, 1H), 7.69 (d, *J* = 9.7 Hz, 1H), 7.45 (s, 1H), 7.18 (d, *J* = 9.9 Hz, 1H), 3.62 (br, 4H), 3.04 (br, 4H), 1.49 (s, 9H) ppm.

^{13}C NMR (151 MHz, $CDCl_3$) δ 154.7, 147.4, 141.1, 136.0, 125.5, 116.4, 107.7, 80.5, 50.2, 43.4 (br), 28.6 ppm.

HRMS (ESI-TOF): calc'd for $C_{15}H_{22}N_5O_2$ ($[M+H]^+$) 304.1773, found 304.1777.

Table 4-A – C-N bond formation on nucleosides

Compound 45

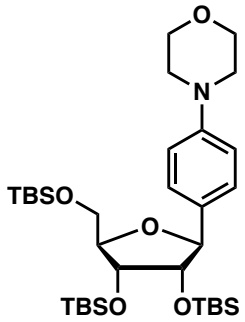

TBS-protected 1-(4-bromophenyl)ribose **45** (0.10 mmol), morpholine (0.15 mmol), DBU (0.2 mmol). Electrolysis was conducted for 4 h (4 mA) following the general procedure. The crude material was purified by PTLC (silica gel, hexanes:EtOAc = 5:1) to give the **46** as a colorless oil (50% yield).

R_f = 0.4 (hexanes:EtOAc = 5:1)

^{1}H NMR (600 MHz, $CDCl_3$) δ 7.31 (d, *J* = 8.5 Hz, 2H), 6.85 (d, *J* = 8.7 Hz, 2H), 4.71 (d, *J* = 7.5 Hz, 1H), 4.13 (dd, *J* = 4.5, 2.1 Hz, 1H), 3.99-4.01 (m, 1H), 3.84-3.87 (m, 5H), 3.75-3.80 (m, 2H), 3.10-3.16 (m, 4H), 0.95 (s, 9H), 0.93 (s, 9H), 0.80 (s, 9H), 0.12 (s, 3H), 0.11 (s, 3H), 0.09 (s, 6H), -0.13 (s, 3H), -0.39 (s, 3H) ppm.

^{13}C NMR (151 MHz, $CDCl_3$) δ 151.3, 132.4, 128.0, 115.7, 85.7, 83.0, 79.5, 73.9, 67.1, 63.9, 49.9, 26.2, 26.1, 26.0, 18.6, 18.3, 18.1, -4.3, -4.4, -5.1, -5.2, -5.4 ppm.

HRMS (ESI-TOF): calc'd for $C_{33}H_{64}NO_5Si_3$ ($[M+H]^+$) 638.4092, found 638.4096.

Compound 46

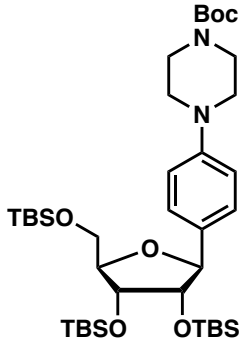

TBS-protected 1-(4-bromophenyl)ribose **45** (0.10 mmol), N-Boc-piperazine (0.15 mmol), DBU (0.2 mmol). Electrolysis was conducted for 4 h (4 mA) following the general procedure. The crude material was purified by PTLC (silica gel, hexanes:EtOAc = 10:1) to give the **47** as a colorless oil (71% yield).

R_f = 0.6 (hexanes:EtOAc = 5:1)

^{1}H NMR (600 MHz, $CDCl_3$) δ 7.31 (d, *J* = 8.6 Hz, 2H), 6.87 (d, *J* = 8.7 Hz, 2H), 4.70 (d, *J* = 7.5 Hz, 1H), 4.12 (dd, *J* = 4.4, 2.0 Hz, 1H), 4.00 (q, *J* = 3.4 Hz, 1H), 3.84 (dd, *J* = 7.5, 4.5 Hz, 1H), 3.77 – 3.78 (m, 1H), 3.57 – 3.58 (m, 4H), 3.06 – 3.12 (m, 4H), 1.48 (s, 9H), 0.94 (s, 9H), 0.93 (s, 9H), 0.79 (s, 9H), 0.12 (s, 3H), 0.11 (s, 3H), 0.09 (s, 6H), -0.13 (s, 3H), -0.41 (s, 3H) ppm.

^{13}C NMR (151 MHz, $CDCl_3$) δ 154.9, 151.3, 132.7, 128.0, 116.6, 85.8, 82.9, 80.0, 79.5, 73.9, 63.90, 50.0, 43.7, 28.6, 26.2, 26.1, 26.0, 18.5, 18.2, 18.1, -4.3, -4.4, -5.1, -5.2, -5.4 ppm.

HRMS (ESI-TOF): calc'd for $C_{38}H_{73}N_2O_6Si_3$ ($[M+H]^+$) 737.4776, found 737.4773.

Compound 47

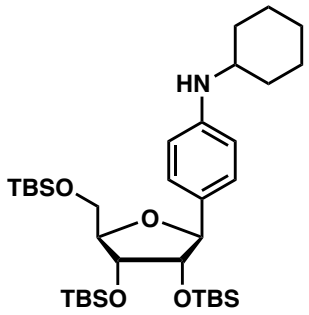

TBS-protected 1-(4-bromophenyl)ribose **45** (0.10 mmol), cyclohexylamine (0.3 mmol), no DBU. Electrolysis was conducted for 4 h (4 mA) following the general procedure. The crude material was purified by PTLC (silica gel, hexanes:EtOAc = 20:1) to give the **48** as a colorless oil (34% yield).

R_f = 0.7 (hexanes:EtOAc = 5:1)

^{1}H NMR (600 MHz, $CDCl_3$) δ 7.17 (d, *J* = 8.5 Hz, 2H), 6.53 (d, *J* = 8.5 Hz, 2H), 4.65 (d, *J* = 7.4 Hz, 1H), 4.12 (dd, *J* = 4.4, 2.3 Hz, 1H), 3.97 (d, *J* = 9.6 Hz, 1H), 3.83 (dd, *J* = 7.4, 4.5 Hz, 1H), 3.76 (d, *J* = 3.7 Hz, 2H), 3.25 (tt, *J* = 10.1, 3.6 Hz, 1H), 2.03-2.05 (m 2H), 1.73-1.76 (m, 2H), 1.63-1.66 (m, 1H), 1.32-1.40 (m, 2H), 1.18-1.25 (m, 1H), 1.08-1.15 (m, 2H), 0.94 (s, 9H), 0.93 (s, 9H), 0.80 (s, 9H), 0.12 (s, 3H), 0.10 (s, 3H), 0.09 (s, 3H), 0.08 (s, 3H), -0.13 (s, 3H), -0.35 (s, 3H) ppm.

^{13}C NMR (151 MHz, $CDCl_3$) δ 147.2, 129.1, 128.3, 113.4, 85.4, 83.3, 79.4, 73.9, 63.9, 52.1, 33.6, 33.5, 26.2, 26.1, 26.1, 26.1, 25.2, 25.2, 18.6, 18.6, 18.6, -4.3, -4.3, -4.4, -5.0, -5.2, -5.4 ppm.

HRMS (ESI-TOF): calc'd for $C_{35}H_{68}NO_4Si_3$ ($[M+H]^+$) 650.4456, found 650.4467.

Compound 48

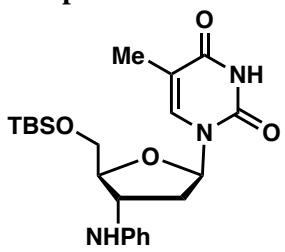

TBS-protected 3-amino thymidine **49** (0.05 mmol), bromobenzene (0.1 mmol), DBU (0.15 mmol) with TMSCl (0.05 mmol). Electrolysis was conducted for 2 h (4 mA) following the general procedure. The crude material was purified by PTLC (silica gel, hexanes:EtOAc = 1:1.5) to give the arylated product in 56% yield as a mixture of **50** and DMA-adduct **SI-1** (**50**:**SI-1** = **1.4**:**1**)

Major isomer **50** was characterized below.

R_f = 0.5 (hexanes:EtOAc = 1:2)

^{1}H NMR (600 MHz, $CDCl_3$) δ 9.09 (br, 1H), 7.56 (s, 1H), 7.19 (t, *J* = 7.8 Hz, 2H), 6.76 (t, *J* = 7.3 Hz, 1H), 6.61 (d, *J* = 7.8 Hz, 2H), 6.36 (t, *J* = 6.7 Hz, 1H), 4.16-4.18 (m, 1H), 4.01-3.97 (m, 2H), 3.87 (dd, *J* = 11.3, 2.2 Hz, 1H), 2.27-2.37 (m, 2H), 1.95 (s, 3H), 0.96 (s, 9H), 0.15 (s, 3H), 0.14 (s, 3H) ppm.

^{13}C NMR (151 MHz, $CDCl_3$) δ 163.9, 150.6, 146.6, 135.4, 129.6, 118.4, 113.4, 111.2, 86.0, 85.0, 63.8, 54.0, 39.3, 26.21, 18.6, 12.8, -5.2 ppm.

HRMS (ESI-TOF): calc'd for $C_{22}H_{34}N_3O_4Si$ ($[M+H]^+$) 432.2319, found 432.2320.

Compound 49

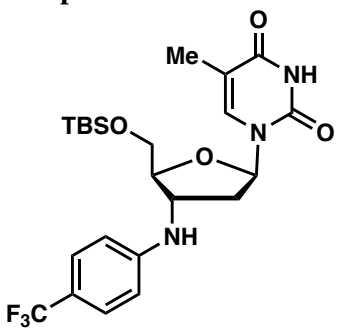

TBS-protected 3-amino thymidine **49** (0.05 mmol), 4-trifluoromethylbromobenzene (0.2 mmol), DBU (0.1 mmol). Electrolysis was conducted for 2 h (4 mA)following the general procedure. The crude material was purified by PTLC (silica gel, hexanes:EtOAc = 1:1) to give the **51** as a white solid (62% yield).

R_f = 0.4 (hexanes:EtOAc = 1:1)

^{1}H NMR (600 MHz, $CDCl_3$) δ 9.32 (br, 1H), 7.54 (s, 1H), 7.42 (d, *J* = 8.0 Hz, 2H), 6.65 (d, *J* = 8.1 Hz, 2H), 6.39 (s, 1H), 4.76 (br, 1H), 4.18 (s, 1H), 4.04 (s, 1H), 3.97 (d, *J* = 11.2 Hz, 1H), 3.88 (d, *J* = 10.8 Hz, 1H), 2.27-2.40 (m, 2H), 1.96 (s, 3H), 0.96 (s, 9H), 0.16 (s, 3H), 0.15 (s, 3H) ppm.

^{13}C NMR (151 MHz, $CDCl_3$) δ 163.8, 150.6, 149.3, 135.2, 126.9, 124.9 (q, *J* = 270.3 Hz), 119.8 (q, *J* = 32.8 Hz), 112.4, 111.4, 85.9, 85.2, 63.8, 53.9, 39.0, 26.1, 18.5, 12.8, -5.2, -5.2 ppm.

^{19}F NMR (376 MHz, $CDCl_3$) δ -61.40 ppm.

HRMS (ESI-TOF): calc'd for $C_{23}H_{33}F_3N_3O_4Si$ ($[M+H]^+$) 500.2192, found 500.2192.

Compound 50a and 50b

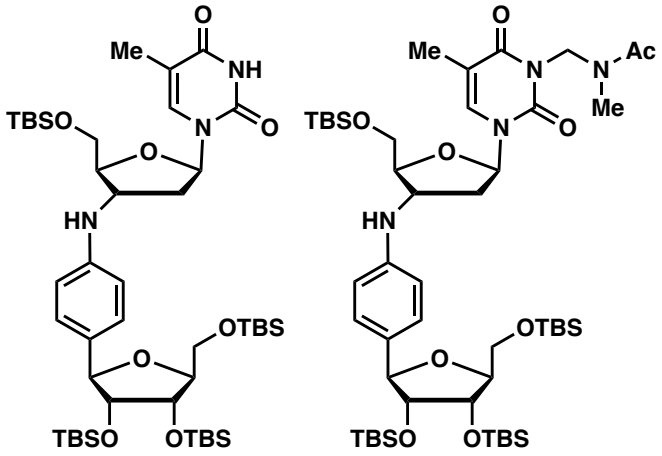

TBS-protected 3-amino thymidine **49** (0.05 mmol), TBS-protected 1-(4-bromophenyl)ribose **45** (0.05 mmol), DBU (0.1 mmol). Electrolysis was conducted for 3 h (4 mA) following the general procedure. The crude material was purified by PTLC (silica gel, hexanes:EtOAc = 1:1) to give the arylated product in 62% yield as a mixture of **52a** and DMA-adduct **52b** (**a**:**b** = 1:2.6).

*Characterization of **52a***

R_f = 0.5 (hexanes:EtOAc = 1:1)

^{1}H NMR (600 MHz, $CDCl_3$) δ 8.05 (s, 1H), 7.56 (s, 1H), 7.25 (d, *J* = 9.1 Hz, 2H), 6.55 (d, *J* = 8.4 Hz, 2H), 6.32 (t, *J* = 6.8 Hz, 1H), 4.67 (d, *J* = 7.6 Hz, 1H), 4.1-4.20 (m, 1H), 4.12-4.13 (m, 1H), 3.97-3.99 (m, 2H), 3.82-3.86 (m, 2H), 3.75-3.78 (m, 2H), 2.31 (t, *J* = 5.8 Hz, 2H), 1.95 (s, 3H), 0.95 (s, 9H), 0.94 (s, 9H), 0.93 (s, 9H), 0.80 (s, 9H), 0.14 (s, 3H), 0.13 (s, 3H), 0.12 (s, 3H), 0.11 (s, 3H), 0.09 (s, 6H), -0.12 (s, 3H), -0.38 (s, 3H) ppm.

^{13}C NMR (151 MHz, $CDCl_3$) δ 163.5, 150.2, 146.1, 135.5, 130.9, 128.5, 113.3, 111.1, 86.0, 85.7, 84.9, 83.1, 79.5, 73.9, 63.9, 63.8, 54.1, 39.4, 29.7, 26.2, 26.1, 26.1, 26.0, 18.6, 18.6, 18.3, 18.1, 12.7, -4.3, -4.3, -5.0, -5.2, -5.2, -5.2, -5.3 ppm.

HRMS (ESI-TOF): calc'd for $C_{45}H_{83}N_3O_8Si_4$ ($[M+H]^+$) 905.5257, found 906.5334.

*Characterization of **52b** (Ligation product DMA adduct)*

R_f = 0.2 (hexanes:EtOAc = 1:1)

^{1}H NMR (600 MHz, $CDCl_3$) δ 7.56-7.60 (m, 1H), 7.23-7.25 (m, 2H), 6.54-6.55 (m, 2H), 6.30-6.36 (m, 1H), 5.49-5.61 (m, 2H), 4.67 (d, *J* = 7.4 Hz, 1H), 4.12-4.19 (m, 2H), 3.96-3.99 (m, 3H), 3.82-3.86 (m, 2H), 3.74-3.79 (m, 2H), 3.00 (s, 0.43H), 2.87-2.88 (m, 2H), 2.43 (s, 2H), 2.28-2.43 (m, 2H), 2.07 (s, 0.60 H), 1.96 (s, 3H), 0.93-0.95 (m, 30H), 0.80 (s, 9H), -0.08-0.04 (m, 18H), -0.12 (s, 3H), -0.38 (s, 3H) ppm.

^{13}C NMR (151 MHz, $CDCl_3$) δ 171.9, 171.2, 163.7, 163.6, 151.1, 150.8, 146.0, 134.4, 134.1, 130.9, 128.5, 128.5, 113.3, 110.3, 110.2, 86.1, 85.9, 85.7, 85.6, 85.6, 85.5, 83.1, 83.0, 79.5, 73.9, 63.9, 63.7, 55.5, 54.1, 54.0, 52.6, 39.5, 35.2, 31.7, 26.2, 26.1, 26.1, 26.0, 22.2, 21.5, 18.6, 18.5, 18.2, 18.1, 13.4, -4.3, -4.3, -4.3, -5.0, -5.0, -5.2, -5.2, -5.3, -5.4 ppm.

HRMS (ESI-TOF): calc'd for $C_{49}H_{91}N_4O_9Si_4$ ($[M+H]^+$) 991.5863, found 991.5861.

Table 4-B – C-N bond formation on oligopeptides

Peptide SI-2

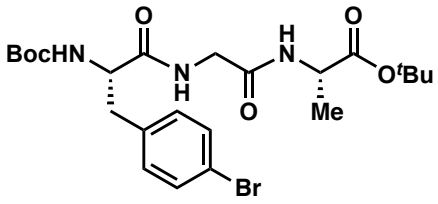

Peptide **SI-1** was synthesized according to a reported procedure on 2 mmol scale.[19] The crude Peptide **SI-2** was purified by preparative reverse-phase HPLC method Narrow 5 to afford peptide **SI-2** (642 mg, 60%) as a white solid following lyophilization.

HPLC trace

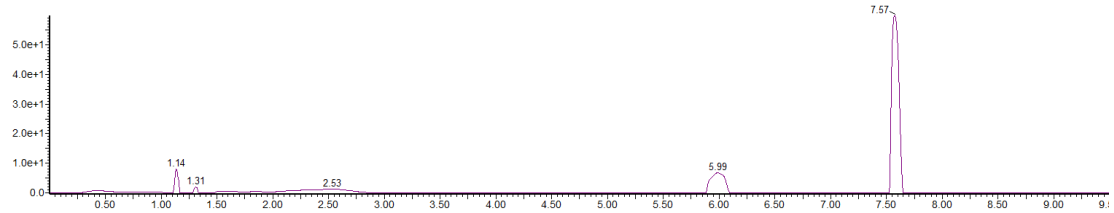

ESI$^-$

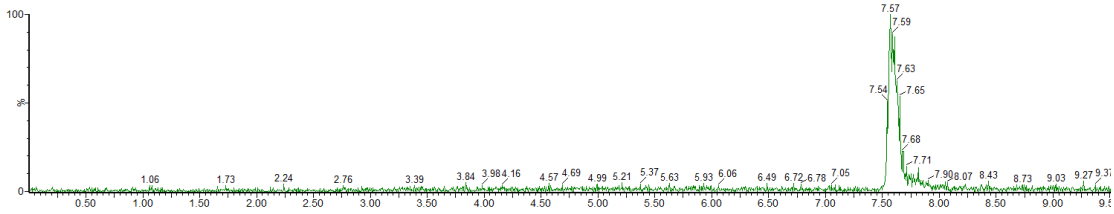

ESI$^+$

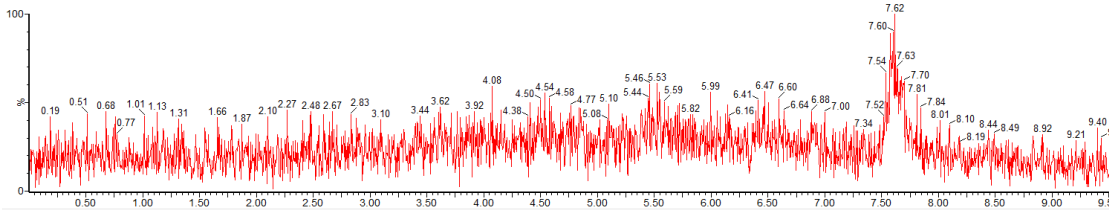

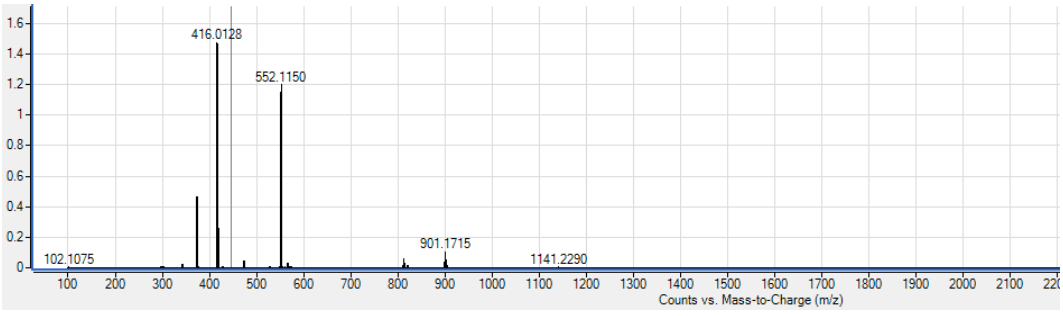

LRMS (ESI-TOF): calc'd for $C_{23}H_{34}BrN_3O_6Na$ $[M+Na]^+$ 552.16; found 552.12.

Peptide SI-3

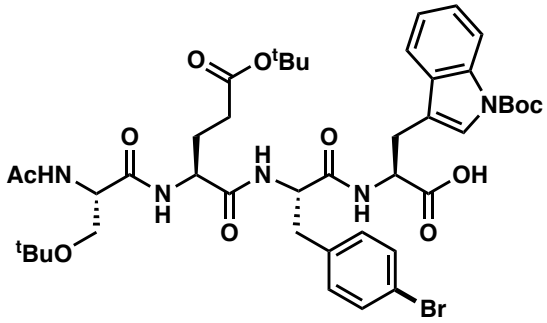

Peptide **SI-3** was prepared on a 300 μmol scale on 2-CTC resin using standard Fmoc-SPPS according to the general procedure. Following cleavage from the resin and ether precipitation, the crude peptide was purified by preparative reverse-phase HPLC method Narrow 5 to afford peptide **SI-3** (110 mg, 41% yield based on the original resin loading) as a white solid following lyophilization.

HPLC trace

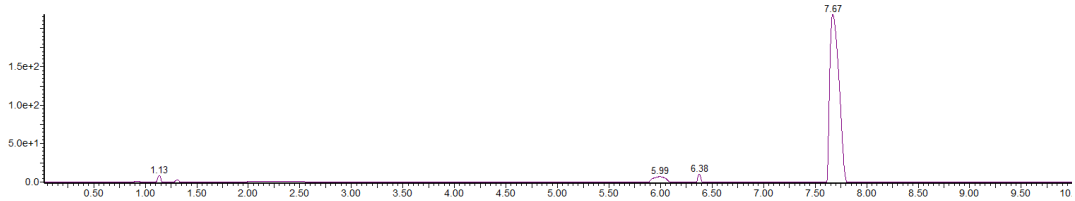

ESI$^-$

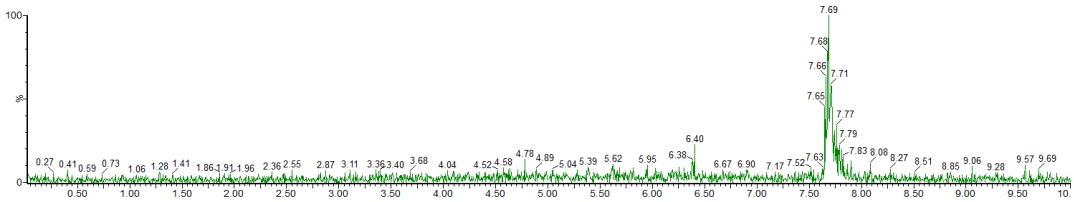

ESI$^+$

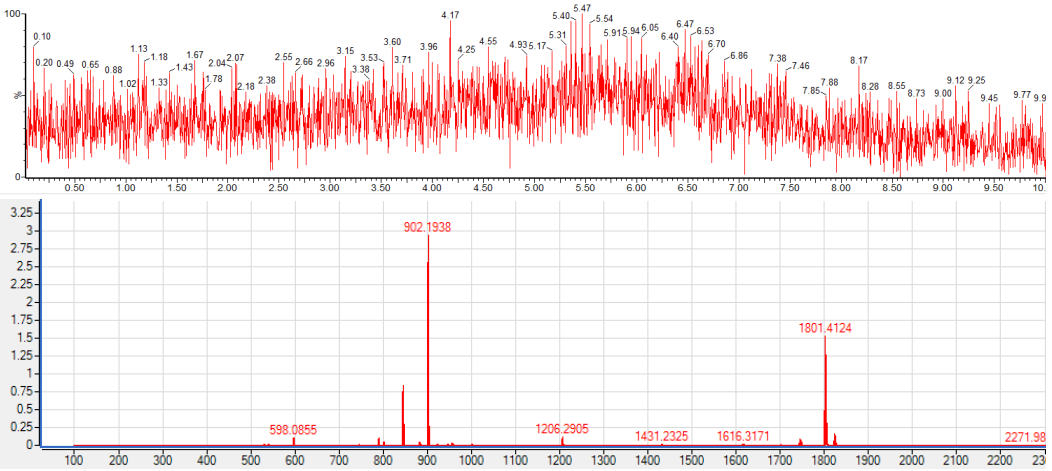

LRMS (ESI-TOF): calc'd for $C_{43}H_{59}BrN_5O_{11}$ $[M+H]^+$ 900.34; found 900.31.

Peptide SI-4

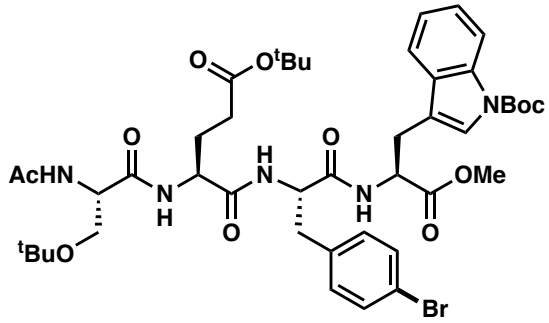

Peptide **SI-4** was prepared on a 300 µmol scale on 2-CTC resin using standard Fmoc-SPPS according to the general procedure esterification step added. Following cleavage from the resin and ether precipitation, the crude peptide was purified by preparative reverse-phase HPLC method Narrow 7 to afford peptide **SI-4** (103 mg, 31% yield based on the original resin loading) as a white solid following lyophilization.

HPLC trace

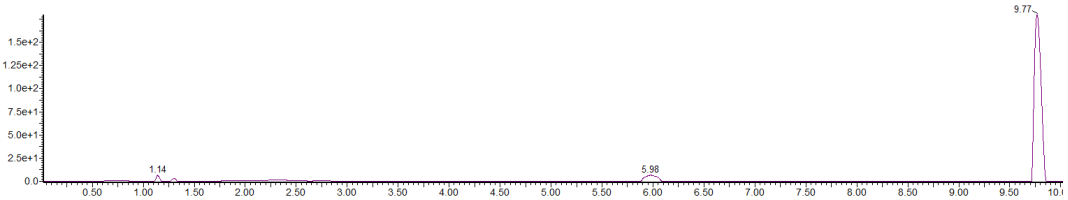

ESI-

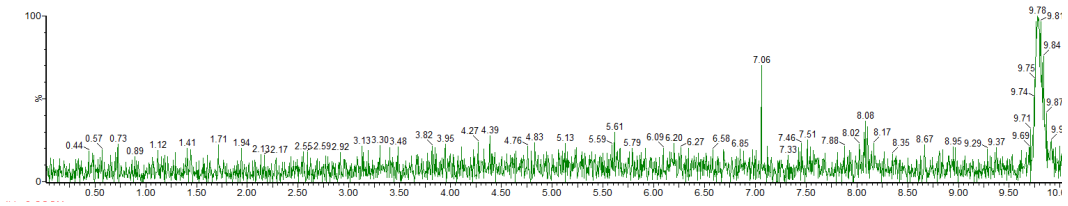

ESI+

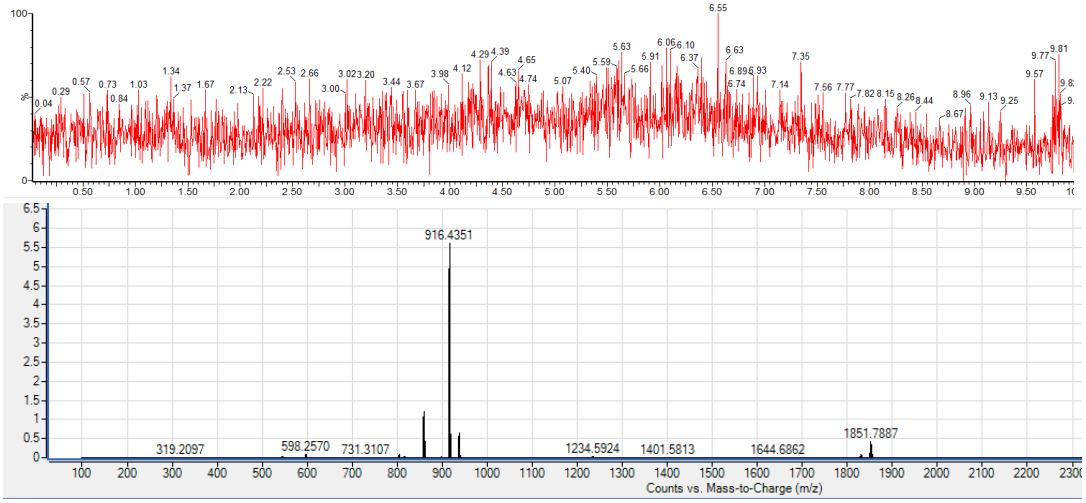

LRMS (ESI-TOF): calc'd for $C_{43}H_{61}BrN_5O_{11}$ $[M+H]^+$ 914.36; found 914.40.

Peptide SI-5

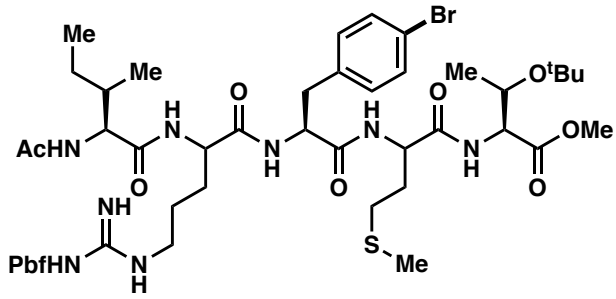

Peptide **SI-5** was prepared on a 300 µmol scale on 2-CTC resin using standard Fmoc-SPPS according to the general procedure esterification step added. Following cleavage from the resin and ether precipitation, the crude peptide was purified by preparative reverse-phase HPLC method Narrow 7 to afford peptide **SI-5** (153 mg, 46% yield based on the original resin loading) as a white solid following lyophilization.

HPLC trace

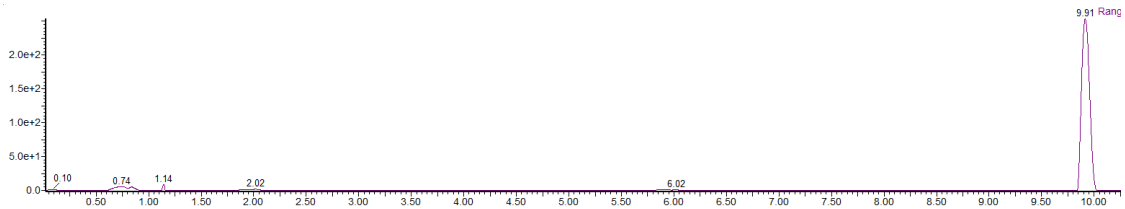

ESI$^-$

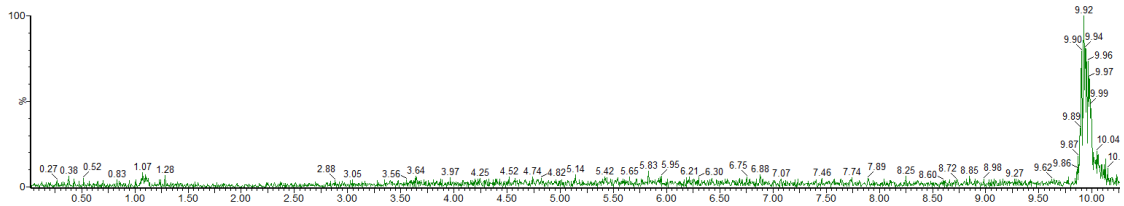

ESI$^+$

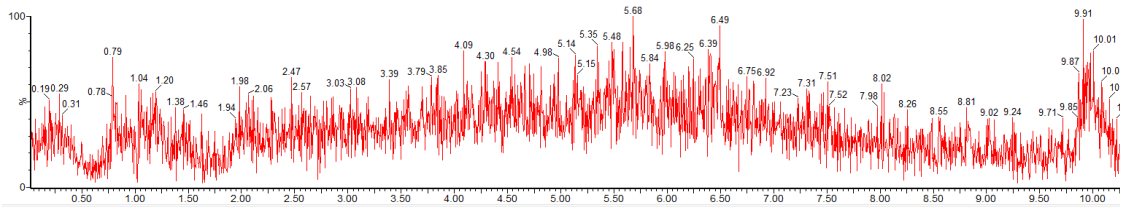

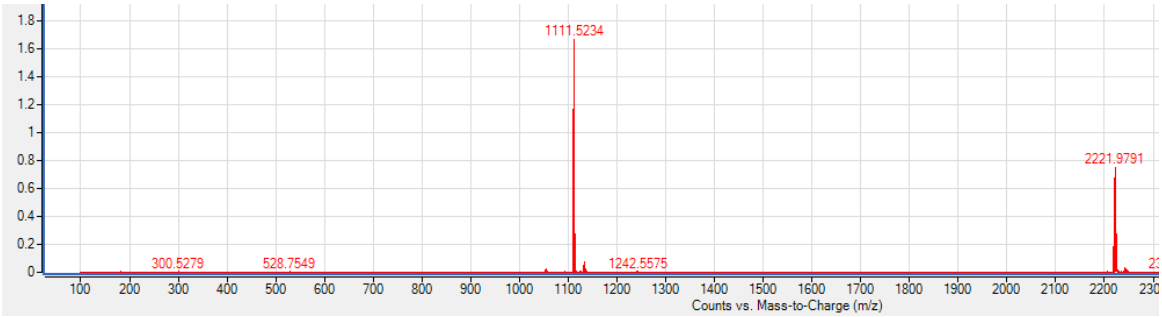

LRMS (ESI-TOF): calc'd for $C_{50}H_{78}BrN_8O_{11}S_2$ $[M+H]^+$ 1109.43; found 1109.32.

Peptide SI-6

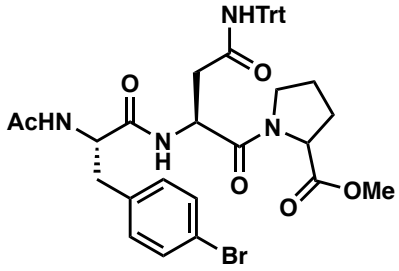

Peptide **SI-56** was prepared on a 300 µmol scale on 2-CTC resin using standard Fmoc-SPPS according to the general procedure esterification step added. Following cleavage from the resin and ether precipitation, the crude peptide was purified by preparative reverse-phase HPLC method Narrow 7 to afford peptide **SI-6** (126 mg, 56% yield based on the original resin loading) as a white solid following lyophilization.

HPLC trace

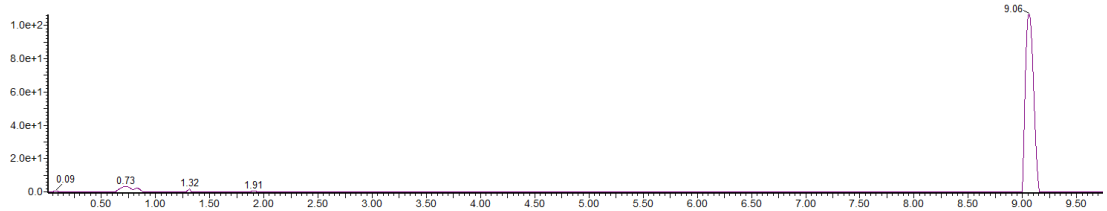

ESI$^-$

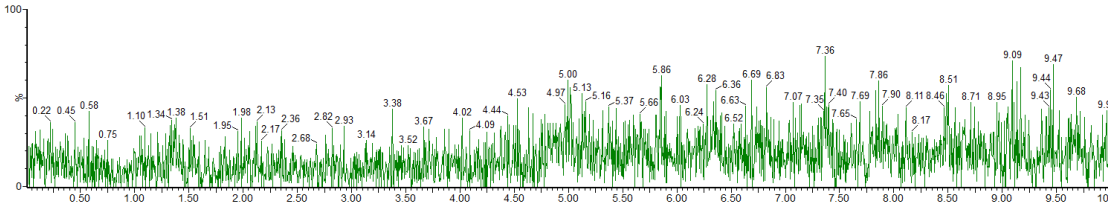

ESI+

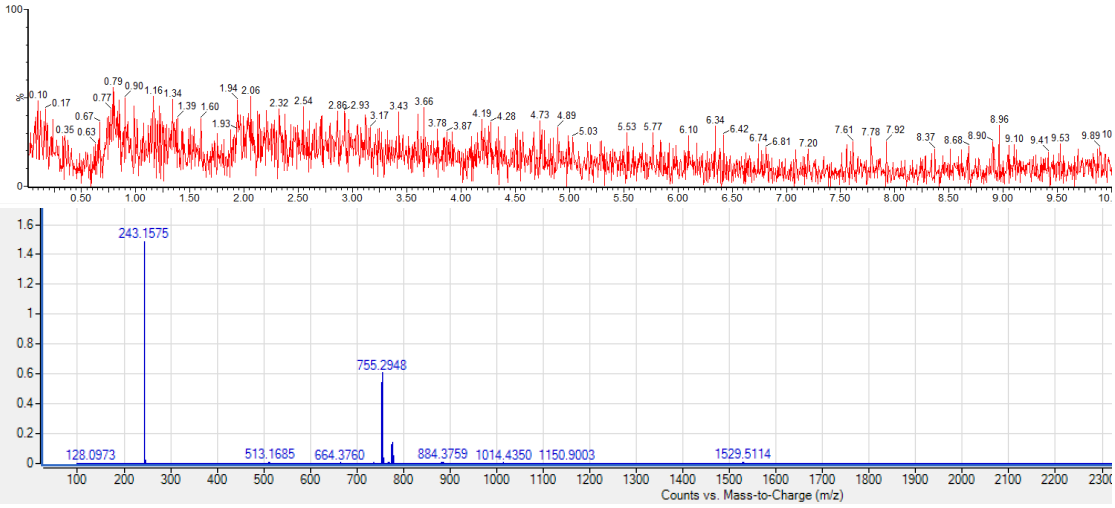

LRMS (ESI-TOF): calc'd for $C_{50}H_{78}BrN_8O_{11}S_2$ $[M+H]^+$ 753.23; found 753.24.

Peptide SI-7

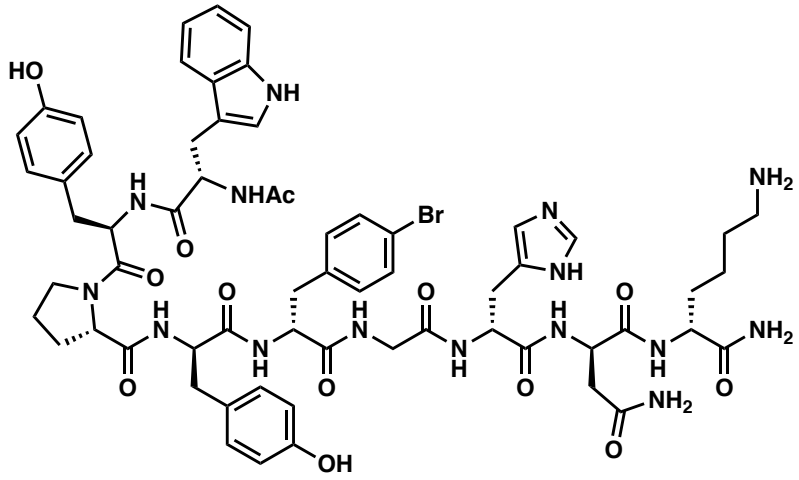

Peptide **SI-7** was provided by Pfizer and was prepared on Rink amide resin using standard Fmoc-SPPS strategy. HPLC and LCMS traces are described below.

HPLC trace

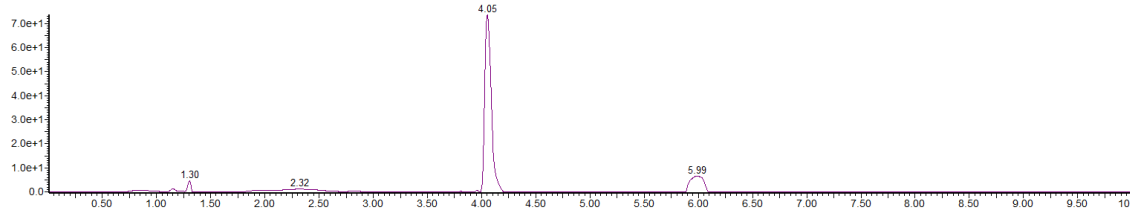

ESI⁻

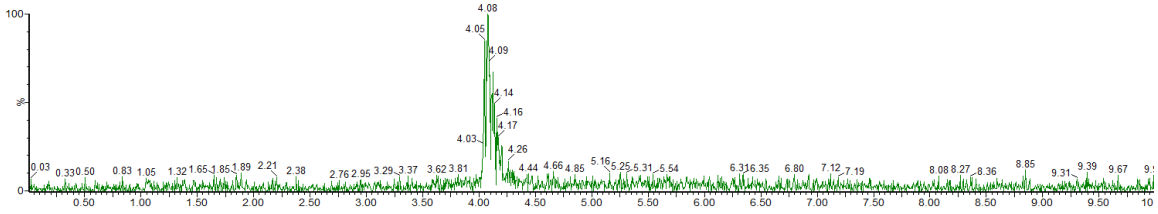

ESI⁺

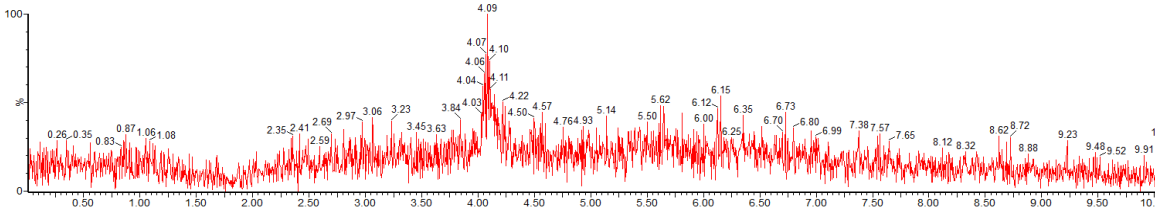

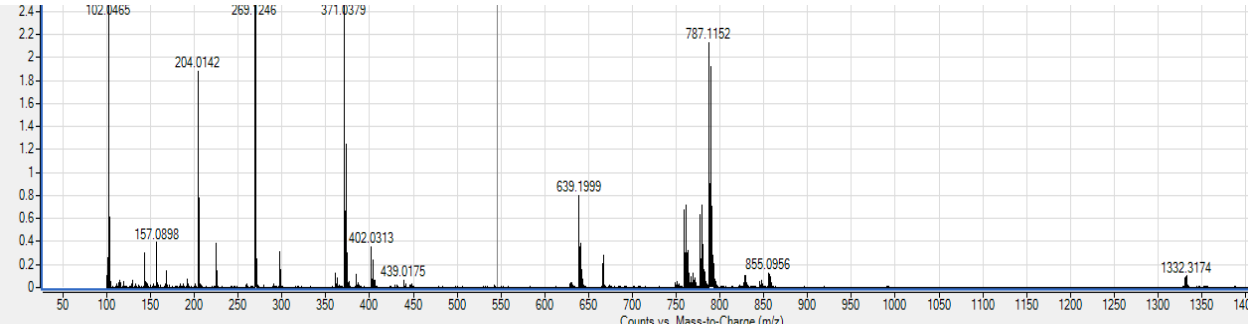

LRMS (ESI-TOF): calc'd for $C_{63}H_{77}BrN_{15}O_{13}$ $[M+H]^+$ 1330.50; found 1330.53.

Peptide – Optimization table

The optimization of the coupling reaction between morpholine and peptide **SI-2** was conducted following the general procedure for peptides.

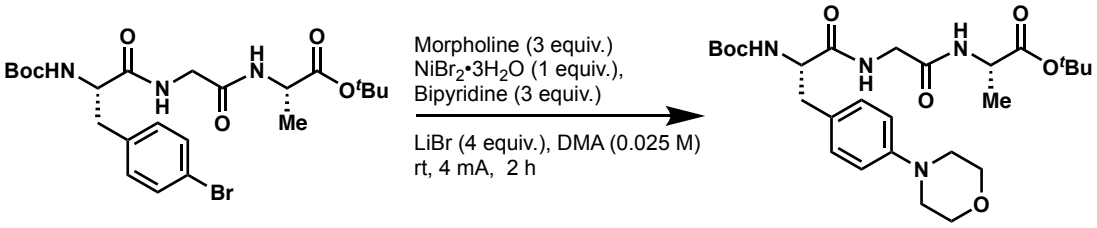

The crude reaction mixtures were analyzed by LCMS and the conversion to the desired product was based on relative integration.

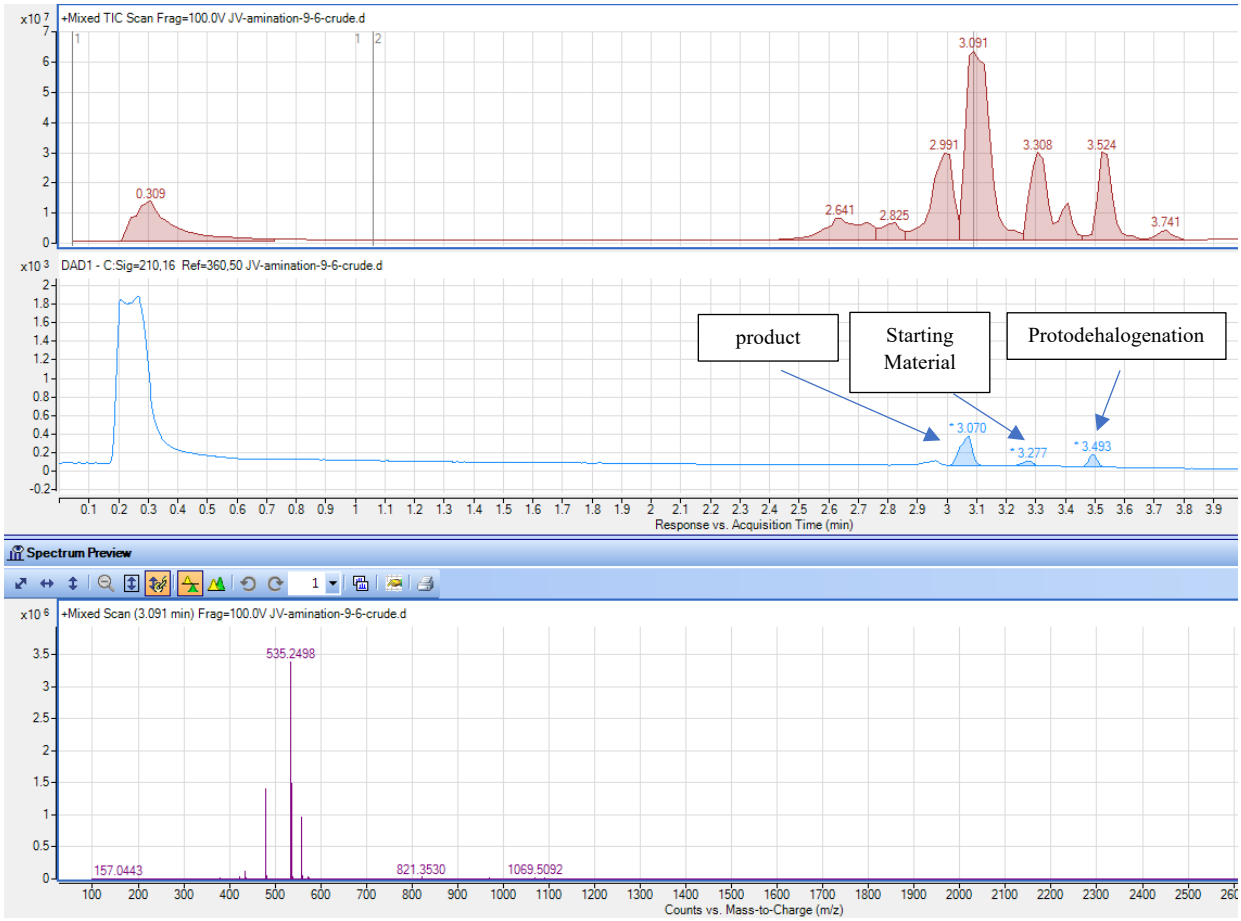

The table below summarized the deviations from standard conditions that led the optimized set of condition:

#	Deviation from standard conditions	Yield %
1	none	37 (32)
2	8 equiv. amine	51
3	2 equiv LiBr	29
4	8 equiv LiBr	40
5	20 equiv LiBr	38
6	8 mA, 1h	29
7	2 mA, 8h	36
8	4 mA, 4h	56
9	4 mA, 6h	63 (57)
10	8 equiv LiBr, 4 mA, 6h	61
11	30 mol% [Ni], 4 mA, 6h	57 (51)
12	30 mol% [Ni] complex, 4 mA, 6h	61 (55)

Compound 51

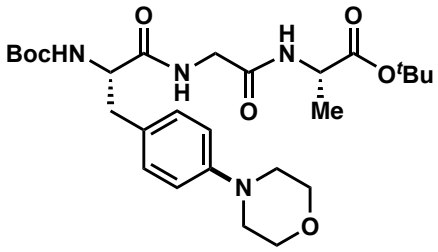

Morpholine (0.15 mmol), peptide **SI-2** (0.05 mmol). Electrolysis was conducted for 6 h following the general peptide procedure. The crude peptide was purified by preparative reverse-phase HPLC method Narrow 7 to afford peptide **53** (13.6 mg, 51%) as a white solid following lyophilization.

HPLC trace

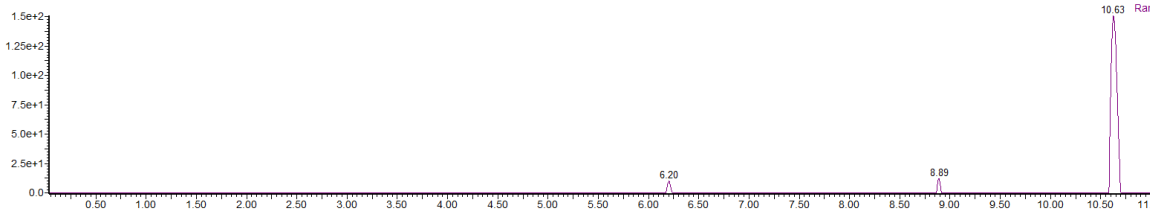

ESI$^-$

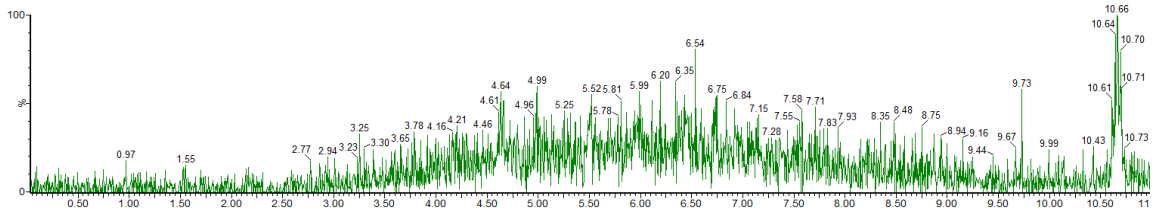

ESI$^+$

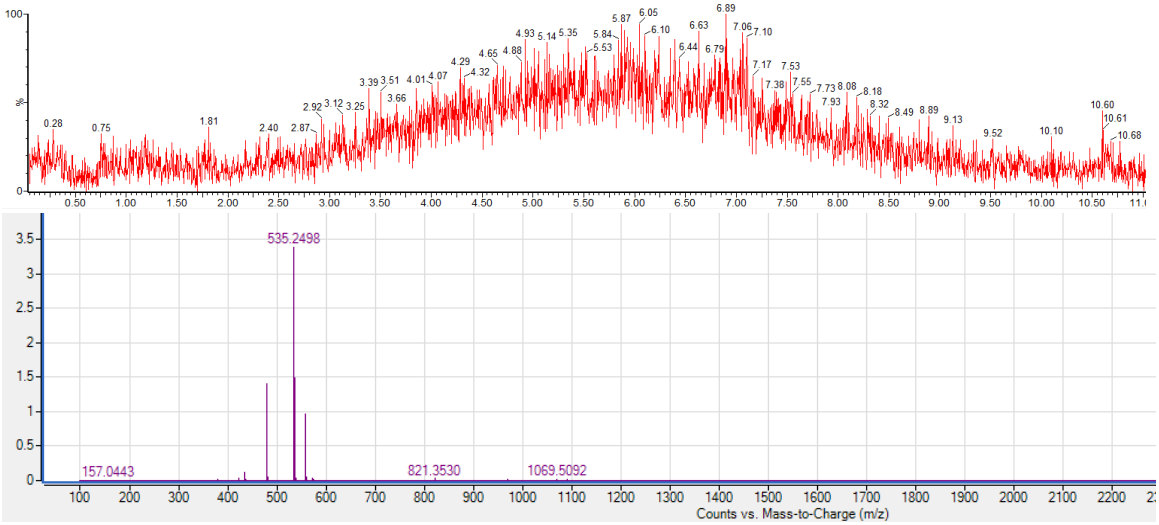

LRMS (ESI-TOF): calc'd for $C_{27}H_{43}N_4O_7$ $[M+H]^+$ 535.31; found 535.25.

Compound 52

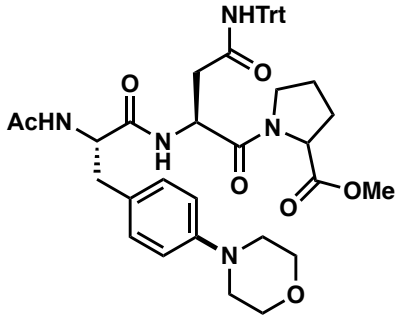

Morpholine (0.15 mmol), peptide **SI-6** (0.05 mmol). Electrolysis was conducted for 6 h following the general peptide procedure. The crude peptide was purified by preparative reverse-phase HPLC method Narrow 7 to afford peptide **54** (21.5 mg, 57%) as a white solid following lyophilization.

HPLC trace

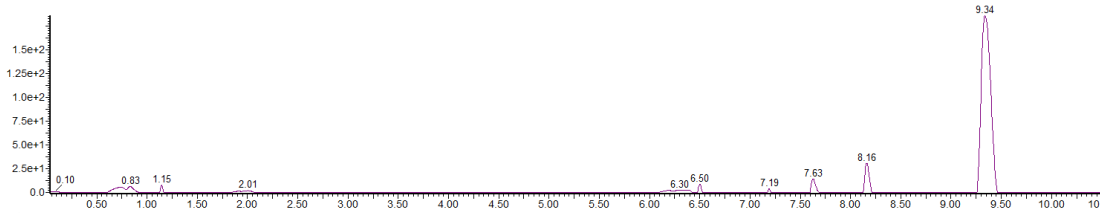

ESI$^-$

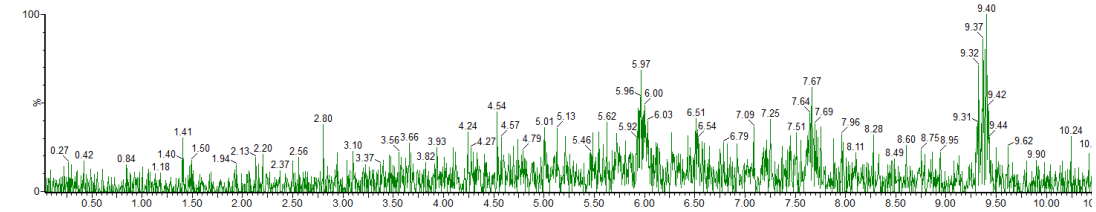

ESI$^+$

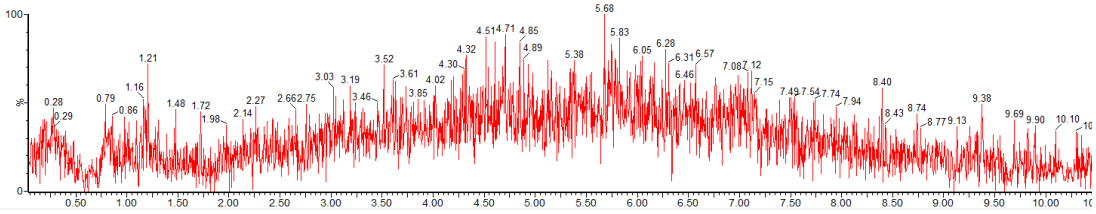

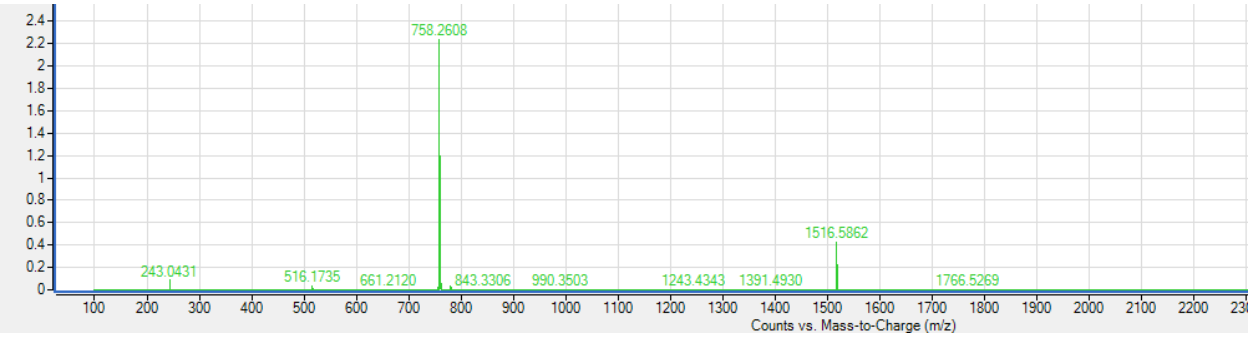

LRMS (ESI-TOF): **calc'd for $C_{44}H_{50}N_5O_7$ $[M+H]^+$ 758.28; found 758.26.**

Compound 53

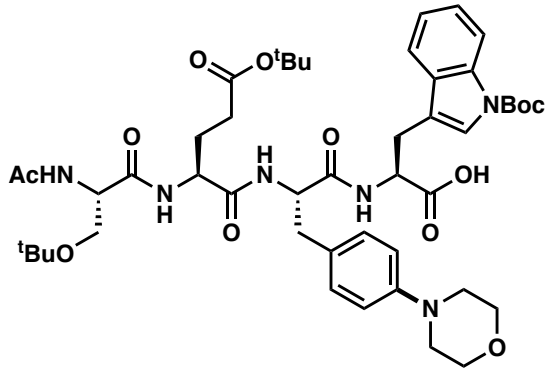

Morpholine (0.15 mmol), peptide **SI-3** (0.05 mmol). Electrolysis was conducted for 6 h following the general peptide procedure. The crude peptide was purified by preparative reverse-phase HPLC method Narrow 5 to afford peptide **55** (10.6 mg, 23%) as a white solid following lyophilization.

HPLC trace

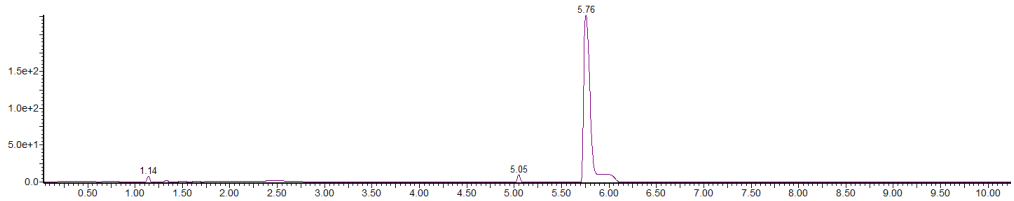

ESI$^-$

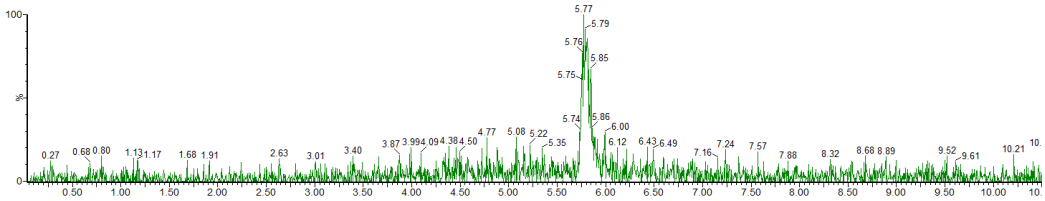

ESI$^+$

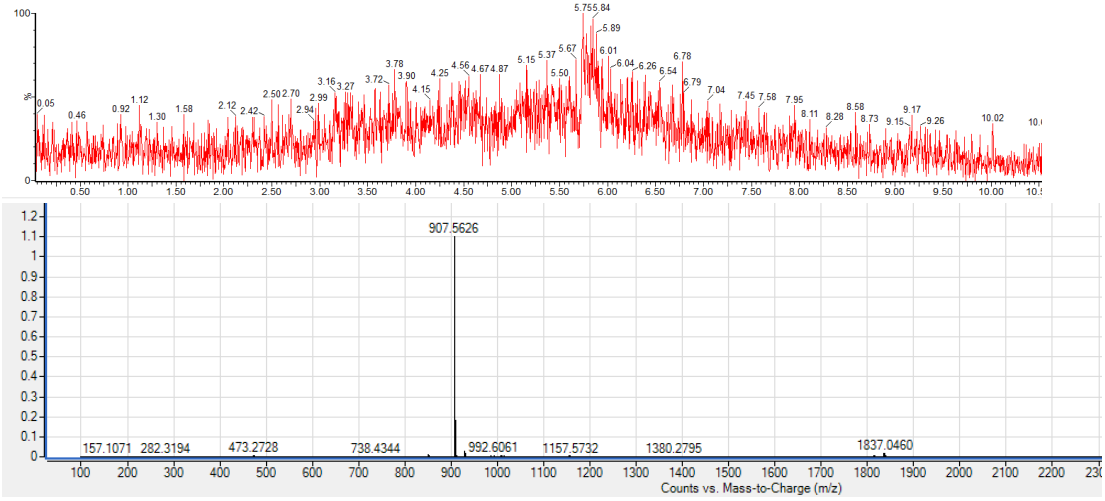

LRMS (ESI-TOF): calc'd for $C_{47}H_{67}N_6O_{12}$ $[M+H]^+$ 907.48; found 907.56.

Compound 54

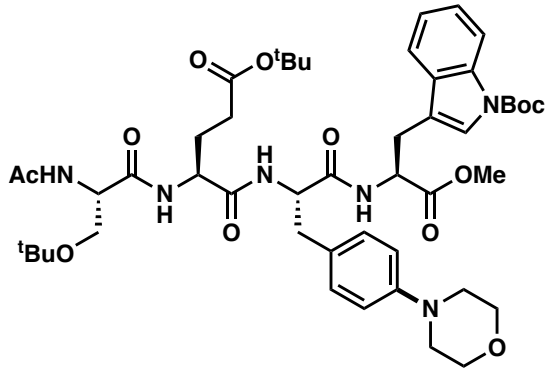

Morpholine (0.15 mmol), peptide **SI-4** (0.05 mmol). Electrolysis was conducted for 6 h following the general peptide procedure. The crude peptide was purified by preparative reverse-phase HPLC method Narrow 6 to afford peptide **56** (14.7 mg, 32%) as a white solid following lyophilization. <u>*Note:*</u> *Peptide **56** was obtained in 45% when using 100 mol% [Ni].*

HPLC trace

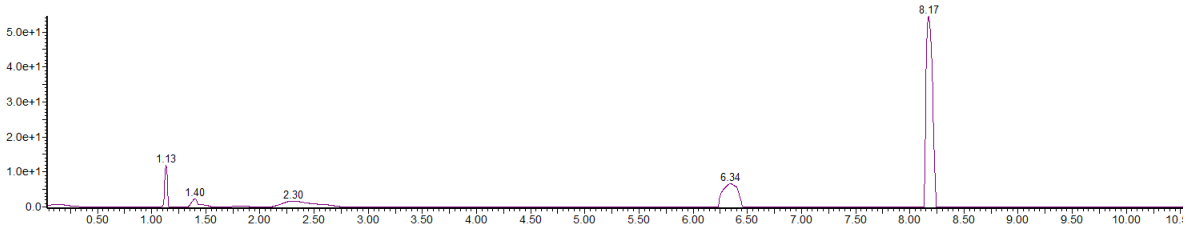

ESI$^-$

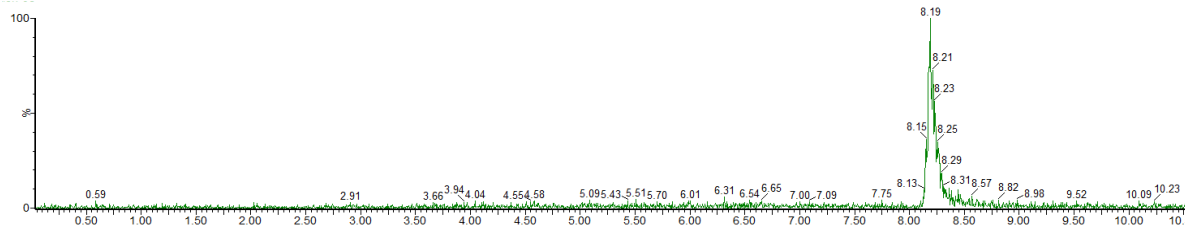

ESI$^+$

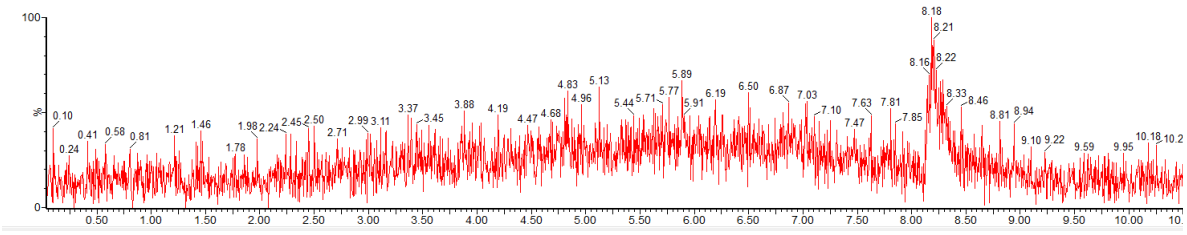

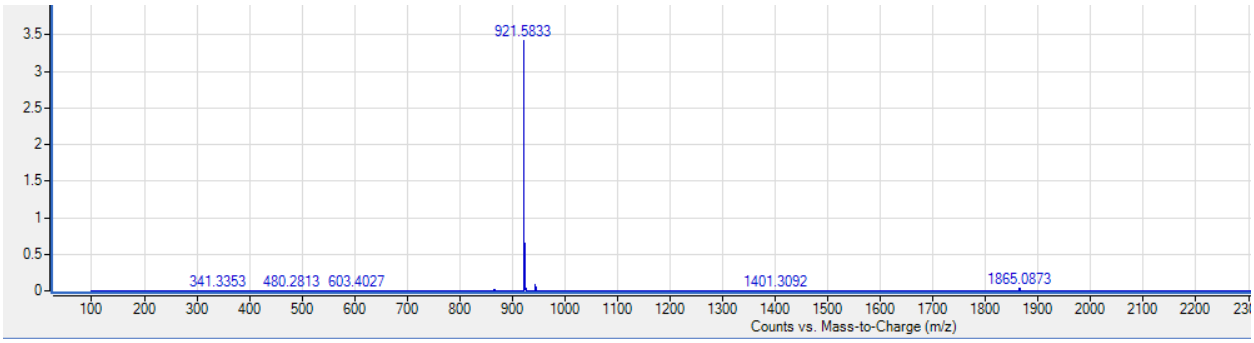

LRMS (ESI-TOF): calc'd for $C_{48}H_{69}N_6O_{12}$ $[M+H]^+$ 921.60; found 921.58.

Compound 55

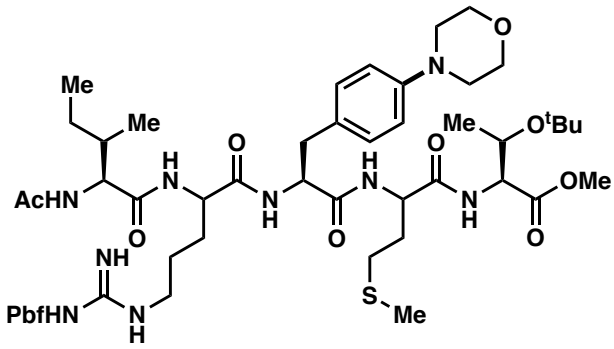

Morpholine (0.15 mmol), peptide **SI-5** (0.05 mmol). Electrolysis was conducted for 6 h following the general peptide procedure. The crude peptide was purified by preparative reverse-phase HPLC method Narrow 6 to afford peptide **57** (21.7 mg, 39%) as a white solid following lyophilization.

HPLC trace

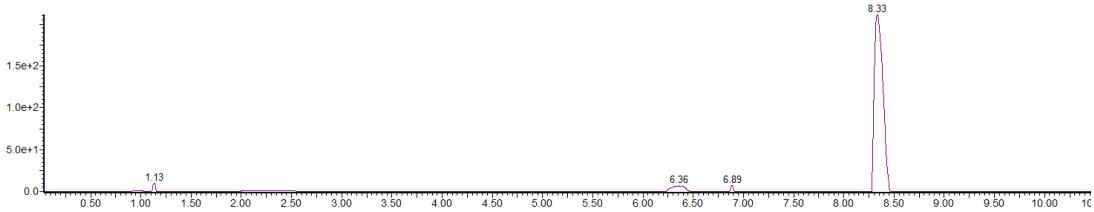

ESI$^-$

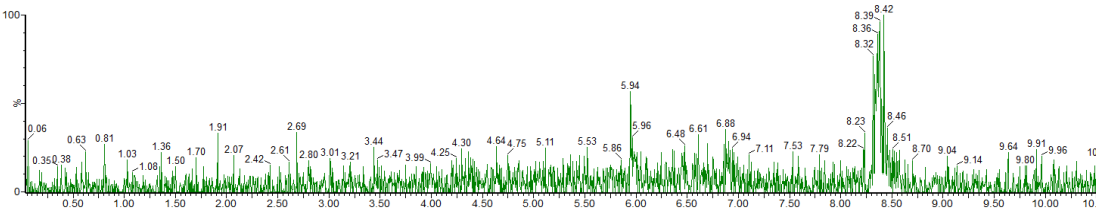

ESI$^+$

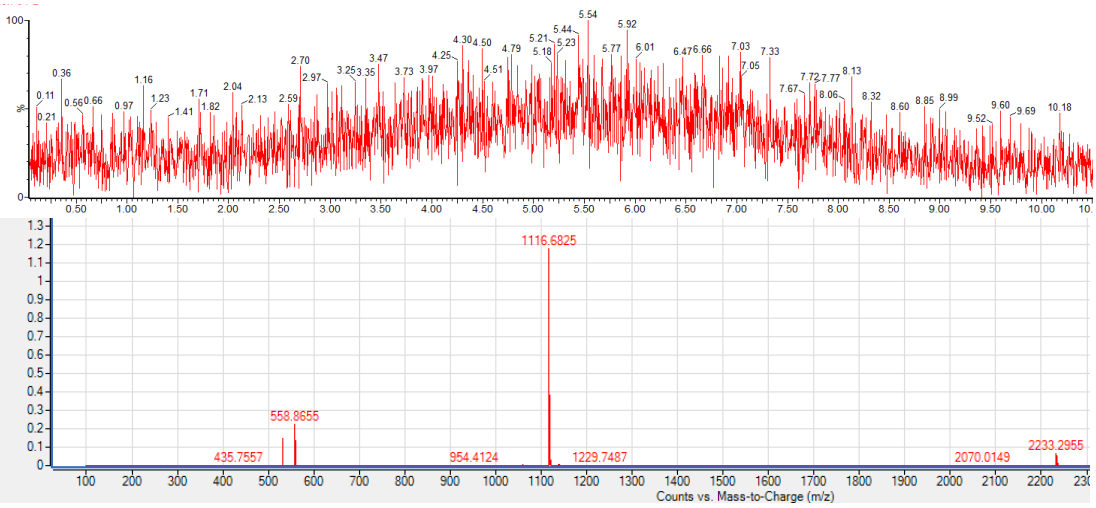

LRMS (ESI-TOF): calc'd for $C_{54}H_{88}N_9O_{12}S_2$ $[M+H]^+$ 1116.56; found 1116.58.

Compound 56

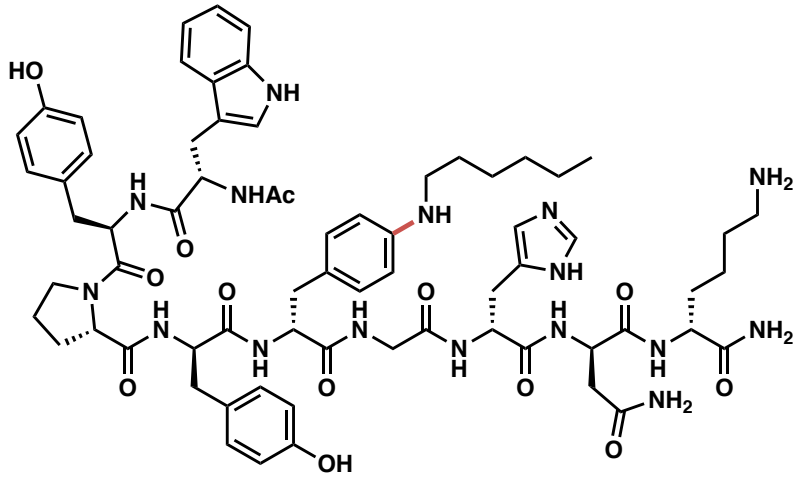

Hexalamine (3mmol), peptide **SI-7** (0.05 mmol), [Ni] (100 mol%). Electrolysis was conducted for 6 h following the general peptide procedure. The crude peptide was purified by preparative reverse-phase HPLC method Narrow 6 to afford peptide **58** (7.4 mg, 11%) as a white solid following lyophilization.

HPLC trace

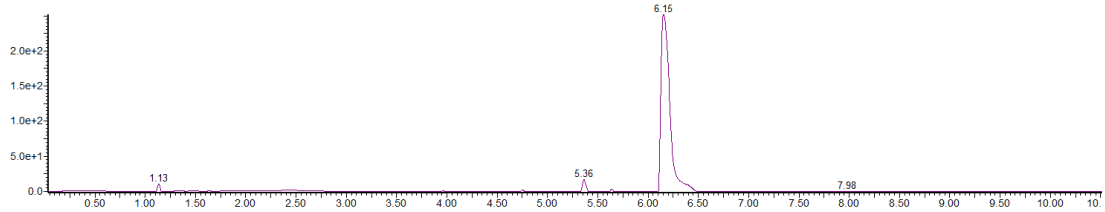

ESI$^-$

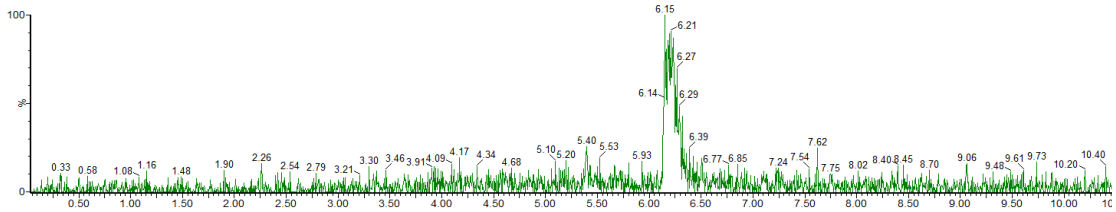

ESI$^+$

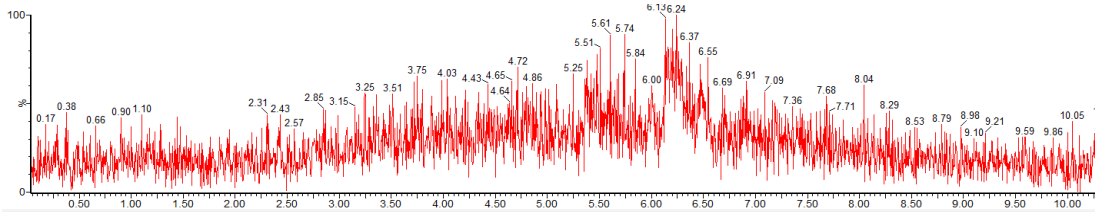

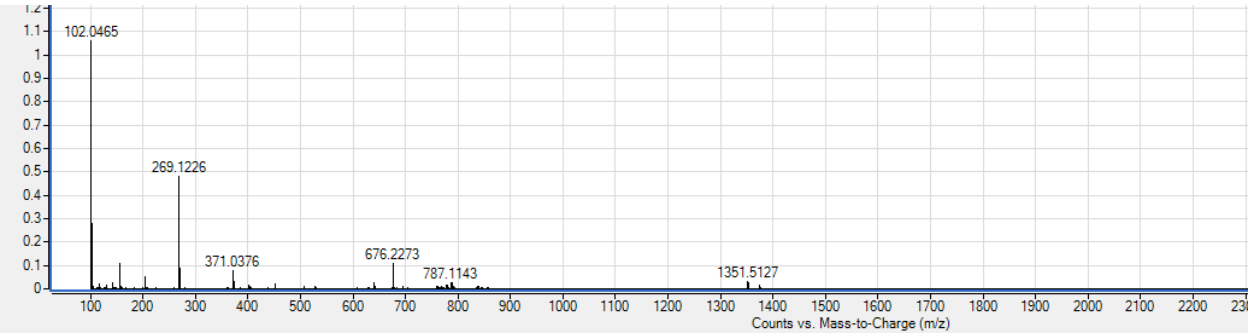

LRMS (ESI-TOF): calc'd for $C_{44}H_{50}N_5O_7$ $[M+H]^+$ 1351.70; found 1351.51.

Figure 4-C – Large scale amination

Experimental detail of 22.5 g scale reaction – Compound 57

Procedure of decagram scale reaction (Performed at Asymchem)

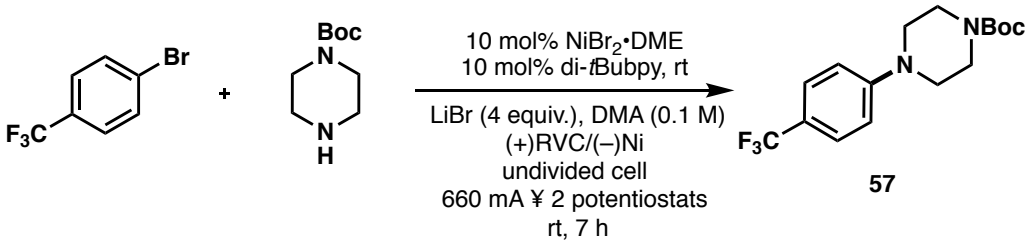

To a clean and dry glass chamber was added DMA (1.5 L), LiBr (52 g, 600 mmol, 4 equiv.), $NiBr_2$•DME (3.08g, 10 mmol, 10 mol%), 4,4'-di-*tert*-butyl-2,2'-bipyridine (2.68g, 10 mmol, 10 mol%), 1-Boc-piperazine (55.88g, 0.3mol, 3 equiv.), and 4-bromobenzotrifluoride (22.50g, 0.1 mol, 1 equiv.). The resulting suspension was stirred until the dissolution of all solids. The RVC anode (two plates) the Ni-foam cathode (two plates) were inserted into the solution; each set of anode/cathode was connected to a potentiostat (EZ-stat pro). The submerged surface area of each electrode was adjusted to 11cm × 15cm. The reaction mixture was deoxygenated by sparging with nitrogen for 30 mins when constant current electrolysis (660 mA for both potentiostats)* was conducted for 7 h under a nitrogen atmosphere. The resulting mixture was poured onto water (7.5 L) and extracted with MTBE (3.4 L × 3). The combined organic layer was concentrated *in vacuo*; the resulting residue was purified by flash column chromatography (silica gel) to afford the desired product **61** as a white solid (22.1 g, 66%).

*Two potentiostats were used as the maximum current output of each unit is 1.0 A.

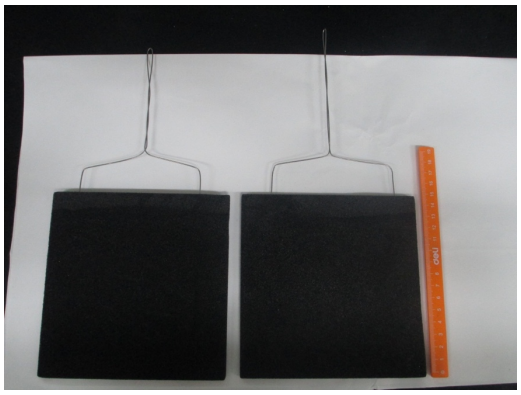

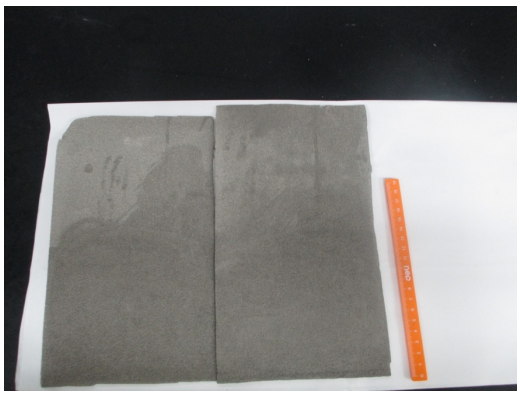

(***Left***) RVC anodes used in the reaction (2 plates, dimensions of each plate: 15 cm × 15 cm × 0.5 cm) (the submerged surface area was 11 cm × 15 cm for each plate). (***Right***) Ni-foam cathodes used in the reaction (2 plates, dimensions of each plate: 15 cm × 25 cm × 0.5 cm) (the submerged exterior surface area was 11 cm × 15 cm for each plate).

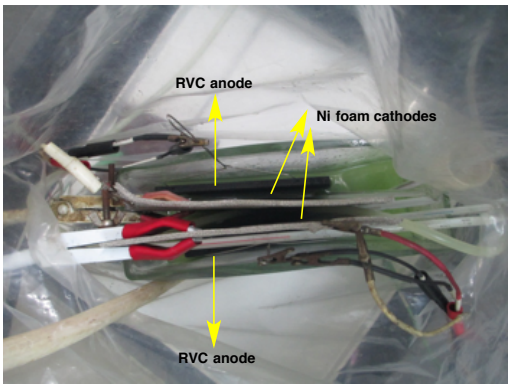

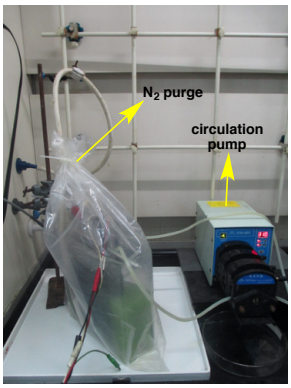

(***Left***) and (***Right***) Electrolysis setup.

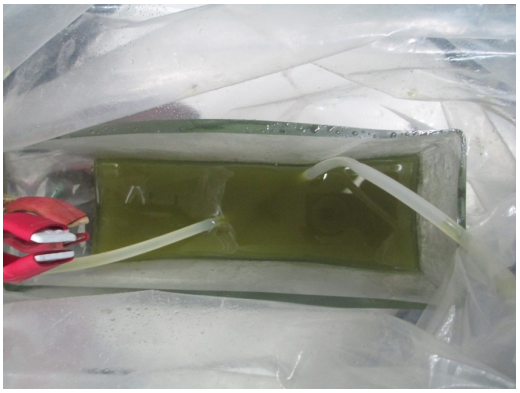

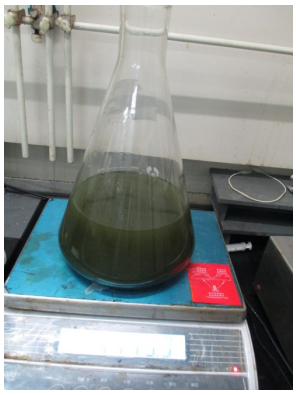

(***Left***) and (***Right***) Reaction mixture after the electrolysis.

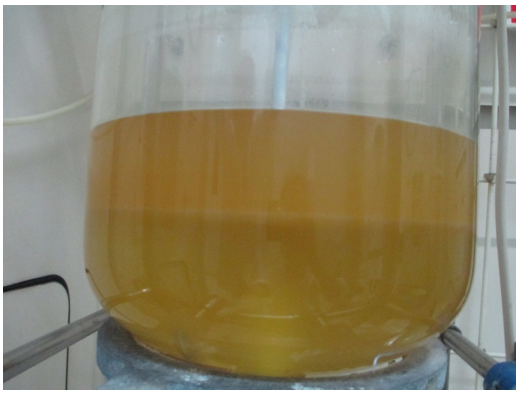

(***Left***) and (***Right***) Extraction of the reaction mixture with MTBE.

Experimental detail of 100 g scale reaction – Compound 36

Multi-Frame Cell setup:

10 stainless steel screws with cap (length: 25.0 cm, diameter: 5.0 mm) were threaded through a base part of multi-frame cell constituted from one Teflon plate (length: 18.0 cm, width: 12.0 cm, thickness: 2.0 cm, with eight holes each has a diameter of 1.0 cm), one Teflon frame block (length: 22.0 cm, width: 12.0 cm, thickness: 2.0 cm, with ten holes each has a diameter of 1.0 cm) and a silicone pad (length: 18.0 cm, width: 12.0 cm, thickness: 2.0 mm, with ten holes each has a diameter of 1.0 cm) between them. The base part with stainless steel screws was then added components topped each layer followed a sequence of silicone pad, graphite plate (as electrode cover, length: 25.0 cm, width: 12.0 cm, thickness: 2.0 mm, with ten holes each has a diameter of 1.0 cm), carbon felt (as electrode, both anode and cathode, length: 15.0 cm, width: 9.0 cm, thickness: 5.0 mm, with an immersion surface area of 13.0 cm×7.0 cm), silicone pad, Teflon frame and carbon felt to form one single working cell. Repeated the adding sequence until a multi-frame cell with total four working cells were packed, ended by putting another base part on the very top layer. The multi-frame cell with a total of 6 frame blocks, 2 Teflon plates, 5 graphite covers, 5 carbon felts and 12 silicone pads were then locked by 10 screw nuts tightened with appropriate force to complete the entire construction. Each side of Teflon frame was screwed a Teflon joint which connected to a rubber tube (6 mm in diameter), the upper joint of four middle frames was connected to the lower joint of its sideward frame, and the joint of two terminal frames was connected to rubber tubes (6 mm in diameter) which through two Teflon tubes (6 mm in diameter) linked with peristaltic pump (as in flow) and external reservoir (as out flow).

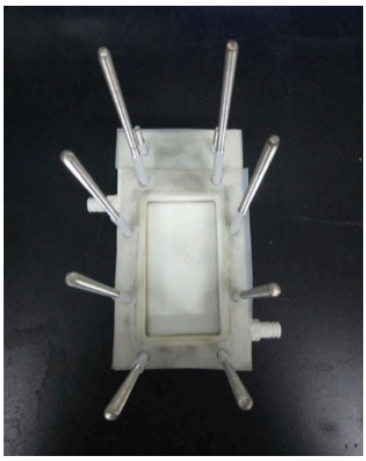

Step 1
Silicon plate on frame

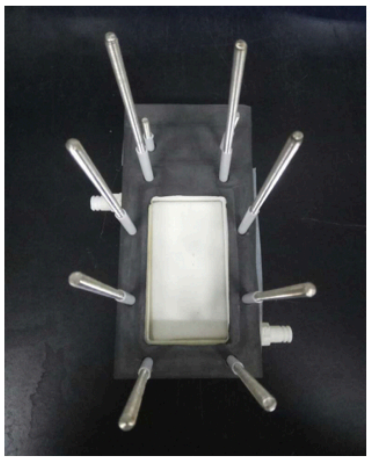

Step 2
Graphite plate on top

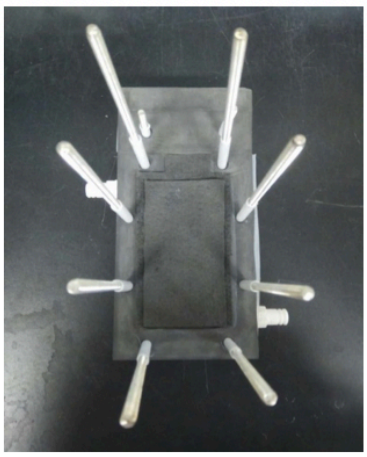

Step 3
Carbon felt on top

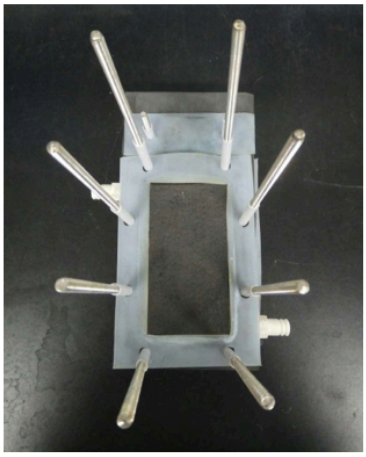

Step 4
Silicon plate on top

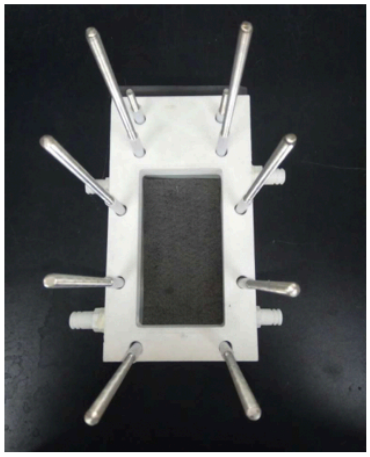

Step 5
Frame on top

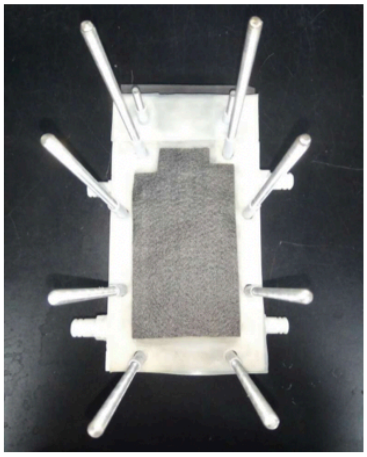

Step 6
Carbon felt on top

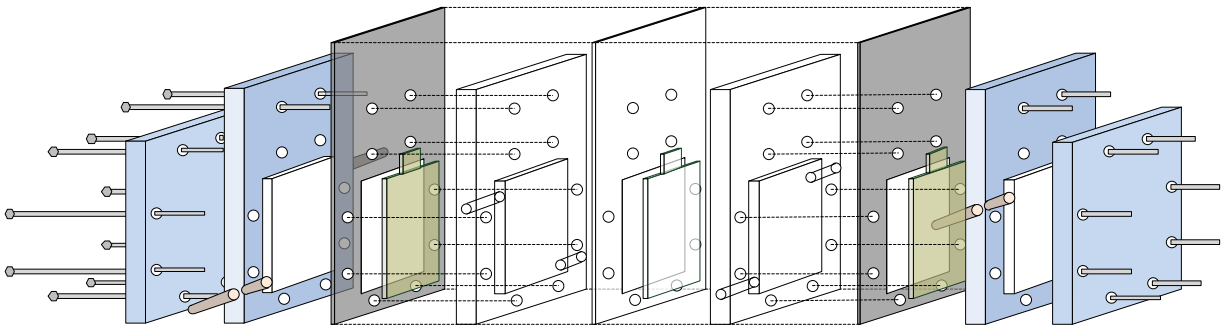

Experimental procedure：

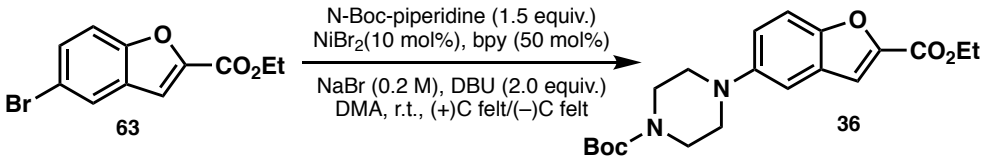

A clean and dry 5.0 L Erlenmeyer flask with a stir bar was charged with $NiBr_2$ (37.2 mmol, 8.13 g, 10 mol%), DMA (3.0 L) was then added and stirred vigorously at room temperature for 10 min until all solid were dissolved and obtained a green color solution. 2,2'-bipyridinyl (186 mmol, 29.0 g, 50 mol%) was added and stirred for another 30 min until solution turn to a pink color. NaBr (0.2 M, 600 mmol, 61.8 g), DBU (744 mmol, 113.1 g, 2.0 equiv.), 5-bromo-benzofuran-2-carboxylic acid ethyl ester **63** (372 mmol, 100.0 g, 1.0 equiv.) and 1-t-Butoxycarbonylpiperazine (558 mmol, 104.3 g, 1.5 equiv.) were added successively under stirring, the obtained solution followed by transferring into a 3.0 L four-necked round bottom as external reservoir. A peristaltic pump was connected to multi-frame cell (4 working cells) and external reservoir (3.0 L four-necked round bottom) by a peristaltic tube (length: 19.0 cm, thickness: 0.8 mm) and two Teflon tubes (length: 15.0 cm to the multi-frame cell and 45.0 cm to the external reservoir, diameter: 6.0 mm) formed a circulatory system. The loop system was then purged with nitrogen for 10 minutes followed by bubbling the reaction mixture with nitrogen for 20 minutes. The reaction mixture was then pumped into multi-frame cell with a flow rate of 500 rpm from external reservoir, set an automatic switch of polarity on all electrodes every 5.0 minutes and electrolyzed under a constant current of 7.2 A provided from a direct current power until the complete consumption of 5-bromo-benzofuran-2-carboxylic acid ethyl ester judged by HPLC. After reaction, all mixture was drove into a 5.0 L Erlenmeyer flask from both multi-frame cell and external reservoir, followed by adding DMA (2x 2.0 L) to the loop and circulated for 10 min to wash the multi-frame cell and flush the residue in tubes twice. The combined solution was poured into three 5.0 L four-necked round bottom with 4.0 L ice water in each and blended vigorously by a two-blade mechanic stir for 30 min. The precipitate was then filtered by a Buchner funnel, the filter cake was crude product as a light brown solid (109.0 g) and was purified by column chromatography (200-300 mesh silica gel, 25.0 cm height in column), washed with eluent (n-Hexane/EtOAc = 10/1) to afford desired product **36** as a light yellow solid (88.9 g, 64 % isolated yield).

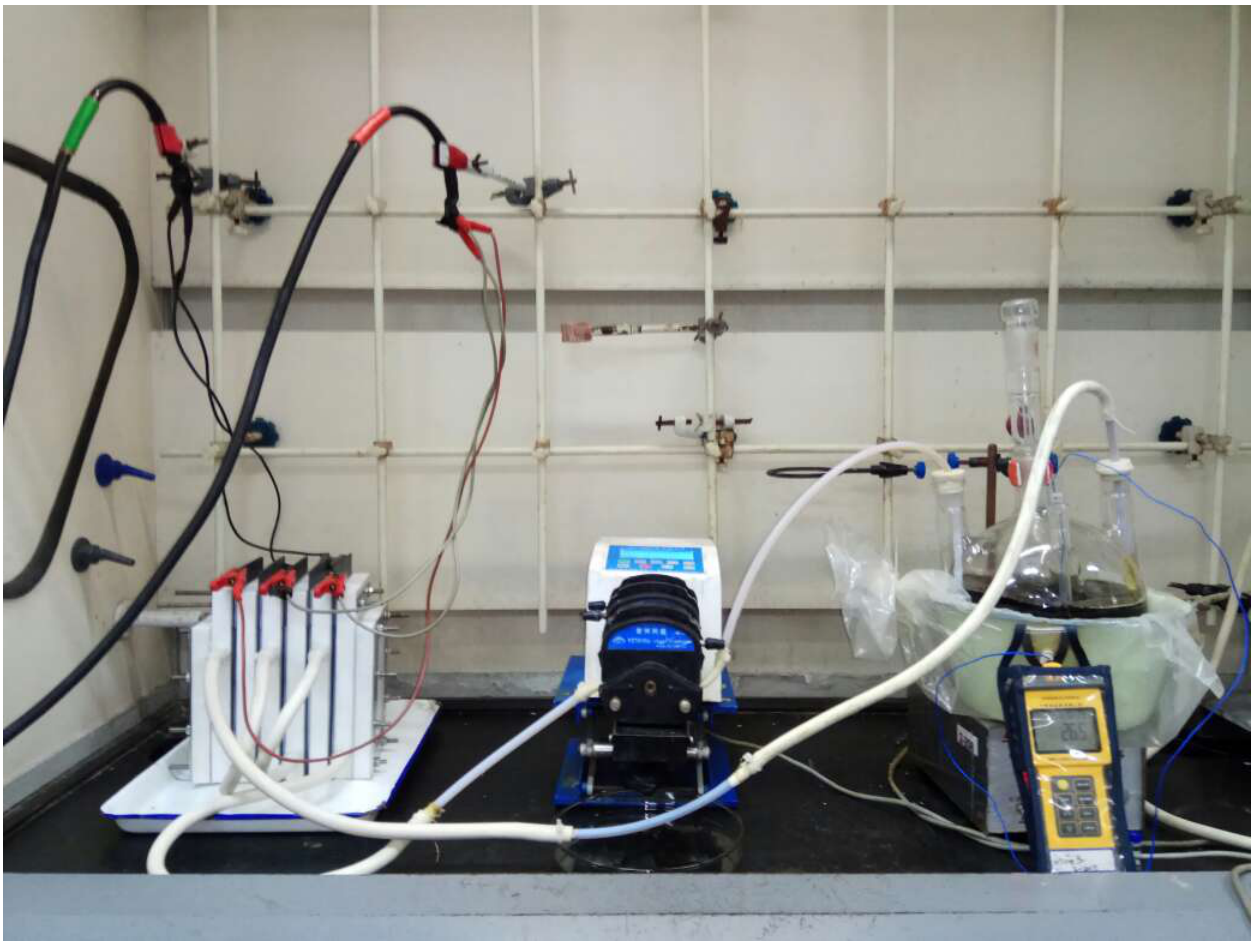

Table 5 – Applicability to previously successful substrates and limitations.

Compound 60

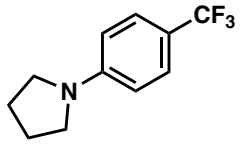

From aryl bromide

Pyrrolidine (0.3 mmol), 1-bromo-4-(trifluoromethyl)benzene (0.2 mmol), DBU (0.4 mmol). Electrolysis was conducted for 4 h following the general procedure. The crude material was purified by PTLC (silica gel, Et_2O:pentane = 1:10) to give the **64** as a colorless oil (54% yield). The spectrum matched with the reported values.[20]

From aryl chloride

Pyrrolidine (0.3 mmol), 1-chloro-4-(trifluoromethyl)benzene (0.2 mmol), DBU (0.4 mmol). Electrolysis was conducted for 4 h following the general procedure. The crude material was purified by PTLC (silica gel, Et_2O:pentane = 1:10) to give the **64** as a colorless oil (69% yield).

From iodide

Pyrrolidine (0.3 mmol), 1-iodo-4-(trifluoromethyl)benzene (0.2 mmol), DBU (0.4 mmol). Electrolysis was conducted for 4 h following the general procedure. The crude material was purified by PTLC (silica gel, Et_2O:pentane = 1:10) to give the **64** as a colorless oil (82% yield).

Compound 61

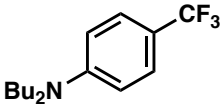

Dibutylamine (0.3 mmol), 1-bromo-4-(trifluoromethyl)benzene (0.2 mmol), DBU (0.4 mmol). Electrolysis was conducted for 4 h following the general procedure. The crude material was purified by PTLC (silica gel, hexanes) to give **65** as a colorless liquid (61% yield). The spectrum matched with the reported values.[20]

Compound 62

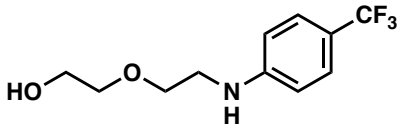

2-(2-aminoethoxy)ethan-1-ol (0.3 mmol), 1-bromo-4-(trifluoromethyl)benzene (0.2 mmol), DBU (0.4 mmol). Electrolysis was conducted for 4 h following the general procedure. The crude material was purified by PTLC (silica gel, Et_2O) to give **66** as a colorless liquid (41% yield). The spectrum matched with the reported values.[20]

Compound 63

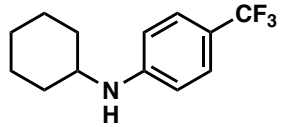

Cyclohexylamine (0.3 mmol), 1-bromo-4-(trifluoromethyl)benzene (0.2 mmol), DBU (0.4 mmol). Electrolysis was conducted for 4 h following the general procedure. The crude material was purified by PTLC (silica gel, EtOAc:hexanes = 1:9) to give the **67** as a colorless liquid (78% yield). The spectrum matched with the reported values.[20]

Compound 64

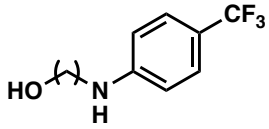

6-aminohexan-1-ol (0.3 mmol), 1-bromo-4-(trifluoromethyl)benzene (0.2 mmol), DBU (0.4 mmol). Electrolysis was conducted for 4 h following the general procedure. The crude material was purified by flash column chromatography (silica gel, EtOAc:hexanes = 3:7) to give **68** as a colorless oil (53% yield). The spectrum matched with the reported values.[20]

Compound 65

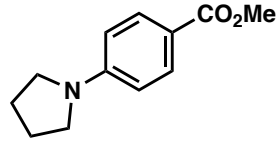

Pyrrolidine (0.3 mmol), methyl 4-(((trifluoromethyl)sulfonyl)oxy)benzoate (0.2 mmol), DBU (0.4 mmol). Electrolysis was conducted for 4 h following the general procedure. The crude material was purified by PTLC (silica gel, Et_2O:hexanes = 3:7) to give the **69** as a white solid (75% yield). The spectrum matched with the reported values.[20]

Compound 66

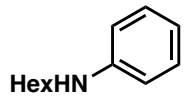

Hexalamine (0.3 mmol), bromophenyl (0.2 mmol), DBU (0.4 mmol). Electrolysis was conducted for 4 h following the general procedure. The crude material was purified by PTLC (silica gel, Et_2O:pentane = 1:15) to give **70** as a colorless liquid (76% yield). The spectrum matched with the reported values.[20]

Compound 67

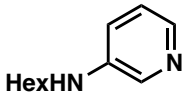

Hexalamine (0.3 mmol), 3-brompyridine (0.2 mmol), DBU (0.4 mmol). Electrolysis was conducted for 4 h following the general procedure. The crude material was purified by flash column chromatography (silica gel, EtOAc:hexanes = 1:3) to give **71** as a white solid (54% yield). The spectrum matched with the reported values.[20]

Compound 68

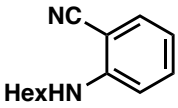

Hexalamine (0.3 mmol), 2-bromobenzonitrile (0.2 mmol), DBU (0.4 mmol). Electrolysis was conducted for 4 h following the general procedure. The crude material was purified by PTLC (silica gel, EtOAc:hexanes = 1:6) to give **72** as a colorless liquid (29 mg, 65% yield). The spectrum matched with the reported values.[20]

Compound 70

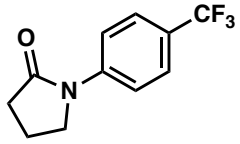

Pyrrolidin-2-one (0.3 mmol), 1-bromo-4-(trifluoromethyl)benzene (0.2 mmol), DBU (0.4 mmol). Electrolysis was conducted for 4 h following the general procedure. The crude material was purified by PTLC (silica gel, EtOAc:hexanes = 2:3) to give **74** as a white solid (29 mg, 67% yield). The spectrum matched with the reported values.[20]

Compound 71

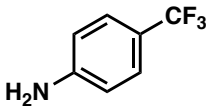

Ammonium hydroxide (2 mmol), 1-bromo-4-(trifluoromethyl)benzene (0.2 mmol), DBU (0.6 mmol). Electrolysis was conducted for 4 h following the general procedure. The crude material was purified by PTLC (silica gel, EtOAc:hexanes = 1:1) to give **75** as a yellow solid (14% yield). The spectrum matched with the reported values.[21]

Compound 73

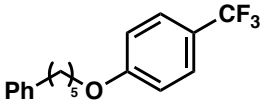

6-phenylhexan-1-ol (0.3 mmol), 1-bromo-4-(trifluoromethyl)benzene (0.2 mmol), DBU (0.4 mmol). Electrolysis was conducted for 4 h following the general procedure. The crude material was purified by PTLC (silica gel, EtOAc:hexanes = 1:20) to give **77** as a colorless oil (37% yield). The spectrum matched with the reported values.[20]

Compound 74

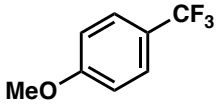

Methanol (2 mmol), 1-bromo-4-(trifluoromethyl)benzene (0.2 mmol), DBU (0.6 mmol). Electrolysis was conducted for 4 h following the general procedure. The crude material was purified by PTLC (silica gel, EtOAc:hexanes = 1:20) to give **78** as a white solid (32% yield). The spectrum matched with the reported values.[22]

Compound 75

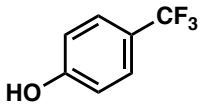

Water (4 mmol), 1-bromo-4-(trifluoromethyl)benzene (0.2 mmol), DBU (0.6 mmol). Electrolysis was conducted for 4 h following the general procedure. The crude material was purified by PTLC (silica gel, EtOAc:hexanes = 1:2) to give **79** as a white solid (43% yield). The spectrum matched with the reported values.[23]

References

1. Varizhuk, A. M.; Kochetkova, S. V.; Kolganova, N. A.; Timofeev, E. N.; Florent'ev, V. L. *Russ. J. Bioorg. Chem.* **2010**, *36*, 199–206.
2. Štefko, M.; Pohl, R.; Klepetářová, B.; Hocek, M. *Eur. J. Org. Chem.* **2008**, *2008*, 1689–1704.
3. Amatore, C.; Azzabi, M.; Calas, P.; Jutand, A.; Lefrou, C.; Rollin, Y., *J. Electroanal. Chem. and Interfacial Electrochem.* **1990,** *288*, 45–63.
4. Denuault, G.; Mirkin, M. V.; Bard, A. J. *Eletroanal. Chem.* **1991**, *308*, 27–38.
5. Newman, J. *J. Electrochem. Soc.* **1966**, *113*, 501–502.
6. Gutierrez, O.; Tellis, J. C.; Primer, D. N.; Molander, G. A.; Kozlowski, M. C., *J. Am. Chem. Soc.* **2015,** *137*, 4896–4899.
7. Kalvet, I.; Guo, Q.; Tizzard, G. J.; Schoenebeck, F. *ACS Cat.* **2017,** *7*, 2126-2132.
8. J. Frisch, G. W. Trucks, H. B. Schlegel, G. E. Scuseria, M. A. Robb, J. R. Cheeseman, G. Scalmani, V. Barone, G. A. Petersson, H. Nakatsuji, X. Li, M. Caricato, A. Marenich, J. Bloino, B. G. Janesko, R. Gomperts, B. Mennucci, H. P. Hratchian, J. V. Ortiz, A. F. Izmaylov, J. L. Sonnenberg, D. Williams-Young, F. Ding, F. Lipparini, F. Egidi, J. Goings, B. Peng, A. Petrone, T. Henderson, D. Ranasinghe, V. G. Zakrzewski, J. Gao, N. Rega, G. Zheng, W. Liang, M. Hada, M. Ehara, K. Toyota, R. Fukuda, J. Hasegawa, M. Ishida, T. Nakajima, Y. Honda, O. Kitao, H. Nakai, T. Vreven, K. Throssell, J. A. Montgomery, Jr., J. E. Peralta, F. Ogliaro, M. Bearpark, J. J. Heyd, E. Brothers, K. N. Kudin, V. N. Staroverov, T. Keith, R. Kobayashi, J. Normand, K. Raghavachari, A. Rendell, J. C. Burant, S. S. Iyengar, J. Tomasi, M. Cossi, J. M. Millam, M. Klene, C. Adamo, R. Cammi, J. W. Ochterski, R. L. Martin, K. Morokuma, O. Farkas, J. B. Foresman, and D. J. Fox, Gaussian, Inc., Wallingford CT, **2016**.
9. Zhao, Y.; Truhlar, D. G. *J. Chem. Phys.* **2006**, *125*, 19410–194118.
10. Dolg, M.; Wedig, U.; Stoll, H.; Preuss, H. *J. Chem. Phys.* **1987**, *86*, 866–872.
11. Bergner, A.; Dolg, M.; Kuechle, W.; Stoll, H.; H, Preuss, H. *Mol. Phys.* **1993**, *80*, 1431–1441.
12. Marenich, A. V.; Cramer, C. J.; Truhlar, D. G. *J. Phys. Chem.* **2009**, *113*, 6378–6396.
13. Henkelman, G.; Uberuaga, B.P., Jónsson, H. J. *Chem. Phys.* **2000**, *113*, 9901–9904.
14. Henkelman, G.; Jónsson, H. *J. Chem. Phys.* **2000**, *113*, 9978–9985.
15. Marcus, Y. Ions in solutions and their solvation, **2015** John Wiley & Sons, Inc.
16. Chowdhury, D. R.; Spiccia, L.; Amritphale, S. S.; Paul, A.; Singh, A. *J. Mater. Chem. A*, **2016**, *4*, 3655–3660.
17. Hendrick, C. E.; Bitting, K. J.; Cho, S.; Wang, Q. *J. Am. Chem. Soc.* **2017**, *139*, 11622–11628.
18. Shao, Q.-L.; Jiang, Z.-J.; Su, W.-K. *Tetrahedron Lett.* **2018**, *59*, 2277–2280.
19. Sommerfeld, T. L.; Seebach, D. *Helv Chim Acta.* **2003**, *76*, 1702–1714.
20. Li, C.; Kawamata, Y.; Nakamura, H.; Vantourout, J. C.; Liu, Z.; Hou, Q.; Bao, D.; Starr, J. T.;

Chen, J.; Yan, M.; Baran, P. S. *Angew. Chem. Int. Ed.* **2017**, *56*, 13088–13093.

21. Han-Sem, K. *Tetrahedron Lett.* **2018**, 59, 4597–4601.
22. Song-Lin, Z.; Wen-Feng, B. *RSC Advances*, **2016**, *6*, 70902–70906.
23. Gao, X.; Geng, Y.; Han, S.; Liang, A.; Li, J.; Zou, D.; Wu, Y.; Wu, Y. *Org. Lett.* **2018**, *20*, 3732–3735.

Compounds Spectra

Compound 15 ^{1}H NMR

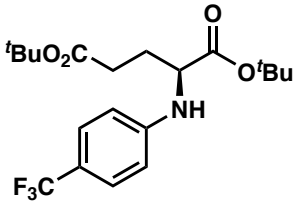

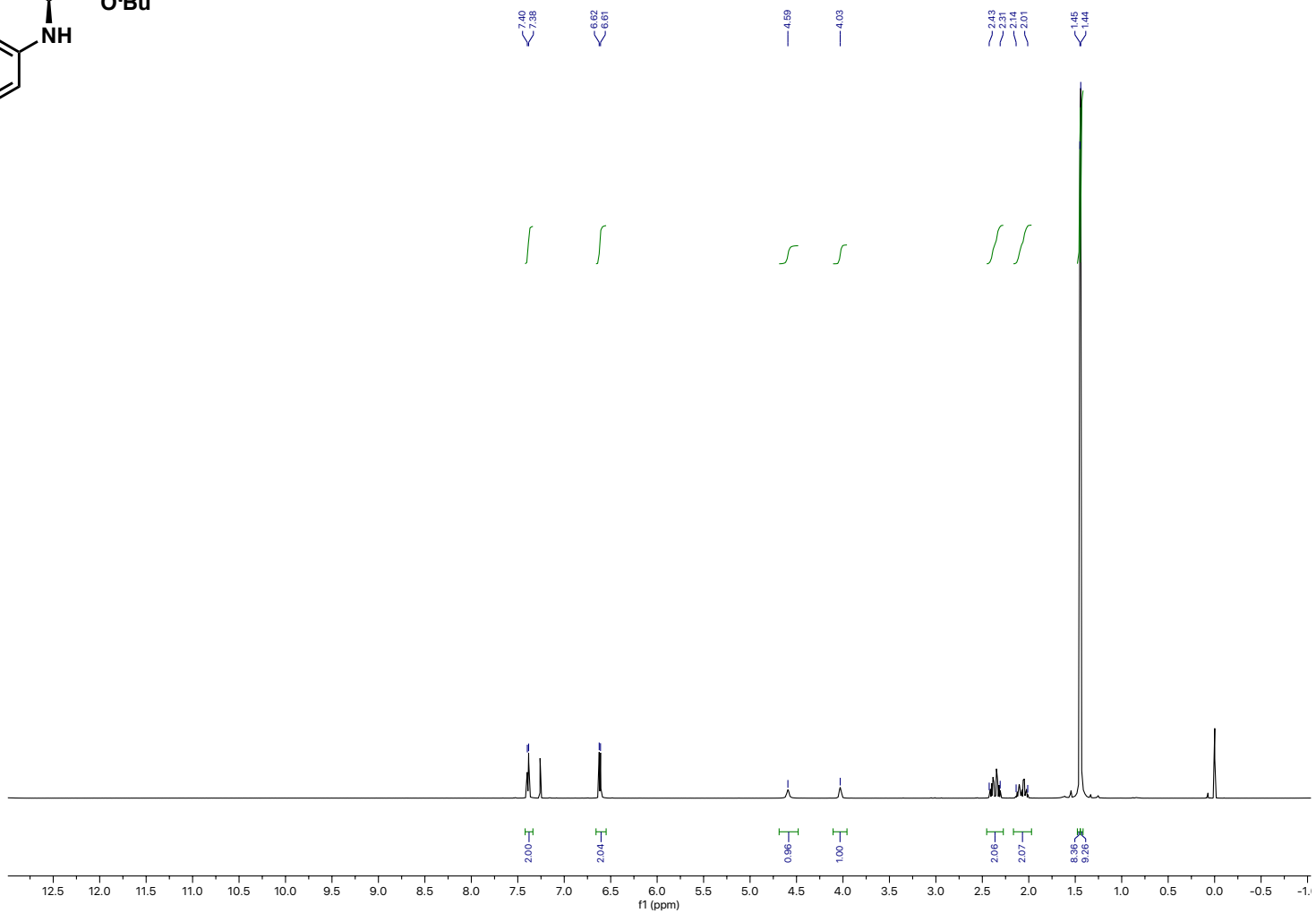

Compound 15 ^{13}C NMR

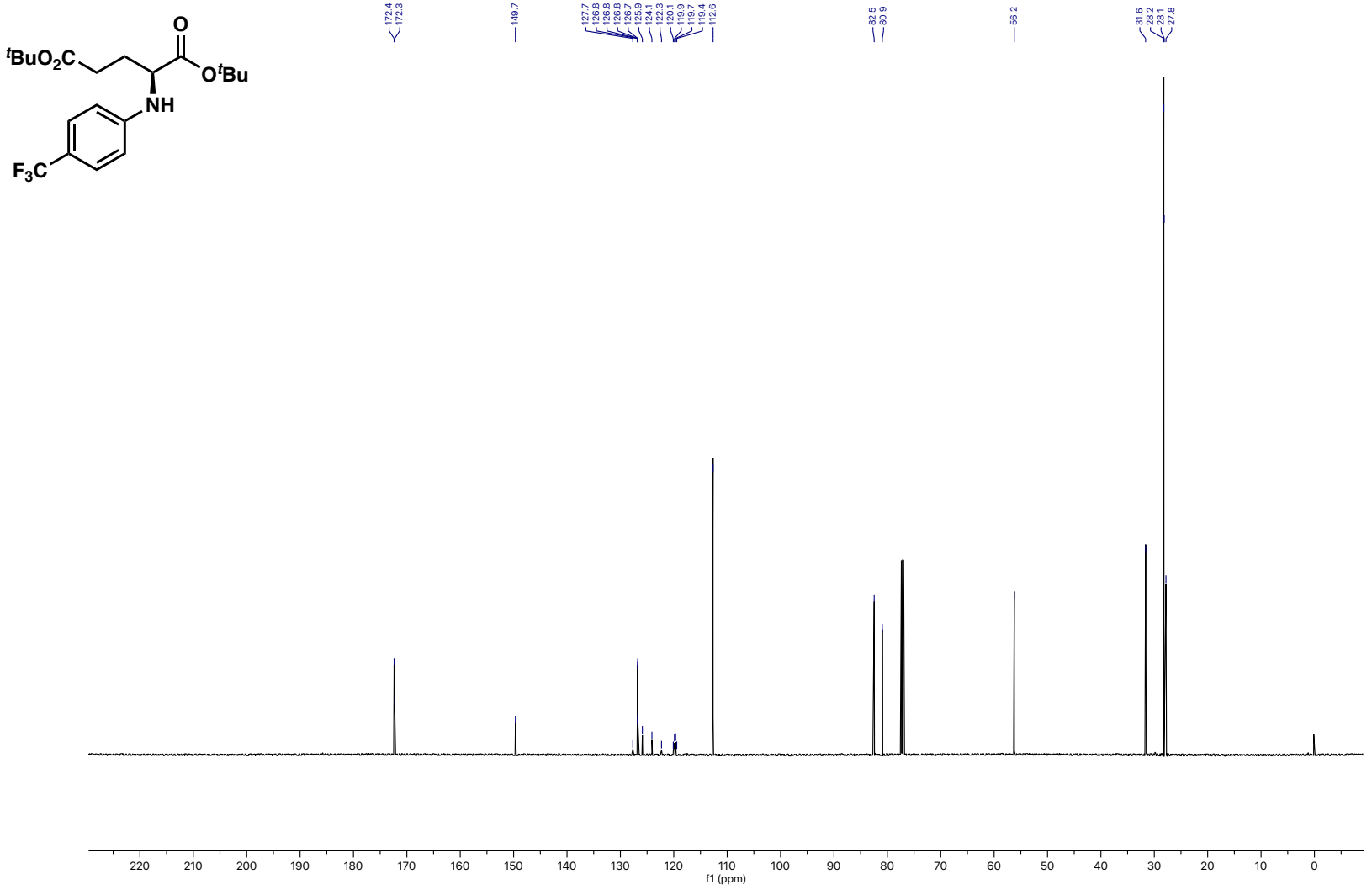

Compound 15 ^{19}F NMR

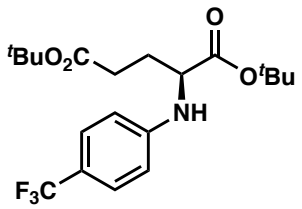

Compound 18 ^{1}H NMR

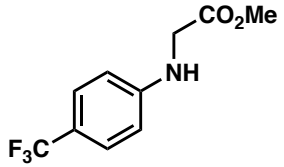

Compound 18 ^{13}C NMR

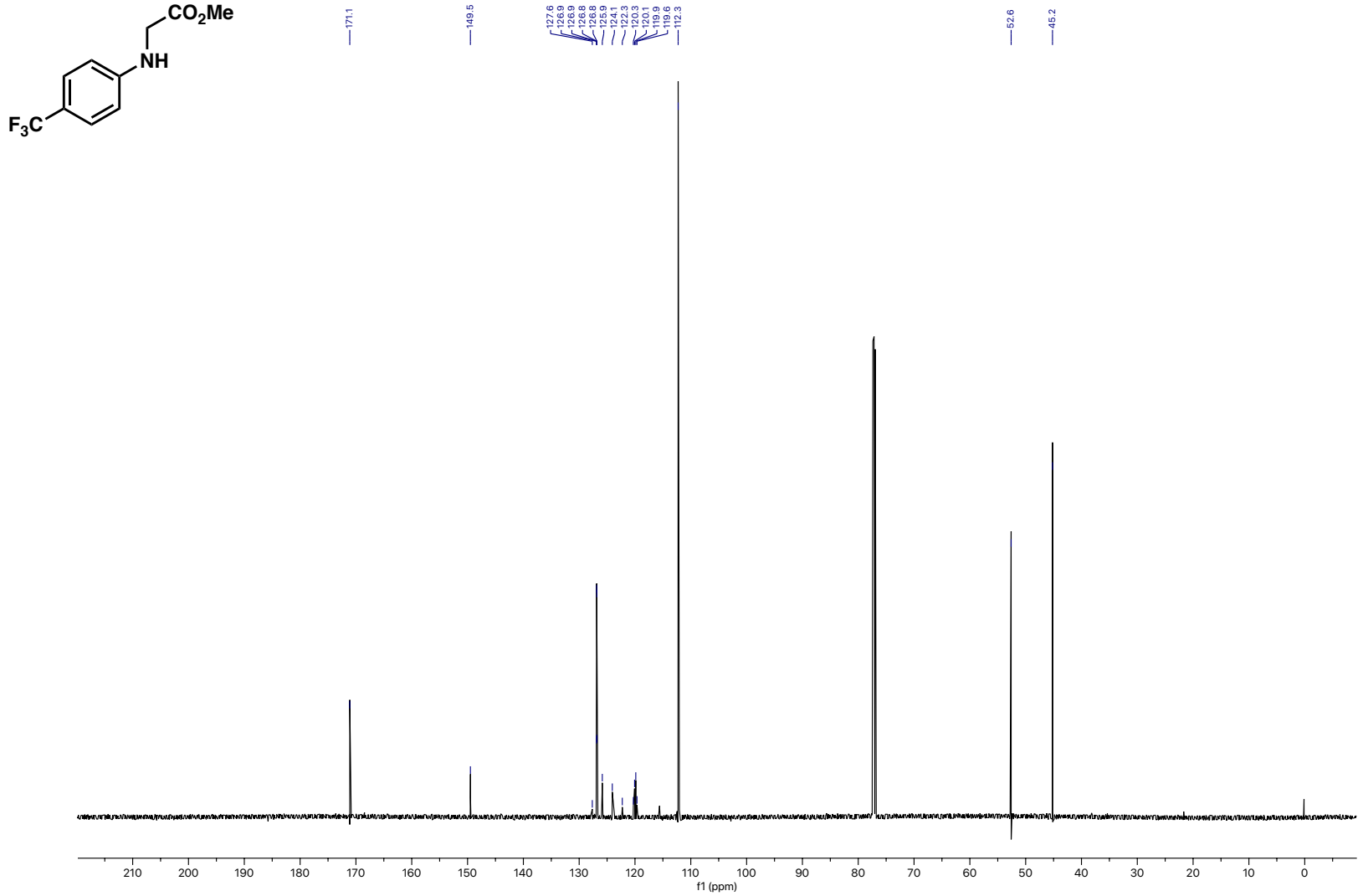

Compound 18 ^{19}F NMR

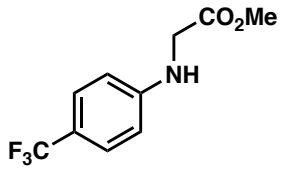

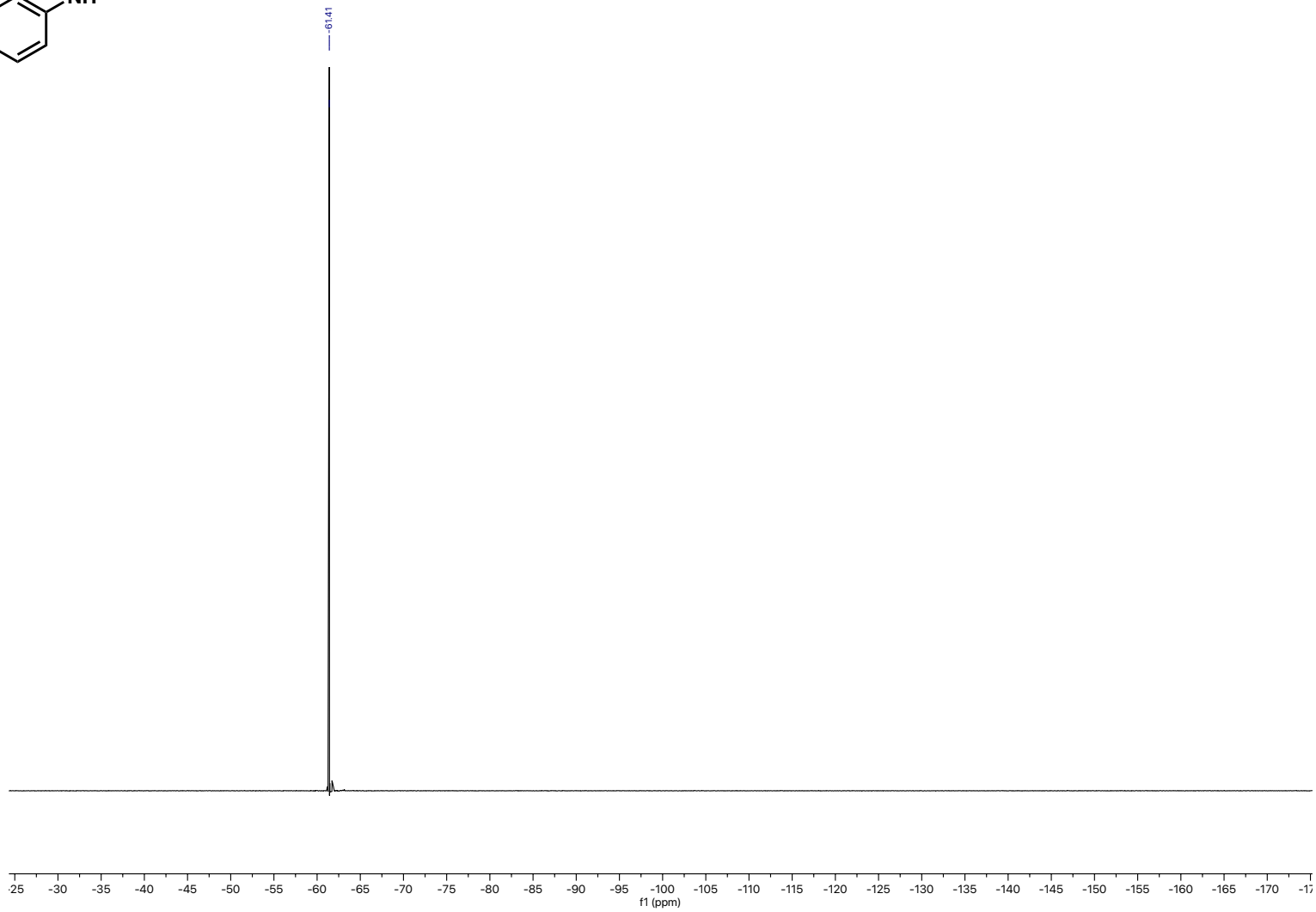

Compound 19 ^{1}H NMR

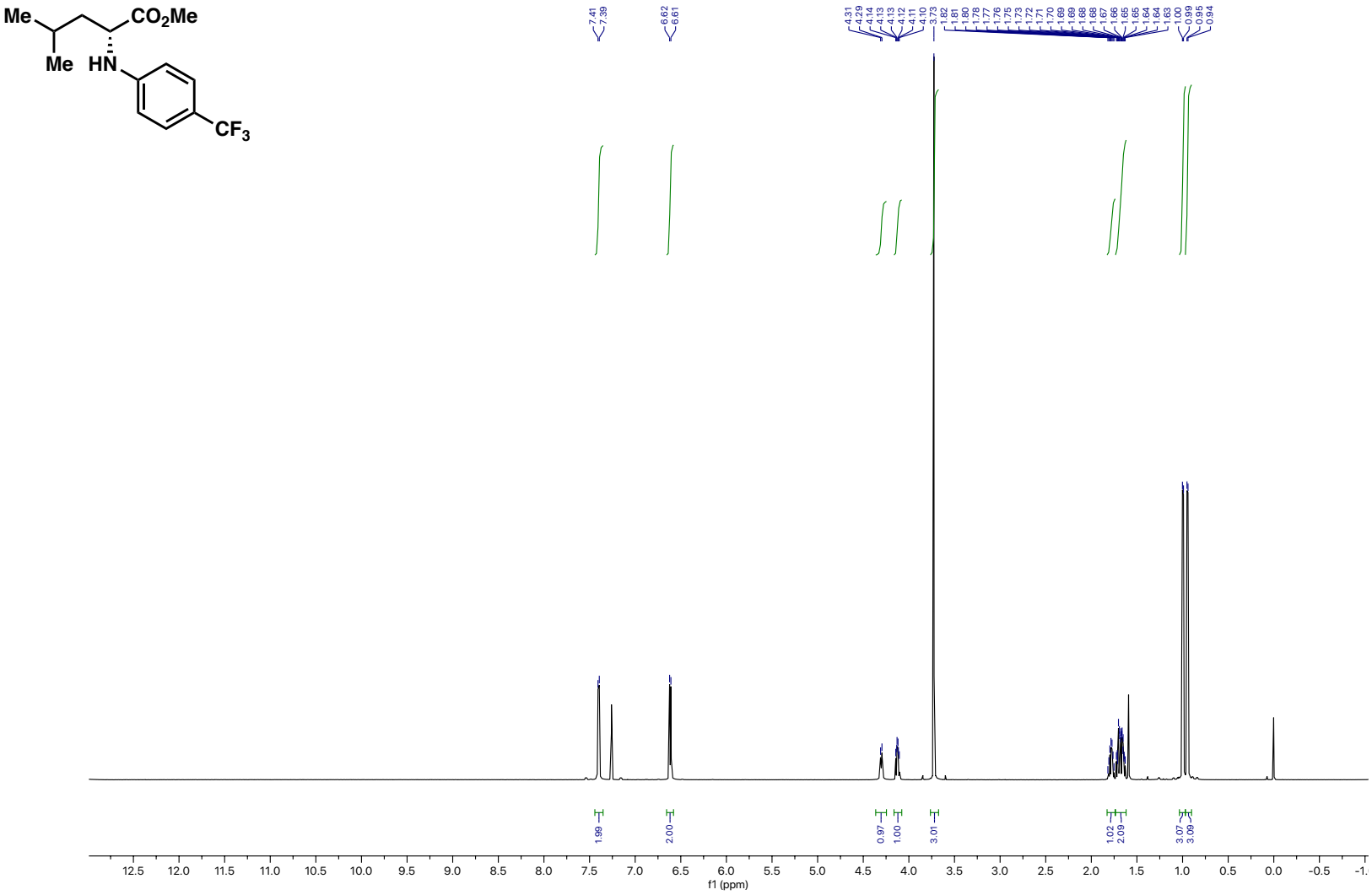

Compound 19 ^{13}C NMR

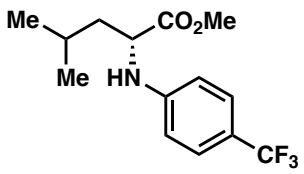

Compound 19 ^{19}F NMR

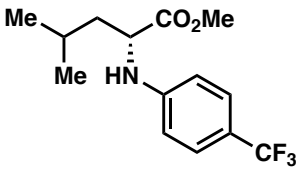

Compound 20 ^{1}H NMR

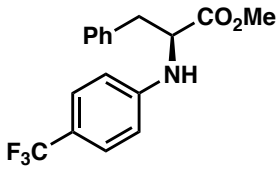

Compound 20 ^{13}C NMR

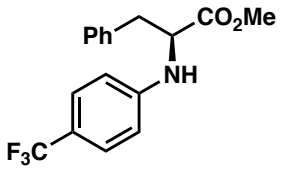

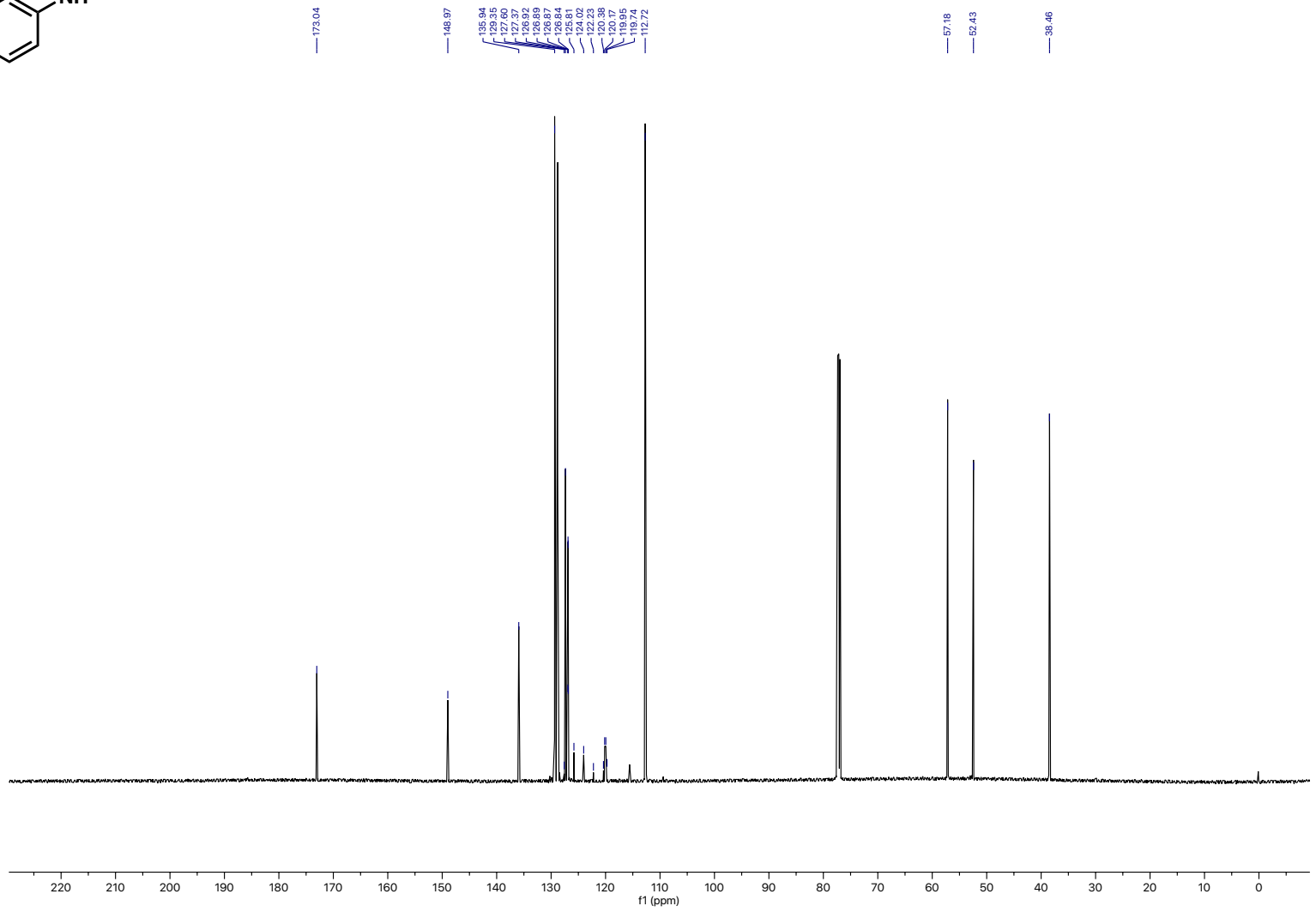

Compound 20 ^{19}F NMR

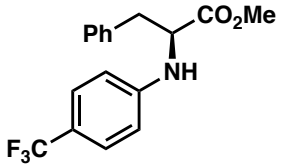

Compound 21 ^{1}H NMR

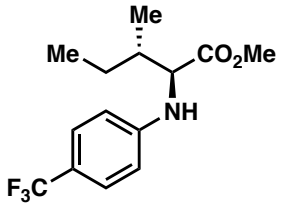

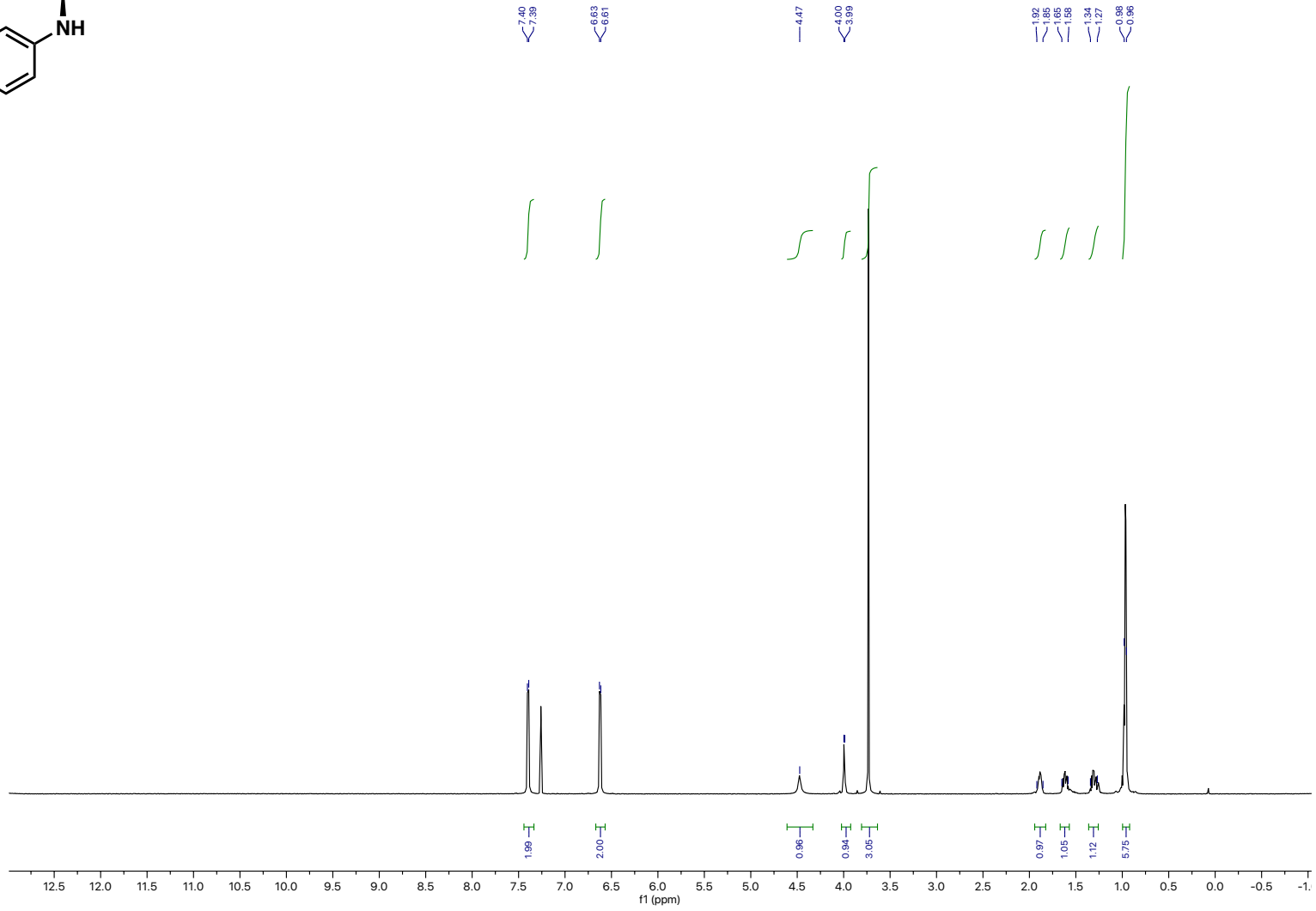

Compound 21 ^{13}C NMR

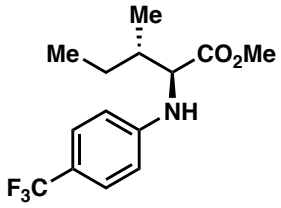

Compound 21 ^{19}F NMR

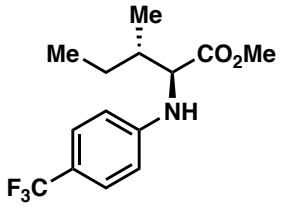

Compound 22 ^{1}H NMR

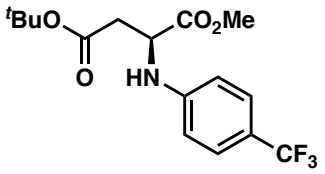

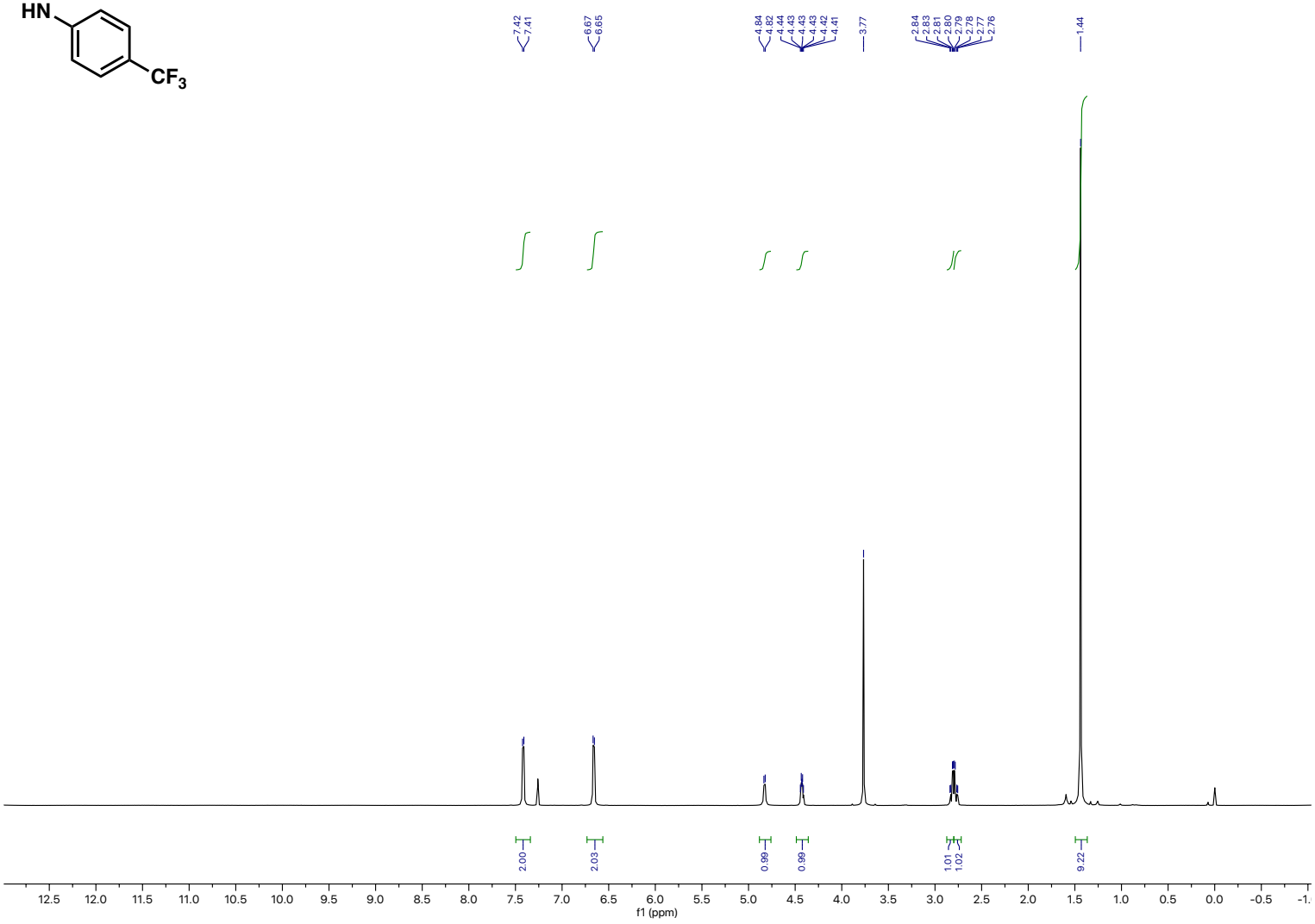

Compound 22 ^{13}C NMR

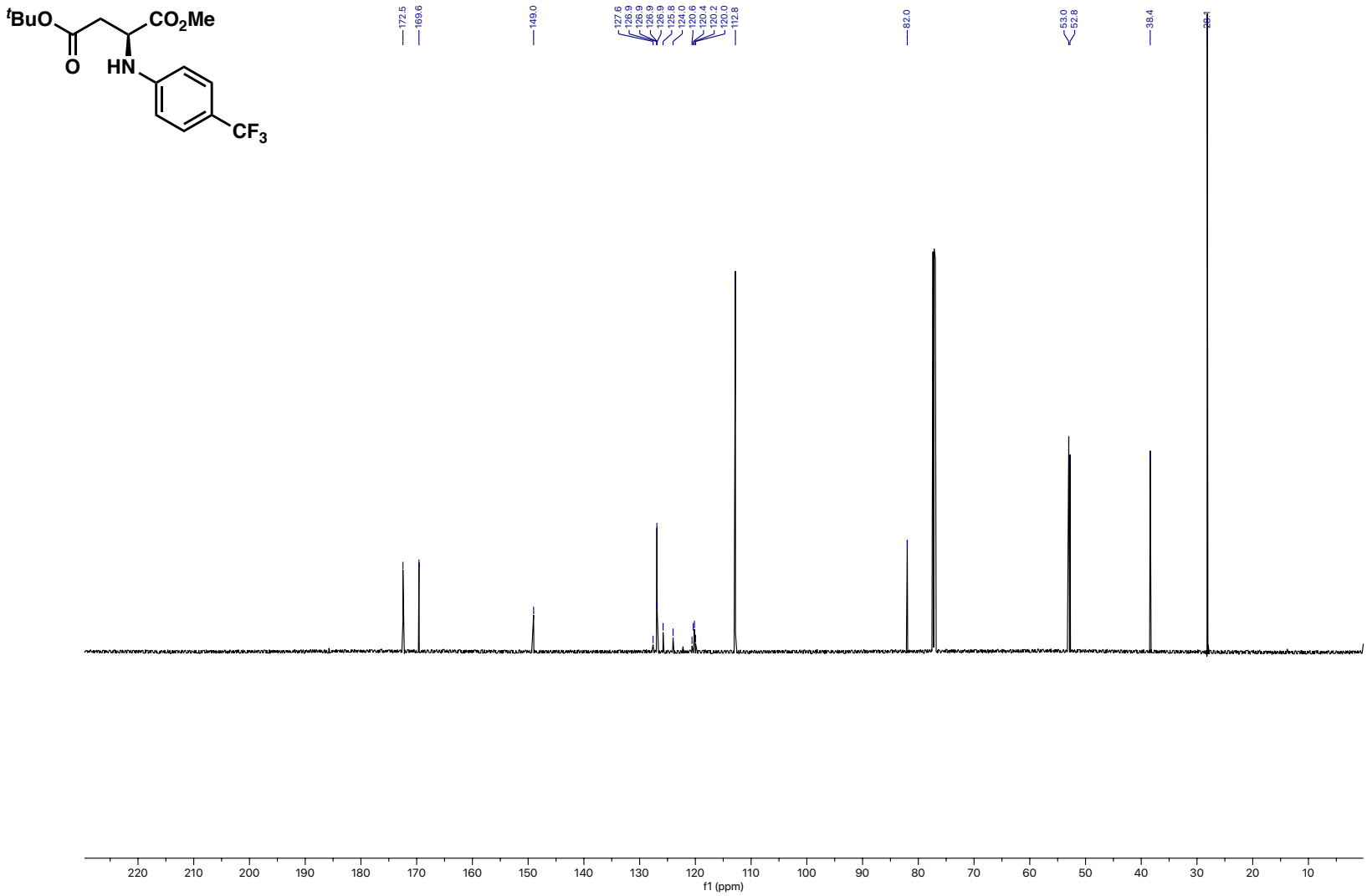

Compound 22 ^{19}F NMR

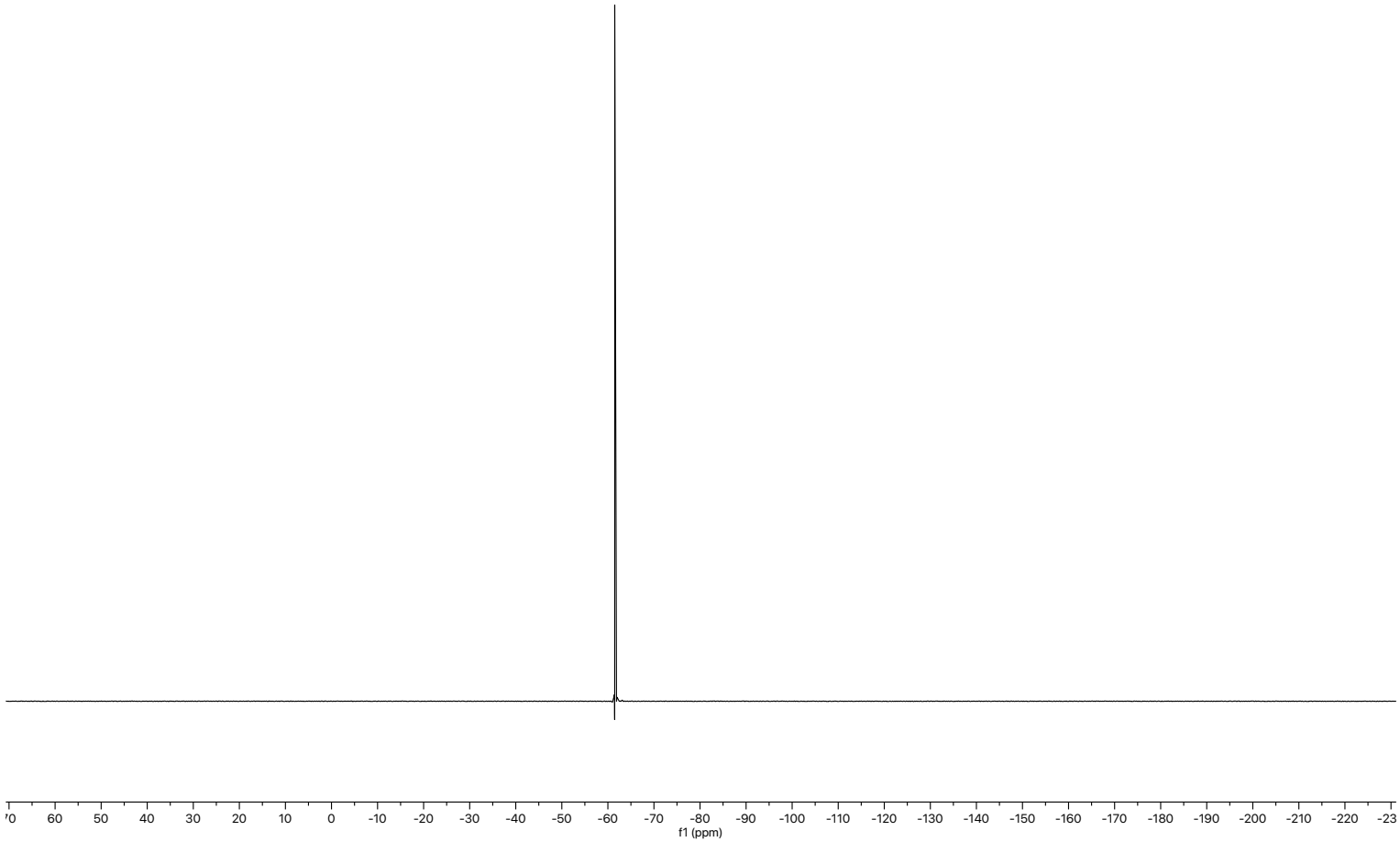

Compound 23 ^{1}H NMR

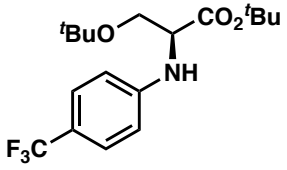

Compound 23 ^{13}C NMR

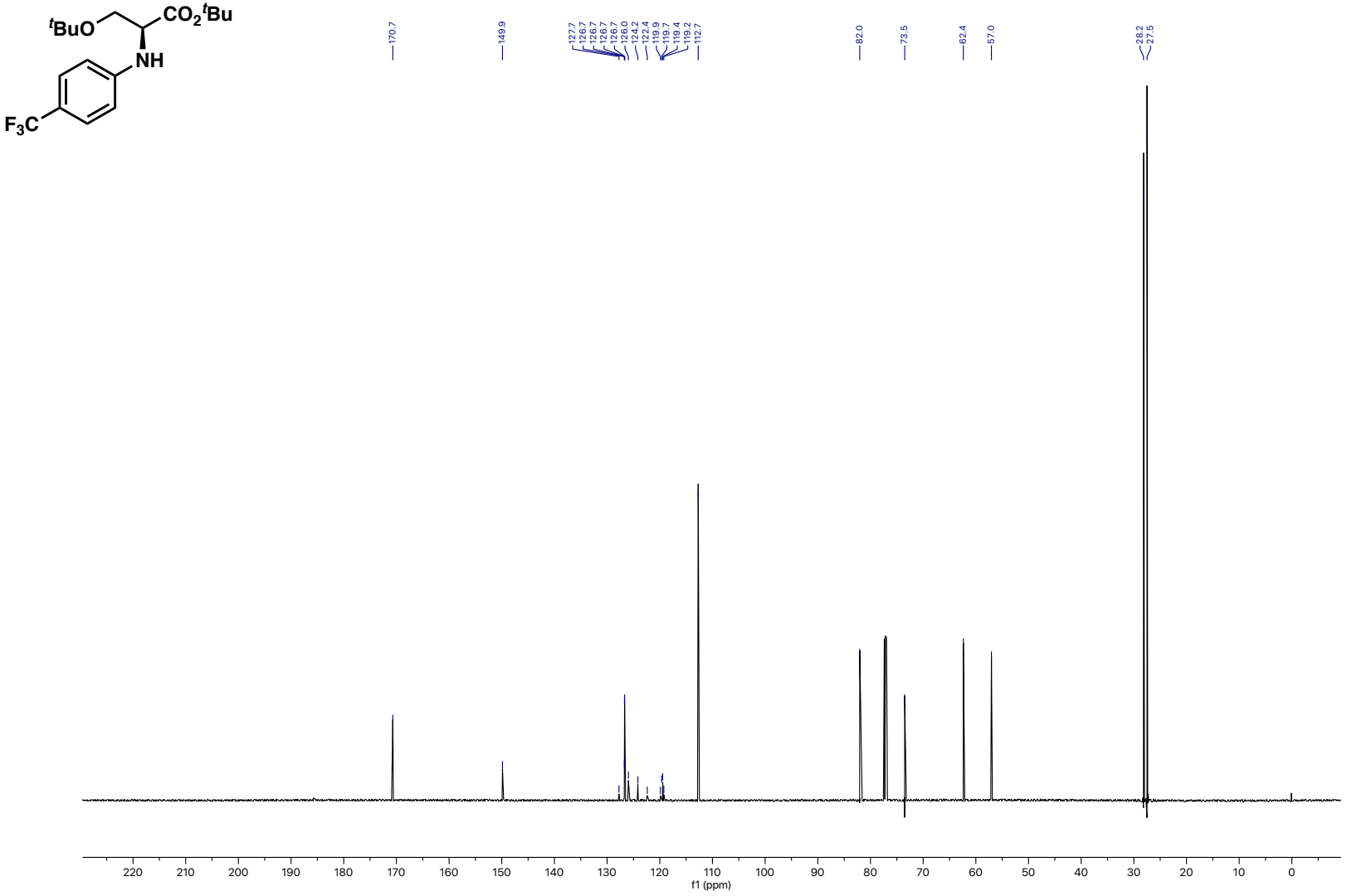

Compound 23 ^{19}F NMR

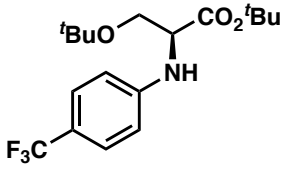

Compound 24 ^{1}H NMR

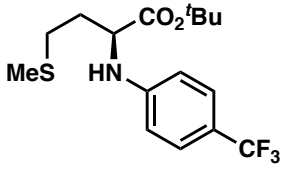

Compound 24 ^{13}C NMR

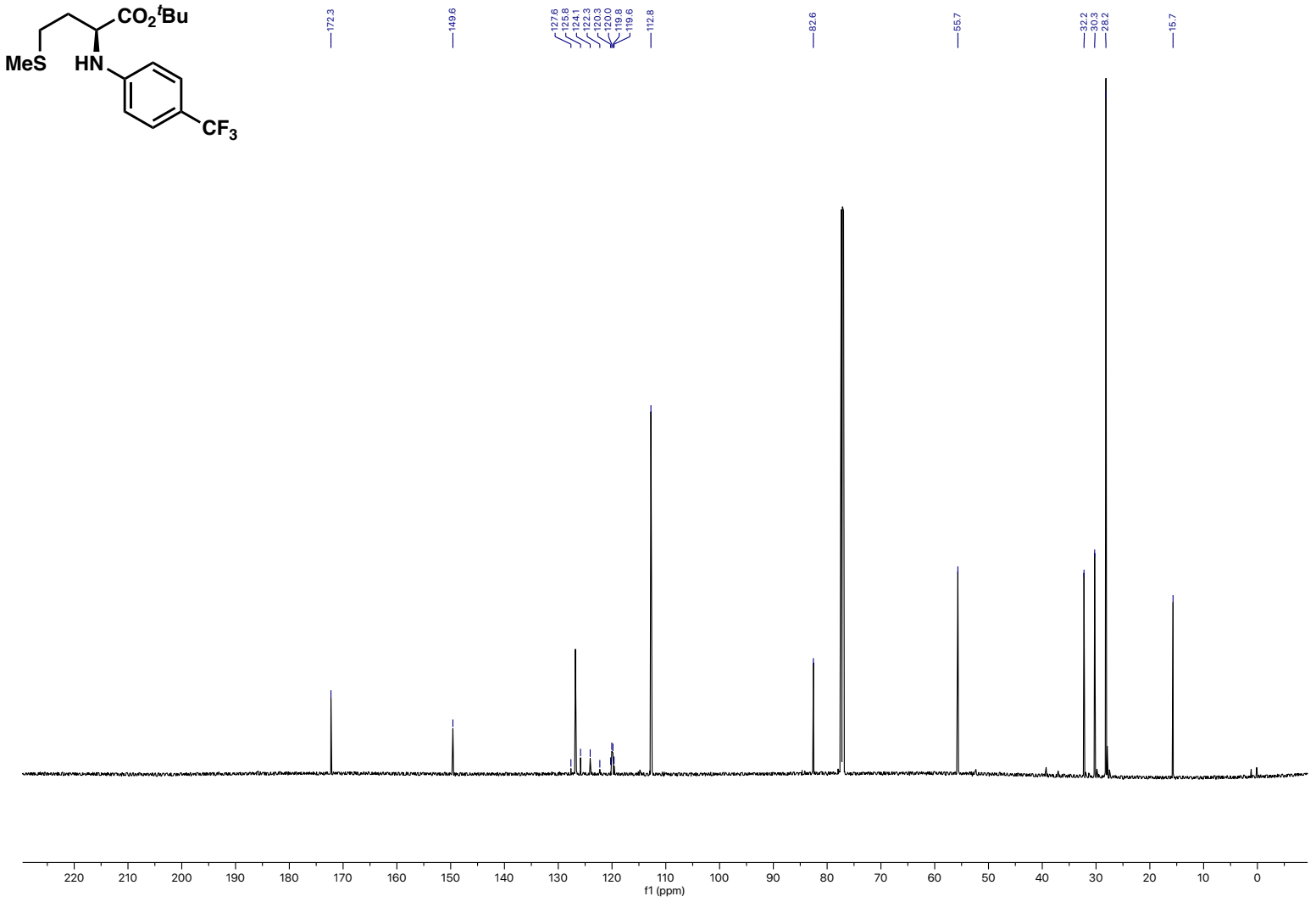

Compound 24 ^{19}F NMR

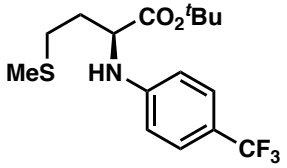

Compound 25 ^{1}H NMR

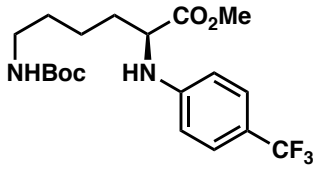

Compound 25 ^{13}C NMR

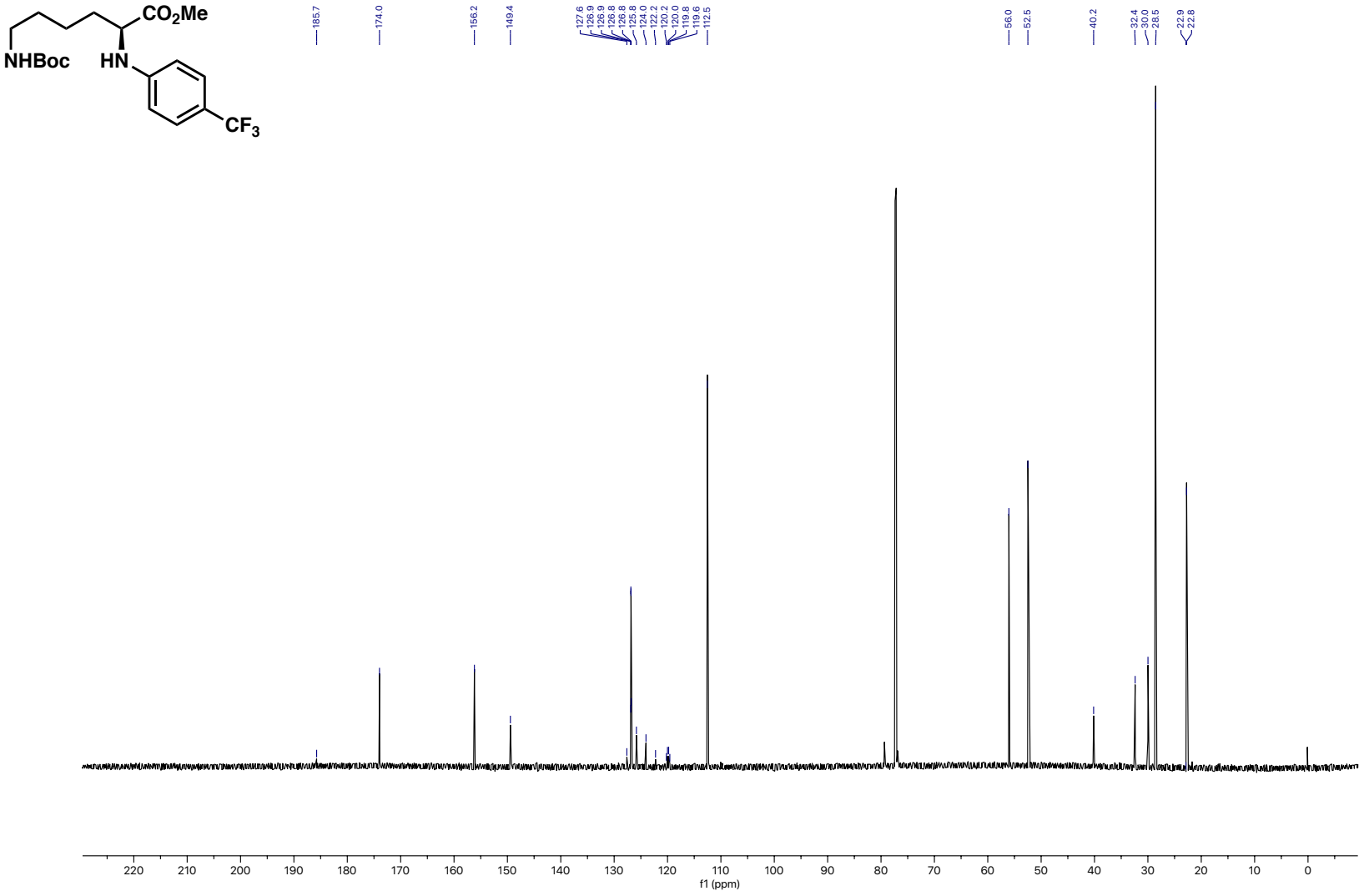

Compound 25 ^{19}F NMR

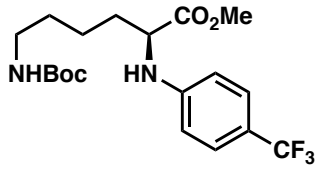

Compound 26 ^{1}H NMR

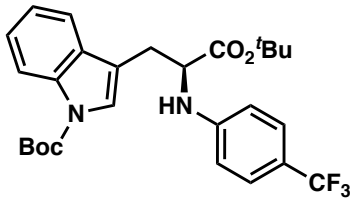

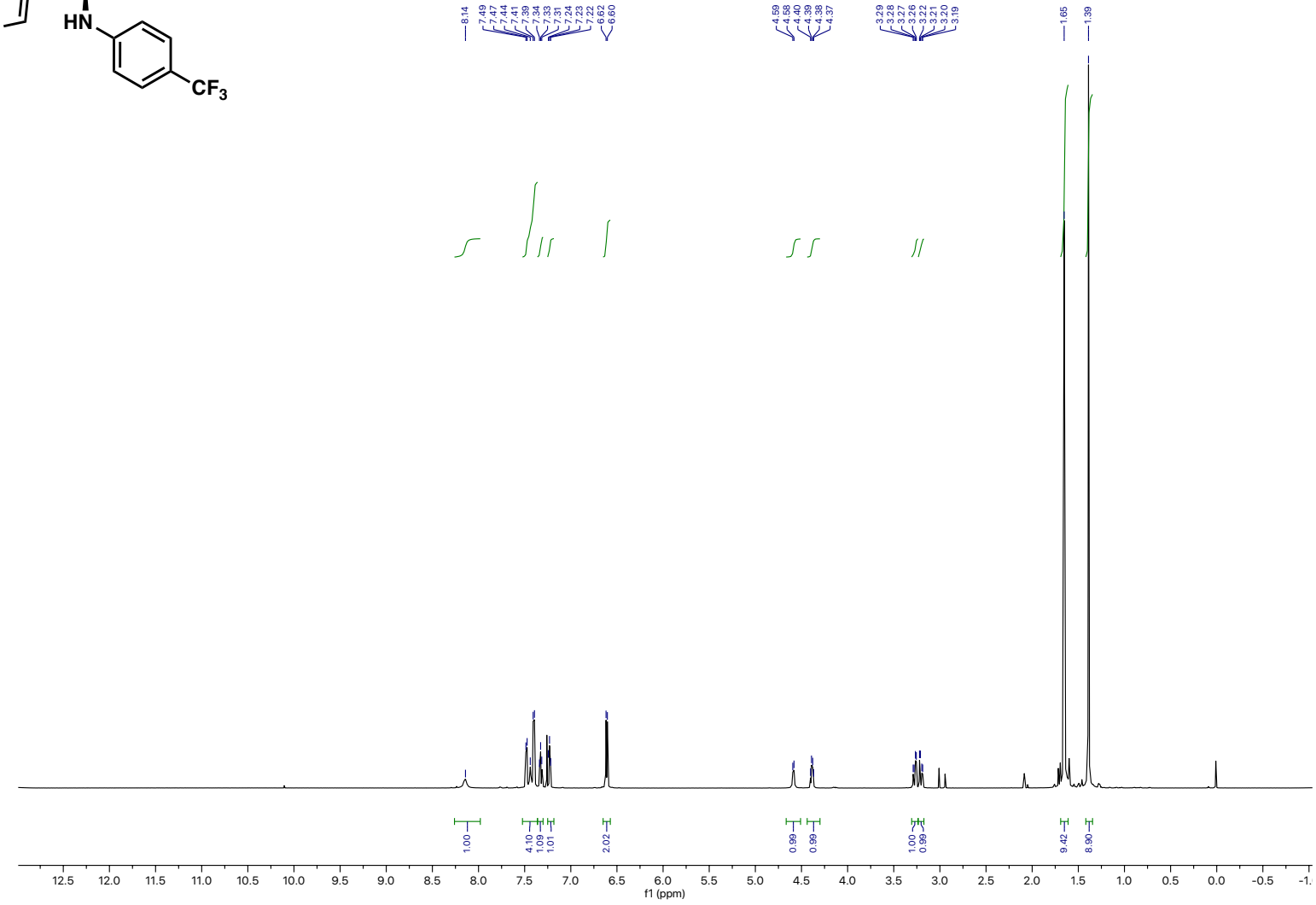

Compound 26 ^{13}C NMR

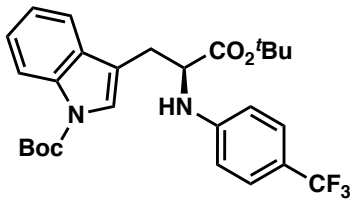

Compound 26 ^{19}F NMR

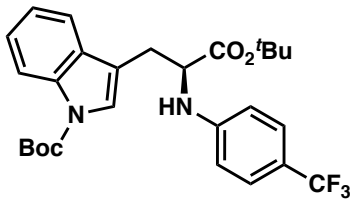

Compound 27 ^{1}H NMR

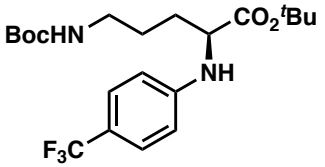

Compound 27 ^{13}C NMR

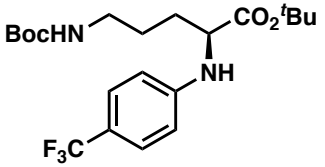

Compound 27 ^{19}F NMR

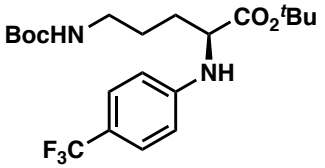

Compound 28 ^{1}H NMR

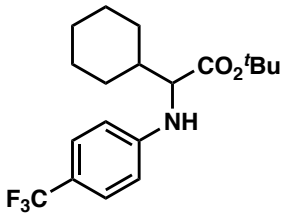

Compound 28 ^{13}C NMR

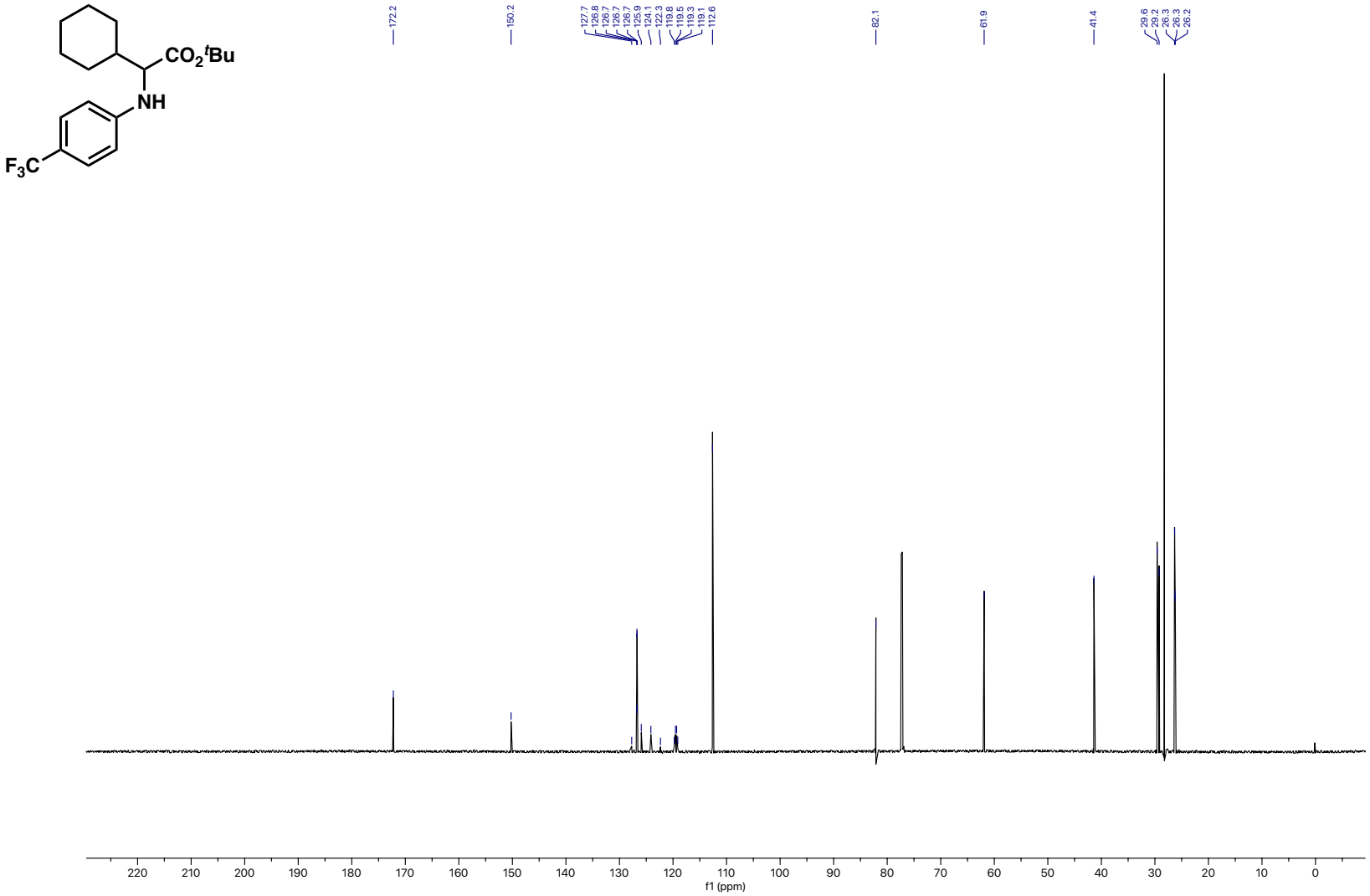

Compound 28 ^{19}F NMR

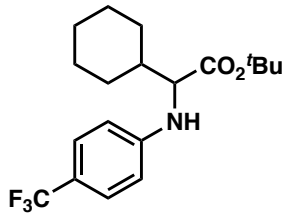

Compound 34 ^{1}H NMR

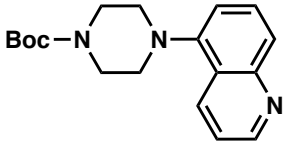

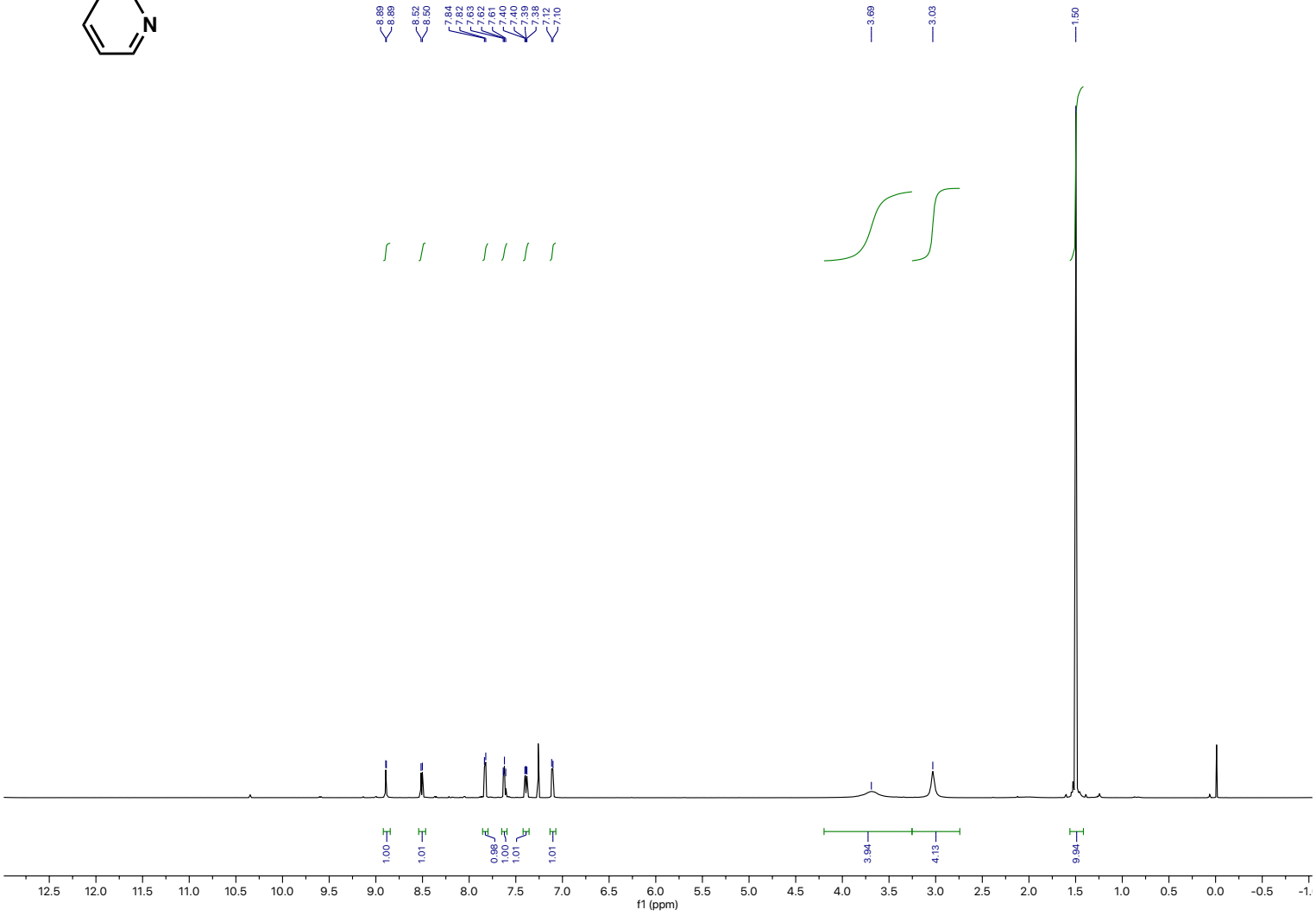

Compound 34 ^{13}C NMR

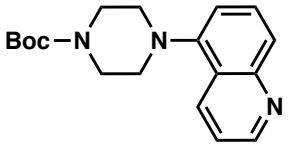

Compound 35 ^{1}H NMR

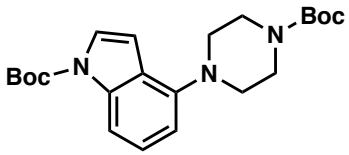

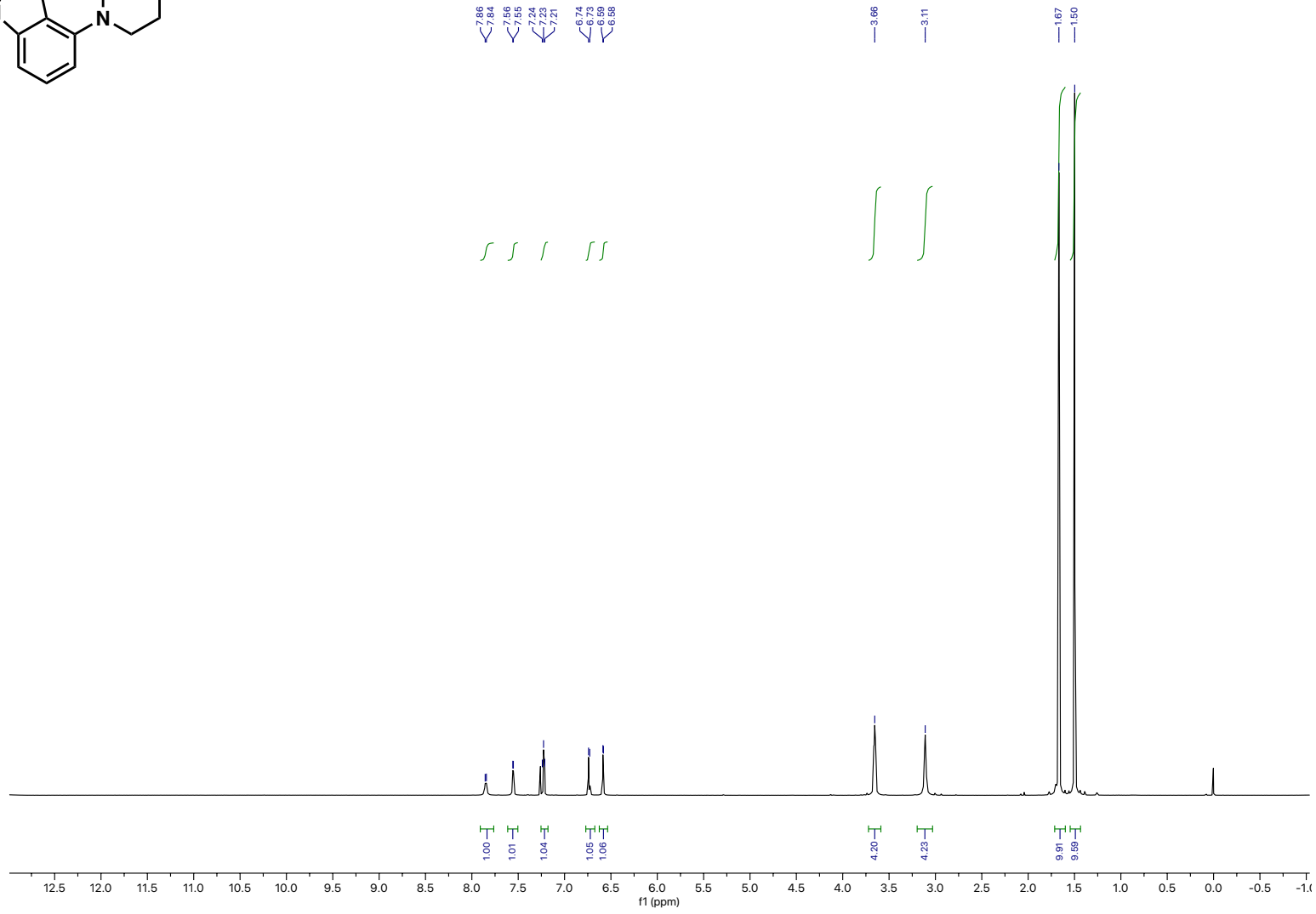

Compound 35 ^{13}C NMR

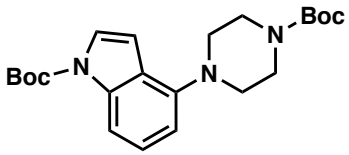

Compound 38 ^{1}H NMR

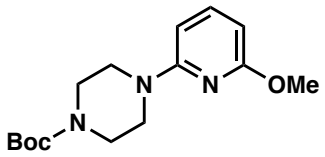

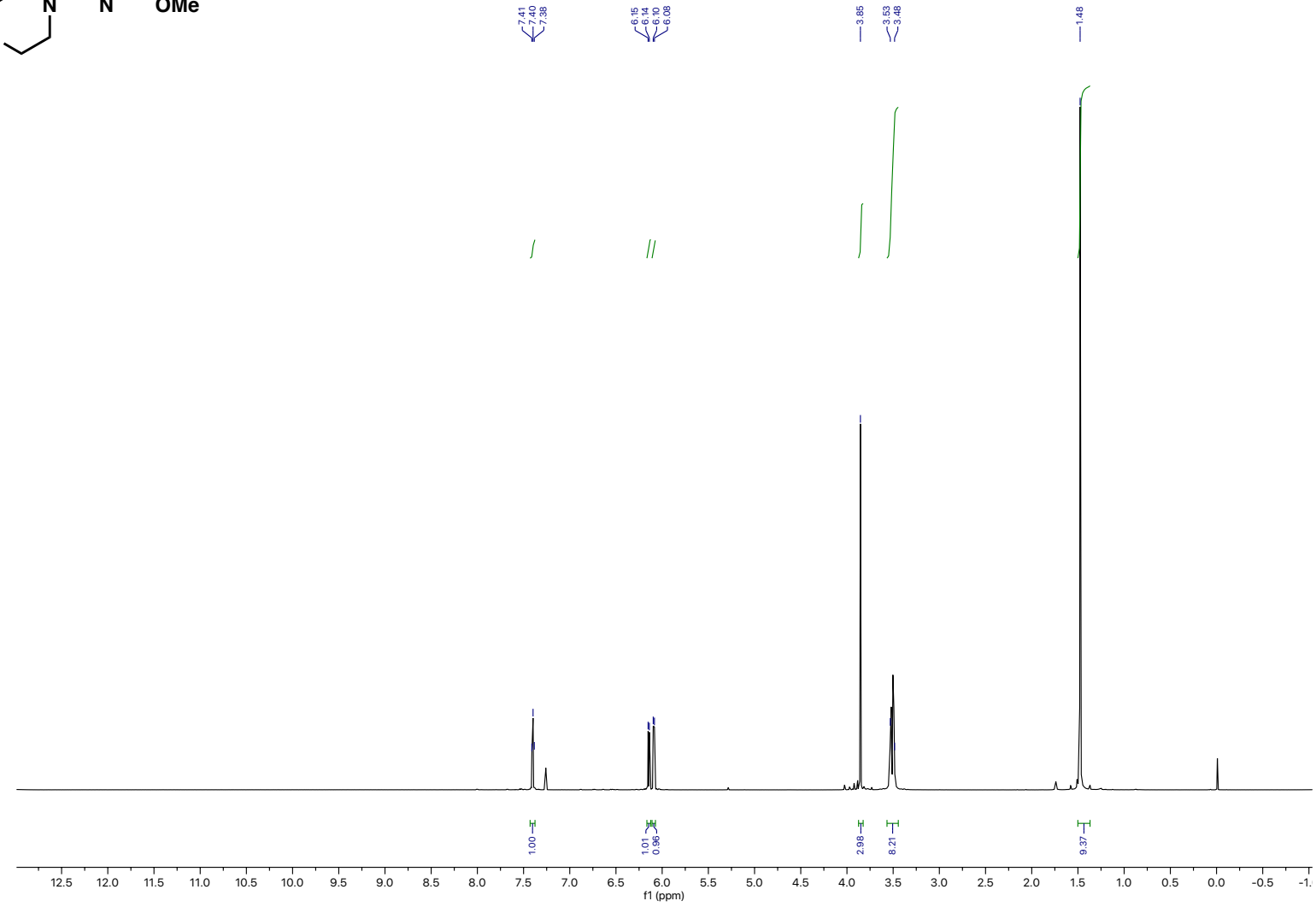

Compound 38 ^{13}C NMR

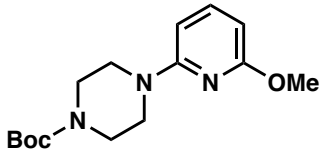

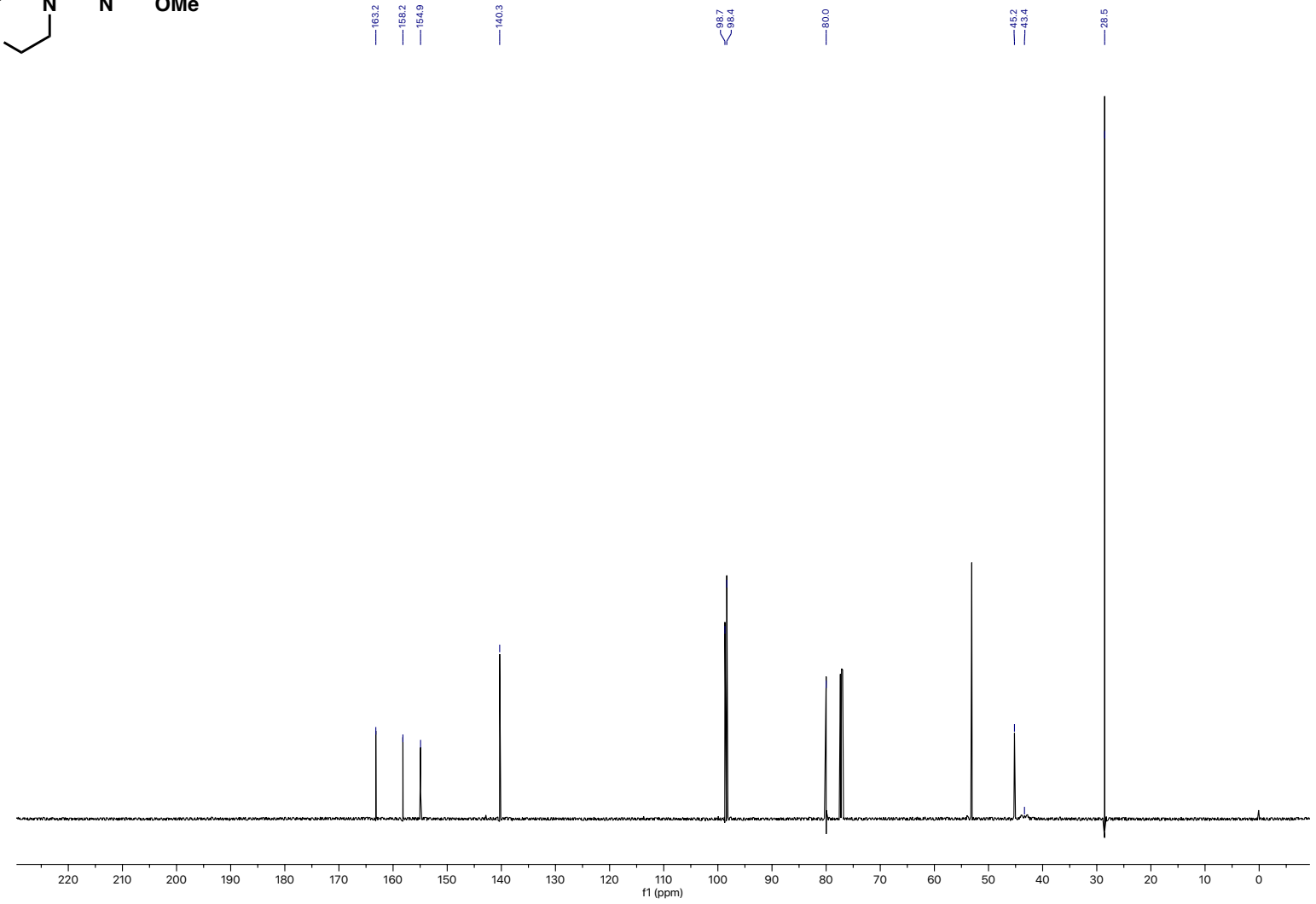

Compound 39 ^{1}H NMR

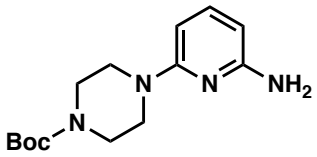

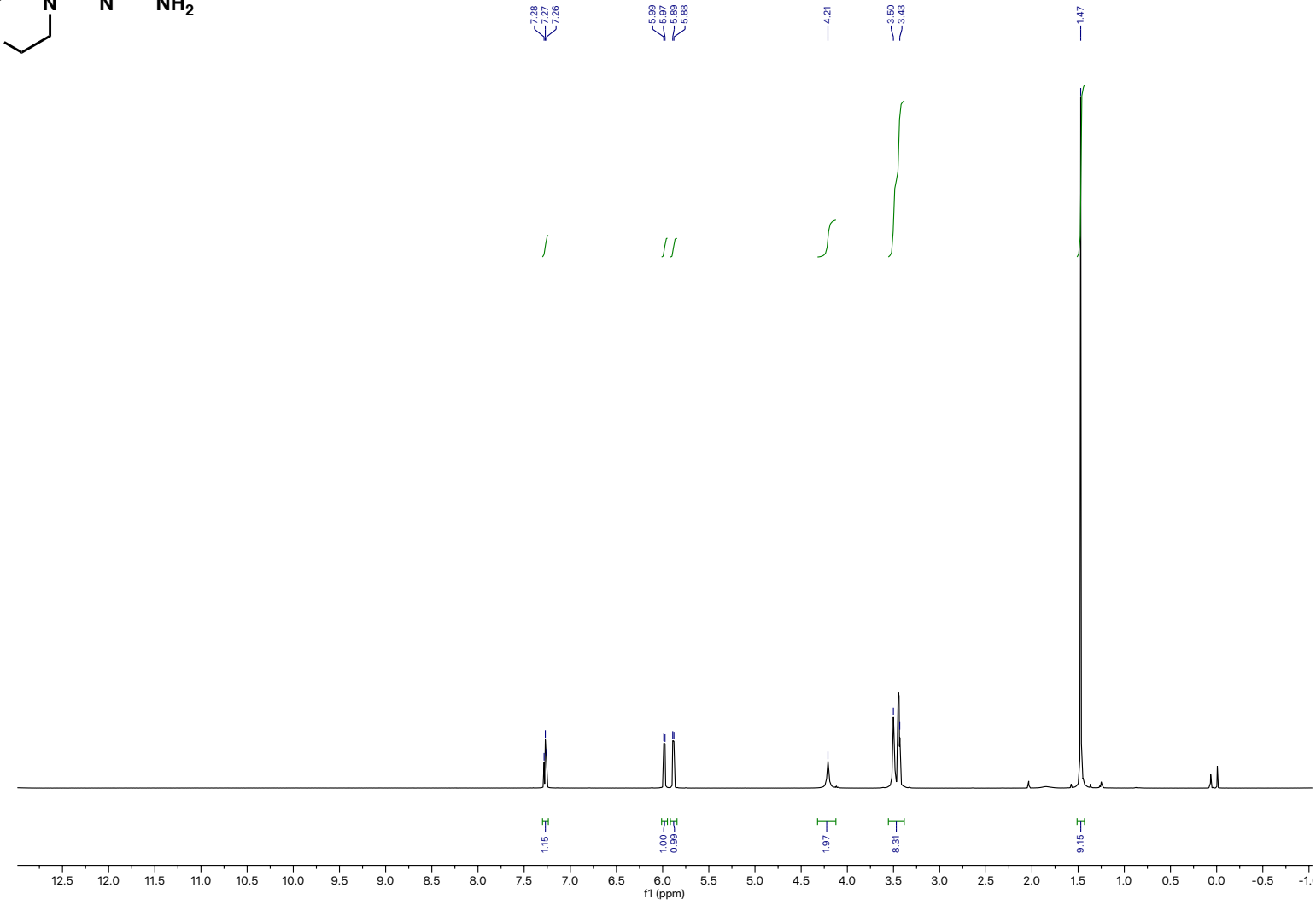

Compound 39 ^{13}C NMR

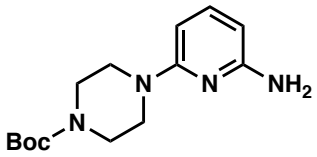

Compound 40 ^{1}H NMR

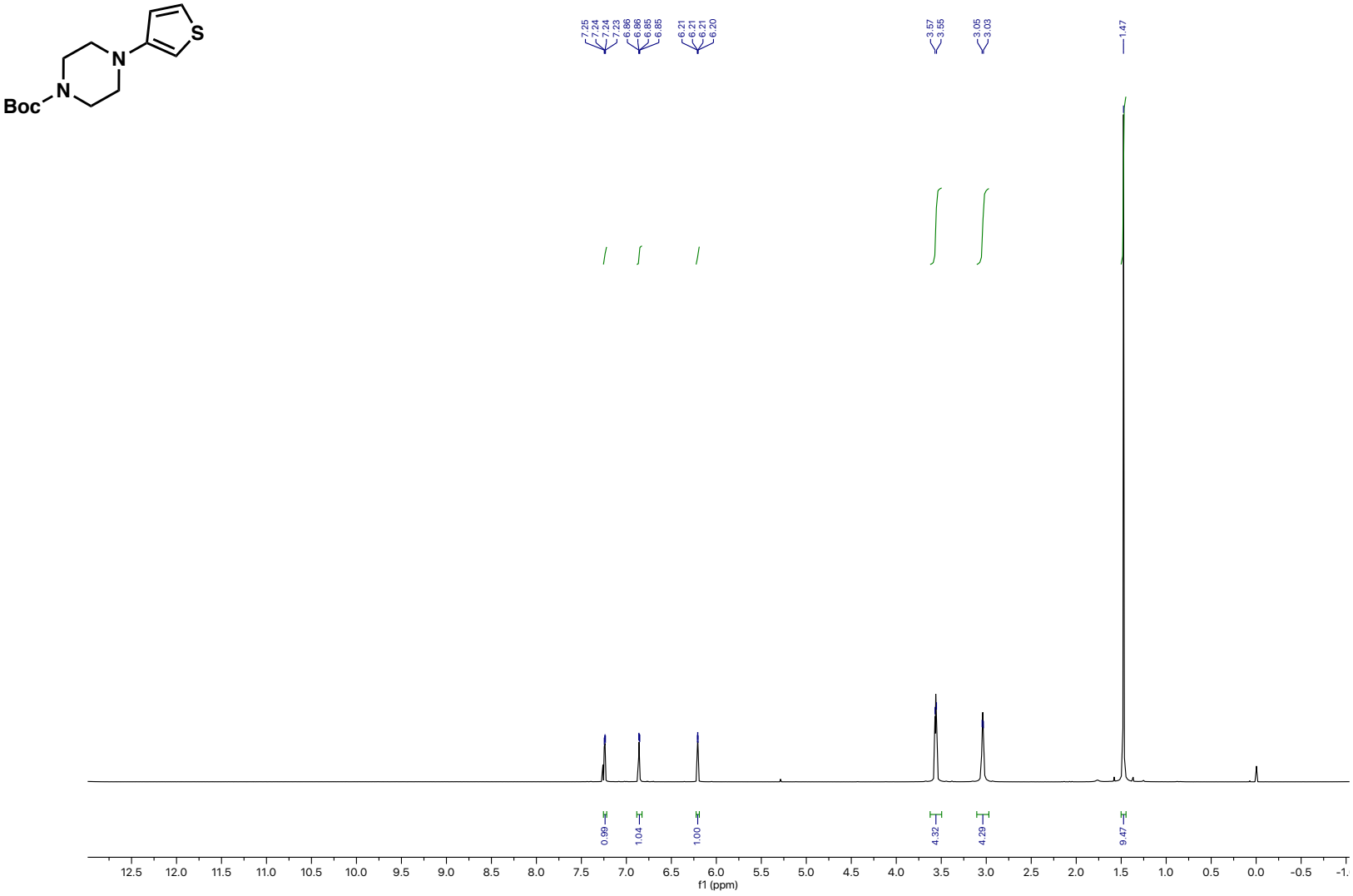

Compound 40 ^{13}C NMR

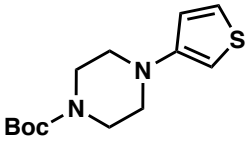

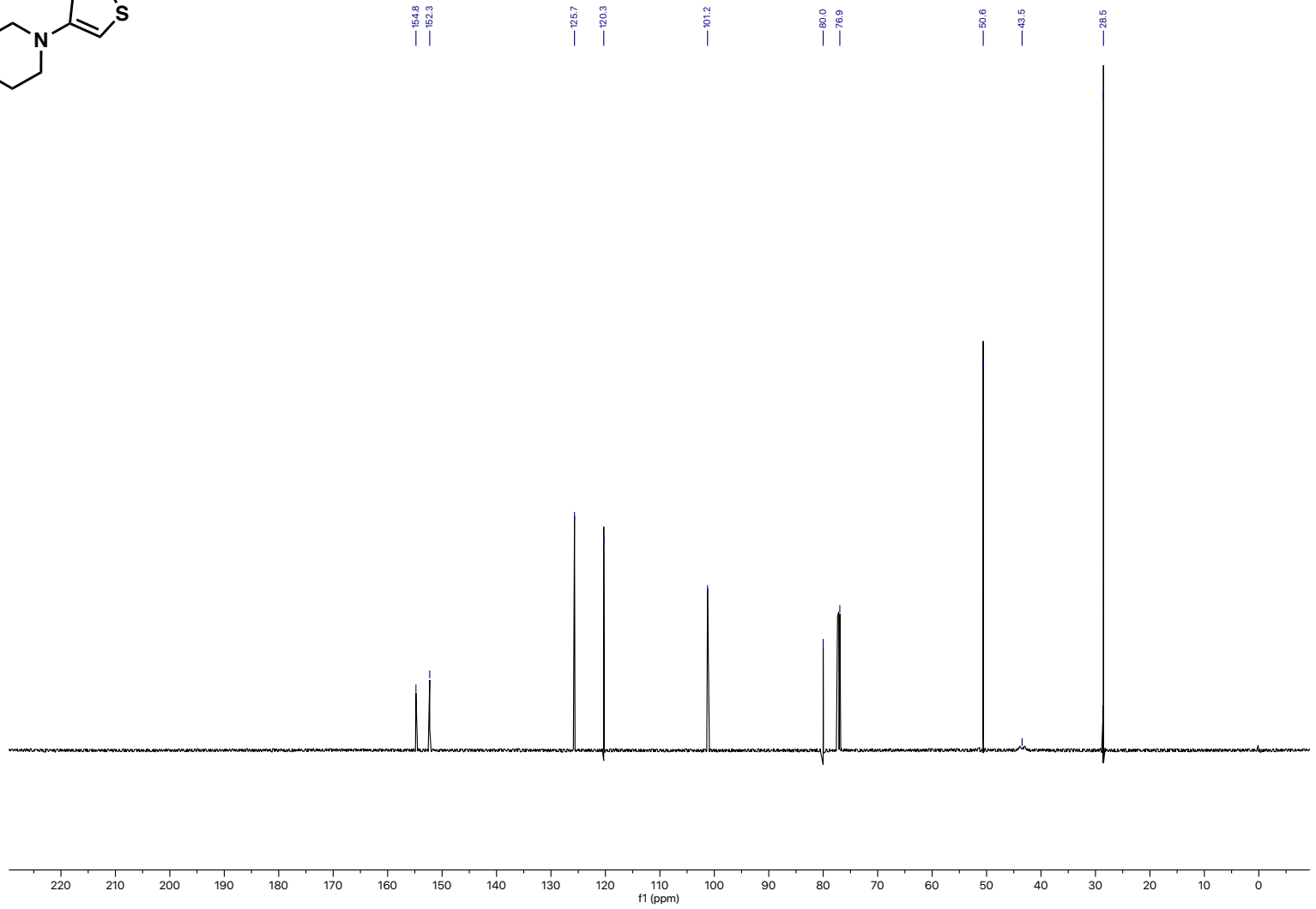

Compound 41 ^{1}H NMR

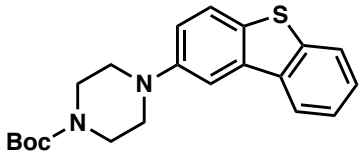

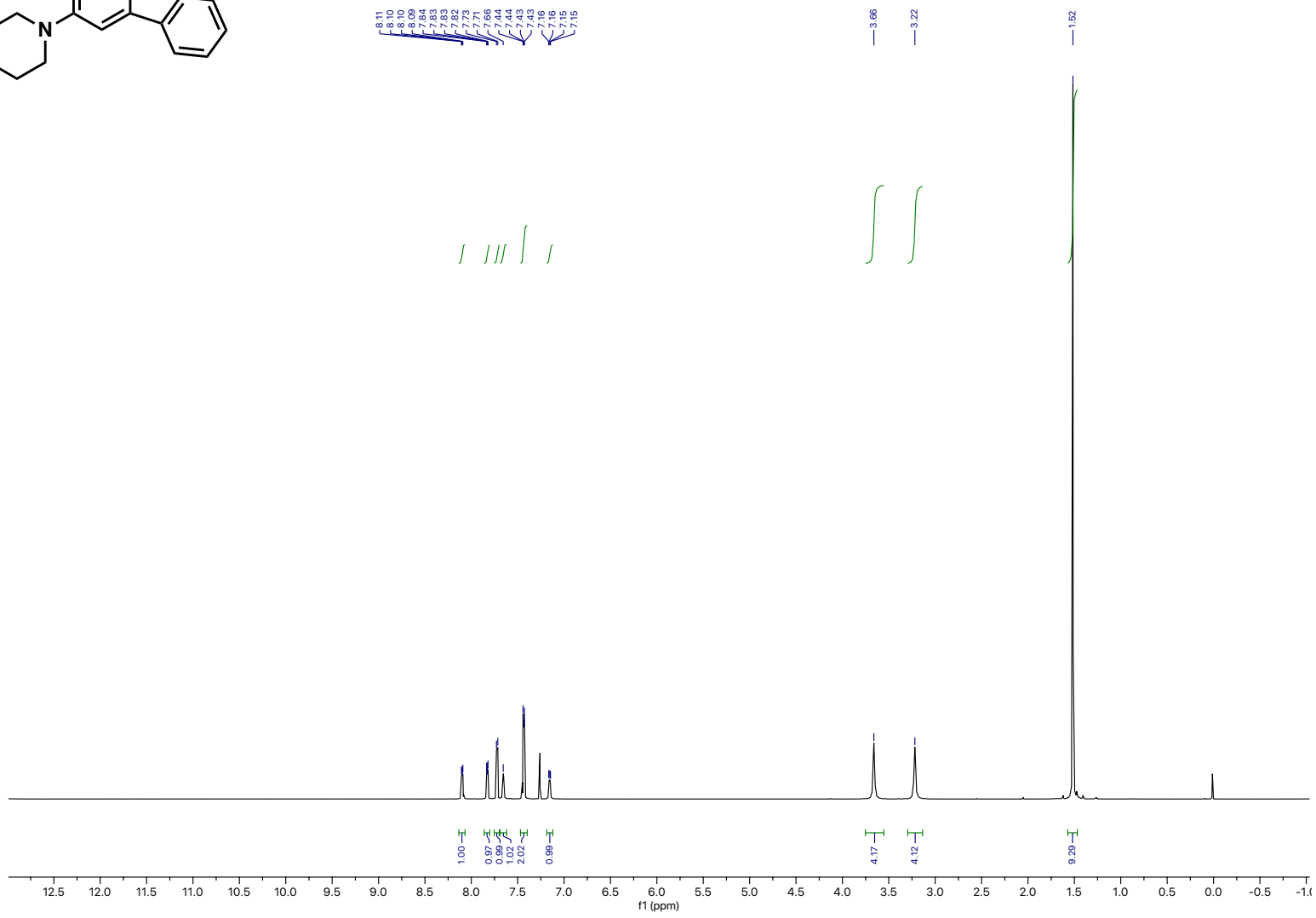

Compound 41 ^{13}C NMR

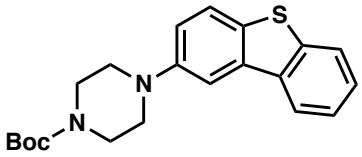

Compound 43 ^{1}H NMR

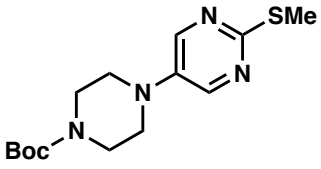

Compound 43 ^{13}C NMR

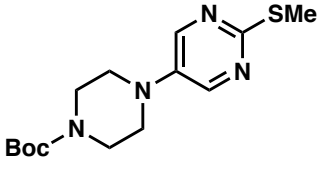

Compound 44 ^{1}H NMR

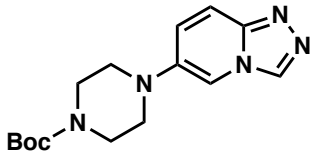

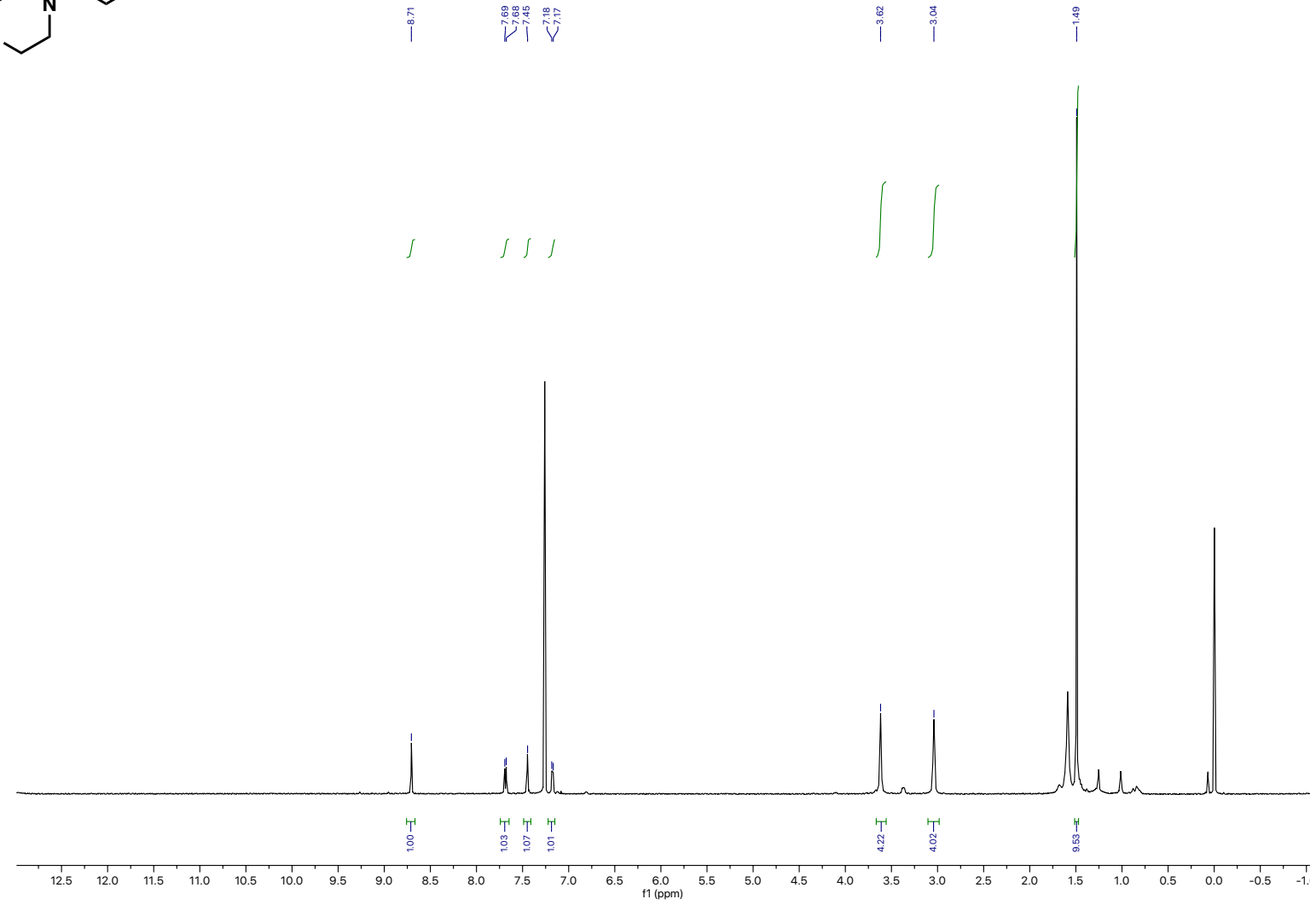

Compound 44 ^{13}C NMR

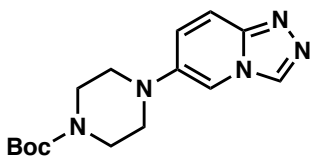

Compound 45 ^{1}H NMR

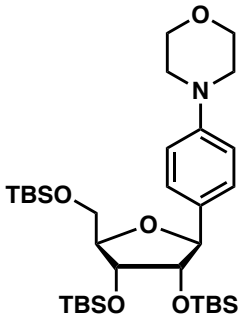

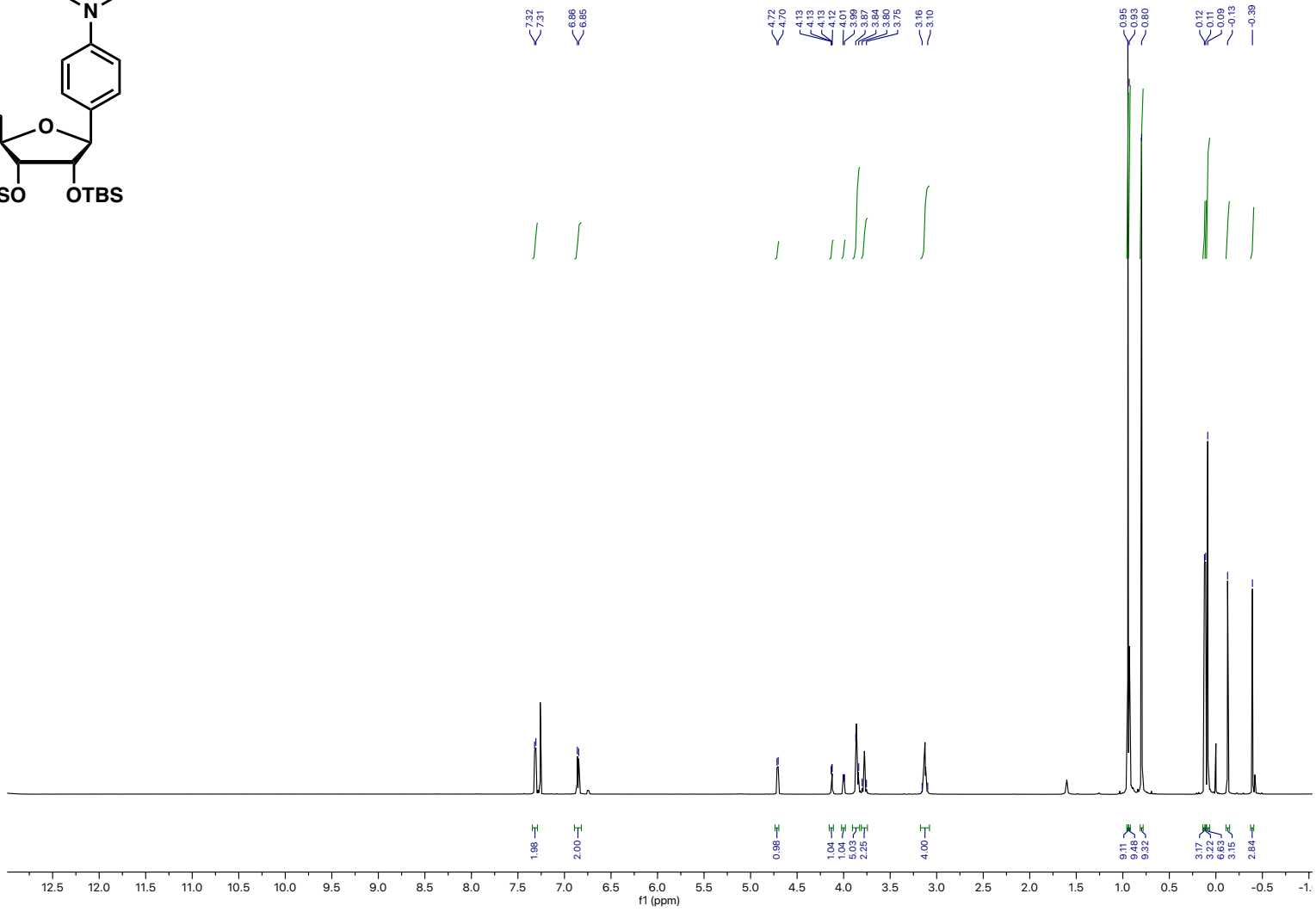

Compound 45 ^{13}C NMR

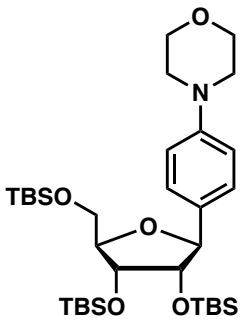

Compound 46 ^{1}H NMR

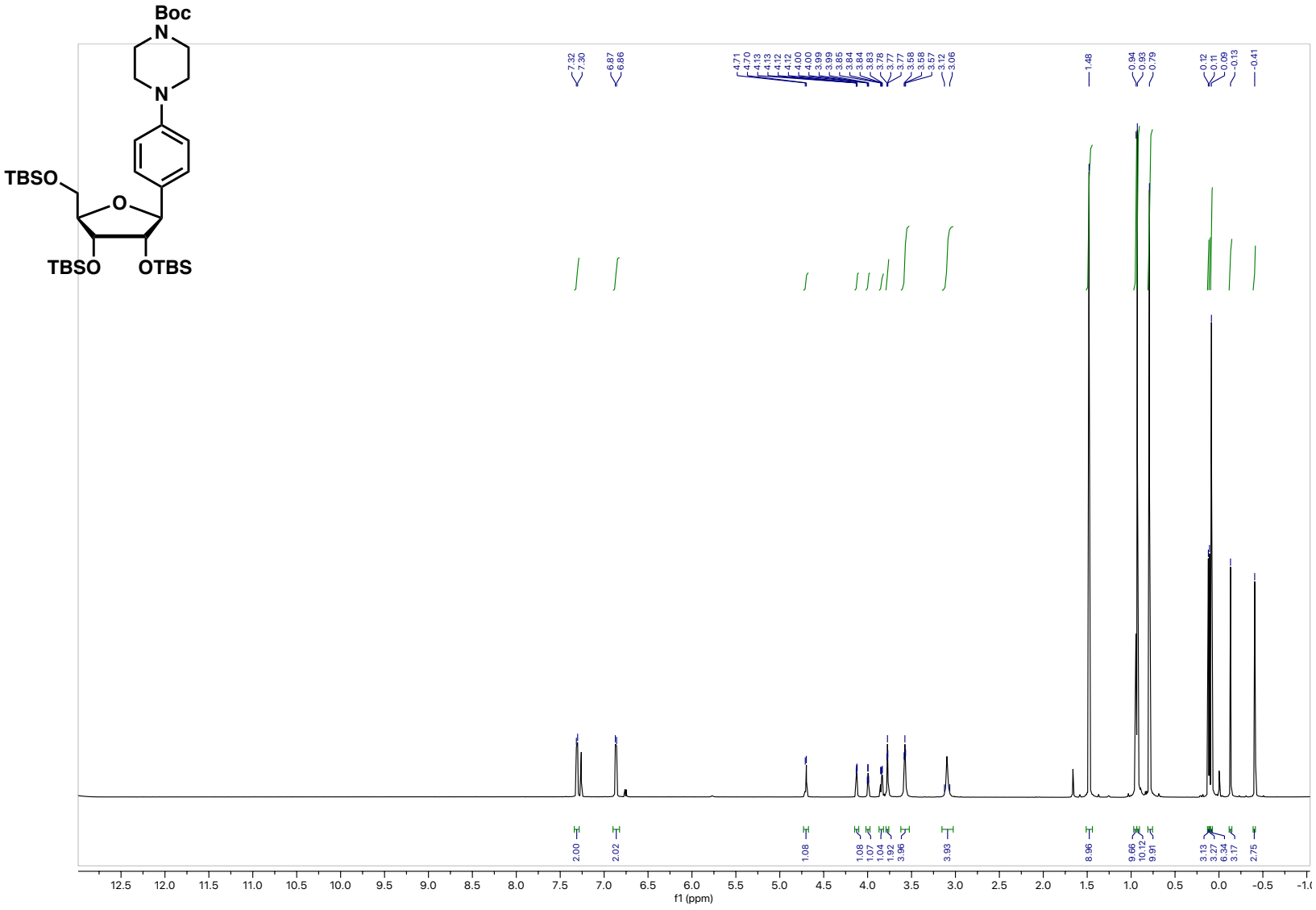

Compound 46 ^{13}C NMR

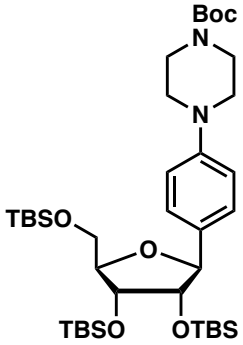

Compound 47 ^{1}H NMR

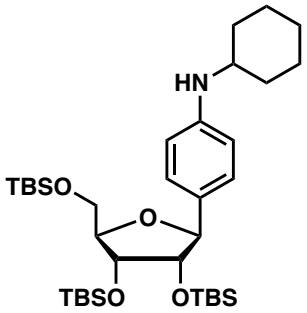

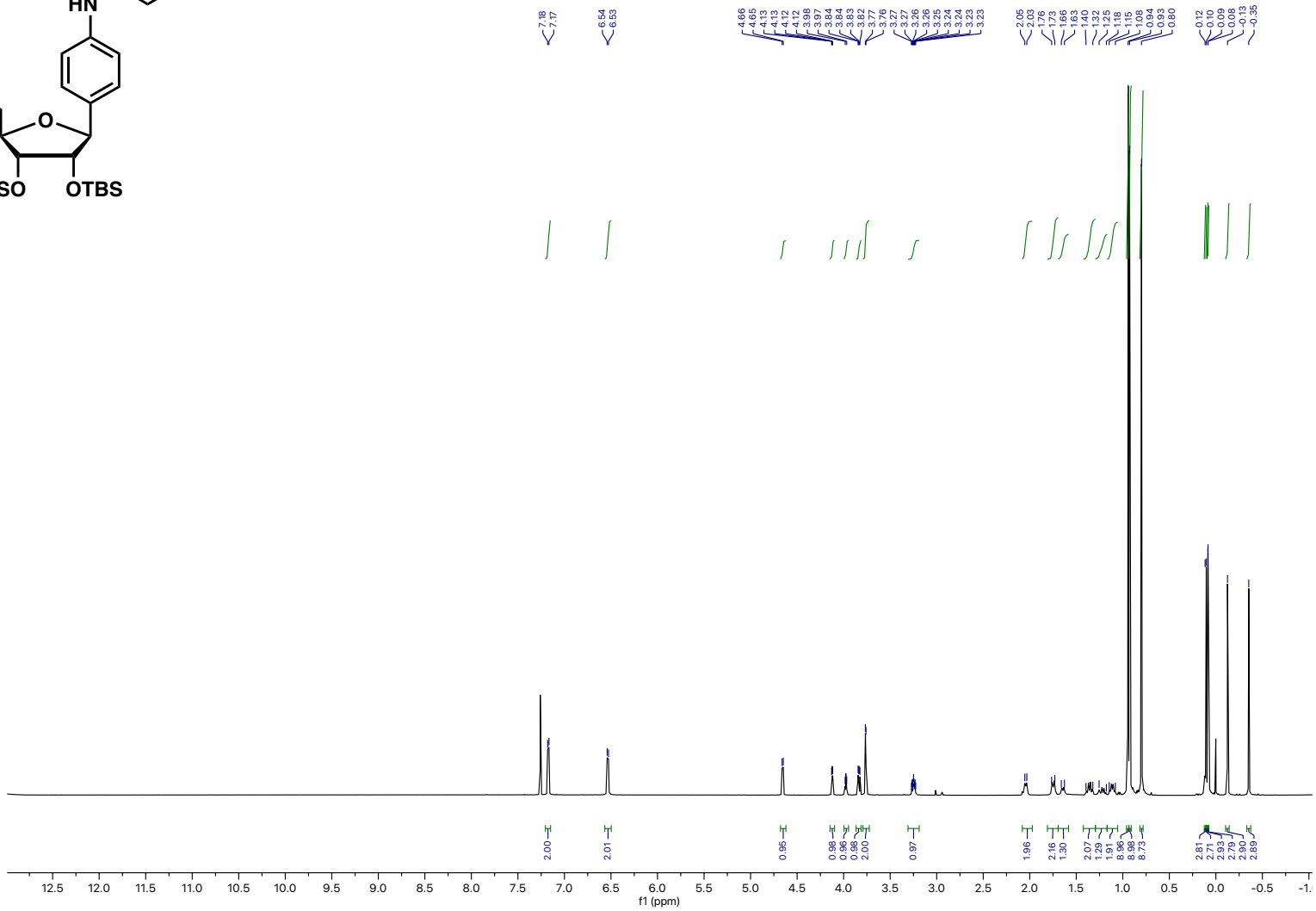

Compound 47 ^{13}C NMR

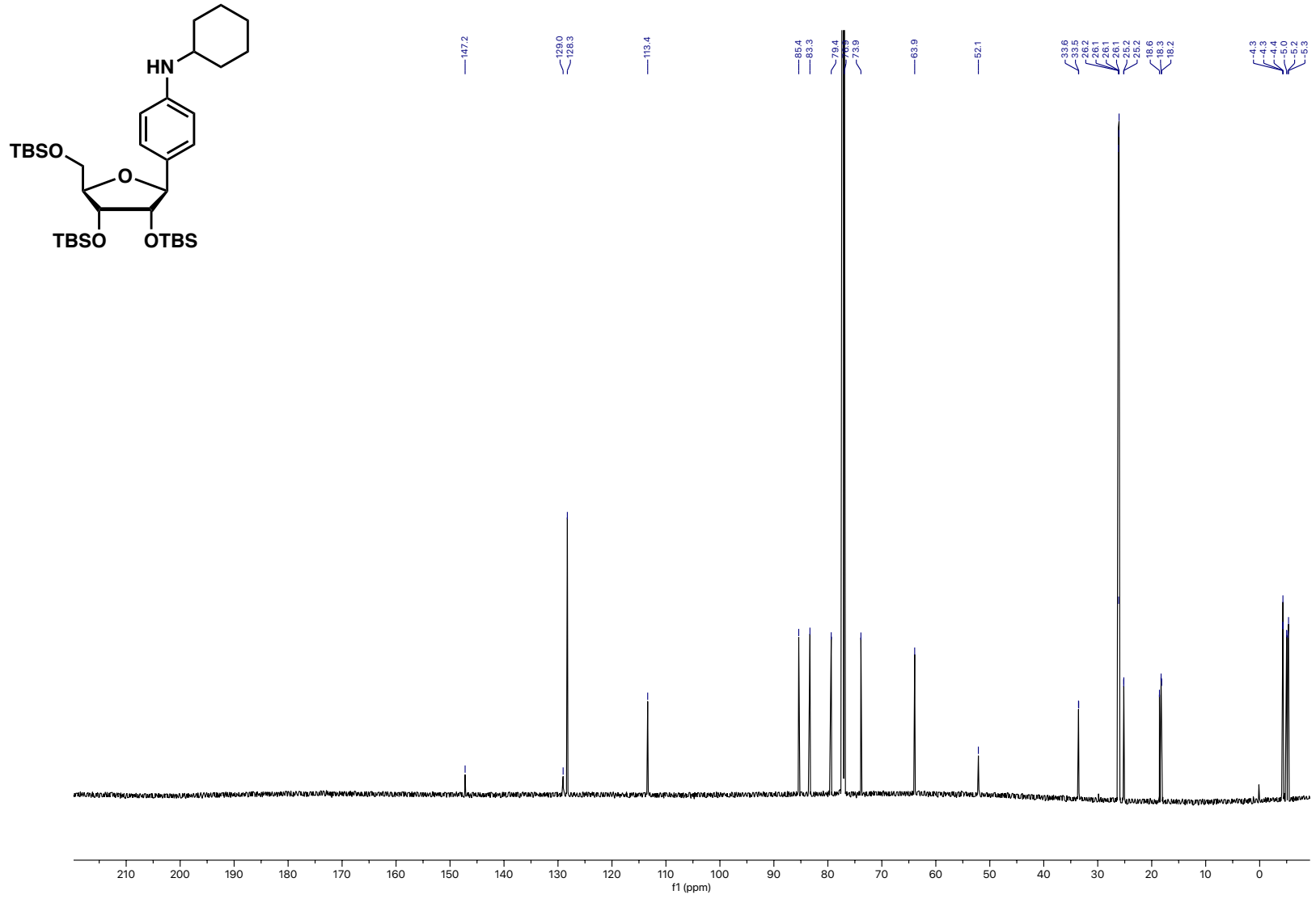

Compound 48 ^{1}H NMR

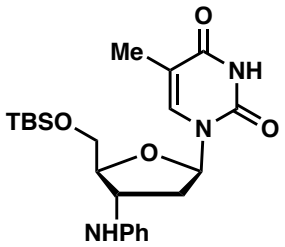

Compound 48 ^{13}C NMR

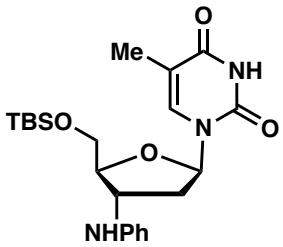

Compound 49 ^{1}H NMR

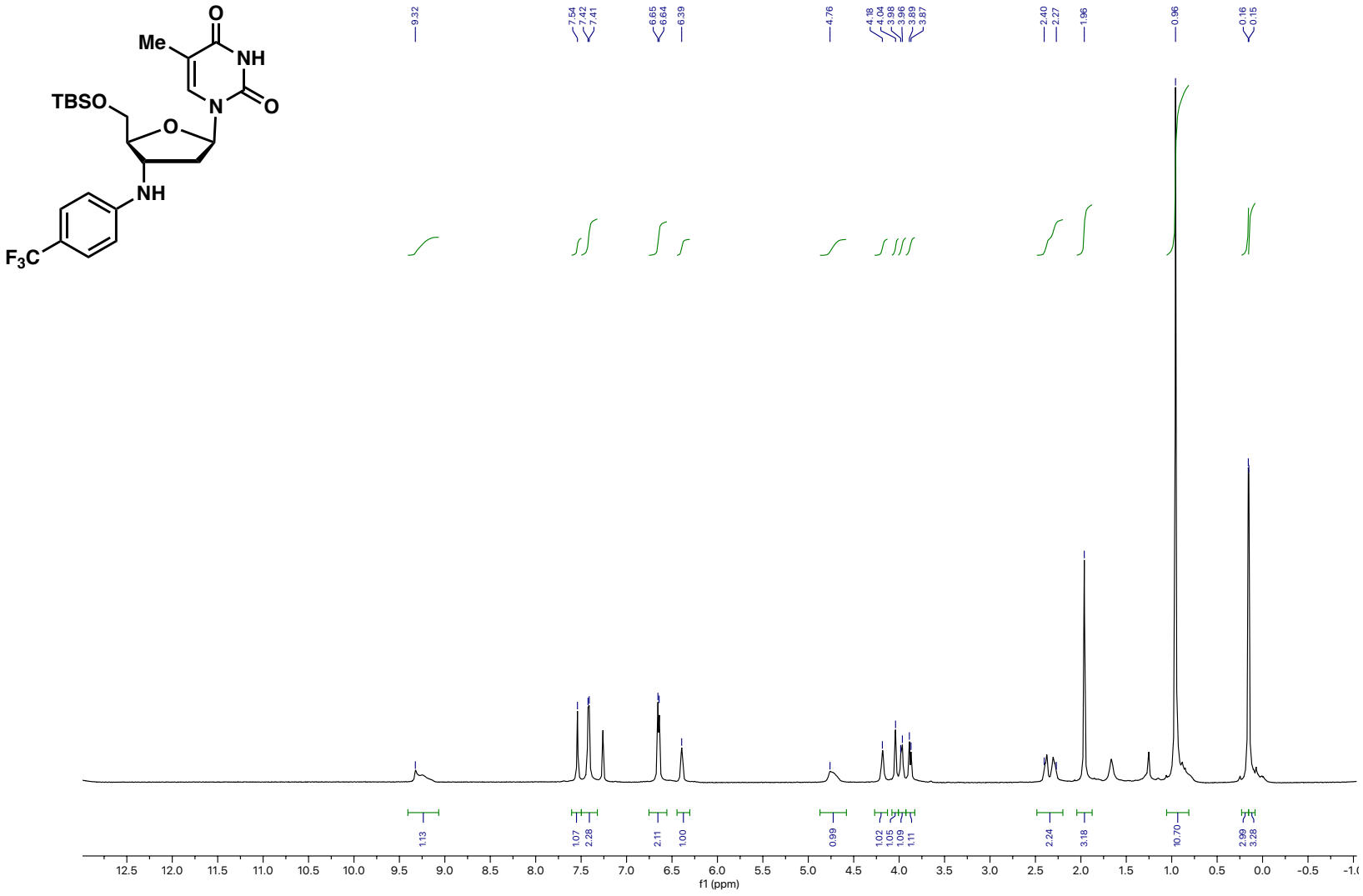

Compound 49 ^{13}C NMR

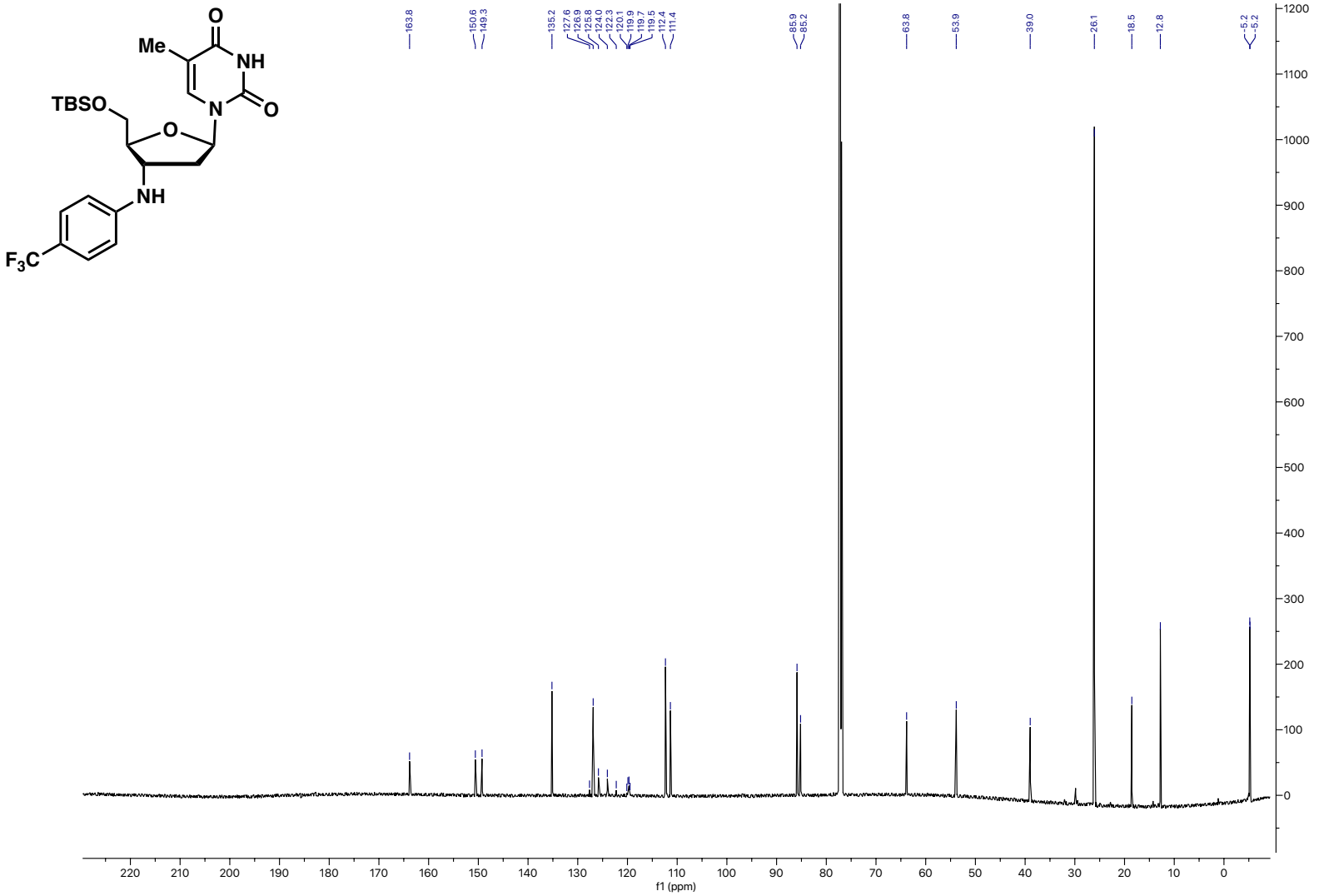

Compound 49 ^{19}F NMR

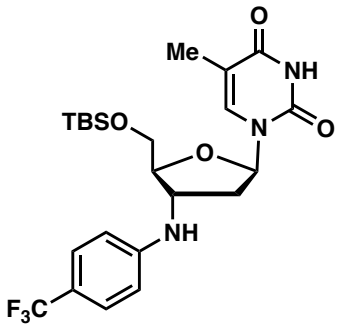

Compound 50a ^{1}H NMR

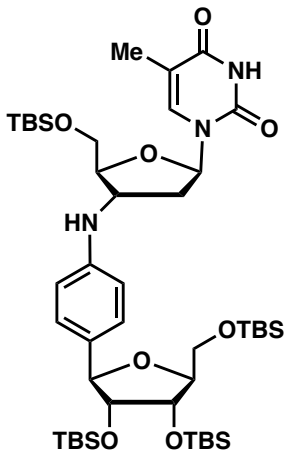

Compound 50a ^{13}C NMR

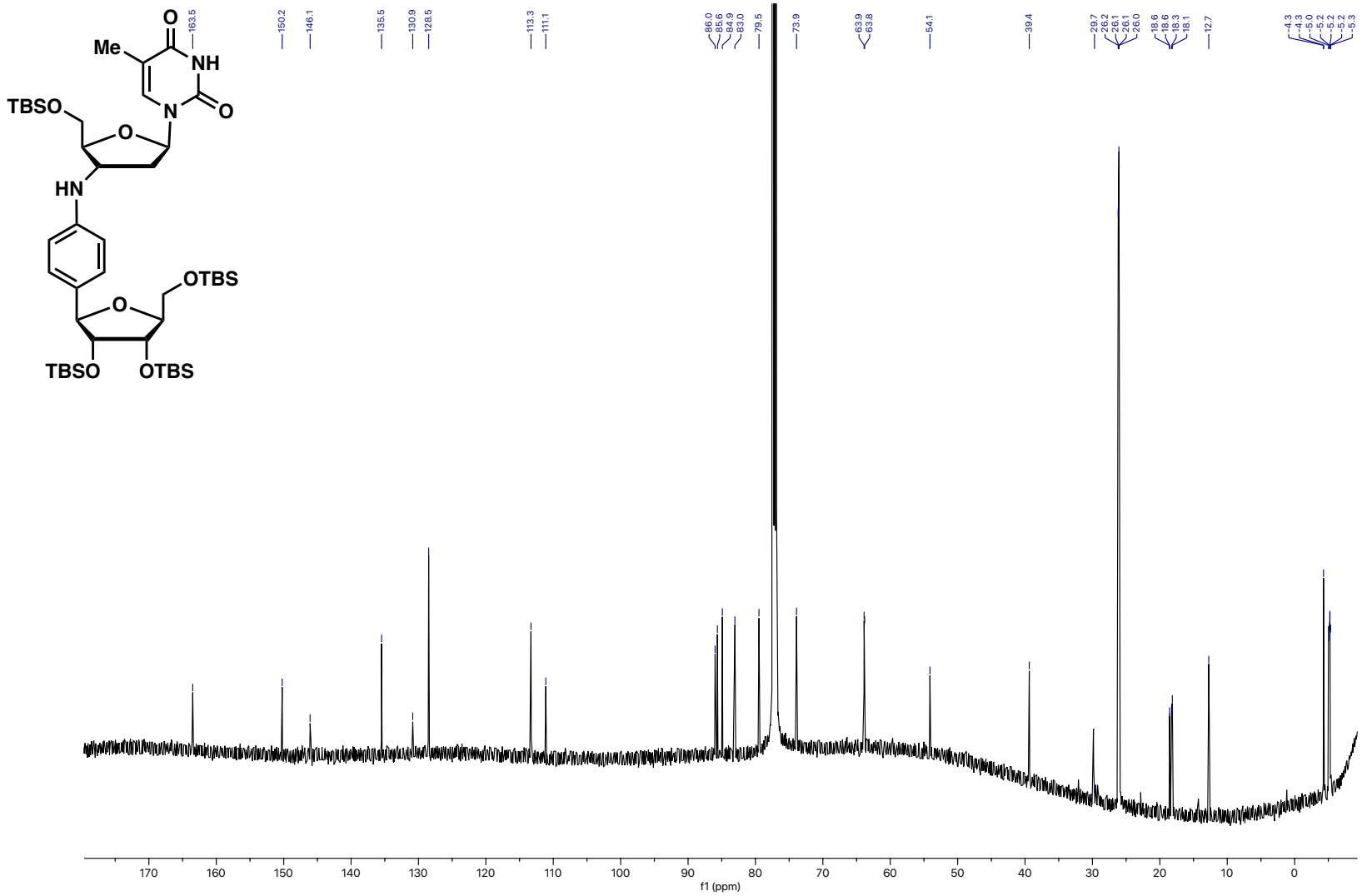

Compound 50b ^{1}H NMR

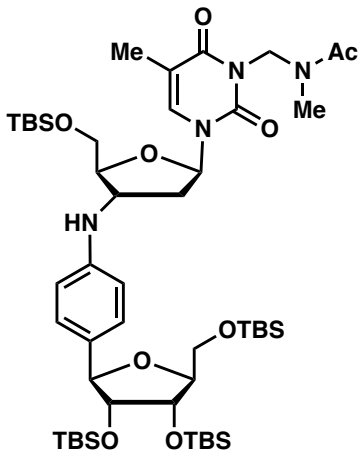

Compound 50b ^{13}C NMR

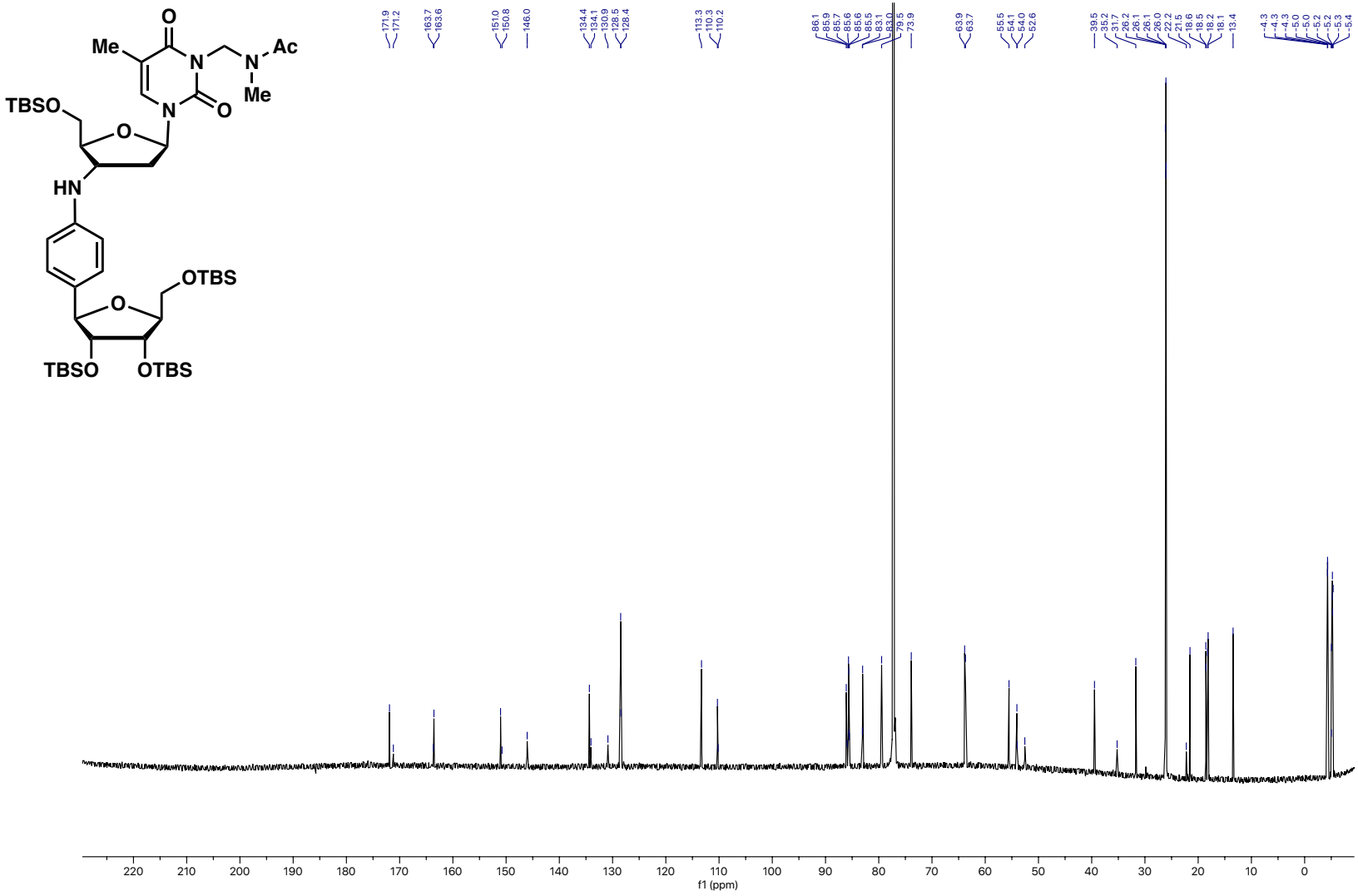

e-Amination 2.0 - Supporting information.pdf (49.03 MiB) view on ChemRxiv • download file